Lappeenranta
University of Technology

Sanna Hokkanen

MODIFIED NANO- AND MICROCELLULOSE BASED ADSORPTION MATERIALS IN WATER TREATMENT

Thesis for the degree of Doctor of Science (Technology) to be presented with due permission for public examination and criticism in the Chamber Music Hall at the Mikaeli Concert and Congress Hall, Mikkeli, Finland on the 7th of November, 2014, at noon.

Acta Universitatis
Lappeenrantaensis 588

Supervisor	Professor Mika Sillanpää Department of Chemical Technology Laboratory of Green Chemistry Lappeenranta University of Technology Finland
Reviewers	Professor Herman Potgieter Department of Analytical Development Manchester Metropolitan University United Kingdom
	Professor Ulla Lassi Department of Chemistry University of Oulu Finland
Opponent	Professor Ulla Lassi Department of Chemistry University of Oulu Finland

ISBN 978-952-265-645-2
ISBN 978-952-265-646-9 (PDF)
ISSN-L 1456-4491
ISSN 1456-4491

Lappeenranta University of Technology

University Press 2014

Abstract

Sanna Hokkanen
Modified nano- and microcellulose based adsorption materials in water treatment
Lappeenranta, 2014
p. 131
Acta Universitatis Lappeenrantaensis 588
Diss. Lappeenranta University of Technology
ISBN 978-952-265-645-2**,** ISBN 978-952-265-646-9(PDF), ISSN-L 1456-4491, ISSN 1456-4491

In recent decades, industrial activity growth and increasing water usage worldwide have led to the release of various pollutants, such as toxic heavy metals and nutrients, into the aquatic environment. Modified nanocellulose and microcellulose-based adsorption materials have the potential to remove these contaminants from aqueous solutions. The present research consisted of the preparation of five different nano/microcellulose-based adsorbents, their characterization, the study of adsorption kinetics and isotherms, the determination of adsorption mechanisms, and an evaluation of adsorbents' regeneration properties.

The same well known reactions and modification methods that were used for modifying conventional cellulose also worked for microfibrillated cellulose (MFC). The use of succinic anhydride modified mercerized nanocellulose, and aminosilane and hydroxyapatite modified nanostructured MFC for the removal of heavy metals from aqueous solutions exhibited promising results. Aminosilane, epoxy and hydroxyapatite modified MFC could be used as a promising alternative for H_2S removal from aqueous solutions. In addition, new knowledge about the adsorption properties of carbonated hydroxyapatite modified MFC as multifunctional adsorbent for the removal of both cations and anions ions from water was obtained. The maghemite nanoparticles (Fe_3O_4) modified MFC was found to be a highly promising adsorbent for the removal of As(V) from aqueous solutions due to its magnetic properties, high surface area, and high adsorption capacity .

The maximum removal efficiencies of each adsorbent were studied in batch mode. The results of adsorption kinetics indicated very fast removal rates for all the studied pollutants. Modeling of adsorption isotherms and adsorption kinetics using various theoretical models provided information about the adsorbent's surface properties and the adsorption mechanisms. This knowledge is important for instance, in designing water treatment units/plants. Furthermore, the correspondence between the theory behind the model and properties of the adsorbent as well as adsorption mechanisms were also discussed. On the whole, both the experimental results and theoretical considerations supported the potential applicability of the studied nano/microcellulose-based adsorbents in water treatment applications.

Keywords: water treatment, nanocellulose, microcellulose, surface modification, heavy metals, H_2S, phosphate, nitrate, adsorption isotherm, adsorption kinetics.

UDC 628.1:502/504:541.183:544.723.2:543.2:539.2

PREFACE

The research work of this thesis was carried out at the Laboratory of Green Chemistry, Lappeenranta University of Technology, Mikkeli, during January 2012- June 2014. Studies were financially supported by the Finnish Funding Agency for Technology and Innovation (Tekes), Nano and microcellulose based materials for water treatment applications –project.

I want to express my gratefulness to supervisor of my thesis professor Mika Sillanpää for providing me the opportunity to carry out this study and for his support, guidance and flexibility that has been very crucial help to execute, keep going on and to finish this thesis.

I express my sincerely gratitude to Professor Ulla Lassi and Professor Herman Potgieter, the reviewers of my thesis, for their valuable comments and improvement suggestions regarding the thesis.

I would like to thank Dr. Eveliina Repo for her invaluable guidance in experimental work, data analysis, writing process of manuscripts, encouragement and friendship. I am thankful to all colleagues at the Laboratory of Green Chemistry for their co-operations, support and company.

It has been pleasure and honor to do research together with creative and inspiring researchers. Special thanks are reserved for Dr. Amit Bhatnagar for his valuable assistance for the preparation of this manuscript and co-authoring. I express my gratitude also to Ms. Terhi Suopajärvi, Dr. Henrikki Liimatainen, Prof. Jouko Niinimäki, Prof. Walter Tang, Dr. Lena Johansson Westholm, Dr. Song Lou and Prof. Tuomo Sainio for their contribution as co-authors. Furthermore, I would like to acknowledge Paula Haapanen for her professional help in revising the language of my work.

I've been blessed with so many caring people around me who have helped me in many things in my life and supported me to achieve this goal. I will never forget you. I owe thanks to the staff at the X-ray department of Lääkärikeskus Mehiläinen Töölö for colleagueship and friendship. I would like to thank all of my friends, who have helped me with this project by providing relaxing and cheerful company at leisure times. Furthermore, I wish to express my

gratitude to the greatest football team in the word: SiMa. I want to thank my teammates for moments of victory and loss, sweating, painful muscles, laughing, screaming etc. You have given so much joy to my life!

Finally I would like to express my deepest gratitude to my family and relatives. I would like to thank my parents and siblings their support throughout my life. The warmest and loving thanks belong to my husband Ari. Thank you for your support and encouragement during these years and for being there for our kids when I was absent-minded and busy struggling with the research. Thank you also for your patient help with mathematical problems, Excel and proof-reading. I am grateful for our children Lotta, Emmistiina and baby-boy Lukas, who was born during this doctoral thesis. You are the most important thing in my life and being your mother makes me proud, every single day.

Helsinki, June 2014
Sanna Hokkanen

LIST OF PUBLICATIONS

I **Hokkanen, S.**, Repo, E., Sillanpää, M., Removal of heavy metals from aqueous solutions by succinic anhydride modified mercerized nanocellulose, Chem. Eng. J. 223 (2013) 40–47.

II **Hokkanen, S.,** Repo, E., Suopajärvi, T., Liimatainen, H., Niinimäki, J., Sillanpää, M., Adsorption of Ni(II), Cu(II) and Cd(II) from aqueous solutions by amino modified nanostructured microfibrillated cellulose, Cellulose 21(2014) 1471-1487.

III **Hokkanen, S.,** Repo, E., Bhatnagar, A., Tang W. Z., Sillanpää, M., Adsorption of hydrogen sulphide from aqueous solutions using modified nano/micro fibrillated cellulose, Environmental Technology 35(2014)2334-2346.

IV **Hokkanen, S.,** Repo, E., Johansson Westholm , L., Lou, S., Sainio, T., Sillanpää, M., Adsorption of $Ni^{2+,}$ Cd^{2+}, PO_4^{3-} and NO_3^- from aqueous solutions by nanostructured microfibrillated cellulose modified with carbonated hydroxyapatite, Chemical Engineering Journal 252 (2014) 64–74.

V. **Hokkanen, S.,** Repo, E., Lou, S., Sillanpää, M., Removal of Arsenic(V) by Magnetic Nanoparticle Activated Microfibrillated Cellulose, Chemical Engineering Journal 260 (2015) 886–894.

The author's contribution in the publications

I The author carried out or supervised all experiments, analyzed the data, and had the main responsibility for writing the manuscript.

II The author carried out all experiments, analyzed most of the data, and had the main responsibility for writing the manuscript.

III The author planned and supervised most of the experiments, analyzed data and had the main responsibility for writing the manuscript.

IV The author carried out all experiments, analyzed data, and had the main responsibility for writing the manuscript.

V The author carried out all experiments, analyzed data, and had the main responsibility for writing the manuscript.

Contents

NOMENCLATURE

List of symbols

A	Surface area	cm^2
B_{DR}	Dubinin-Radushkevich constant	$mmol^2/J^2$
BE	Elovich model parameter	g/mmol
C	Intraparticle diffusion constant	mmol/g
C_e	Equilibrium concentration	mmol/L
C_i	Initial concentration	mmol/L or mg/L
G	Standard Gibbs free energy	
	J or J/mol	
k_1	Pseudo-first-order rate constant	1/min
k_2	Pseudo-second-order rate constant	g/mmol min
K_d	Distribution ratio	mL/g
K_F	Freundlich affinity constant	
	L/mmol	
K_L	Langmuir affinity constant	
	L/mmol	
K_{RP}	Redlich-Peterson affinity constant	L/mmol
K_S	Sips affinity constant	L/mmol or
M	Molecular mass	g/mol
m	Weight of the adsorbent	g
n	Quantity of material / Number of data points mol /	-
N	Primary hydration number	-
n_F	Freundlich heterogeneity factor	-
n_{RP}	Redlich-Peterson heterogeneity factor	-
n_S	Sips heterogeneity factor	-
q_e	Equilibrium adsorption capacity	mmol/g

q_m	Maximum adsorption capacity	mmol/g
q_t	Adsorption capacity at time t	mmol/g
R^2	Coefficient of determination/correlation coefficient	-
T	Temperature	K or ^oC
V	Volume of the solution	L or cm^3

Abbreviations

AA	Acrylic acid
ACH	Alachlor
AIBN	Azobisisobutyronitrile
AN	Acrylonitrile
APS	Aminopropyltriethoxysilane
ASBC	Ammonium sulfamate-bacterial cellulose
ATPR	Atom transfer radical polymerization
ATR	Atrazine
BCA	Bifunctional chelating agents
BC	Bacterial cellulose
BNC	Bacterial nanocellulose
BPEI	Branched polyethylenimines
CA/OMMT	Cellulose acetate/organo-montmorillonite
CA/ZPNC	Cellulose acetate–zirconium (IV) phosphate nanocomposite
CAN	Ceric ammonium nitrate
CCHBs	Biodegradable collagen/cellulose hydrogel beads
CDI	N,N-carbonyldiimidazole
CE	Cellulose ether
CEL	Cellulose
Cell-PMAN	Cellulose-polymethacrylonitrile
CHA	Carbonated hydroxyapatite
CMC	Carboxy methylated cellulose

CP	Coir pith
CS	Citosan
DEAE-Cell	Diethylaminoethyl cellulose
DMAEMA	Dimethylaminoethyl methacrylate
DMSO	Dimethyl sulfoxide
DP	Degree of polymerization
DS	Disaccharide
DTX	Dithiooxamide
EB	Electron beam
EDAX	Energy dispersive analysis of X-ray
EDTA	Ethylenediaminetetraacetic acid
EDTAD	Ethylenediaminetetraacetic dianhydride
F-CMC	Fibrous carboxymethyl cellulose
Fe(III)-AM-PGMA Cell	Iron(III)- coordinated amino-functionalized poly(glycidyl methacrylate)-grafted cellulose
FESEM	Field Emission Scanning Electron Microscope
FTIR	Fourier transform infrared spectroscopy
GMA	Glycidyl methacrylate
HA	Humic acid
HAP	Hydroxyapatite
HCE	Hydroxyethyl cellulose
HEC	Hydroxyethyl cellulose
HEMC	Hydroxyethyl methyl cellulose
HPLC	High Performance Liquid Chromatograph
HPMC	Hydroxypropyl methyl cellulose
IPN	Interpenetrating networks
KC	Kaolin Clay
LNR	Linuron
LPEI	Linear polyethylenimines
MAAc	Methacrylic acid

MBA	N,N’-methylenebisacrylamide
MCC	Microcrystalline cellulose
MFC	Microfibrillated cellulose
NBC	Nanobanana cellulose
NC	Nanochitosan
NCC	Nanocrystalline cellulose
NFC	Nanofibrilled cellulose
NMBA	*N*’-methylene bisacrylamide
NP	Nanoparticle
PAA	Polyacrylamide
PANI	Polyaniline
PE	Polyethylene
PEGDA	Poly(ethyleneglycol diacrylate)
PEI	Polyethylenimine
PES	Poly(ether-sulfone)
PPy	Polypyrrole
PS1	Pseudo-first-order
PS2	Pseudo-second-order
PVA	Polyvinylalcohol
PVC	Polyvinyl chloride
RIG	Radiation-induced grafting
SA	Sodium alginate
SEM	Scanning electron microscope
TECAM	Triolein embedded-cellulose acetate membrane
TEMPO	2,2,6,6-tetramethylpiperidine-1-oxy radical
TEOS	Tetraethoxysilane
UV	Ultraviolet
XNBC	Xanthate nanobana cellulos

1. INTRODUCTION

Rapid human population and industrialization growth has increased environmental problems such as water, air and land pollution [1-4]. Heavy metals can be considered as some of the most problematic pollutants due to their non-biodegradable nature. In recent years, water pollution by heavy metals has posed one of the most severe environmental problems. For example, cadmium, lead, cobalt, copper, mercury, chromium, nickel, selenium and zinc are carcinogenic to human beings if consumed in high quantities. Because of the high solubility and bioavailability of heavy metals in aquatic environments, they can be absorbed by living organisms. Once they enter the food chain, large concentrations of heavy metals may accumulate in the human body. If the metals are ingested beyond the permitted concentration, they can cause serious health disorders such as developmental retardation, various cancers, kidney damage, autoimmunity, and in extreme cases, even death [2]. Therefore, it is necessary to treat metal contaminated wastewater prior to its discharge into the environment.

Several treatment technologies are available to reduce the pollutants' concentrations in wastewater, including chemical oxidation and reduction, membrane separation, liquid extraction, ion exchange, electrolytic treatment, electroprecipitation, coagulation, flotation, evaporation, hydroxide and sulfide precipitation, crystallization, ultrafiltration, and electrodialysis [1, 3]. These methods differ in their effectiveness and cost. The main advantages and disadvantages of the various physico-chemical methods for water treatment are generally summarized in Table 1.

Table 1. The main advantages and disadvantages of the various physico-chemical methods for water treatment

Treatment method	Advantages	Disadvantages	References
Chemical precipitation	Low capital cost, simple operation	Sludge generation, extra operational cost for sludge disposal	[5]
Membrane filtration	Small space requirement, low pressure, high separation selectivity	Small space requirement, low pressure, high separation selectivity	[5]
Electrodialysis	High separation selectivity	High operational cost due to membrane fouling and energy consumption	[6]
Adsorption	Low-cost, easy operating conditions, high metal binding capacities	Low selectivity, production of waste products	[3]

Adsorption has become one of the alternative treatments for wastewater treatment due to its high removal efficiency without the production of harmful by-products [1-3]. The process of adsorption involves the separation of a substance from one phase accompanied by its accumulation or concentration at the surface of another. The adsorbing phase is the adsorbent, and the material concentrated or adsorbed at the surface of that phase is the adsorbate. Similar to surface tension, adsorption is a consequence of surface energy. In a

bulk material, all the bonding requirements (ionic, covalent or metallic) of the constituent atoms of the material are filled. However, atoms on a (clean) surface experience a bond deficiency, due to the fact that they are not wholly surrounded by other atoms. Thus the bonding is energetically favourable for them. The exact nature of the bonding depends on the details of the species involved, but the adsorbed material is generally classified as exhibiting physisorption or chemisorption. Physisorption or physical adsorption is a type of adsorption in which the adsorbate adheres to the surface only through van der Waals (weak intermolecular) interactions, which are also responsible for the non-ideal behavior of real gases. Chemisorption is a type of adsorption whereby a molecule adheres to a surface through the formation of strong chemical bonding, as opposed to the van der Waals forces [3].

Adsorption phenomena are operative in most natural physical, biological, and chemical systems, and adsorption operations employing solids, such as activated carbon and synthetic resins, are widely used in industrial applications and for the purification of water and wastewater. Adsorption experiments are typically performed in a sequence of three essential steps: (1) the reaction of an adsorbate with an adsorbent contacting a fluid phase of known composition under controlled temperature and applied pressure for a prescribed period of time; (2) the separation of the adsorbent from the fluid phase after reaction; and (3) the quantitation of the chemical substance undergoing adsorption, both in the supernatant fluid phase and in the separated adsorbent slurry that includes any entrained fluid phase [5]. The reaction step can be performed in either a closed system (batch reactor) or an open system (flowthrough reactor), and can proceed over a time period that is either quite short (adsorption kinetics) or very long (adsorption equilibration) as compared to the natural timescale for achieving a steady composition in the reacting fluid phase.

In the 1940's, activated carbon was introduced for the first time as the water industry's main standard adsorbent for the reclamation of municipal and industrial wastewater to a potable water quality [4]. It has been found as a versatile adsorbent due to its high capacity of adsorption because of small particle sizes and active free valences. In spite of this, due to its high cost of production, activated carbon could not be used as the adsorbent for large scale

water treatment. Moreover, the regeneration of activated carbon is difficult due to the use of costly chemicals, high temperatures, and hence, its regeneration is not easily possible on a commercial scale. Commercial activated carbon, which has high surface area and adsorption capacity, is a potential adsorbent for removing heavy metals from wastewater. However, preparing activated carbon is relatively complicated and involves carbonization and activation stages.

The use of low-cost sorbents has been investigated as a replacement for current costly methods of removing heavy metals from solutions. Recently, numerous approaches (e.g. use of microorganisms to detoxify the metals by valence transformation, extracellular chemical precipitation, or volatilization) have been studied for the development of cheaper and more effective technologies, both to decrease the amount of wastewater produced and to improve the quality of the treated effluent. Natural materials or waste products from certain industries with a high capacity for heavy metals can be obtained, employed, and disposed of with little cost [2, 6-8].

Cellulose is argued to be the most abundant polymer in nature and constitutes the main component of plant fibres, giving the plant rigidity. In addition, it is one of the most promising bio-based raw materials due to its abundance, easy availability, and low cost. It is a linear polysaccharide with long chains that consists of β-D-glucopyranose units joined by β-1.4 glycosidic linkages [8-10]. In one repeating unit of cellulose molecule, there are methylol (1) and hydroxyl (2) groups as functional groups. Due to absence of side chains or branching, cellulose chains can exist in an ordered structure. Therefore, cellulose is a semicrystalline polymer, and it contains both crystalline and amorphous phases. Although it is a linear polymer and contains two types of hydroxyl groups, primary hydroxyl in the methylol group ($–CH_2OH$) at C-6 and secondary hydroxyl groups (–OH) at C-3 and C-4, both of which are hydrophilic, it does not dissolve in water and in common solvents due to strong hydrogen bonds between the cellulose chains. As a result, the hydrogen bonds between the cellulose chains and van der Waals forces between the glucose units lead to the formation of crystalline regions in cellulose [9].

Cellulose can be derived from a variety of sources, such as woods, annual plants, microbes, and animals. These include seed fiber (cotton), wood fibers (hardwoods and softwoods), bast fibers (flax, hemp, jute, ramie), grasses (bagasse, bamboo), algae (*Valonica ventricosa*), and bacteria (*Acetobacter xylinum*). In addition to cellulose, these materials also contain hemicelluloses, and a comparably small amount of lignin. Wood and cotton are the raw materials for the commercial production of cellulose. Cellulose in its natural state serves as a structural material within the complex architecture of plant cell walls with variation in its content. In wood, it constitutes about 40–50%; in leaf fibers: sisal fibers (55–73%), in bast fibers: flax 70–75%, hemp 75–80%, jute 60–65%, ramie 70–75%, kenaf 47–57%, in canes: bamboo 40–55%, baggase 33–45%, and in cereal straw: barley 48%, oat 44–53%, rice 43–49%, rye 50–54%, wheat 49–54%. Cotton seed hairs, the purest source, contain 90–99% cellulose [9].

Currently, the isolation, characterization, and search for applications of novel forms of cellulose, variously termed crystallites, nanocrystals, whiskers, nanofibrils, and nanofibers, is generating much activity [11]. Novel methods for their production range from top-down methods involving enzymatic/chemical/physical methodologies for their isolation from wood; from wood pulp, pulp industry wastes, native cellulose in the form of cotton, cellulosic agricultural residues (e.g., sugar beet pulp) or microcrystalline cellulose (MCC) by acid hydrolysis and forest/agricultural residues to the bottom-up production of cellulose nanofibrils from glucose by bacteria.

It is well known that cellulosic-based materials can be obtained and employed as cheap adsorbents, and their performance to remove heavy metal ions can be affected by chemical treatment. In general, chemically modified cellulose materials exhibit higher adsorption capacities than unmodified forms. Numerous chemicals, which include mineral and organic acids, bases, oxidizing agents, and organic compounds have been used for modifications. In the present literature review, an extensive list of celluose and nanocellulose-based adsorbents is presented and their methods of modification discussed. A comparison of

adsorption efficiency between chemically modified and unmodified adsorbents is also reported.

2. CHEMICALLY MODIFIED CELLULOSE BASED ADSORBENTS

An important aim of chemical functionalization is the introduction of stable negative or positive electrostatic charges on the surface of cellulose [12]. This is done to obtain better colloidal dispersion and to tune the surface characteristics of cellulose to improve its compatibility, especially when used in combination with nonpolar or hydrophobic matrices in nanocomposites. Due to the abundance of hydroxyl groups on the surface of cellulose, different chemical modifications have been carried out. These include treatment with base solutions (sodium hydroxide, calcium hydroxide, sodium carbonate), with mineral and organic acid solutions (hydrochloric acid, nitric acid, sulfuric acid, tartaric acid, citric acid, thioglycollic acid), with organic compounds (ethylenediamine, formaldehyde, epichlorohydrin, methanol), and with oxidizing agents (hydrogen peroxide). In these cases, the purpose has been to remove soluble organic compounds, to eliminate the coloration of the aqueous solutions, or to increase efficiency for metal adsorption.

2.1 Monomer-grafted cellulose adsorbents

Grafting of other monomers onto cellulose is an important tool for the modification of cellulose. In this process, side chain grafts are covalently attached to a main chain of a polymer backbone to form a branched copolymer. Depending on the monomer grafted onto cellulose, it gains new properties. Figure 1 shows the functional groups, which are widely used in monomer grafting. The grafting can be performed in a heterogeneous or homogeneous medium [14]. In the grafting performed in a heterogeneous medium, the reaction is carried out in an aqueous solution using a suitable initiator. As an initiator, radiation or chemical initiators, such as ceric ammonium nitrate (CAN), various persulfates, azobisisobutyronitrile (AIBN), or Fenton reagent (Fe(II)–H_2O_2), are mostly used. In the case of a CAN initiator, the grafting should be performed in an acidic medium in order to prevent its

hydrolysis. In homogeneous grafting reactions, either a water-soluble cellulose derivative is used in grafting or cellulose is dissolved in a suitable solvent before grafting. A higher number of grafts per cellulose chain is obtained in homogeneous grafting compared to heterogeneous grafting. The examples where monomer graft cellulose adsorbents have been used are outlined in Table 2.

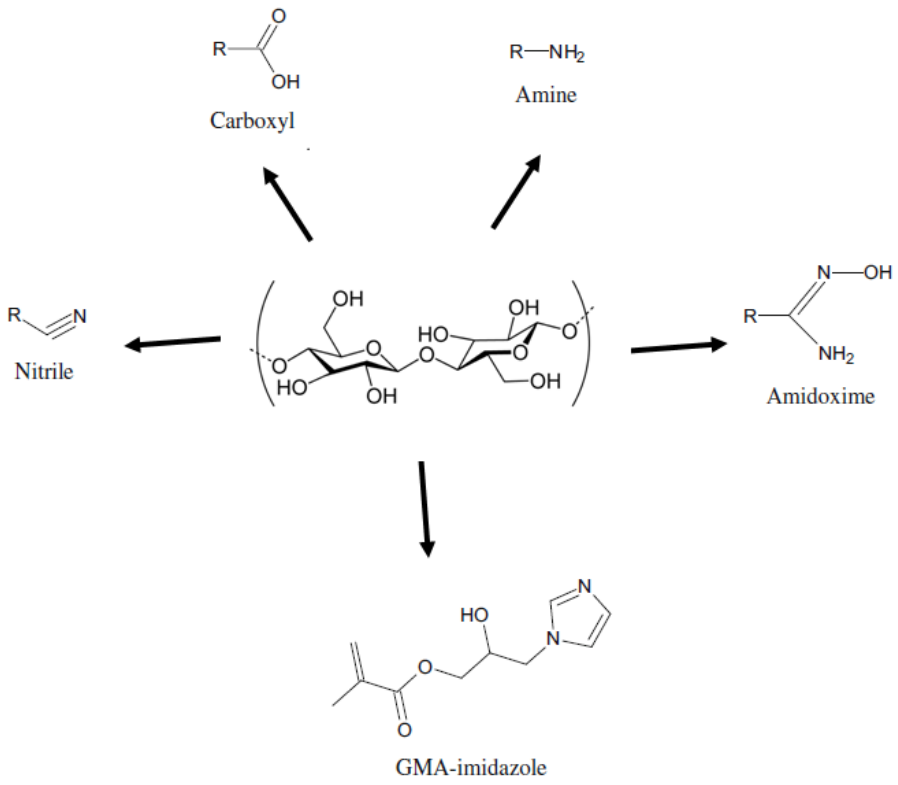

Figure 1. Functional groups on grafted cellulose with good adsorption properties [9].

Table 2. Chemically modified and grafted celluloses and associated adsorption capacities.

Grafted Cellulose Adsorbent	Grafting Agent (Chelating group)	Adsorption capacity (mg/g)	Isotherm model	Reference
Banana stalk	(1) Acrylamide (2) Ethylenediamine (3) Succinic anhydride (Carboxyl)	Hg(II) 138	L	[56]
Banana stalk	Acrylonitrile (Fe^{2+}-H_2O_2)-	Pb(II) 99.8% Cd(II) 90.1% Hg(II) 99.3		[40]
Cellulose	(1) Glycidyl methacrylate (Imidazole)	Cu(II) 68.5 Ni(II) 48.5 Pb(II) 75.8	L	[45-47]
Cellulose	Epichlorohydrin (Carboxyl)	NO_3^- 232.6	L	[49]
Cellulose	Glycidylmethacrylate (GMA) onto titanium dioxide cellulose (TDC) followed by amination and ethylation reactions. (Amino)	Cr(VI) 123.6		[50]
Cellulose	Acrylic acid (AA) (Carboxyl)	Pb(II) 351.9 and Cd(II) 95.2		[51]
Cellulose	-g-acrylicacid (Carboxyl)	Cu(II) 329.0 Ni(II) 299.0 (extracted cellulose) Cu(II) 286.0		[52]
Cellulose	Polyacrylonitrile (Amino)	Ni(II) 270.0 Cd(II) 131.0 Cu(II) 121.0 Cd(II) 154.0		[13]

	Poly(acrylic acid) (Carboxyl)	Cu(II) 148.0 Cd(II) 88.0		
	Unmodifed cellulose	Cu(II) 0.8		
Cellulose	Glycidyl methacrylate (GMA, N,N'-methylenebisacrylamide (MBA) ethylenediamine ferric chloride (Amino, Chloride)	As(V) 78.8		[102]
Cellulose	Acrylonitrile N,N-methylenebisacrylamide (Amino)	Cd(II) 21.4	L	[55]
Cellulose	Polyacrylamid (Amino)	Hg(II) 748.0		[57]
Cellulose bead	(1) Acrylonitrile (2) Sodium hydroxide (Carboxyl)	Cr(III) 73.5 Cu(II) 70.5	L,F	[59]
Cellulose pulp	(1) Acrylic Acid (2) Acrylamide Carboxyl (Amino)	Cu(II) 49.6	F	[35]
Porous cellulose	(1) Glycidyl methacrylate (2) Polyethyleneimine (Amine)	Cu(II) 60.0 Co(II) 20.0 Zn(II) 27.0	L	[48]
Sawdust	Acrylic Acid (Carboxyl)	Cu(II) 104.0 Ni(II) 97.0 Cd(II) 168.0		[61]
Sugarcane bagasse cellulose	Urea (Amino)	Cu(II) 76.0 Hg(II) 280.0	L	[36]
Sunflower stalks	(1) Acrylonitrile (2) Hydroxylamine (Amidoxime)	Cu(II) 39.0	F	[58]
Wood pulp	(1) Acrylonitrile (2)Tetraethyleneamine (Amino)	Cu(II) 30.0		[15]
Wood pulp	(1) Acrylonitrile (2) Hydroxylamine	Cu(II) 51.0		[20]

Cotton cellulose	(Amidoxime) Acrylonitrile methacrylic acid (Amidoxime)	U 95%	[34]

L= Langmuir; F= Freundlich

2.1.1 Photografting

Photochemical initiation is a useful means for introducing various vinyl monomers onto cellulose materials [15-23]. The energy from the incident ultraviolet light is absorbed by a sensitizer, monomer, and/or polymer, or by an electron band structure of the excited cellulose molecule. The chromophore of macromolecule absorbs light, and the excited molecule inter- mediate may dissociate into reactive free radicals and initiate the grafting process. If the absorption of light does not lead to the formation of free radical sites through bond rupture, the process can be promoted by the addition of photosensitizers (e.g., benzoin ethyl ether), dyes such as acrylated azo dye, or aromatic ketones. Photochemical grafting can be achieved with or without a sensitizer [16-19].

The mechanism without a sensitizer involves the generation of free radicals on the cellulose backbone, which react with the monomer free radical to form the graft copolymer. In the mechanism with the sensitizer, the sensitizer forms free radicals, which can undergo diffusion so that they abstract hydrogen atoms from the base polymer, producing radical sites required for grafting to take place [16-19].

In the presence of vinyl monomers, these free radicals initiate the growth of polymer chains from the surface of the activated cellulose and also homopolymerisation of the vinyl monomers [17]. Photografting has many advantages including readily available UV light sources, selective reaction and low photoenergy requirements (relative to other higher energy sources such as γ-ray and electron beam), resulting in the reduced deterioration of polymeric materials.

Novel ion-exchangers were prepared by grafting cotton fabric with (1) glycidyl methacrylate (GMA) followed by aminization, (2) dimethylaminoethyl methacrylate (DMAEMA) followed by quaternization, and (3) acrylic acid (AA) [23]. Grafting was carried out on a pilot scale using a thiocarbonate– H_2O_2 redox system. For direct and reactive dyes, the percentage of exhaustion followed the order of aminized GMA > quaternarized DMAEMA > DMAEMA, whereas for acid dye the percentage of exhaustion followed the order of quaternarized DMAEMA > DMAEMA > aminized GMA. On the other hand, poly(AA) –cotton copolymer was very effective in the removal of basic dye. With respect to heavy metal (Cu(II) and Co(II)) ion removal, the copolymers showed the following order: AA > aminized GMA > quaternarized DMAEMA > DMAEMA, while dichromate removal followed the order of quaternarized DMAEMA > DMAEMA > aminized GMA.

Dye removal capacity varied from 40.6% to 99.0% depending on the ion exchange material. The complete (100%) removal of these selective ions could be achieved by the poly(AA)–cotton copolymer before and after being subjected to the regeneration process. The percentage of Cu(II) and Co(II) ion removal lay between 3 – 6% for quaternized poly(DMAEMA)–cotton copolymer and Poly(DMAEMA)–cotton copolymer, while it went up to 54.0 and 40.0 % for the poly(AA)–cotton copolymer in the case of Cu(II) and Co(II) ions, respectively. Absence of the cationic properties, particularly in quaternized poly(DMAEMA)–cotton copolymer and Poly(DMAEMA)–cotton copolymer, accounted for this observation [23].

Acrylonitrile was grafted to the cellulose surface using the photografting technique; subsequently, the cyano groups were amidoximated by reaction with hydroxylamine [15]. The ability of these cellulose amidoximated samples to adsorb Cu(II) was examined and the maximum adsorption capacity achieved was found to be 51 mg/g.

Later, the resultant AN-grafted celluloses were subjected to reactions with triethylenetetraamine (Trien). The sample containing triethylenetetraamine groups showed an ability to adsorb Cu(II) to the extent of 30 mg/g [20].

2.1.2 High energy radiation grafting

Radiation-induced grafting offers unique advantages for the preparation of functional copolymers for various reasons, including the simplicity and the flexibility of reaction initiation with commercially available ionizing radiation sources (e.g., no additive is needed for the initiation, homogeneous and temperature-independent initiation, polymer formation eventually together with crosslinking and sterilization) [21- 23]. This technique enables imparting tailored modifications ranging from surface to the bulk of backbone polymers, unlike photo and plasma initiation, which impart surface modification only. Commercial radiation sources include electromagnetic radiation such as γ-rays (from Co-60) and particulate radiation such as electron beam (EB).

Radiation-induced grafting can be performed by two main methods: (1) simultaneous irradiation (direct or mutual) and (2) pre-irradiation methods. In the first method, the backbone polymer is irradiated while immersed in a pure monomer or a monomer solution [22, 24]. A side reaction of homopolymerization, which might be initiated, may be suppressed by applying low irradiation dose rates and/or adding inhibitors into the grafting solutions.

The preirradiation method means that the backbone polymer is irradiated in vacuum or inert medium to generate radicals, and subsequently is brought into contact with a monomer under controlled conditions [19, 24, 25]. Alternatively, the backbone polymer may be irradiated in air forming either peroxy or hydroperoxy groups in a procedure called the peroxy (peroxidation) or hydroperoxy (hydroperoxidation) method. The stable peroxy products are then treated with the monomer at an elevated temperature when the peroxides undergo decomposition to radicals, which then initiate grafting.

A radiation-induced grafting technique has been used to impart and improve flame the retardancy, water impermeability, abrasion resistance, and rot resistance of cellulose [26-28]. It is also used to improve anti-crease and thermo-responsive properties, and properties for antibacterial or bio-medical applications, and in fabrication of adsorbents for water purification.

The benefits of a high energy radiation grafting method was demonstrated in sorption studies of Cu(II) ions using some cellulose graft copolymers as adsorbent [29]. A method of synthesis for grafting copolymers had a tremendous effect on sorption behavior. For identical graft levels, graft copolymers synthesized by gamma radiation initiation sorbed three times more ions as compared to the graft copolymers initially synthesized with the persulphate redox system.

Amidoximated polymer surfaces have strong metal-binding abilities for certain ions. After investigating 200 functional groups, it was found that amidoxime showed the best chelating properties [30]. Amidoximated polymers have both N and O atoms available for chelate formation. The chelate formed with $UO_2(OH)^+$ ions in AN grafted, amidoximated, and AN/MAAc grafted and amidoximated polymer surfaces is shown in Figure 2.

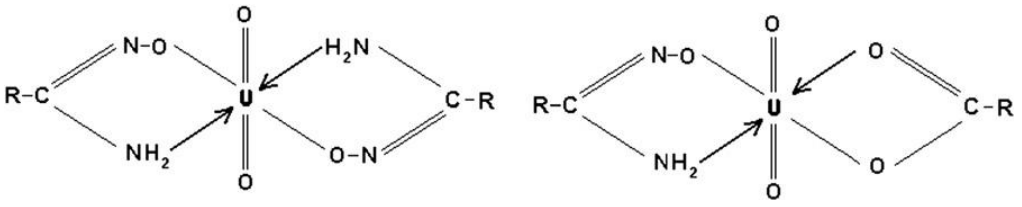

Figure 2. Chelate formation with uranium(VI) ion: AN grafted, amidoximated (left) and AN/MAAc grafted and amidoximated (right) polymer surfaces [15].

A reactive cloth filter was fabricated by grafting acrylonitrile/methacrylic acid onto cotton cloth. A irradiation technique was used for grafting. After subsequent amidoximation, the material was used for the recovery of uranium from radioactive waste obtained from nuclear fuel fabrication laboratories. The cellulose content of the cotton fiber was 85-90 % [32-34]. The effect of the hazardous ions chelation from the radioactive waste on the morphological and chemical structure was studied. The high capacity for uranium uptake with the amidoximated cloth filter was attributed to the complexation and formation of a ring structure with uranyl ion. Authors suggested that the fabricated cloth filter could be used for low-level radioactive waste treatments.

Microwave radiation was utilized to produce bifunctional chelating agents (BCA) from sugarcane bagasse by reacting urea with reactive sites, such as hydroxyl and carboxylic groups, present in bagasse [35], and in the copolymerization of acrylic acid and acrylamide onto cellulose [36, 37]. At optimal adsorption conditions, a maximum adsorption capacity of 49.6 mg/g for Cu(II) with adsorption efficiency up to 99.2% was obtained for the acrylic acid and acrylamide-grafted polymers. This adsorbent resin could be regenerated using 8 wt% $NH_3 \cdot H_2O$, which had a good regeneration effect and after regeneration, the material still possessed over 90.0% adsorption efficiency. BCA adsorbent showed a maximum chelating capacity of 76 mg/g for Cu(II) and 280 mg/g for Hg(II).

Adsorbents produced by radiation-induced graft copolymerization of maize starch/acrylic acid and natural byproduct wood pulp have been used for the removal of metal ions from the investigated wastewater [38]. The absorbed dose is an important parameter in any radiation grafting system because an increase in the absorbed dose enhances the formation of radicals in the system and the percentage conversion of the studied material. The factors affecting the abilities of the prepared materials for removing heavy metal ions and dyes from aqueous solutions were studied. It was found that the maximum metal uptake followed the sequence Fe(III)> Cr(III)> Pb(II)> Cd(II). The adsorption capacity of the investigated metal ions increased with the increasing pH.

2.1.3 Chemical initiation grafting

Chemically initiated grafting can be achieved by free radical or ionic polymerization [39]. The role of the initiator is very important as it determines the path of the grafting in the chemical process. Ceric ammonium nitrate (CAN), various persulfates, azobisisobutyronitrile (AIBN), and Fenton reagent ($Fe(II)–H_2O_2$) are mostly used as initiators [19, 38-40]. In ionic polymerization, often a Lewis base liquid e.g. alkylaluminium (R_3Al) or BF_3 is used as the reactant. Apart from the general free-radical mechanism, grafting in the melt and atom transfer radical polymerization (ATRP) are the techniques used to carry out grafting.

By grafting monomers, new functional groups are introduced on the surface of cellulose. Acrylonitriles are widely used monomers. Cellulosic materials containing various amounts of grafted polyacrylonitrile and poly(acrylic acid) molecules were used to remove Cd(II), Cu(II) [40], Zn(II) and Cr(III) [7] ions from aqueous solutions. It was found that grafting enhanced the metal ion binding capacity of the cellulosic material; the extent of enhancement depended on the type of the metal ion and the level and nature of the incorporated graft polymer [40]. Reuse of the grafted cellulosic materials after one sorption cycle resulted in less than 10.0% reduction in the sorption capacity of the material, suggesting that the grafted cellulosic materials were multiple-use adsorbents. The recovery of the adsorbed metal ions from the grafted cellulosic materials using 2% (v/v) HNO_3 was quantitative. In another study, cellulosic graft copolymers were prepared by reacting bast fibers of the kenaf plant (Hibiscus cannabinus) with acrylonitrile and methacrylonitrile monomers in aqueous media initiated by the ceric ion-toluene redox pair [7]. For Zn(II) and Cr(III) ions, the cellulose-polymethacrylonitrile (Cell-PMAN) graft copolymer was a more effective sorbent than the Cell-PMAN derivative. The amount of ions sorbed decreased with an increase in percentage graft and over the range 38.0% of the graft the amounts of Zn(II) and Cr(III) ions sorbed by Cell-PAN decreased by 44.0% and 56.0%, respectively.

Cellulose powder was grafted with acrylic acid (AA), N,N'-methylene bisacrylamide (NMBA), 2-acrylamido-2-methylpropane sulphonic acid ($AASO_3H$) and a mixture of acrylic acid (AA) and 2-acrylamido-2-methylpropane sulphonic acid ($AASO_3H$) [42]. Ceric ammonium nitrate (CAN) was used as the initiator in all cases. All four grafted cellulose materials were compared in the adsorption of Pb(II), Cu(II) and Cd(II) under competitive conditions. The obtained metal uptakes were 0.27, 0.24 and 0.02 mmol/g for cellulose grafted with p(AA), p(AA-NMBA) and p($AASO_3H$), respectively. Cellulose-g-pAA proved to be the most efficient adsorbent under these conditions with its carboxyl groups responsible for chelating the divalent metal ions.

The amidoxime group has both acidic and basic parts, and for the coordination two lone pairs of electrons are available on the oxygen and one lone pair on each N atom [43, 44]. Amidoxime groups form stable complexes with different metal ions, and consequently,

polymers with amidoxime groups can be successfully used for the preconcentration of trace metals from aqueous solutions. In a study, cyano groups on the poly(acrylonitrile) chains coming off the cellulose backbone polymer were amidoximated by reacting them with hydroxylamine in methanol [44]. An alkali treatment of amidoxime functionalized cellulose further accelerated the sorption of metal ions.

Regenerated cellulose wood pulp was grafted with the vinyl monomer glycidyl methacrylate (GMA) using CAN as initiator and was further functionalized with imidazole to produce a novel adsorbent material, cellulose-g-GMA-imidazole [45-47]. Adsorption capacities of this material for Cu(II), Ni(II) and Pb(II) reached 68.5 mg/g, 48.5 mg/g and 75.8 mg/g, respectively. The cellulose-g-GMA material was found to contain 1.75 mmol/g of epoxy groups. These epoxy groups permitted the introduction of metal binding functionalities to produce the cellulose-g-GMA-imidazole as a final product.

The modification of cellulose for heavy metal adsorption was conducted by the graft polymerization of glycidyl methacrylate utilizing the ceric ammonium nitrate initiator [48]. This was followed by the functionalization of the reactive epoxy groups present in poly(glycidyl methacrylate) with polyethyleneimine to introduce nitrogenous ligands. The produced material showed an adsorption capacity of 60 mg/g for Cu(II), 20 mg/g for Co(II) and 27 mg/g for Zn(II) from wastewater.

A cellulose-grafted epichlorohydrin (Cell-g-E) copolymer was synthesized and its functionalization carried out using polyethylenimine (Cell-g-E/PEI) [49]. A batch adsorption reaction was carried out for the removal/recovery of nitrate ions and maximum adsorption capacity was obtained at pH 4.5. The adsorption process was spontaneous and exothermic. Batch adsorption/desorption studies over six cycles showed the repeatability and regeneration capability of the adsorbent.

Ethylated aminated polyglycidylmethacrylate-grafted-densified cellulose (Et-AMPGDC) was successfully prepared via graft polymerization of Glycidyl methacrylate (GMA) onto titanium dioxide cellulose (TDC) followed by amination and ethylation reactions [50]. The maximum

adsorption capacity of Cr(VI) onto Et-AMPGDC was found to be 123.60 mg/g at 30 °C. The adsorbent was also tested in an electroplating industrial wastewater sample containing Cr(VI) ions, and it was determined that it could be effectively regenerated by treating it with 0.1 M NaOH.

A crosslinked hydroxyethyl cellulose-g-poly(acrylic acid) (HEC-g-pAA) graft copolymer was prepared by grafting acrylic acid (AA) onto hydroxyethyl cellulose (HEC) using the $[Ce(NH_4)_2(NO_3)_6]/HNO_3$ initiator system in the presence of a poly(ethyleneglycol diacrylate) (PEGDA) crosslinking agent [51]. The carboxyl content of the copolymer was determined by the neutralization of –COOH groups with a NaOH solution, and sodium salt of the copolymer (HEC-g-pAANa) was swelled in distilled water in order to determine the equilibrium swelling value of the copolymer. Both dry HEC-g-pAA and swollen HEC-g-pAANa copolymers were used in the removal of heavy metal ions from three different aqueous ion solutions as follows: a binary ion solution with equal molar contents of Pb(II) and Cd(II), a triple ion solution with equal molar contents of Pb(II), Cu(II) and Cd(II), and a triple ion solution with twice the Cu(II) molar content of Pb(II) and Cd(II). Higher removal values for swollen HEC-g-pAANa were observed in comparison to those on the dry polymer. The presence of Cu(II) decreased the adsorption efficiencies of Pb(II) and Cd(II) ions on both types of HEC copolymers. However, with a further increase in Cu(II) content, both dry and swollen copolymers became apparently selective to Cu(II) removal, and Cu(II) removal values exceeded the sum of adsorption values for Pb(II) and Cd(II). Maximum metal ion removal capacities were 370.5 and 95.2 mg/g (Me(II)/g polymer) on swollen HECg-pAANa and dry HEC-g-pAA, respectively.

The cellulose was extracted from the sisal fiber using chemical and mechanical treatments (steam explosion method) and the extracted cellulose and cellulose-g-acrylicacid copolymer were used as an adsorbent for the removal of Cu(II) and Ni(II) [52]. The adsorption capacities for Cu(II) and Ni(II) were evaluated by varying the operational parameters, such as solution pH, agitation time, ion concentration, and adsorbent concentration. The adsorption capacities of extracted cellulose were 286 mg/g for Cu(II) and 270 mg/g for Ni(II) and those of cellulose-g-acrylicacid 329 mg/g for Cu(II) and 299 mg/g for Ni(II).

Different modified cellulose fibers were prepared and their efficiency as adsorbents for the removal of several aromatic organic compounds and three herbicides (i.e. Alachlor (ACH), Linuron (LNR) and Atrazine (ATR)) investigated [53]. The evolution of the adsorption capacity according to the solute structure and the modification sequence was explored. The modification was carried out under heterogeneous conditions using N,N-carbonyldiimidazole (CDI) as an activator and different amino derivatives as the grafting agent. By varying the structure of the amino derivative and the reaction sequence, different organic structures bearing diverse functional groups were generated on the surface. It was shown that the chemical modification of the fibers' surface greatly enhanced the adsorption capacity toward organic compounds dissolved in water. The adsorption capacity evolved from 20 to 50 mmol/g for the virgin fibers to between 400 and 1000 mmol/g for the modified substrates, depending on the solute structure and the modification sequence.

The iron (II)–hydrogen peroxide system (Fenton reagent) is a cheap and easily available redox initiator, and grafting with it can be carried out in low temperatures [54]. Iron(III)-coordinated amino-functionalized poly(glycidyl methacrylate)-grafted cellulose was prepared through the graft copolymerization of glycidyl methacrylate (GMA) onto cellulose (Cell) in the presence of N,N'-methylenebisacrylamide (MBA) as a cross linker using a benzoyl peroxide initiator, followed by treatment with ethylenediamine and ferric chloride in the presence of HCl (Fig.ure 3). The adsorbent was used for the adsorption of arsenic(V) from aqueous solutions. Equilibrium data fitted well with the Sips isotherm model, with a maximum adsorption capacity of 78.8 mg/g at 30°C. Furthermore, over 98.0% desorption of As(V) was achieved with 0.1 M NaCl solution.

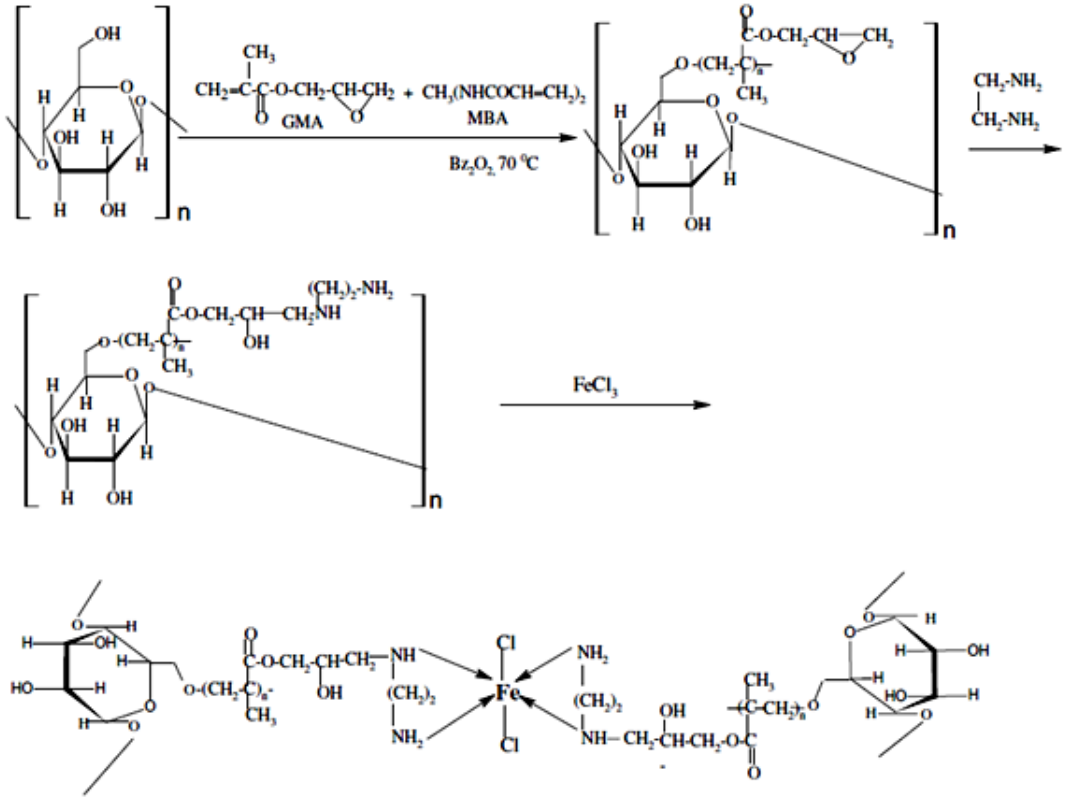

Figure 3. Preparation of Fe(III)-AM-PGMA Cell [54]

Isolated cellulose from corn stalks was graft copolymerized using acrylonitrile as monomer, N,N-methylenebisacrylamide as cross linker and $KMnO_4$ as an initiator [55]. The results showed that AGCS-cell had better adsorption potential for cadmium ion than unmodified cellulose because of the addition of functional groups (CN and OH groups) and the lower crystallinity.

Banana stalks are largely composed of cellulose, which enables its use as adsorbent for heavy metals after chemical initiation grafting. The adsorbent (PGBS-COOH), having a carboxylate functional group at its chain end, was synthesized by (Fe^{2+}-H_2O_2)-initiated graft copolymerization of acrylamide onto banana stalks, followed by succinic anhydride functionalization [40]. Synthetic wastewater samples were treated with the adsorbent to

demonstrate its efficiency in removing Pb(II) and Cd(II) ions from industrial wastewaters. The maximum uptake of Pb(II) and Cd(II) from their aqueous solutions was found to be 99.8 and 90.1%, respectively, at an initial concentration of 25 mg/L and at pH 6.5. The adsorbed Pb(II) and Cd(II) ions were effectively desorbed by 0.2 M HCl and PGBS-COOH was reused successfully after regeneration. The study examined the effectiveness of a new adsorbent prepared from banana stalks, one of the abundantly available lignocellulosic agrowastes, in removing Pb(II) and Cd(II) ions from aqueous solutions. The same adsorbent was used to remove Hg(II) from a water solution [56].The maximum adsorption capacity of the adsorbent for Hg(II) was found to be 138.0 mg/g .

Polyacrylamide grafted onto cellulose has been demonstrated to be a very efficient and selective sorbent for the removal of mercuric ions from aqueous solutions [57]. The mercury-uptake capacity of the graft polymer was as high as 710 mg/g and sorption was also reasonably fast. The Hg(II) sorption was selective and no interferences were observed in the presence of Ni(II), Co(II), Cd(II), Fe(III), Zn(II) ions in 0.1 M concentrations at pH 6. The regeneration of the loaded polymer could be achieved using hot acetic acid without losing its original activity.

A sunflower stalk graft cellulose copolymer was prepared by reacting ground sunflower stalks (SFS) with acrylonitrile (AN) in an aqueous solution initiated by a $KMnO_4$-citric acid (CA) system [58]. It was shown that the grafting parameters, such as the concentration of $KMnO_4$, AN, and CA, had a significant effect on graft copolymerization. The amidoximation of the grafted stalks was performed by the reaction between grafted SFS with hydroxylamine hydrochloride in an alkaline medium to obtain amidoximated sunflower stalks (ASFS). The maximum uptake capacity of this adsorbent for Cu(II) was found to be 39.0 mg/g.

The removal and recovery of Cr(III) and Cu(II) from aqueous solutions using a spheroidal cellulose adsorbent containing the carboxyl anionic group was investigated [59, 60]. A saponification reaction using sodium hydroxide was subsequently carried out on this material. The saponification converts the same grafted poly(acrylonitrile) with its cyano groups as the main group to both amide ($–CONH_2$) and carboxylate (–COONa) groups. The

adsorption of Cr(III) on the amide functionalized compound reached 73.5 mg/g whereas the Cu(II) uptake on the carboxylate functionalized compound was 70.5 mg/g. A 1.2 mol/L HCl aqueous solution was finally chosen to recover the Cr(III) ions using column operation. The recovery percentage for Cu(II) was approximately 85.2%. The maximum percentage of recovery was approximately 100% when a 2.4 mol/L HCl solution was used. In addition, only 7.2% of the adsorption capacity was lost after 30 replications of adsorption and desorption.

Polyacrylic with $KMnO_4$ as the initiator was used for grafting chains onto sawdust to obtain an inexpensive adsorbent [61]. The material had a high adsorption capacity for Cu(II) 104.0 mg/g, Ni(II) 97.0 mg/g and Cd(II) 168.0 mg/g.

The monomer glycidyl methacrylate was also chosen as a reactive monomer for grafting due to the subsequent availability of its reactive epoxy groups for further functionalization [57]. The epoxy groups are highly reactive to amines, alcohols, phenols, carboxylic acids, carboxylic anhydrides, and Lewis acids and their complexes [62]. A sorbitol-containing resinous polymer has been prepared starting from crosslinked polystyrene divinylbenzene (DVB) resin beads by the following series of reactions: (1) chlorosulfonation, (2) sulfonamidation with N-propylamine, (3) condensation of sulfonamide with epichlorohydrin, and (4) modification with sorbitol. The resulting sorbitol-modified polymer has been demonstrated to be a selective, efficient and regenerable sorbent for the removal of boron in ppm levels [57].

2.2 Adsorbents produced by the direct modification of cellulose

Unmodified cellulose has a low heavy metal adsorption capacity as well as variable physical stability. However, a chemical modification of cellulose can be executed to achieve adequate structural durability and an efficient adsorption capacity for heavy metal ions and other water pollutants [43]. The properties of cellulose, such as its hydrophilic or hydrophobic character, elasticity, water sorbency, adsorptive or ion exchange capability, resistance to microbiological attack and thermal resistance, are usually modified by chemical treatments.

The β-D glucopyranose on the cellulose chain contains one primary hydroxyl group and two secondary hydroxyl groups. Functional groups may be attached to these hydroxyl groups through a variety of reactions. The main routes of direct cellulose modification in the preparation of adsorbent materials are esterification, etherification, halogenations, oxidation and alkali treatment.

2.2.1 Esterification

Cellulose esters are cellulose derivatives which result from the esterification of free hydroxyl groups of the cellulose with one or more acids, whereby cellulose reacts as a trivalent polymeric alcohol. Cellulose esters are commonly derived from natural cellulose by reacting with organic acids, anhydrides, or acid chlorides. Table 3 presents the esterification methods of cellulose leading to adsorbent materials for water treatment.

Table 3. Cellulose modification using esterification methods and associated adsorption capacities.

Adsorbent	Modifying chemicals (Chelating group)	Maximum adsorption (mg/g)	Isotherm	Reference
Cellulose	Succinic anhydride a)(Carboxyl) b)(Carboxylate)	Cu(II) 30.4 Cd(II) 86 Pb(II)205.9		[65]
Cellulose	Succinic anhydride+Triethylenetetramine (Carboxyl, Amine)	Cr (VI) 43.1		[63]
Cellulose	Triethylenetetramine (Amine)	Cu(II) 56.8 and 69.4 Cd(II) 68.0 and 87.0 Pb(II) 147.1 and 192.3		[64]
Hardwood sawdust	Unmodified Oak Unmodified Black locus Formaldehyde mod. Oak(Carboxyl) Formaldehyde mod Black locus(Carboxyl)	Cu(II) 9.3 , Zn(II) 7.1 Cu(II) 4.4 , Zn(II) 0.08 Cu(II) 3.1 / Zn(II) 6.1 Cu(II) 2.9 Zn(II) 5.3	L	[108]
Cellulose bagasse	HCl, HNO_3, NaOH tartaric, citric and oxalic acids (Carboxyl)	Raw bagasse: Zn(II) 8.0 , Cd(II) 14.0 , Pb(II) 36.0 This was improved about 27–62% upon modification with HNO_3 and NaOH. Treatments with citric, oxalic and tartaric acid did not have a significant effect in adsorption capacity		[87]

Cellulose	Maletic anhydride (Carboxyl)	Methyl violet dye 106.4 (Unfunctionalized 43.7)		[71]
Wood pulp	Succinic anhydride (Carboxyl)	Cd(II) 169		[61]
Cellulose	Succinic anhydride (Carboxyl)	Co(II) 144.9 Ni(II) 144.4		[66]
Cellulose	Maleic anhydride (Carboxyl)	Hg(II) 172.5		[71]
Cellulose	Succinic anhydride (Carboxyl)	Cd(II) 185.2 and 178.6		[68]
Bagasse fibers	Succinic anhydride (Carboxyl)	Cu(II) 95.3 Ni(II) 105.7 Cr(II) 130.0 Fe(II) 346.0		[66]
Cellulose **Sugarcane bagasse**	Ethylenediaminetetraaceti c dianhydride (EDTAD) (Carboxyl, Amine)	Ca (II)15.6 - 54.1 Mg(II) 13.5 -42.6		[74]
Apple pomace	Succinic anhydride+Triethylenetetr amine (Carboxyl, Amine)	Cd(II) 4.5 and 91.8	L and F	[70]
Cotton cellulose	Sulfuric acid	Au(III) 6.		[90]
Sugarcane bagasses	Succinic anhydride (Carboxyl) EDTA dianhydride (Amine)	Etherdiamine 869.6 and 1203.5		[73]
Cellulose (junpier)	Sulfuric acid (Carboxyl)	Cd(II) 16.6		[89]
Pineapple peel fibers with	Succinic anhydride (Carboxyl)	Cu(II) 27.7 Cd(II) 34.2 Pb(II) 70.3		[67]
Wood pulp	Citric acid	Cu(II) 24.0 Pb(II) 83.0	L	[72]

	(Carboxyl)		
	Citric acid	Cu(II) 9.5	[88]
Sugarcane bagasse	(Carboxyl)	Cu(II) 8.9	
Peanut shells		Cu(II) 36.8	
Macadamia nut hulls		Cu(II) 20.3	
Rice hulls		Cu(II) 32.4	
Cottonseed hulls		Cu(II) 11.4	
Corn cob		Cu(II) 34.9	
Soybean hulls		Cu(II) 17.2	
Almond shells		Cu(II) 42.6	
Almond hulls		Cu(II)25.4	
Pecan shells		Cu(II) 25.4	
English walnut shells		Cu(II) 32.4	
Black walnut shells			
Corncobs	Sulfuric acid (Carboxyl)	Co(II) 31.5	[83]
Rice husk	Hydrochloric acid Epichlorohydrin (EDTA) (Carboxyl)	Cd(II) 11.1	[75]
Sugarbeet pulp	Hydrochloric acid (Carboxyl)	Cu(II) 9.5 Zn(II) 11.8	[80]
Rice husk	Tartaric acid (Carboxyl)	Cu(II) 31.9 Pb(II) 20.5	[81]
Wheat bran	Sulfuric acid (Carboxyl)	Cu(II) 51.5	[84]
Wheat bran	Sulfuric acid (Carboxyl)	Cd(II) 101.0	[85]

Corncorb	Sodium iodate Nitric acid Citric acid (Carboxyl)	Cd(II) 19.0 (Sodium iodate) 19.3 (Nitric acid) 55.2 (Citric acid)	[78]
Carrot residues	Hydrochloric acid (Carboxyl)	Cr(III) 45.1 Cu(II) 32.7 Zn(II) 29.6	[79]
Sawdust	Sulfuric acid (Carboxyl)	Cu(II) 92% (untreated sawdust 47%)	[82]

The treatments of cellulose with cyclic anhydrides, such as succinic anhydride, are widely studied methods to add carboxyl groups to the surface of cellulose [62-70]. EDTA dianhydride, citric acid anhydride and maleic anhydride were also used for esterification [69-71]. The reaction of succinic anhydride on cellulose is presented in Figure 4. The mercerization of cellulose before a succinylation reaction is commonly used due to the fact that the mercerization of cellulose increases the separation of polysaccharide chains and reduces the packing efficiency, thereby facilitating the penetration of succinic anhydride [64]. It was observed that the modified mercerized cellulose showed a higher adsorption capacity for Cu(II), Cd(II) and Pb(II) ions than modified non-mercerized cellulose. Modified mercerized cellulose in relation to modified non-mercerized cellulose presented an increase in the mass gain and concentration of carboxylic functions of 68.9% and 2.8 mmol/g, respectively, and an increase in the adsorption capacity for Cu(II) (30.4 mg/g), Cd(II) (86 mg/g) and Pb(II) (205.9 mg/g); it demonstrated that metal ion adsorption efficiency was proportional to the number of carboxylic acids introduced. Chemically modified cellulose (EMC) and sugarcane bagasse (EMMB) were also prepared from mercerized cellulose and twice-mercerized sugarcane bagasse using ethylenediaminetetraacetic dianhydride (EDTAD) as the modifying agent [74]. Sodium hydroxide, sodium carbonate and epichlorohydrin-treated cellulose material had enhanced adsorption capacity for cadmium [75].

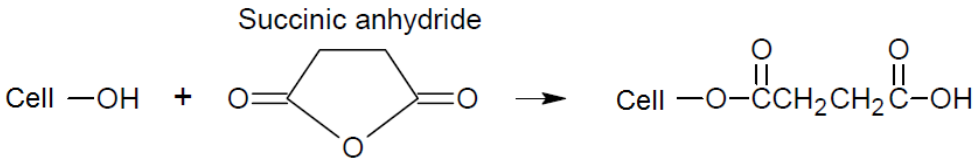

Figure 4. Modification reactions between wood cellulose and succinic anhydride [63].

Further processing after esterification would give better properties for binding metals from water solutions. The esterified cellulose is ommonly treated with a saturated sodium bicarbonate solution because carboxylate functions have better chelating capacities than the carboxylic group [63, 66, 68, 70, 74]. The other pre-tretatment method was reacting carboxylic groups with triethylenetetramine to introduce amine functionality to carboxylated material [64].

The new cellulose-based ion exchanger polysaccharide was prepared by adding cellulose directly to molten succinic anhydride in a quasi-solvent-free procedure [66]. This biopolymer/anhydride ion exchanger was able to exchange cations from an aqueous solution through a batchwise methodology to obtain 144.9 mg/g and 144.4 mg/g adsorption capacities for Co(II) and Ni(II) cations, respectively.

The sawdusts of oak and black locust hardwood were found to possess good adsorption capacities for heavy metal ions [76]. The leaching of coloured organic matter during the adsorption could be prevented by the following adsorbent pre-treatments: with formaldehyde in acidic medium, with sodium hydroxide solution after formaldehyde treatment, or with sodium hydroxide only. The adsorption of Zn(II) and Cu(II) was studied. The studies indicated that the leaching of coloured matter from modified hardwood sawdust was less than that from unmodified hardwood sawdust, namely between 70 and 94%, depending on the wood species and the method of modification. At the same time, the adsorption capacities of modified adsorbents were higher than those of unmodified adsorbents when sodium hydroxide was applied for modification. When formaldehyde was applied, the adsorption capacities of adsorbents remained unchanged. Only the application of sodium hydroxide was recommended for modification of hardwood sawdust.

The adsorbent for the removal of Pb(II) and Hg(II) was prepared through two common reactions, which included the esterification of starch with excess maleic anhydride in the presence of pyridine, and the cross-linking reaction of the obtained macromonomer with acrylic acid by using potassium persulphate as the initiator [77]. It was found that the adsorption capacities of the adsorbent for lead and mercury ions were 123.2 and 131.2 mg/g, respectively. In addition, the adsorbent was able to remove *ca.* 51–90% of Pb(II) and Hg(II) ions that existed in the decoctions of four medicinal herbs.

Meanwhile, most acids used for the treatment of cellulosic plant wastes, such as sulfuric acid, hydrochloric acid and nitric acid, have been in a dilute form [78-86]. When rice husk is treated with hydrochloric acid, adsorption sites on the surface of the rice husk are protonated, leaving the heavy metal ions in the aqueous phase rather than being adsorbed on the adsorbent surface. The adsorption study of copper was carried out by modifying rice husks using various kinds of carboxylic acids (citric acid, salicylic acid, tartaric acid, oxalic acid, mandelic acid, malic and nitrilotriacetic acid) and it was reported that the highest adsorption capacity was achieved by tartaric acid modified rice husk [81]. Esterified tartaric acid modified rice husk, however, significantly reduced the uptake of Cu and Pb. The maximum adsorption capacities for Pb and Cu were reported as 108.0 and 29.0 mg/g, respectively. The effect of sulfuric acid treatment on poplar sawdust was also studied [82]. Sulfuric acid poplar sawdust removed Cu(II) well (92.4%), while untreated sawdust only removed 47%.

It was reported that when corncobs were treated with sulfuric acid while heating at 150 ^{o}C, the functional groups present in the adsorbent were mainly oxygen-containing groups such as –OH, –COOH and –COO [83]. The maximum adsorption capacity for copper was 31.5 mg/g. Adsorption was more favoured at a higher pH value (4.5) due to the low competing effect of protons for the adsorption sites. The effect of interfering ions, such as Zn(II), Pb(II) and Ca(II), was also studied. It was noticed that copper removal efficiency was reduced by 53%, 27% and 19% in the presence of Pb(II), Ca(II) and Zn(II), respectively. A regeneration

study indicated that sulfuric-acid-treated corncobs could be regenerated by acidified hydrogen peroxide solution and as much as 90% of the copper was recovered.

HCl, HNO_3, NaOH, tartaric, citric and oxalic acids were used to modify agave bagasse and the obtained materials were tested for the removal of Cd(II), Pb(II) and Zn(II) ions from water [87]. Raw bagasse had an adsorption capacity of approximately 8.0, 14.0 and 36.0 mg/g for zinc, cadmium and lead, respectively and this was improved by 27–62% upon modification with HNO_3 and NaOH. Treatments with citric, oxalic and tartaric acid did not have any significant effect on the adsorption capacities. Raw agave bagasse had appreciable adsorption capacity for metal cations and it could be partly regenerated (45%), since the biosorption mechanism involved ion exchange and complexation.

The interesting finding in which a linear relationship between total negative charge and amount of copper ions adsorbed was observed for 12 types of cellulosic agricultural byproducts (sugarcane bagasse, peanut shells, macadamia nut hulls, rice hulls, cottonseed hulls, corn cob, soybean hulls, almond shells, almond hulls, pecan shells, English walnut shells and black walnut shells) after modification with citric acid, was reported [88]. In this comprehensive study, it was found that after washing with a base (NaOH) and modified with citric acid, the total negative charge of all 12 types of agricultural by-products increased significantly. Among the 12 adsorbents, soybean hulls (a low density material) showed the highest copper uptake and had a high total negative charge value, which can be explained by the increase in carboxyl groups after thermochemical reaction with citric acid. On the other hand, nutshells (high density materials) displayed low total negative charge values, indicating a low number of carboxyl groups. Due to the high bulk density, the lignin in nutshells might have completely blocked or only allowed little penetration of citric acid to reactive sites, hence a lower copper ion uptake was observed.

Cellulose sulfates are the most frequently investigated of all other inorganic cellulose esters. Sulfonated juniper was found to have at least twice the sorption capacity for cadmium removal from water compared to that of untreated juniper [89]. Cotton cellulose was

chemically modified with concentrated sulfuric acid to prepare a novel kind of adsorption gel for gold [90]. The maximum adsorption capacity for Au(III) was evaluated as 6.21 mmol/g.

In addition to metal ions, the adsorption of etherdiamine [73] methyl violet dye [91, 92] and crystal violet [93] dyes were also studied using esterificated cellulose material. Furthermore, a comparative study has been carried out for the removal of methyl violet dye using unfunctionalized and functionalized cellulose [91]. The functionalization was achieved through the esterification of cellulose with maletic andhydride (furan-2,5-dione). Functionalized cellulose (106.4 mg/g) showed a higher dye removal capability than unfunctionalized cellulose (43.7 mg/g) [91].

Cellulose acetate is a semi-synthetic polymer obtained through the esterification of acetic acid with cellulose. The material is used in a broad range of commercial applications including the general areas of films, fibers, plastics and coatings. The ability of cellulose acetate for composite material in water treatment applications has also been studied. More details about this area are presented in section 2.3.

2.2.2 Halogenation

Halogenation is a chemical reaction that involves the reaction of a compound with a halogen and results in the halogen being added to the compound [92]. Various methods are suitable to prepare halogenated cellulose derivatives (Table 4). Chlorine is the most effective halogen with polymers, and different chemicals are used as precursors, with the objective of transferring the halogen element to the cellulosic polymeric chain.

Table 4. Halogenation of cellulose and associated adsorption capacities.

Adsorbent	Modifying chemicals (Chelating group)	Maximum adsorption capacity at optimum conditions (mg/g)	Reference
Cellulose powder	Trimethylammonium chloride (Carbonyl, chloride)	Cr(VI) 71.8	[92]
Cellulose	Thionyl chloride modified. (Chloride)	Cu(II) 6.4 Co(II) 5.5 Ni(II) 4.3 Zn(II) 4.6	[94]
Cellulose	Thionyl chloride (Carboxyl)	Cu(II) 36.0 Pb(II) 105.0 Ni(II) 9.3	[93]
	Cysteine (Amino + Carboxyl)	Cu(II) 22.0 Pb(II) 28.0 Ni(II) 8.0	
	a-Thioglycerol (Hydroxyl)	Cu(II) 2.0 Pb(II) 6.0 Ni(II) 10.0	
	3-Mercaptopropionic acid (Carboxyl)	Cu(II) 24.0 Pb(II) 20.0 Ni(II) 1.0	

A novel method for the immobilization of D-glucose (D-Glu) and trimethylammonium chloride onto the surface of cellulose powder was studied [92]. Cellulose powder was grafted with a vinyl monomer (GMA), using CAN as an initiator, and further derived with quaternary ammonium groups to build the D-GluN+-type cellulose absorbent (Cell-g-GMA-D-GluN+) (Figure 5). Epoxy cellulose was found to contain 5.48 mmol/g of epoxy groups. The maximum adsorption capacity of chromium (VI) reached a value of 71.79 mg/g. Adsorption–desorption tests of the D-GluN+-type cellulose derivatives showed a good regenerability of the adsorbent so that the adsorbent could be reused at least six times.

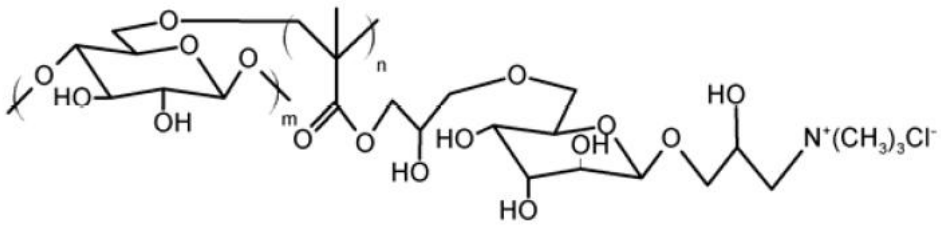

Figure 5. Structure of D-GluN+-type cellulose derivatives [92]

The adsorption properties of 6-(2'-aminomethylpyridine)-6-deoxycellulose produced by reacting 2-aminomethylpyridine with thionyl-chloride-modified cellulose has also been studied [93]. The modified cellulose exhibited maximum sorption capacities of 6.4, 5.5, 4.3 and 4.6 mg/g for Cu(II), Co(II), Ni(II) and Zn(II), respectively.

Furthermore, the adsorption of heavy metals was studied using 6-deoxy-6-mercaptocellulose and its S-substituted derivatives from 6-bromo-6-deoxycellulose [94]. The reactivity of cellulose and bromine compared to cellulose and chlorine was higher. Carboxyl, amino, isothiouronium, mercapto, and additional hydroxyl groups were introduced to the cellulose and their adsorption behavior for metal ions was examined. The derivatives containing carboxyl groups due to the reaction with 2-mercaptobutanedioic acid had adsorption capacities of 36 mg/g, 9 mg/g and 104 mg/g for Cu(II), Ni(II) and Pb(II), respectively. The derivatives with amino and carboxyl groups, due to the reaction with cysteine, had adsorption capacities of 22.0, 8.0 and 28.0 mg/g for Cu(II), Ni(II) and Pb(II), respectively. In another case, by reacting cellulose powder with thionyl chloride in dimethylformamide solvent, chlorodeoxycellulose was synthesized. After that, it was functionalized with ethylenediamine, thiourea, thiosemicarbazide, thioacetamide, hydroxylamine, and hydrazine [95]. These derivatives were found to be able to remove Hg(II) ions to an extent greater than 99.0% from a 10 ppm aqueous solution of mercuric chloride.

2.2.3. Oxidation

Cellulose derivatives can also be prepared by oxidation and the subsequent functionalization of the oxidized cellulose (Table 5). The behavior of the ion exchange of carboxylate groups in the 2,2,6,6-tetramethylpiperidine-1-oxy radical (TEMPO)-oxidized fibrous cellulose prepared from cotton linters was compared with that of fibrous carboxymethyl cellulose (F-CMC) with almost the same carboxylate content as that of the TEMPO-oxidized cellulose [96]. The native cellulose was treated by catalytic oxidation with 2,2,6,6-tetramethylpiperidine-1-oxy radical (TEMPO)/NaBr/NaClO under aqueous conditions. The adsorption selectivity of metal ions on the TEMPO-oxidized cellulose was also studied using aqueous solutions containing multiple metal salts and the following selectivity order was obtained: Pb(II)>La(III)>Al(III)>Cu(II)>Ba(II)>Ni(II)> Co(II)>Cd(II), Sr(II), Mn(II), Ca(II)>Mg(II).

Dialdehyde cellulose was prepared by the periodate oxidation of cellulose [97]. This dialdehyde cellulose was further oxidized using mildly acidified sodium chlorite. The adsorption capabilities for Ni(II) and Cu(II) were 184.0 mg/g and 236.0 mg/g, respectively. Cellulose-hydroxamic acid derivatives were synthesized from dialdehyde cellulose obtained by the previous periodate oxidation method and their heavy metal adsorption capacities were investigated. These materials were capable of adsorbing 246 mg/g of Cu(II) from an aqueous solution [98]. Hydrogen-peroxide-bleached magnesium bisulfate softwood pulp was used as the raw material for an acid process of N_2O_4-mediated oxidation. Oxidized cellulose was effectively used in the form of filter sheets to remove some metal ions from water and from aqueous solutions. Furthermore, oxycellulose was applied in an ion-exchange column and in a batch process [99].

Table 5. Cellulose modification using oxidation methods and associated adsorption capacities.

Adsorbent	Modifying chemicals (Chelating group)	Maximum adsorption capacity at optimum conditions (mg/g)	Reference
Cellulose powder	Sodium metaperiodate (Carboxyl)	Ni(II) 184.0 Cu(II) 236.0	[97]
Cellulose powder	Sodium metaperiodate Hydroxamic acid (Amino)	Cu(II) 246	[98]
Softwood pulp	Nitrogen tetroxide	Cd(II)30.9 Ni(II) 9.6 Zn(II) 16.9	[99]

2.2.4. Etherification

Cellulose ethers (CEs) are synthesized from cellulose through the process of etherification, during which C-2, C-3, and C-6 OH groups of an anhydroglucose unit in cellulose molecule are at least partially substituted by other groups [100]. Hydroxyethyl cellulose and its hydrophobically modified derivatives are widely used in many industrial applications such as pharmaceuticals, cosmetics, textiles, and paint and mineral industries. The etherification methods of cellulose leading to adsorbent materials for water treatment are presentnted in Table 6. The reaction of cellulose with ethylene oxide or other epoxides yielded, for example, HPMC (hydroxypropyl methyl cellulose), HEMC (hydroxyethyl methyl cellulose) and HEC (hydroxyethyl cellulose). A typical hydroxypropylation reaction was carried out in two steps – alkalization and etherification of cellulose reacted with epichlorohydrin, yielding reactive epoxy groups for further functionalization with polyethyleneimine as a chelating agent. The adsorption properties of these cellulose ethers have been studied for some heavy metal ions [101]. The prepared adsorbent had metal uptake affinities of 2.5 mg/g, 38.0 mg/g

and 12.0 mg/g for Co(II), Cu(II) and Zn(II), respectively. The coconut coir pith (CP) adsorbent carrying a dimethylaminohydroxypropyl weak base functional group was synthesized by reacting CP with epichlorohydrin and dimethylamine followed by a treatment of hydrochloric acid. Batch adsorption–desorption studies illustrated that a CP– anion exchanger could be used to remove As(V) from ground water and other industrial effluents. Maximum removal was found to be 99.2 % (12.5 mg/g) [102]. The spent adsorbent could be regenerated by 0.1 N HCl.

Cellulose hydroxyls can also be made to add across-activated double bonds as in the formation of cyanoethyl cellulose from a reaction with acrylonitrile [103, 104]. A typical cellulose etherification involving Michael addition of an activated C=C bond of acrylonitrile (AN) to a partially anionized cellulosic hydroxyl in an aqueous alkaline medium is represented below (Figure 6).

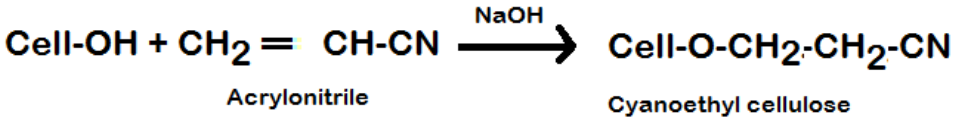

Figure 6. Formation of cyanoethyl cellulose from reaction with acrylonitrile [105]

The cellulose of sawdust [103] and corn stalk [104] were chemically modified by reacting acrylonitrile with the cellulose through an etherification reaction in order to add cyano groups to the cellulose structure. The maximum uptake of Cd(II) by modified corn stalk cellulose was 12.7 mg/g and by unmodified corn stalk cellulose 3.4 mg/g. The cyano groups of sawdust cellulose were then amidoximated by reaction with hydroxylamine. This amidoximated sawdust had high adsorption capacities for Cu(II) and Ni(II) (246 mg/g and 188.0 mg/g, respectively).

Agricultural wastes, for example, rice straw, sugarcane bagasse, saw dust, cotton stables, orange mesocarp, weeds, and Eichoria crassipes have been used as a base material for the production of carboxy methylated cellulose (CMC), differing in their disaccharides (DS) and

properties using a different set of reaction conditions depending upon the degree of polymerization (DP) and composition of the cellulosic material [105]. Carboxymethylated and non-carboxymethylated material sugarcane bagasse fibres were doped with Fe(II) ions by dipping them in aqueous iron chloride solutions of different concentrations [106]. This material was used to remove phosphate from water. When about 4% of iron is adsorbed on the fibres, 97.0% of phosphate is captured on the carboxymethylated material and 94.0% on the non-carboxymethylated material material. The presence of Fe^{2+} ions on the surface fibres increases the phosphate adsorption capacity by about 45.0% and the maximum adsorption capacity was 152 mg/g for phosphate.

Table 6. Cellulose modification using etherification methods and associated adsorption capacities.

Adsorbent	Modifying chemicals (Chelating group)	Maximum adsorption capacity at optimum conditions (mg/g)	Isotherm	Reference
Cellulose	(1) Sodium methylate (2) Epichlorohydrin (3) Polyethyleneimine (Amino)	Hg(II) 288.0	L	[101]
Coconut coir pith (CP)	Epichlorohydrin, dimethylamine (mino)	As(V) 12.5		[102]
Cellulose powder	Acrylonitrile Hydroxylamine (Amidoxime)	Cu(II) 238.8 Cr(III) 202.8		[104]
Corn stalk	Acrylonitrile Hydroxylamine (Amidoxime)	Cd(II) 12.7 (unmodified 3.4)		[55]
Cellulose	Cyclohexane/ethanol + Fe(II) treatment	PO_4^{3-} 152.0		[106]

2.2.4 Alkaline treatment

Alkaline treatment induces changes on the wood's surface by increasing its surface area, average pore volume, and pore diameter. Sodium hydroxide is a good reagent for saponification or the conversion of an ester group to carboxylate and alcohol. Associated adsorption capacities of NaOH treated cellulose for uptake metal ions from aquous solutions are listed in Table 7. A detailed analysis on the ideal concentration of NaOH for modifying juniper fibre for the adsorption of cadmium ions was carried out by Min et al. [107]. Based on the FTIR analysis, it was found that as the concentration of NaOH increased (from 0 to 1.0 M), the amount of carboxylates also increased. After a base treatment, the maximum adsorption capacity of cadmium increased by approximately three times (from 9.2 to 29.5 mg/g) compared to untreated juniper fibre despite a decrease in specific surface area for the treated adsorbent.

Two kinds of sawdust, poplar and fir wood, were treated with NaOH (fibre-swelling agent) and Na_2CO_3 solutions, and the adsorption capacities were compared with the untreated sawdusts [108]. For unmodified sawdust, both types of woods showed higher uptakes of Cu(II) ions than Zn(II) ions, and adsorption followed the Langmuir isotherm model. Equivalent amounts of adsorption capacities were recorded by both types of sawdust for Zn(II) and Cu(II) ions, although these two adsorbents have different anatomical structures and chemical compositions. After treating with NaOH, a marked increase in adsorption capacity was observed for both heavy metal ions, and especially for Zn(II) ions. The increase was 2.5-fold for Cu(II) and 15-fold for Zn(II).

A comparative study on the adsorption efficiency of untreated and NaOH-treated sawdust of cedrus deodar wood was conducted by Memon et al. [109]. Cadmium removal was more favored by NaOH-treated sawdust as the value of adsorption capacity was four times greater than that of untreated sawdust. Rehman et al. [110] on the other hand, reported the removal of Ni(II) ions by using the sodium-hydroxide-treated sawdust of Dalbergia sissoo, a byproduct of sawmills. They stated that the treatment of sawdust with NaOH resulted in the

conversion of methyl esters, which are the major constituents in cellulose, hemicellulose and lignin, to carboxylate ligands. The maximum adsorption capacity of Ni(II) ions was found to be 10.5 mg/g.

The effectiveness of Pb(II) adsorption by sodium–hydroxide-treated lalang or *Imperata cylindrica* leaf powder was studied [111]. The value of maximum adsorption capacity obtained by NaOH-treated *Imperata cylindrica* (13.5 mg/g) was much higher than that of the untreated adsorbent (5.9 mg/g).

Table 7. Alkaline treatment of cellulose and associated adsorption capacities.

Adsorbent	**Modifying chemicals (Chelating group)**	**Maximum adsorption capacity at optimum conditions (mg/g)**	**Isotherm**	**Reference**
Cellulose (*Juniper* fiber)	Sodium hydroxide (Hydroksyl)	Cd(II) 29.5		[107]
Wood sawdust	Sodium hydroxide (Hydroksyl)	Cd(II) 72.8	L	[109]
Sawdust (*Dalbergia sissoo*)	Sodium hydroxide (Hydroksyl)	Ni(II) 10.8		[110]
***Imperata cylindrica* leaf powder**	Sodium hydroxide (Hydroksyl)	Pb(II) 15.5		[111]

2.2.5 Silynation

Silane-based surface modification is a popular way to modify cellulosic fibers. Therefore, interactions of silane coupling agents with natural fibers are very well-known [112]. Coupling agents usually improve the degree of cross-linking in the interface region and offer a perfect bonding. Silanes undergo hydrolysis, condensation, and a bond formation stage. Silanols can

form polysiloxane structures by reacting with a hydroxyl group of the cellulose fibers. In the presence of moisture, the hydrolyzable alkoxy group leads to the formation of silanols. The silanols then react with the hydroxyl groups of the fiber, forming stable covalent bonds to the cell wall. Adsorption properties of functionalized silanes have been widely investigated and they have been found as effective adsorbents for the removal of metals from aqueous solutions [112]. Nevertheless, cellulose-coupled aminosilanes have not been widely investigated for water treatment applications.

The adsorbent, cellulose-dithiooxamide (Cel –DTX), was synthesized using a simple two-step methodology (Figure 7) [113]. Dithiooxamide is a complexing agent that is generally used in the spectrometric determination of certain solution phase metals, including copper, iron, nickel, and cobalt, among others. The maximum amount of metal species extracted from the solution was determined to be 3.7 and 8.1 mg/g for Cu(II) and Cd(II), respectively. The pre-concentration results led to the conclusion that the material showed high stability and that the material could be reused for at least 20 cycles.

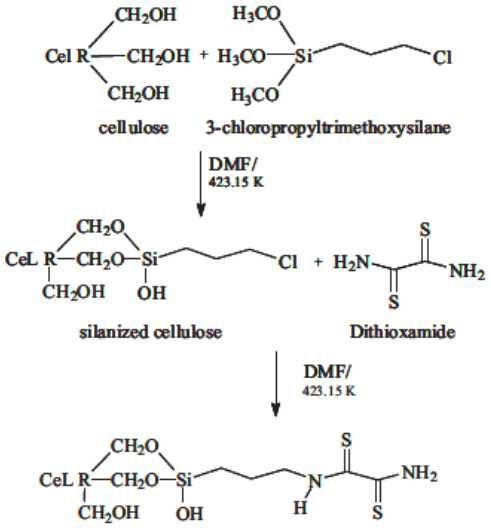

Figure 7. The simple two-step methodology for preparing Cellulose-Dithiooxamide adsorbent [113].

2.3 Cellulose-based composite materials

Composite materials (also called composites) are materials made from two or more constituent materials with significantly different physical or chemical properties, which, when combined, produce a material with characteristics different from the individual components. In practice, most composites consist of a bulk material (the matrix) and a reinforcement of some kind added primarily to increase the strength and stiffness of the matrix. This reinforcement is usually in fibre form [114]. Cellulose macro and nanofibers can be used as reinforcement in composite materials because of enhanced mechanical, thermal, and biodegradation properties of composites. Cellulose fibers are hydrophilic in nature, so it becomes necessary to increase their surface roughness for the development of composites with enhanced properties. In the present section, the surface modification of cellulose fibers by various methods is reviewed. Hence, the modification and processing methods are not discussed in this section, but the different cellulose-based composite materials for water treatment are reviewed. The typical cellulose-based composite materials as water treatment adsorbents are presented in Table 8.

Table 8. Cellulose-based composite materials and their applications in water treatment.

Composite material	Process	Reference
Graphene oxide/carboxymethyl cellulose monoliths	Metal removal	[128]
Carboxymethyl cellulose Ce(IV) molybdophosphate composite	Cation-exchanger	[131]
Cellulose acetate membrane coated with polyaniline or polypyrrole	Gold–iodide complex remova	[132]
Cellulose acetate–organo-montmorillonite	Anionic dye removal	[129]

Acetate/zeolite composite fiber	Heavy metal removal	[130]
Cellulose triacetate membranes added with activated carbon	Heavy metal removal	[135]
Cellulose/chitin beads	Heavy metal removal	[123]
Chitosan-cellulose composite	Microcystin removal	[125]
Chitin/cellulose composite	Heavy metal removal	[122]
DEAE/cellulose	Au(II) removal	[137]
Chitosan/cellulose acetate membrane	Heavy metal removal	[121]
Epoxy functionalized poly(ether-sulfone) incorporated cellulose acetate ultrafiltration membrane	Heavy metal removal	[117]
Carboxymethyl cellulose Sn(IV) phosphate composite	Cation exchanger	[132]
Magnetic cellulose/Fe_3O_4/activated carbon composite	Congo red removal	[136]
Cellulose-graft-polyacrylamide/hydroxyapatite composite hydrogel	Heavy metal removal	[115]
Hydroxyapatite/cellulose Composite	Heavy metal removal	[125]
Cellulose/hydroxyapatite nanocomposites	Fluoride removal	[126]
Hydroxyl ethyl cellulose blending porous composite	Heavy metal removal	[124]
Poly(vinyl alcohol)/cellulose composite membrane	Metal removal	[134]

Zeolite/cellulose acetate	Heavy metal removal	[130]
Carboxymethyl cellulose-g-poly (acrylic acid)/attapulgite hydrogel composites	Heavy metal removal	[116]
Zirconium/cellulose	Fluoride removal	[135]

The excellent properties of epoxy (good adhesion, mechanical properties, low moisture content, little shrinkage, and ease of processing) make it one of the best matrix materials for composites [117]. Epoxy functionalized poly(ether-sulfone) (EPES) was prepared and utilized as the hydrophilic modification agent for the preparation of high performance cellulose acetate (CA) membranes by the phase inversion technique. It was concluded that CA ultrafiltration membranes prepared by the incorporation of EPES may be valuable in the removal of chromium ions from aqueous streams.

There is some literature, which reports on the use of cellulose immobilized on chitosan or chitin to form chitosan or chitin–cellulose composite beads. For example, chitosan/cotton cellulose fiber composites were prepared to remove Au(III), Pb(II), Ni(II), Cd(II), Cu(II), and Hg(II) [118-123] from an aqueous solution. Chitin/cellulose blend membranes were successfully prepared in a 7 wt% NaOH/12 wt% urea aqueous solution via a freezing/thawing method to dissolve chitin, and then coagulating with 5 wt% Na_2SO_4 to regenerate it. The results of the adsorption study revealed that the composite membranes exhibited the efficient removal of heavy metal ions (mercury, copper and lead) from an aqueous solution as a result of their microporous structure, large surface area and affinity on metal ions. The uptake capacity of the heavy metal ions on chitin/cellulose blend membranes increased with the chitin content. Moreover, the chitin/cellulose membranes could be easily regenerated [122]. The chitin/cellulose composite was also found to have superior mechanical strength (from cellulose) and excellent adsorption capability for microcystin-LR, which is a deadly toxin produced by cyanobacteria [124].

A novel porous composite adsorbent was prepared by using sodium alginate and hydroxyl ethyl cellulose blending as an immobilization matrix for humic acid and then crosslinked by glutaraldehyde [125]. Humic acid is a principal component of humic substances, which are the major organic constituents of soil (humus), peat, coal, many upland streams, dystrophic lakes, and ocean water. The adsorbent was prepared using polyethylene glycol (PEG) as the porogen and was used to remove Cd(II) ions from an aqueous solution. The maximum uptake capacity of the GA-HA/SA-HEC for Cd(II) ions was 148.9 mg/g.

As a kind of inorganic/organic hybrid polymeric material, charged hybrids have attracted great attention in recent years, because they not only combine the advantages of organic and inorganic materials but also acquire some distinguished properties, such as structural flexibility, and thermal and mechanical stability. Hydroxyapatite (HA) has an excellent ion-exchangeability and is expected to be used as an agent for the removal of heavy metal ions from wastewater. However, due to the high specific surface area and very small particle size, the agglomeration of powdery HA is very general. Thus, the pure hydroxyapatite was mixed with cellulose to utilize its ion-exchangeability. The removal ratios of some heavy metal ions with hydroxyapatite composite were examined with regard to their reaction time and the amount of hydroxyapatite composite. The ion-exchangeability of the hydroxyapatite composite did not seem to be interfered with by the cellulose matrix during heavy metal ion removal [126]. The HA-Cellulose composite was also found to have a strong affinity toward fluoride [127].

The shaped solid composites of biopolymers and clay minerals have great potential in the efficient removal of hazardous pollutants from wastewater. Graphene oxide/carboxymethyl cellulose monoliths composite [128], cellulose acetate/organo-montmorillonite (CA/OMMT) [129], and cellulose acetate/zeolite [130] composites have been found to be effective adsorbents for various heavy metal ions.

Cellulose is an interesting polymeric material for the immobilization of metal particles and metal nanoparticles as it contains six hydroxyl groups per cellubiose (repeating) unit of cellulose polymer. These hydroxyl groups can be functionalized by chemical modification for loading metal particles on the cellulose fibers. The thermodynamics of nicotinic acid adsorption from an aqueous solution on carboxymethyl cellulose Ce(IV) molybdophosphate composite cation exchanger synthesized by sol-gel method was studied by Inamuddin et al. [131]. The thermodynamic parameters showed that the adsorption of nicotinic acid onto composite cation exchanger was feasible, spontaneous and exothermic, suggesting its suitability for the potential application of nicotinic acid removal from wastewater. The same research group also studied the ion-exchange mechanism of heavy metal ions on the surface of carboxymethyl cellulose Sn(IV) phosphate composite. The results showed that the ion-exchange phenomenon was more feasible on the surface of this composite cation exchanger as compared to the other ion exchangers [132]. This indicated the usefulness of this composite as ion exchanger in various applications.

The effects of incorporation of natural fibers in petrochemical-based plastics matrices have been extensively studied quite recently. Polyacrylamide (PAA), polyvinyl chloride (PVC), polyvinylalcohol (PVA), polyaniline (PANI) (Castillo-Ortega), and polypyrrole (PPy) are reportedly used matrices for cellulose-based fiber-reinforced polymer composites in water treatment applications [133, 134]. In the first case, cellulose acetate membranes with controlled thickness were coated with PANI or with PPy in order to adsorb and subsequently desorb a gold–iodide complex. In the second study, composite poly(vinyl alcohol) (PVA)/cellulose membranes were prepared by coating PVA mixture solutions on filter paper for Fe(II) and Cu(II) adsorption from water solution.

The ultrafiltration removal of uranium from water with composite-activated carbon cellulose triacetate membranes (AC-CTA) was investigated [135]. Removal efficiencies were calculated measuring solutions' radioactivities and uranyl removal was 35.7%.

A novel ultrasound-assisted methodology was used for the impregnation of zirconium into a cellulose matrix [136]. These composite materials were used as adsorbents for fluoride from

aqueous solutions. Fluoride interacted with the cellulose hydroxyl groups and the cationic zirconium hydroxide, reaching a maximum adsorption capacity of 4.6 mg/g.
The adsorption of congo red dye onto the novel Magnetic cellulose/Fe3O4/activated carbon composites m-(Cell/Fe_3O_4/ACCs) was studied as a function of contact time, initial concentration of congo red, adsorbent dosage, and solution pH [137]. The magnetic adsorbent showed characteristics of superparamagnetism, which indicated that m-Cell/Fe_3O_4/ACCs could be separated from a treated solution using a magnetic process.

Diethylaminoethyl cellulose (DEAE-Cell) is a common biopolymer derivative. It is a positively charged resin and widely used in ion exchange chromatography, a type of column chromatography, used in protein and nucleic acid purification/separation [138]. The effects of different recovery parameters on the efficiency of gold recovery using this composite were studied in detail. A gold recovery efficiency of 99% was attained under conditions of 20–40 g DEAE-cellulose per liter at a shaking rate of 130 rpm for 30 min at room temperature.

Novel NH_2-functionalized cellulose acetate (CA)/silica composite nanofibrous membranes were successfully prepared by sol–gel combined with electrospinning technology [139]. Tetraethoxysilane (TEOS) as a silica source, CA as precursor and 3-ureidopropyltriethoxysilane as a coupling agent were used in membrane preparation. The maximum adsorption capacity for Cr(VI) was estimated to be 19.46 mg/g.
A new type of composite membrane, triolein embedded-cellulose acetate membrane (TECAM) was prepared and used for the uptake of six organochlorine pesticides. Results indicated that TECAM quickly and efficiently accumulated hydrophobic organochlorine pesticides (OCPs) from water [140, 141].

Tetrakis (1-methyl-4-pyridinio) porphyrin tetra (p-toluenesulfonate), an optical indicator ligand for cadmium ions, was immobilized onto a porous chitosan/cellulose acetate blend base membrane through polymer brushes grafted onto the membrane's surface via a surface-initiated atom transfer radical polymerization (ATRP) method [142]. The prepared

membrane was found to be capable of displaying distinctive color changes in response to the presence of cadmium ions in aqueous solutions. In addition, it also showed significantly enhanced performance for the adsorptive removal of cadmium ions. Experimental results indicated that the developed membrane can exhibit rapid (within 2 min) color change (from yellow to green) when it was in contact with cadmium ions in a solution even at relatively low concentrations (e.g. 5 mg/L). The interference study revealed that the functionalized membrane also possessed selectivity towards cadmium ions when other cationic species such as K^+, Na^+, Ca(II) and Mg(II) ions existed together in the solutions.

2.4 Summary of literature

This literature review shows that the study of chemically modified cellulose-based adsorption for pollutant removal has attracted the attention of many scientists. Most studies focused on the removal of heavy metal ions, such as Cd, Cu, Pb, Zn, Ni and Cr(VI) ions. Approaches to the modification of cellulose, as reviewed in this paper, have been based on a direct chemical modification or the grafting of suitable polymeric chains onto the cellulose backbone followed by functionalization. The most common chemicals used for the treatment of cellulosic-based materials are acids and bases. The latter has enabled the addition of amine, amide, amidoxime, carboxyl, hydroxyl, and imidazole-type binding ligands to the cellulose adsorbent backbone. Chemical modification in general has improved the adsorption capacity of adsorbents probably due to a higher number of active binding sites after modification, better ion-exchange properties and formation of new functional groups that favors metal uptake.

As cellulose has prodigious hydroxyl groups at the surface, compounds that react with alcohols (e.g. isocyanates, epoxides, acid halides) and acid anhydrides are the most common for direct attachment. These reactions can be used to form a host of alternate surface chemistries such as amine, ammonium, alkyl, hydroxyalkyl, ester (acetate, propionate, etc.), acid, among others. Alternatively, many studies seek to change the chemistry of the hydroxyl group. TEMPO-mediated oxidation, for instance, has been used to convert alcohol groups to

carboxylic acid moieties for better dispersibility. Other methods to modify the surface, such as using sulfuric acid, can also be used to form sulfate esters.

Furthermore, chemical modification in general has improved the adsorption capacity of adsorbents compared to unmodified materials. The regeneration and reuse of a number of the modified cellulose adsorbents is demonstrated in a number of papers reviewed in this work. Many of the adsorption interactions between the modified cellulose adsorbents and heavy metals have been characterized by the Langmuir approach or in a lesser number of cases by the Freundlich model.

Since there are a variety of cellulose-based adsorbents, the argument regarding which type of adsorbent is better in adsorption is still ongoing. There is no definite answer to this since each adsorbent has its own advantages and disadvantages. Comparing adsorbents is almost impossible since the parameters and the adsorbates used are different. Good metal ion sorption capacities were found in many studies, however, the results obtained in different laboratory conditions may differ considerably. This field of research has great room for improvements, with the hope that cellulose-based adsorption materials can be applied commercially instead of only at the laboratory scale.

3. APPLICATIONS OF NANOCELLULOSE FOR WATER TREATMENT

3.1 General

Nanocelluose, variously termed crystallites, nanocrystals, whiskers, nanofibrils, and nanofibers, has been the subject of extensive research covering the isolation, characterization, and search for applications of novel forms of cellulose, and has been reviewed in a number of books and journal articles due to its biodegradable nature, low density, high mechanical properties, economic value, and renewability [143-153].

Nanocellulose can be produced from wood and forest/agricultural residues by three different main methods: physical, chemical and bacterial methods from various lignocellulosic sources [143-147]. As is apparent from Table 5, the nomenclature of

nanocelluloses has not been used in a completely uniform manner in the past. Herein, the terms microfibrillated cellulose (MFC), nanocrystalline cellulose (NCC), and bacterial nanocellulose (BNC) are used in this paper. Nanocelluloses combine important cellulose properties, such as hydrophilicity, broad chemical-modification capacity, and the formation of versatile semicrystalline fiber morphologies. The specific features of nanoscale are mainly caused by the high surface area of these materials. On the basis of their dimensions, functions, and preparation methods, which in turn depend mainly on the cellulosic source and on the processing conditions, nanocelluloses may be classified in three main subcategories as presented below (Table 9). The main steps involved in the preparation of cellulose nanoparticles ares presented in Figure 8.

Table 9. The classification of nanocellulose materials [151].

Type of cellulose	Synonyms	Typical sources	Formation and size
Microfibrillated cellulose (MFC)	microfibrillated cellulose nanofibrils and microfibrils nanofibrillated cellulose	wood, sugar beet, potato tuber, hemp, flax delamination of wood pulp by	mechanical pressure before and/or after chemical or enzymatic treatment diameter: 5–60 nm
Nanocrystalline cellulose (NCC)	cellulose nanocrystals, crystallites, whiskers,rodlike cellulose microcrystals tunicates, algae, bacteria	wood, cotton, hemp, flax, wheat straw, mulberry bark, ramie, Avicel, tunicin	cellulose from algae and bacteria acid hydrolysis of cellulose from many sources diameter: 5–70 nm length: 100–250 nm (from plant celluloses); 100 nm to several micrometers
Bacterial nanocellulose (BNC)	bacterial cellulose, microbial cellulose, biocellulose	low-molecular-weight sugars and alcohols	synthesis using bacterial diameter: 20–100 nm; different types of nanofiber networks

MFC is normally produced from wood through the high pressure homogenization of pulps. Different pretreatments have been proposed to facilitate this process, for example, mechanical cutting, acid hydrolysis, enzymatic pretreatment, and the introduction of charged groups through carboxymethylation or 2,2,6,6-tetramethylpiperidine-1-oxyl (TEMPO)-mediated oxidation; due to this, the production route has high energy consumption for fiber delamination without these pretreatment procedures. Being the

smallest structural unit of plant fiber, MFC consists of a bundle of stretched cellulose chain molecules with long, flexible and entangled cellulose nanofibers of approximately 1–100 nm size. They consist of alternating crystalline and amorphous domains [147,148].

NCC is the term often used for cellulose nanocrystals prepared from natural cellulose by strong acid hydrolysis. During the acid hydrolysis process, the hydronium ions can penetrate the cellulose chains in the amorphous domains promoting the hydrolytic cleavage of the glycosidic bonds. Finally, after mechanical treatment, it releases individual crystallites. Hydrochloric and sulfuric acids have been extensively used to degrade cellulose fibers. However, phosphoric, hydrobromic and nitric acids have also been reported for the preparation of crystalline cellulosic nanoparticles. The nanocrystals formed from wood pulp are shorter and thinner than MFC [147-152].

Cellulose fibers are also pepared by gluconacetobacter (Acetobacter, Agrobacterium, Alcaligenes, Pseudomonas, Rhizobium, or Sarcina [153]. The most efficient producers of BNC is *Acetobacter Xylinum* or *Gluconacetobacter Xylinus*, witch are gram-negative strains of acetic-acid-producing bacteries, having active motility, and high ubiquity [4]. BNC formed has the same molecular formula as plant cellulose but is fundamentally different because of its nanofiber structure. After simple purification, BNC contains no impurities and no functional groups other than hydroxy groups. Owing to its nanoscale fiber structure, the properties of BNC are quite different from those of common plant celluloses. Therefore, BNC opens up new fields of application for cellulose materials [153].

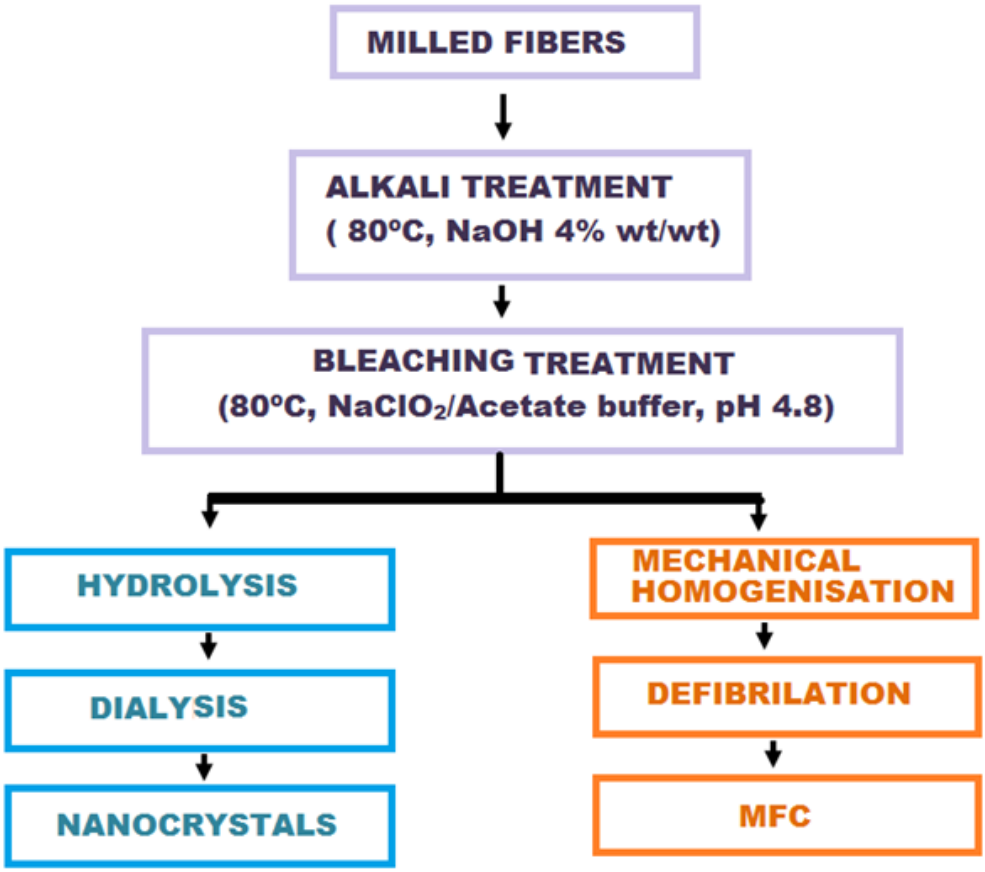

Figure 8. The main steps involved in the preparation of cellulose nanoparticles [143-154].

3.2 Nanocellulose-based materials for water treatment

The method of surface chemistry modification of nanocellulose is through the use of direct chemical modification and/or covalent attachment of molecules. Due to high specific surface areas and numerous reactive groups, excellent adsorption performance may be obtained with different types of modified nanocelluloses. The techniques are generally the same as those presented earlier in case of conventional cellulose (Chapter 2).

Nanotech reinforcement of native cellulose significantly enhanced metal removal efficiency compared to rice straw and cellulose fibers. Nanocellulose fibers were prepared using the physico-chemical treatment of rice straw, and were characterized and explored for the remediation of some toxic metals from wastewater [153]. Nanocellulose fibers were found to have a long rod-like elongated nanofibrillated morphology, with an average grain size of 6 nm. The prepared nanocellulose fibers in batch experiments showed a removal efficiency of 9.7 mg/g Cd (II), 9.4 mg/g Pb(II), and 8.6 mg/g Ni (II) ions. The regeneration studies signified that nanocellulose fibers could be successively used for up to three cycles of regeneration.

Given the high surface area of the nanocellulose, an adsorbent based on modified nanocellulose might afford an interesting alternative to conventional adsorbents like activated carbon, ion exchange resins, or zeolite. This new area of potential use of nanocellulose in the field of water treatment was explored by several recent publications that showed the possibility to prepare adsorbents based on modified nanocellulose for removing not only for heavy metal ions but also for organic pollutants. The surface modification of the nanocellulose was obtained by adding specific groups such as carboxyl [154, 155], amine [156, 157], ammonium [158] and xanthate [159] on the surface of cellulose.

Oxolane-2,5-dione-modified cellulose nanofibres were used for the adsorption of cadmium and lead ions from model wastewater samples for the first time. The maximum adsorption demonstrated the higher capacity of cellulose-g-oxolane-2,5-dionenanofibres for Pb(II) and Cd(II) removal as compared with oxolane-2,5-dione functionalized raw cellulose fibres (for cellulose nanofibres adsorption capacities were 12.0 and 2.9 mmol/g for Pb(II) and Cd(II), respectively, in comparison to 0.002 mmol/g for raw cellulose) [160].

As reported above, succinic anhydride is an active agent containing one anhydride group, which can react with the hydroxyl groups of cellulose. In recent decades, there have been many investigations concerning the modification of cellulose with succinic anhydride for the removal of heavy metal ions. However, modification of CNCs with succinic anhydride has

also been reported. The maximum adsorption capacities of succinic anhydride modified nanocellulose (SCNCs) and NaSCNCs for Pb(II) and Cd(II) were 367.6 mg/g, 259.7 mg/g and 465.1 mg/g, 344.8 mg/g, respectively [155]. Comparing these results with cellulose modified with the same method, the maximum adsorption capacities were higher for modified nanocellulose. SCNCs and NaSCNCs showed high selectivity and interference resistance from coexisting ions for the adsorption of Pb(II). NaSCNCs could be efficiently regenerated with a mild saturated NaCl solution with no loss of capacity after two recycles.

Nanocellulose-ethylenediaminetetraacetic acid (EDTA) conjugates were synthesized by the esterification of non-mercerized and mercerized cellulose with ethylenediaminetetraacetic dianhydride (EDTAD) (Figure 9). The adsorption of Cu(II), Cd(II), and Pb(II) ions were investigated from aqueous solutions. These materials showed maximum adsorption capacities for Cu(II), Cd(II), and Pb(II) ions ranging from 38.8 to 92.6 mg/g, 87.7 to 149.0 mg/g, and 192.0 to 333.0 mg/g, respectively. The modified mercerized materials showed larger maximum adsorption capacities than modified non-mercerized materials [161]. In another study, the adsorption of Pb(II) ions was investigated using regenerated cellulose fiber functionalized by anhydrous EDTA. The maximum adsorption capacity was 140.0 mg/g, which was less than half of the capacity using nanocellulose-based chelating material [162].

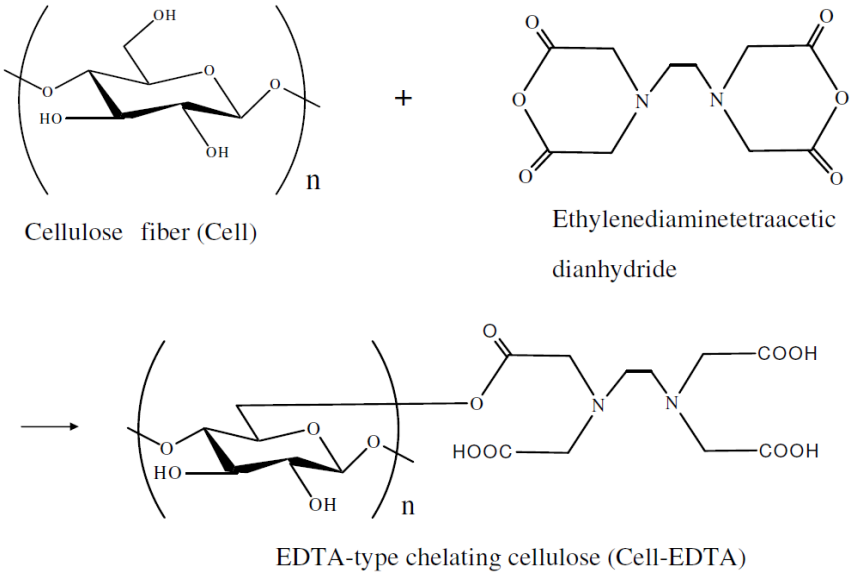

Figure 9. Cellulose fiber functionalized by anhydrous EDTA [162]

The high surface-to-volume ratio and size effects, and the ability to tune surface properties through molecular modification, give good properties for metal remediation to nanocrystalline cellulose (NCC). The removal capacities for succinated and aminated nanocrystalline cellulose were 95.0 % for Cr(III) and 98.0% for Cr(VI). The capacities of unmodified NCC were 64.0 % for Cr(III) and 6.0 % for Cr(IV). Structurally functionalized succinated and aminated biomaterial could be used up to five times, compared to three cycles of MCC (microcrystalline cellulose) and NCC [157].

Cellulose reacts with carbon disulfide (CS_2) in the presence of sodium hydroxide (NaOH) to produce sodium cellulose xanthate. This esterification reaction was used for acid-hydrolysis-prepared nano banana cellulose (NBC). The maximum biosorption capacity of xanthate nanobana cellulose (XNBC) for Cd(II) was found to be 154.3 mg/g. Among the various desorbing agents tested, the desorbing efficiency was found to be maximal with 0.1 mol/ L HCl [160].

Bacterial cellulose (BC) has the potential as a new adsorbent for effective separation of heavy metal ions due to its unique properties, including high water holding capacity, a fine fiber network, and high tensile strength, lack of secondary pollution, high specific surface area, porous structure and presence of many hydroxyl groups in the chains [163, 165]. The adsorption capacity of unmodified BC was found to be relatively low. Therefore, it was necessary to modify the surface of BC, in order to increase its adsorption capacity.

Diethylenetriamine-bacterial cellulose (EABC) [163], ammonium sulfamate-bacterial cellulose (ASBC), xanthogenated bacterial cellulose (Deng) and carboxymethylated-bacterial cellulose (CM-BC) were investigated as adsorbents for Cr(VI), Cd(II), Pb(II), and Cu(II). Ammonium sulfamate-bacterial cellulose (ASBC) was prepared through chemical modifications of bacterial cellulose. A new adsorbent, ammonium sulfamate-bacterial cellulose (ASBC) was prepared by taking ammonium sulfamate as a monomer. Meanwhile, the adsorption property of Pb(II) by ASBC was studied, and the results showed that adsorption property of ASBC was improved compared to that of BC [164]. The maximum adsorption capacity of modified cellulose was 22.7 mg/g.

Carboxymethylated-bacterial cellulose (CM-BC) was synthesized by Acetobacter xylinum by adding water-soluble carboxymethylated cellulose (CMC) in the culture medium [161]. The CM-BC was examined for the removal of Cu(II) and Pb(II) ions from an aqueous solution and compared with BC. The effects of performance parameters such as pH, adsorbent dose, and contact time on copper and lead ion adsorption were analyzed. Both BC and CM-BC showed good adsorption performance at an optimized pH of 4.5. Compared with BC, CM-BC performed better with the value of 9.7 mg (copper)/g and 22.6 mg (lead)/g for BC and 12.6 mg (copper)/g and 60.4 mg (lead)/g for CM-BC, respectively.

A summary of modified and unmodified nanocellulose as adsorbents for the removal of heavy metal ions from aqueous solutions is shown in Table 10.

Table 10. Modified and unmodified nanocellulose as adsorbents for the removal of heavy metal ions from aqueous solutions

Material	**Modification**	**Maximum adsorption capacity (mg/g)**	**Reference**
Nanocellulose fibers		Cd(II) 9.7 Pb(II) 9.4 Ni(II) 8.6	[153]
Nanocellulose	Glycidylmethacrylate and tetraethylenepentamine	Hg(II) 414.0 Cu(II) 96.0 Ag(I) 129.6	[154]
Nanocellulose	Oxolane-2,5-dione	Pb(II) 78.0 Cd(II) 32.0	[160]
Nanocellulose	Succinic anhydired	Pb(II) 367.6 - 465.1 Cd(II) 259.1 - 344.8	[155]
Nanocellulose	Ethylenediaminetetraaceti c acid (EDTA)	Cd(II) 38.8 - 92.6 Cu(II) 87.7 - 149.0 Pb(II) 192.0 - 333.0	[161]
Nanocellulose	Anhydrous EDTA	Pb(II) 140.0	[162]
Nanocellulose	Succination and amination	Cr(III) 95.0 % Cr(IV) 98.0 % (unmodified Cr(III) 64.0 % Cr(IV) 6.0 %)	[157]
NBC, nano banana cellulose	Carbon disulfide (CS_2) in presence of sodium hydroxide (NaOH)	Cd(II) 154.3	[159]
Bacterial cellulose	Carboxymethylation	Cu(II) 12.6 Pb(II) 60.4 (unmodified Cu(II) 9.7 , Pb(II) 22.6)	[165]

3.3 Cellulose-based nanocomposite materials for water treatment

Nanocomposites, in general, comprise multiphase materials where at least one constituent phase has one dimension in the nanometer range (1–100 nm). When comparing naocomposite materials with conventional composite materials, the advantages of nanocomposite materials are their superior thermal, mechanical and barrier properties at low reinforcement levels (e.g., B5 wt%), as well as their better recyclability, transparency and low weight [166]. The refered nanocellulose-based composite materials used for water treatment are shown in Table 11.

Nano-scale cellulose fiber materials (e.g., microfibrillated, nanofibrilled and bacterial cellulose) are promising candidates for bio-nanocomposite production, due to their abundance, high strength and stiffness, low weight and biodegradability. It is well known that the properties of nanocomposite materials depend on addition to the properties of their individual components, also on morphological and interfacial characteristics arising from the combination of distinct materials. Therefore, the use of polymers such as cellulose, starch, alginate, dextran, carrageenan, and chitosan among others, gain great relevance due to their renewable nature and biodegradability, and also because a variety of formulations can be exploited depending on the envisaged functionality [167, 168].

Metal nanoparticles have properties that differ from the bulk analogues due to size and surface effects. Thus, the properties of the final composite materials can be modified with various size, shape and particle size distribution of the nanofillers as well as by interactions occurring with the cellulose fibers' surfaces. The unique material is a composite of nanocellulose and magnetic nanoparticles [169]. Celluolose nanofibril is decorated with magnetic nanoparticles that are uniformly distributed on the nanofibril. These materials combine the biological and mechanical properties of nanocellulose, which are enhanced with magnetic nanoparticle characteristics. A novel amino-functionalized magnetic cellulose composite was prepared by a process that involved: (1) the synthesis of magnetic silica nanoparticles using the co-precipitation method followed by the hydrolysis of sodium silicate, (2) coating with cellulose (3) grafting of glycidyl methacrylate using cerium initiated

polymerization and (4) the ring-opening reaction of epoxy groups with ethylenediamine to yield amino groups. This composite material should be a promising adsorbent for Cr(VI) removal, with the advantages of high adsorption capacity, rapid adsorption rate, and convenient recovery under a magnetic field.

The spherical Fe_3O_4/BC nanocomposites had high adsorption capacities for Pb(II), Mn(II), and Cr(III) and were recyclable after the elution of heavy metal ions [170]. Compared with conventional preparation procedure for cellulose spheres, spherical Fe_3O_4/BC nanocomposites can be readily prepared without sophisticated steps and this adsorption material has high adsorption and elution capacities

Gels consist of a solid three-dimensional network, including large amounts of solvent and ensnares it through surface tension effects. Mainly, hydrogels are structures formed from biopolymers and/or polyelectrolytes, and contain large amounts of trapped water [29, 146]. Composite hydrogels from cellulose and other polymers have been prepared by blending, complex formation, and interpenetrating networks (IPN) technology. These materials combine the different properties of cellulose and other polymers. Cellulose-based hydrogel can be used as matrices to incorporate inorganic nanoparticles for preparing cellulose-inorganic hybrid hydrogels. This strategy is suitable for fabricating novel cellulose-based hydrogels with multifunctional properties.

A novel adsorbent, biodegradable collagen/cellulose hydrogel beads (CCHBs), was prepared by reconstitution from 1-butyl, 3-methylimidazolium chloride ([C_4mim]Cl) and the adsorption properties of the CCHBs for Cu(II) ion removal from aqueous solutions were investigated [171]. The maximum adsorption capacity of CCHB3 (collagen/cellulose mass ratio of 3/1) was found to be 63.6 mg/g. The CCHBs maintained good adsorption properties after the fourth cycle of adsorption–desorption.

Another good candidate for the preparationof hydrogels is polyvinyl alcohol (PVA), which can be cross-linked using several methods [172, 173]. Novel magnetic hydrogel beads (m-CS/PVA/CCNFs), consisting of carboxylated cellulose nanofibrils (CCNFs), amine-functionalized magnetite nanoparticles and poly(vinyl alcohol) (PVA) blended chitosan (CS), were prepared by an instantaneous gelation method. The magnetic hydrogels were employed as absorbents for the removal of Pb(II) ions from aqueous solutions and the fundamental adsorption behavior was studied. Experimental results revealed that the m-CS/PVA/CCNFs hydrogels exhibited a higher adsorption capacity with the value of 171.0 mg/g, and the carboxylate groups on the CCNFs surface played an important role in Pb(II) adsorption. Additionally, Pb(II)-loaded m-CS/PVA/CCNFs hydrogels could be easily regenerated in a weak acid solution and the adsorption effectiveness of 90% could be maintained after the four cycles.

The synergistic adsorption of heavy metal ions and organic pollutants were investigated using novel supramolecular polysaccharide composites from cellulose (CEL), chitosan (CS) and benzo-15-crown 5 (B15C5) [174]. Butylmethylimidazolium chloride [$BMIm^+Cl^-$], an ionic liquid (IL), was used as the sole solvent for the dissolution and preparation of the composites. The [CEL/CS + B15C5] composites obtained retained the properties of their components, namely superior mechanical strength (from CEL) and excellent adsorption capability for heavy metal ions and organic pollutants (from B15C5 and CS). Moreover, the pollutants adsorbed on the composites could be quantitatively desorbed to enable the [CS + CEL + B15C5] composites to be reused with similar adsorption efficiency.

Chitosan and chitin are two of the most abundant natural biopolymers after cellulose. The chitosan was converted into chitosan nanoparticles and, to improve its adsorption efficiency, it was mixed separately with kaolin clay and methylcellulose to form the binary composites NC+KC and NC+MC [175]. These nanocomposites acted as good adsorbents to remove Pb(II) ions from synthetic wastewater. Chitin/cellulose-composite membranes exhibited the efficient removal of heavy metal ions (mercury, copper and lead) from an aqueous solution as a result of their microporous structure, large surface area and affinity on metal ions [174]. The uptake capacity of the heavy metal ions on chitin /cellulose-blend membranes increased

with the chitin content. The amount of metal ions adsorbed onto the unit amount of the membrane (q_e) was in the order of Hg(II) > Pb(II) > Cu(II), indicating a good adsorption of Hg(II). Moreover, the chitin/cellulose membranes could be easily regenerated. This work provided a “green” pathway for the removal of the hazardous materials in wastewater.

Nanocellulose acetate was used as composite material together with zirconium (IV) phosphate and zeolite [4, 176] for the removal of heavy metals from aqueous solutions. Cellulose acetate–zirconium (IV) phosphate nanocomposite (CA/ZPNC) showed an ion-exchange capacity of 1.4 mequiv./g for Na^+ and was highly selective for Pb(II) and Zn(II) over many other metal ions.

Dyeing wastewater is an important class of pollutants, which can be identified by the naked eye. Nano-cellulose hybrids containing polyhedral oligomeric silsesquioxane with multi-N-methylol (R-POSS) [177] and fabricate porous nanocomposite gels based on partially hydrolyzed polyacrylamide and cellulose nanocrystals [172] could be used as biosorbents for dyes. Reactive dyes, Yellow B-4RFN and Blue B-RN and methylene blue were investigated and it was concluded that nano-cellulose hybrids have a potential application as biosorbents in low concentration dyeing wastewater treatment.

Table 11. Nanocellulose-based composite materials for water treatment

Composite material	**Maximum adsorption capacity (mg/g)**	**Reference**
(CCNFs)/poly(vinyl alcohol) (PVA)/ chitosan (CS)	Pb(II) 171.0	[173]
Amino-functionalized magnetic cellulose composite	Cr(VI) 171.5	[170]
Cellulose acetate–zirconium (IV) phosphate nanocomposite (CA/ZPNC)	Ion-exchange capacity of 1.4 mequiv/g Na^+ Pb(II) and Zn(II)	[4]
Chitin/nanocellulose	Hg(II) 0.8 Cu(II) 0.1 Pb(II) 0.5	[175]
Chitosan nanoparticles/kaolin clay	Pb(II) 907	[174]
Chitosan nanoparticles/methylnanocellulose	Pb(II) 976	
Collagen/cellulose hydrogel	Cu(II) 63.6	[171]
Fe_3O_4/BC	Pb(II) 65.0 Mn(II) 33.0 Cr(III) 25.0	[170]
Nanocellulose acetate (CA)/zeolite (Z)	Ni(II) 28.6 Cu(II) 17.0	[176]
Nanocellulose hybrids containing polyhedral oligomeric silsesquioxane with multi-N-methylol (R-POSS)	Reactive Blue B-RN 14.4 Reactive Yellow B-4RFN 16.6	[177]
Nanocellulose/poly(vinyl alcohol) (PVA)	Methylene blue (Maximum adsorption capacity are not available)	[172]

Several studies on the chemical surface modification of cellulose fibres for water treatment applications have been published. Based on the literature review, while the reactions and modification methods as such are well known, the reports of their use to modify nano/microcellulose for water treatment are very limited. It is well known that the surface of cellulose microfibrils carries a large number of hydroxyl groups, which makes the nano/microfibrils suitable for the introduction of new functionalities and more exploration is needed in this research field. The preparation of a nano/microcellulose-based multifunctional adsorbent for removal of cations and anions from water has yet to be reported.

4. OBJECTIVES AND STRUCTURE OF THE WORK

The overall aim of the thesis was to investigate the potential of modified nano and microcellulose adsorbents for water treatment applications (Figure 10). The research focus was on cations and anions. The specific objectives of this study were:

- to prepare five different kinds of nano/microscellulose-based adsorbents (1) Succinic anhydride modified mercerized nanocellulose for metals removal (Paper I); (2) aminosilane-modified nanostructured microfibrillated cellulose for hydrogen sulfide and metals removal (Paper II, III); (3) epoxy-modified nanostructured microfibrillated cellulose for hydrogen sulfide removal (Paper III); (4) hydroxyapatite-modified nanostructured microfibrillated cellulose for hydrogen sulfide, metals, phosphate and nitrate removal (Papers III, IV) and (5) Fe_3NP -activated microfibrillated cellulose for arsenate removal (Paper V).

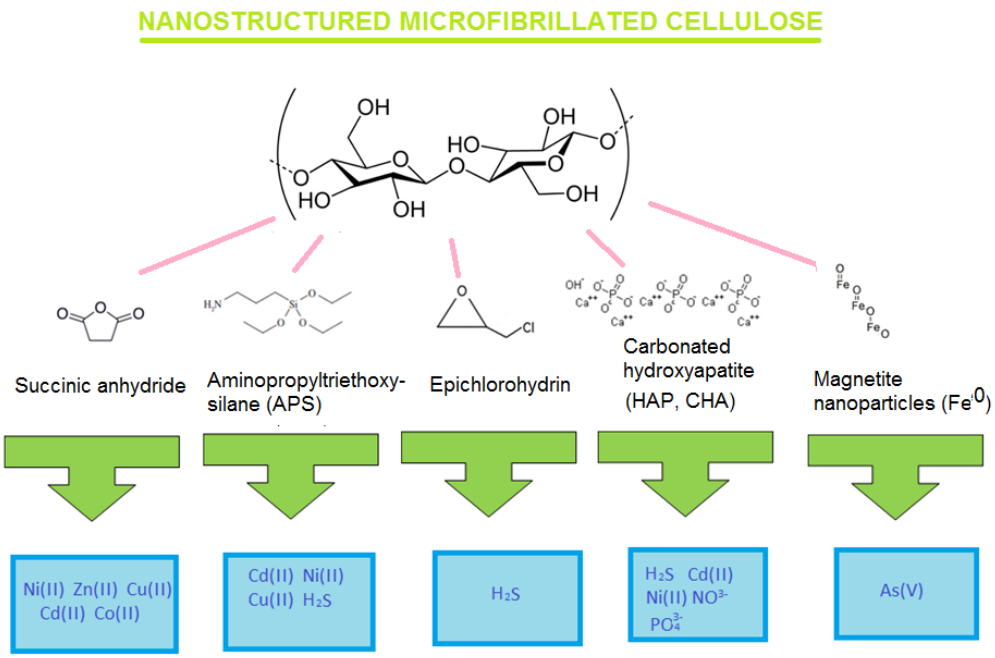

Figure 10. Schematic overview of the contents of this thesis

- to investigate the effects of solution pH, contact time, and contaminants or pollutants' concentration as well as regenerability of the spent adsorbents. Moreover, the reaction mechanism of the adsorption processes was also described
- to fit the experimental data obtained from the isotherm and kinetic studies to various kinetic and isotherm models that could describe the experimental data. The fitting results from isotherm and kinetic modeling for the investigated experimental data range is presented in Papers I, II, IV and V. Paper III presents the fitting results from isotherm modeling.

5. MATERIALS AND METHODS

5. 1 Synthesis of the adsorbents

Five different nanocellulose adsorbents were synthesized: the synthesis of succinic anyhdried modified MFC is described in detail in Paper I, the aminosilane (APS) modification in Papers II and III, the epichlorohydrin modification (Epoxy/MFC) in Paper III, the carbonated hydroxyapatite (HAP/MFC and CHA/MFC) in Papers III and IV and the nanomagnetic particle activation FeNP/MFC in Paper IV.

Briefly, the succinylated cellulose was prepared using merzerated MFC and the deprotonation of the free carboxylic acid group was achieved by treatment with a saturated $NaHCO_3$ aqueous solution (Paper I). The synthesis of aminopropyltriethoxysilane (APS)-modified microfibrillated cellulose (MFC) was obtained by reacting MFC with a coupling agent, APTES in an ethanol/water mixture (Papers II and III). Alkaline-treated MFC was reacted with epichlorohydrin-DMSO solution and 1,4-butanediol diglycidyl ether, resulting in an Epoxy/MFC adsorbent (Paper III). A carbonated hydroxyapatite-MFC (HAP/MFC or CHA/MFC) adsorbent was developed via the embedding of prepared hydroxyapatite into MFC (Papers III and IV). The preparation of the Fe^0-modified MFC was done by mixing Fe_3O_4 nanoparticles with NaOH- sulfocarbamide-urea-treated MFC (Paper V).

5.2 Characterization of the adsorbents

Elemental analysis was conducted to determine the surface coverage of APS/MFC, Epoxy/MFC and CHA/MFC using Organic Elemental Analyzer Flash 2000 (Thermo Scientific, Germany) (Papers II and III, IV). The surface morphology was examined using a Hitachi S-4100 scanning electron microscope (SEM). Fourier Transform Infrared Spectroscopy (FTIR) type Vertex 70 by Bruker Optics (Germany) was used to identify the surface functional groups of unmodified and modified MFC (Papers I-V). Zetasizer Nano Series model ZEN 3500 (Malvern, the UK) was employed to measure isoelectric points (Papers II and III). The energy dispersive analysis of X-rays (EDAX) was used to determine the chemical composition of Fe^0 and CHA-modified MFC (Papers IV and V). The surface morphology and chemical composition of FeNP/MFC was also examined using transmission electron microscope (HT7700 120kV High-Contrast/High-Resolution Digital TEM) (Paper V).

5.3 Adsorption and desorption experiments

Adsorption and desorption experiments as well as the study of adsorption kinetics are described in detail in Papers I-V. For the adsorption isotherm experiments, solutions containing known concentrations of adsorbates were mixed with a known dose of adsorbent for a designated time, after which the adsorbent was separated from the solution. The equilibrium adsorption capacity (q_e, mmol/g) was calculated as follows:

$$q_e = \frac{(C_i - C_e)}{M} V \qquad (1)$$

where C_i and C_e are the initial and the equilibrium concentrations (mmol/L) of adsorbates, while m and V are the weight of the adsorbent (g) and the volume of the solution (L), respectively.

The regeneration efficiency (%RE) of the adsorbent was calculated as follows:

$$(\%RE) = \frac{q_r}{q_0} \times 100 \qquad (2)$$

where q_0 and q_r are the adsorption capacities of the adsorbents (mmol/g) before and after regeneration, respectively.

The kinetics of the adsorption experiments was investigated by measuring the adsorption capacity of the adsorbent for a set time that was varied from one minute until equilibrium was attained (Papers I, II, IV and V).

The effect of the solution pH on the adsorption capacity of the adsorbent for target anions was studied by performing adsorption experiments. This was executed by adjusting the solution pH from 2.0 to 9.0 using 0.1 M HCl and 0.1 M NaOH with a known initial target anion concentration and adsorbent dose (Papers I-V).

5.4 Analysis of solutions

After centrifugation, metal concentrations were analyzed by the inductively coupled plasma optical atomic emission spectrometry (ICP-OES) model iCAP 6300 (Thermo Electron Corporation, USA). Zn(II) was analyzed at a wavelength of 202.548 nm (Papers I and II), Ni(II) at 231.605 nm (Papers I, II and IV), Cu(II) at 324.754 nm (Papers I and II), Co(II) at 228.616 nm (Paper I), Cd(II) at 226.502 nm (Paper I, II and IV), S at 180.731 (Paper III) and As(V) at 193.696 nm (Paper V). A HPLC (High Performance Liquid Chromatograph, Shimadzu) was used for the analysis of PO_4^{3-} and NO^{3-}. The used anion columns were IC SI-50 4E and SI-90G (Shodex®) and 3.2 mM Na_2CO_3 + 1.0 mM $NaHCO_3$ was used as the eluent. The detailed description of H_2S analysis is presented in Paper III.

5.5 Modeling of adsorption isotherms and kinetics

5.5.1 Adsorption isotherms

An adsorption isotherm is a quantitative measurement of the adsorption equilibrium during the adsorption process. Langmuir (Papers I-V), Sips (Papers I-V), Dubinin-Radushkevich (Paper II) and Freundlich (Paper V) isotherms were used for modeling the adsorption. Modeling calculations were conducted using Microsoft Office Excel 2007 software.

Langmuir model

The Langmuir model is a very simple theoretical model for monolayer adsorption onto a surface with a finite number of identical adsorption sites. The equation is applicable for homogeneous systems where the adsorption process has equal activation energy, based on the following basic assumptions: (a) molecules are adsorbed at a fixed number of well-defined localized sites, (b) each site can hold one adsorbate molecule, (c) all sites are energetically equivalent, and (d) there are no interactions between molecules adsorbed on neighbour sites.

The general Langmuir equation is written as follows:

$$q_e = \frac{q_m K_L C_e}{1 + K_L C_e} \qquad (3)$$

where q_e (mmol/g) is the equilibrium adsorption capacity and q_m (mmol/g) is the maximum amount of the ions adsorbed per unit weight of the adsorbent. The latter also describes a formation of the complete monolayer coverage on the surface at a high equilibrium H_2S concentration C_e (mmol/L) and practical limiting adsorption capacity. K_L (L/mmol) is the Langmuir equilibrium constant related to the affinity of the binding sites and also indicates the binding energy of the adsorption reaction between adsorbate and adsorbent.

Freundlich isotherm

The Freundlich expression is an empirical equation applicable for the non-ideal adsorption on heterogeneous surface as well as multilayer adsorption. The model is given as

$$q_e = K_f C_e^{1/nf} \qquad (4)$$

If the concentration of the solute in the solution at equilibrium, C_e, is raised to the power of 1/nf with the amount of solute adsorbed being q_e, $C_e^{1/nf}$ /q_e is constant at a given temperature. K_f is a relative indicator of adsorption capacity, while the dimensionless 1/nf indicates the energy or intensity of the reaction and suggests the favorability and capacity of the adsorbent/adsorbate system. According to the theory, nf > 1 represents favorable adsorption conditions.

Sips isotherm

The Sips isotherm model is a combination of the Langmuir and Freundlich isotherm type models and is expected to describe a heterogeneous surface much better than its two constituent models. At low adsorbate concentrations, the Sips isotherm approaches the Freundlich isotherm, whereas it approaches the Langmuir isotherm at high concentrations. The model can be written as:

$$q_e = \frac{q_m (K_S C_e)^{n_S}}{1 + (K_S C_e)^{n_S}} \qquad (5)$$

where q_m (mg/g) is the maximum amount of H_2S adsorbed per unit mass of adsorbent, K_S (L/mg), is the Sips constant related to the energy of adsorption, and n_S could be regarded as a parameter characterizing system heterogeneity.

The Dubinin-Radushkevich (D-R) isotherm model was applied to the data in order to deduce the heterogeneity of the surface energies of adsorption and the characteristic porosity of the adsorbent. The linear form of the D-R isotherm is given as follows:

$$lnq_e = lnq_D - B_D(RTln(1 + \frac{1}{C_e}))^2 \qquad (6)$$

The apparent energy of adsorption, E was calculated by

$$E = \frac{1}{(2B_D)^{1/2}} \qquad (7)$$

The constants q_D(mol/g) is the D-R constant representing the theoretical saturation capacity and B_D(mol^2/J^2) is a constant related to the mean free energy of adsorption per mol of the adsorbate, R is the ideal gas constant, (8.314 J/mol K) , T (K) is the temperature of adsorption and E (kJ/mol) is the mean free energy of adsorption per molecule of the adsorbate when transferred to the surface of the solid from infinity in solution.

Isotherm parameters were determined by minimizing the Sum of the Squares of the Errors (ERRSQ) function across the concentration range studied:

$$\sum_{i=1}^{p}\left(q_{\mathrm{e,exp}} - q_{\mathrm{e,calc}}\right)^2 \qquad (8)$$

5.5.2 Kinetic modeling

Investigating the mechanism of adsorption and its potential rate-controlling steps that include mass transport and chemical reaction processes, two kinetic models (pseudo-first-order and pseudo-second-order) were employed to analyze the experimental data (Papers IV and V).

The pseudo-first-order model is widely used for sorption in liquid/solid systems. To distinguish a kinetic equation based on the adsorption capacity of an adsorbent, the equation for the pseudo-first-order kinetics is presented as follows:

$$\frac{dq}{dt} = k_1(q_e - q) \qquad (9)$$

By integrating this particular equation at the boundary conditions q = 0 at t = 0 and q = q_t at t = t, this can be transformed into a logarithmic function as follows:

$$ln(q_e - q_t) = lnq_e - k_1 t \qquad (10)$$

where q_t and q_e are the adsorption capacity (mg/g) at time t (min) and at equilibrium respectively, while k_1 represents the pseudo-first-order rate constant (min^{-1}).

The pseudo-second-order model, which assumes that the rate-determining step may be a chemical surface reaction, is presented as follows:

$$\frac{dq}{dt} = k_1(q_e - q)^2 \qquad (11)$$

An integration of Eq. (6) at the boundary conditions, q = 0 at t = 0 and q = q_t at t = t, would give:

$$\frac{t}{q_t} = \frac{1}{k_2 q_e^2} + \frac{1}{q_e} t \qquad (12)$$

where q_t and q_e (mmg/g) represent the amount of metals adsorbed at time t (min) and at equilibrium, respectively, while k_1 (1/min) and k_2 (g /mmol min) are the rate constants of pseudo-first and pseudo-second order sorption. The initial adsorption rate (min) can be determined from k_2 and q_e values using:

$$h = k_2 q_e^2 \qquad (13)$$

To investigate if the film or pore diffusion was the controlling step in the adsorption, a model of intraparticle diffusion was tested as follows:

$$q_t = X + K_i t^{0.5} \qquad (14)$$

where q_t is the amount of metal ion adsorbed at time t, K_i is the intraparticle diffusion rate constant (mmol/g $min^{-0.5}$), and X represents the boundary layer diffusion effects.

6. RESULTS AND DISCUSSION

6.1 Characterization

The surface morphologies are important characteristics of adsorption materials. The morphological characteristic of the unmodified and modified MFC was investigated with FESEM (Papers I-V). SEM-images presented in Figure 11 show the differences between the surface morphology of studied adsorbents. The fibrous nanostructure of MFC remained largely unchanged after all modifications. FESEM images also verified that the structure of the adsorbent material was nano-sized (20- 50 nm). TEM analysis was used to confirm the distribution of iron nanoparticles on the surface of MFC (Paper V). High resolution TEM image (Figure 12a) shows overall structure of the studied material and dark field image (Figure 12b) locations of the nanoparticles. TEM analysis show that most of the material is composed of very short fibers indicating that hydrolysis of cellulose occurred during the modification step

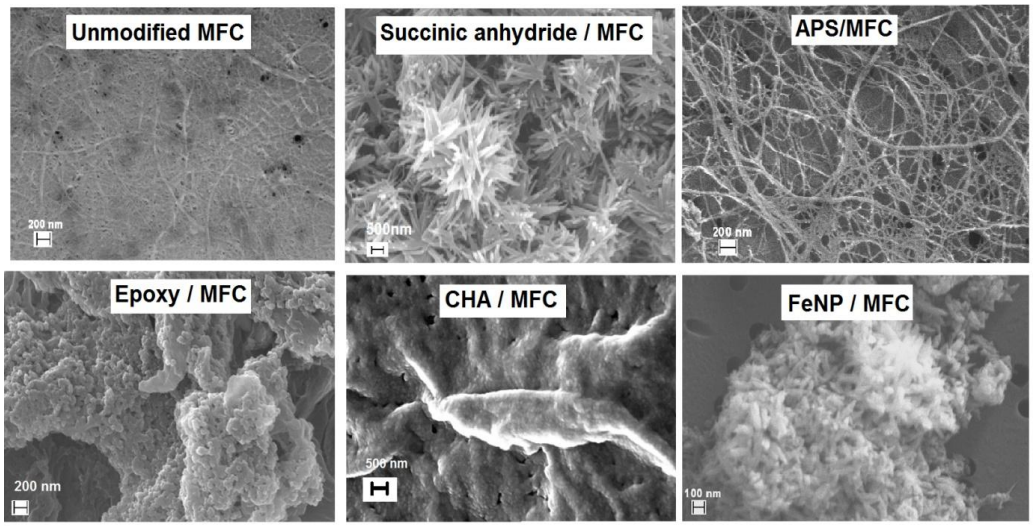

Figure 11. The SEM pictures of unmodified and modified MFC (Papers I-V)

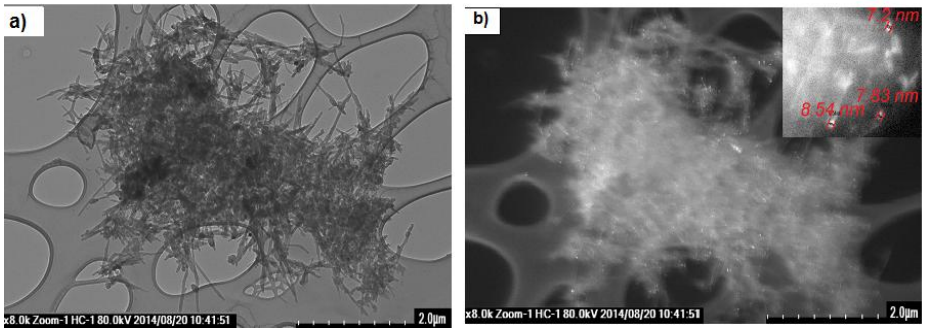

Figure 12. (a) High resolution and (b) dark field TEM images of FeNP/MFC.

The elemental analysis of the unmodified MFC and APS/MFC (Paper II), CHA or HAP/MFC (Paper II and IV) shows a high level of carbon (33.05 mol-% and 35.46 mol-%) and oxygen (66.51 mol-% and 60.70 mol-%), and a low level of hydrogen (0.44 mol-% and 0.46 mol-%) and nitrogen (3.43 mol-% only for APS modified MFC). After modification with aminosilane (APS/MFC), an obvious increase in nitrogen content corresponds to the introduction of amine groups on the cellulose surface. The most notable difference in the contents of elements was observed between the unmodified MFC and CHA or HAP/MFC. The level of carbon was much lower after modification and the levels of hydrogen and oxygen higher due to the high amount of the calcium caused by the modification. A clear relationship was found between the EDAX analysis and the elementary analysis. Low concentrations of C and high concentrations of Ca and P indicate that MFC can bind to a much larger amount of CHA than its own mass (Paper IV).

The isoelectric point was determined by zeta potential measurements for unmodified MFC, APS/MFC and Epoxy/MFC (Papers II and III). The isoelectric point for unmodified MFC was around pH 3.9; for APS/MFC the isoelectric point was found to be at pH 5.65 and for the Epoxy/MFC at a pH above 6.5. A change in isoelectric point after modification is caused by the new functional groups on the surface of the modified cellulose (amino and epoxy). The surface charge dependency on the solution pH of both unmodified and modified MFC followed a similar trend. A positive surface charge at an acidic pH indicated a protonation of the surface groups and negative surface charge in alkaline conditions the release of protons into the solution.

The functional groups on the adsorbent surface were analyzed by FTIR-spectroscopy (Papers I-V). The spectrum of unmodified MFC is shown in Figure 13. The band at around 2900 cm^{-1} belongs to O-H stretching, while the O-H bending mode of adsorbed water is registered at around 1640 cm^{-1}. The weak band at 1590 cm^{-1} confirms the presence of the COO− group. The other weak bands at 1428 cm^{-1} are assigned to HCH and OCH vibrations and the band at 1366 cm^{-1} to the CH bending mode. The band at 895 cm^{-1} corresponds to the COC, CCO and CCH deformation modes. Table 12 summarizes the characteristic absorption bands after different modifications. Furthermore, FTIR spectra after H_2S adsorption on APS/MFC, Epoxy/MFC and CHA or HAP/MFC as well as Ni(II), Cd(II), PO_4^{3-} and NO^{3-} adsorption was measured and adsorption mechanism confirmed from the change of bands (Papers III and IV, Table 12).

Table 12. The characteristic bands of modified MFC (Papers I-V).

Adsorbent	Wavelenght (cm^{-1})	Process
Succinic anhydride MFC	1724	Asymmetric and symmetric stretching of ester C-O
	1570 and 1415	Asymmetric and symmetric stretching vibrations – COO-
APS/MFC:	1625	Vibration and bending of N-H
	1350 - 1250	Bending of C-N
	1100 and 980	The –Si–O–Si– linkage and –Si–O– cellulose bond
	2574	SH stretching vibration modes appeared after H_2S adsorption
Epoxy/MFC	2930 and 2890	Asymmetric and symmetric stretching of CH_2 and CH_3 of the epoxy resin
	1608, 1580 and 1497	The benzene ring of epoxy or C-C stretching of aromatic ring
	1244 and 920	The C–O stretching of epoxide ring vibration
	1158, 1070 and 1022	The molecular vibrations of C—S bonds after H_2S adsorption

CHA or HAP/MFC	962-1023 and 562 -643	The asymmetric and symmetric stretching vibrations of PO_4^{3-}
	1420	The presence of carbonate (CO_3^{2-})
	2182-1996	The combination and overtone bands of PO_4^{3-} ions in the adsorbent
	2576	SH stretching vibration modes appeared after H_2S adsorption
	bi-modal peak at 1010 and 980 and peaks at 600- 560	Phosphate vibrations in Cd^{2+} and Ni^{2+} substituted CHA after adsorption
	1450-1370	The nitro-complex stretching after NO_3^- adsorption
FeNP/MFC	580	Vibration of the Fe-O bond

.

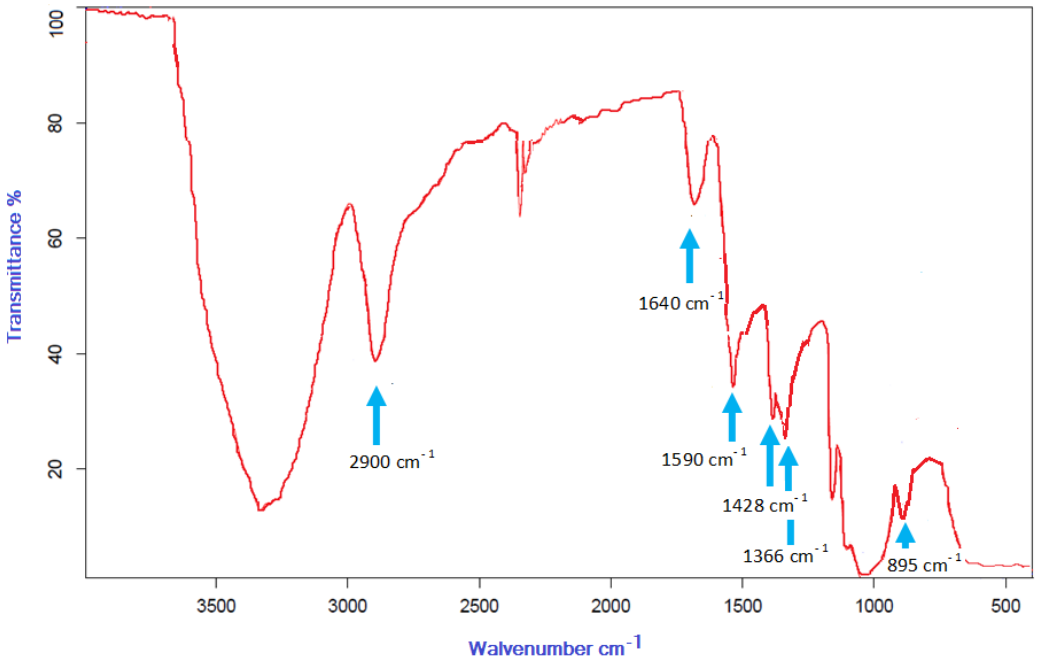

Figure 13. The FTIR-spectra of unmodified MFC

6.2 Adsorption studies

6.2.1 Effect of solution pH

The removal of metal ions from aqueous solutions by adsorption depends on the solution pH since the acidity of the solution affects the ionization of the metal ions and concentration of the counter H^+ ions of the surface groups. To maximize the removal of heavy metals by the adsorbents, knowledge of an optimum pH is important.

The adsorption efficiency of all studied metals, H_2S, PO_4^{3-} and NO_3^- ions were shown to be dependent on the solution pH (Papers I-V). A similar trend was observed for all metal ions, except As(V): adsorption efficiency increased with the increasing pH (Paper I, II, IV). At low pH, protons competed with metals for the adsorption sites and metal adsorption was inhibited. The maximum adsorption of metals occurred at a pH range of 3 to 7 for succinic anhydride modified MFC (Paper I). The optimum pH for Cd(II), Cu(II) and Ni(II) adsorption by APS/MFC was found to be in the pH range of 4–6 (Paper II) and for CHA or HAP/MFC, the

results illustrate that the pH does not affect the percentage removal of Ni(II), Cd(II), PO_4^{3-} and NO_3^- at pH 5 and above. However, at a pH below 5 it has a significant effect (Paper IV).

As(V) was strongly adsorbed on the Fe_3O_4/MFC surface from acidic solutions at pH 2. The acidic conditions caused the positive surface charge of the adsorbent and accordingly, made the surface more attractive to As(V), which is in $H_2AsO_4^-$ form at pH 2 and 5 (Paper V).

Adsorption efficiency increased when approaching a neutral pH and at pH<7, the adsorption efficiency was highest for all the adsorbents studied. This can be attributed to the increasing positive surface charge of the adsorbents with decreasing pH (surface protonation) making the surface more attractive for sulfide species (H_2S and HS^-) (Paper III).

6.2.2 Adsorption kinetics

In order to determine the equilibration time for the maximum adsorption of studied metals, PO_4^{3-} and NO_3^- on the modified MFC adsorbents, the adsorption was studied as a function of contact time (Paper I, II, IV and V).

In the case of succinic-anhydride-modified MFC at lower temperatures, diffusion was slowed down and therefore the increase of adsorption efficiency occurred later than at room temperature (Paper I). Figure 14 shows the effect of contact time on the adsorption of Zn(II), Ni(II), Cu(II), Co(II), Cd(II) and As(V) by modified MFC. The kinetic curve for the studied metal ions showed that the adsorption was initially rapid for all adsorbents. At the initial adsorption stage, the surface of all adsorbents contained many available active sites for metal binding and fast adsorption took place.

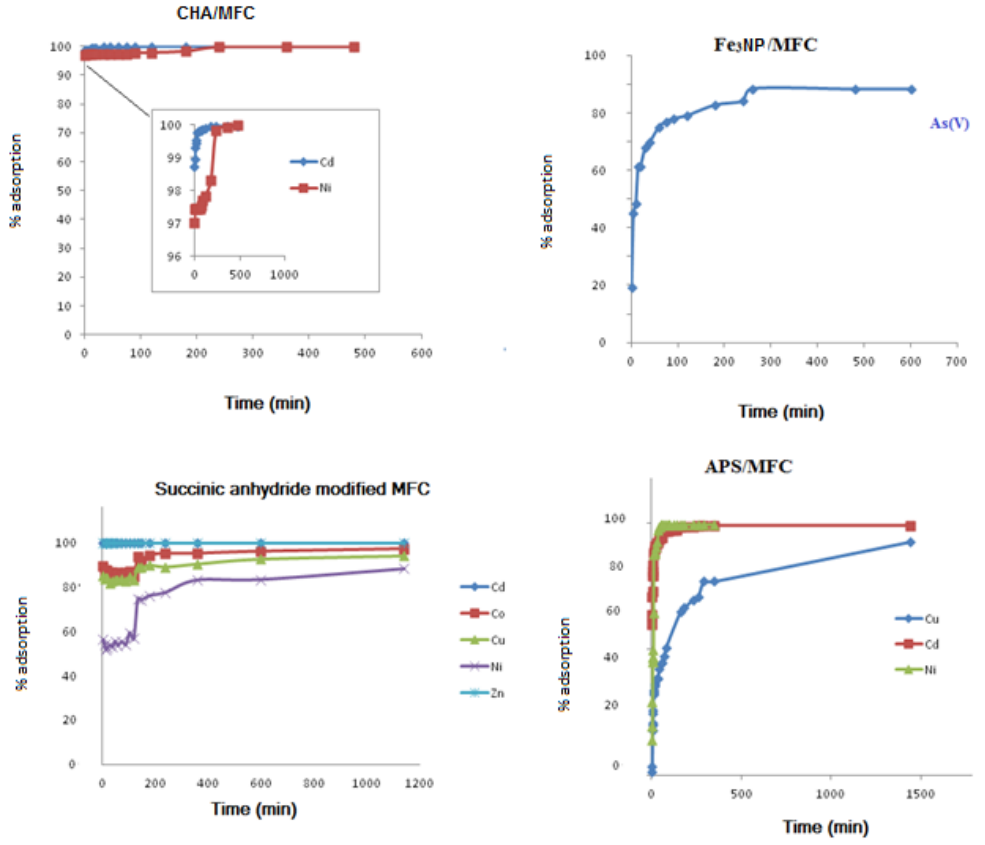

Figure 14. The effect of contact time on the adsorption of Zn(II), Ni(II), Cu(II), Co(II), Cd(II) and As(V) by modified MFC

Adsorption kinetics of PO_4^{3-} and NO_3^- from aqueous solutions by CHA/MFC was also fast; for PO_4^{3-} more than 85% and for NO_3^- more than 80% was adsorbed within 5 min (Paper IV). In the case of a multi-component solution of Ni(II), Cd(II), PO_4^{3-} and NO_3^-, the other components hardly affected the adsorption of Ni(II) and for Cd(II) ions, but the adsorption capacity of NO_3^- decreased drastically and the adsorption kinetics became irregular. This is due to the fact that metal solutions were prepared using metal nitrate salts for which reason the total nitrate concentration was much higher than the other compounds in the multi-component solution. Furthermore, the CHA/MFC residue contains some chlorides, which may have decreased the nitrate removal efficiency. Also for PO_4^{3-} maximum adsorption

capacity decreased and the equilibrium time became longer. This indicates that there are less adsorption sites for anions on the surface of CHA/MFC. Hence, PO_4^{3-} and NO_3^- have to compete with each other for the free adsorption sites. The removal capacity for the different ions on the CHA/MFC is in the order of Ni^{2+} ~ Cd^{2+} > PO_4^{3-} > NO_3^-. (Paper V).

The kinetics of Ni(II), Cd(II), PO_4^{3-} and NO_3^- adsorption on CHA/MFC (Paper V), As(V) adsorption kinetics on Fe_3O_4/MFC and Cd(II), Cu(II), and Ni(II) on the APS/MFC (Paper II) were also analyzed using pseudo-first-order and pseudo-second-order kinetic models.

The kinetic parameters for adsorption are given in Table 13. Based on the obtained correlation coefficients, the pseudo-second-order equation was the model that yielded the best fit for the experimental kinetic data with Ni(II), Cd(II) and Cu(II) for APS/MFC (Paper II). Both models were found to be in agreement with the experimental data and can be used to favorably explain the sorption of Ni(II), Cd(II), PO_4^{3-} and NO_3^- on CHA/MFC, but the pseudo-first-order model gave the best fit to the experimental data since $q_{e,exp}$ and $q_{e,model}$ were very close to each other (Paper IV). The pseudo-second-order model was better fitted with the experimental data since the calculated q_e was closer to the experimental one, and the correlation coefficient was 0.957 in the case of As(V) adsorption on FeNP/MFC (Paper V).

Table 13. Kinetic parameters for Cd(II), Cu(II), Ni(II). PO_4^{3-} and NO_3^-

CHA/MFC

		Pseudo-first-order			Pseudo-second-order		
Adsorbate	q_e (mmol/g)	q_t (mmol/g)	k_1 (1/min)	R^2	q_t (mmol/g)	k_2 (g/mg* min)	R^2
Cd(II)	0.495	0.494	4.58	1.000	0.495	158.70	1.000
Ni(II)	0.497	0.489	4.25	1.000	0.490	93.40	0.998
PO_4^{3-}	0.207	0.204	3.02	1.000	0.204	71.80	0.993
NO_3^-	0.415	0.415	1.00	1.000	0.451	1.56	0.998

APS/MFC

		Pseudo-first-order			Pseudo-second-order		
Adsorbate	q_e (mmol/g)	q_t (mmol/g)	k_1 (1/min)	R^2	q_t (mmol/g)	k_2 (g/mg* min)	R^2
Cd(II)	2.910	2.830	0.50	0.642	2.922	0.34	0.927
Cu(II)	2.930	2.320	0.02	0.798	2.561	0.01	0.895
Ni(II)	2.960	2.980	0.11	0.970	3.148	0.06	0.942

FeNP/MFC

		Pseudo-first-order			Pseudo-second-order		
Adsorbate	q_e (mmol/g)	q_t (mmol/g)	k_1 (1/min)	R^2	q_t (mmol/g)	k_2 (g/mg* min)	R^2
Cd(II)	1.413	4.92	0.99	0.854	4.27	0.04	0.957

6.2.3 Equilibrium studies

To determine the adsorption potential of modified MFC for Zn(II), Ni(II), Cu(II), Co(II), Cd(II), As(V), PO_4^{3-} and NO_3^-, the equilibrium adsorption was studied as a function of varying initial adsorbate concentration (Paper I-V). In the following sections, adsorption equilibria of different species are summarized and discussed.

6.2.3.1 Adsorption of metals

To determine the adsorption potential of modified MFC for Zn(II), Ni(II), Cu(II), Co(II), Cd(II) and As(V), the equilibrium adsorption was studied as a function of varying initial adsorbate concentration (Paper I, II, IV, V). Comparisons of metals adsorption on different adsorption materials are shown in Table 14. The highest adsorption capacity was obtained for APS/MFC.

Table 14. The maxium adsorption capacites for metal ions

	Adsorbents			
Type of metal	Succinic anhydride/MFC	APS/MFC	CHA/MFC	FeNP/MFC
	q_m (mmol/g)	q_m (mmol/g)	q_m (mmol/g)	q_m (mmol/g)
Zn(II)	1.610			
Ni(II)	0.744	2.734	2.021	
Cu(II)	1.900	3.150	1.224	
Co(II)	1.338			
Cd(II)	2.062	4.195		
As (V)				1.414

The adsorption equilibrium data of Zn(II), Ni(II), Cu(II), Co(II) and Cd(II) were analyzed using Langmuir and Sips isotherm models (Paper I and Table 10). The results in Table 10 show that the equilibrium data fit well with both the Sips and the Langmuir isotherms. However, q_m values estimated by the Sips model corresponded to the experimentally obtained values of $q_{m,exp}$ slightly better than those estimated by the Langmuir model. Moreover, the correlation coefficients for the Sips model were higher in most cases. The K_S indicated the highest affinity of Cd(II) and the other results are consistent with the Langmuir model.

In the isotherm studies of Ni(II), Cu(II), and Cd(II) ions adsorption on APS/MFC, the experimental maximum adsorption capacities ranged from 2.72 to 4.20 mmol/g (Paper II and Table 11). Langmuir, Sips and Dubinin-Radushkevich models were used to model the adsorption. The Sips isotherm model provided the best fit to the experimental adsorption data for these ions, revealing maximum adsorption capacities of 3.09, 2.59, and 3.47 mmol/L for Ni(II), Cu(II) and Cd(II), respectively.

The results of the adsorption study showed that CHA-modified MFC was very effective for Ni(II) and Cd(II) removal from an aqueous solution; the adsorption efficiency was > 90 % (Paper IV). The equilibrium isotherm data was fitted to the Langmuir and Sips models. The results in Table 10 show that for adsorbates, the q_m value estimated by the Sips model corresponded to the experimentally obtained $q_{m,exp}$ better than that estimated by the Langmuir model. For Ni(II), the Langmuir model seemed to provide a better approximation for q_m, but the R^2 values were higher for all the metals with the Sips model. The relatively poor correlation coefficients (R^2 values < 0.990) observed for all the metal ions with both the Langmuir and Sips models may be attributed to the unequal distribution of the adsorption surface area and active sites in samples due to the high water concentration of CHA/MFC. Very high K_L values of Ni^{2+} and Cd^{2+} ions correlated well with their fast adsorption.

Fe^0-bearing materials are widely used in arsenic adsorption because of the selectivity and affinity of Fe^0 toward inorganic arsenic species. Therefore, only the adsorption of As(V) was studied using Fe^0-bearing adsorbent (Paper V). The maghemite nanoparticles (Fe_3O_4)-modified MFC showed greatly improved uptake properties of As(V). As shown in Table 10, according to the correlation coefficients (R^2), the order of the three models used was Langmuir, Freundlich and Sips. Thus, the Langmuir model was the most suitable to describe the adsorption process of arsenic onto an adsorbent and the adsorption was a monolayer adsorption process. The maximum adsorption capacity (q_m) for As(V) from the Langmuir model was 2.460 mmol/g. The values of R_L, which denotes the adsorption nature, were calculated. The results (0.706–0.964) indicated that the adsorption process was favorable. Furthermore, the value of 1/n obtained (Table 15) from the Freundlich model was less than 1, which also revealed the favorable adsorption of arsenic onto an adsorbent. Comparison of the adsorption capacities of Fe^0 nanoparticles and FeNP/MFC for the removal of As(V) observed that the capacities of FeNP/MFC was relatively higher. The maximum adsorption Langmuir capacity is 2.460 mmol As(V)/g for FeNP/MFC and 0.042 mmol As(V)/g for Fe^0. These results are consistent with the results of some other Fe^0 nanoadsorbents for arsenate removal with batch experiments [178]

Table 15. The isotherm modeling parameters for metal ions

Adsorbent	Type of metal	Modeling parameters			
			Langmuir		
		$q_{m,}$(mmol/g)	K_L	R^2	
	Ni(II)	1.500	59.213	0.902	
	Cu(II)	0.716	12.318	0.964	
	Co(II)	1.879	58.889	0.849	
	Cd(II)	1.304	3.548	0.984	
Succinic	Zn(II)	1.954	691.004	0.923	
anhydride/MFC			**Sips**		
		$q_{m,exp}$ (mmol/g)	n_s	K_S	R^2
	Ni(II)	1.600	0.426	53.677	0.864
	Cu(II)	0.722	0.737	10.335	0.977
	Co(II)	1.828	0.808	56.190	0.857
	Cd(II)	1.321	0.737	3.256	0.991
	Zn(II)	1.954	0.579	555.179	0.962
			Langmuir		
		q_m (mmol/g)	K_L	R^2	
	Cd(II)	3.611	61.298	0.892	
	Cu(II)	3.078	4.072	0.770	
	Ni(II)	2.663	52.194	0.969	
APS/MFC			**Sips**		
		q_m (mmol/g)	n_s	K_S	R^2
	Cd(II)	3.472	1.100	53.667	0.894
	Cu(II)	2.593	2.387	5.761	0.965
	Ni(II)	3.092	1.038	62.973	0.970
			Dubinin-Radushkevich		
		q_D (mmol/g)	B_d	E	R^2
	Cd(II)	1.445	0.007	8.111	0.964
	Cu(II)	1.446	0.007	8.379	0.805
	Ni(II)	1.048	0.007	8.392	0.981
			Langmuir		
		q_m(mmol/g)	K_L	R^2	
	Ni^{2+}	2.277	293.040	0.931	
	Cd^{2+}	1.028	676.279	0.878	

			Sips		
		q_m (mmol/g)	n_s	K_S	R^2
	Ni^{2+}	0.616	0.735	5.984	0.965
CHA/MFC	Cd^{2+}	1.688	0.293	1.950	0.917
			Langmuir		
		q_m(mmol/g)	K_L	R^2	
FeNP/MFC	As(V)	2.460	0.167	0.968	
			Sips		
		q_m (mmol/g)	n_s	K_S	R^2
	As(V)	6.282	0.019	0.866	0.919
			Freudlich		
		K	n (1/n)	R^2	
	As(V)	0.296	1.167 (0.857)	0.968	

6.2.3.2 Adsorption of H_2S

In the adsorption study of H_2S, the experimental maximum adsorption capacities were 104.0, 13.4 and 12.7 mg/g for APS/MPS, HAP/MPS and Epoxy/MPS, respectively. The adsorption mechanisms were analyzed by the Langmuir, Freundlich and Sips isotherm models. The results of the isotherm modeling are shown in Table 16. The poor fitting results of the isotherm models tested may be attributed to the high water concentration of the used adsorbents. Wet adsorbents were used in this study because a dry modified MFC became very hard and lost its adsorption capacity. When wet adsorbent was used, it was difficult to know the exact water concentration of the adsorbent. Therefore, the samples were not homogenous with regard to the adsorbent. Furthermore, the volatility of H_2S could also affect the fitting results. Reference samples were used for detecting the volatility and the average volatility was +/- 0.44 mg/L per sample. The values of R_L were very close to unity for all the adsorbents and concentrations, suggesting that the APS/MFC, HAP/MFC and Epoxy/MFC are favorable for the adsorption of H_2S under conditions used in this study. These results are consistent with the Freundlich model, which gave nf > 1 for all the adsorbents suggesting favorable adsorption.

Table 16. The results of the isotherm modeling for H_2S.

APS/MFC			
	Langmuir		
q_m (mg/g)	K_L (L/mg)		R^2
1807.564	0.000967		0.759
	Freundlich		
	K_f	n_f	R^2
	1.215150	1.081	0.644
	Sips		
q_m (mg/g)	K_S (L/mg)	ns	R^2
0.513	0.816887	1.081	0.677
HAP/MFC			
	Langmuir		
q_m (mg/g)	K_L (L/mg)		R^2
1549.752	0.000148		0.687
	Freundlich		
	K_f	n_f	R^2
	0.005306	2.062	0.770
	Sips		
q_m (mg/g)	K_S (L/mg)	n_s	R^2
709.476	0.003689	2.180	0.770
Epoxy/MFC			
	Langmuir		
q_m (mg/g)	K_L (L/mg)		R^2
1267.150	0.000269		1.000
	Freundlich		
	K_f	n_f	R^2
	0.004806	2.268	0.959
	Sips		
q_m (mg/g)	K (L/mg)	n_s	R^2
173.170	0.010727	2.390	0.958

6.2.3.3 Adsorption of PO_4^{3-} and NO_3^-

The results of the adsorption study showed that CHA-modified MFC was very effective for PO_4^{3-} removal from an aqueous solution; the adsorption efficiency was > 90%. The adsorption efficiency for NO_3^- was > 50% (Paper IV). Equilibrium isotherm data was fitted using the Langmuir and Sips models (Table 17). Among these models, the Sips model was in good agreement with the experimental data with high R^2 values.

Table 17. The modeling parameters for PO_4^{3-} and NO_3^-.

		Langmuir			
Adsorbate	$q_{m,exp}$ (mmol/g)	q_m(mmol/g)	K_L	R^2	
PO_4^{3-}	0.843	0.911	6.995	0.977	
NO_3^-	0.209	0.180	3.665	0.561	
		Sips			
Adsorbate	$q_{m,exp}$ (mmol/g)	q_m (mmol/g)	n_s	K_S	R^2
PO_4^{3-}	0.843	0.974	0.673	4.559	0.979
NO_3^-	0.209	7.591	4.538	2.945	1.000

6.2.3.4 Adsorption of Ni(II), Cd(II), PO_4^{3-} and NO_3^- in multi component solution

Adsorption of Ni(II), Cd(II), PO_4^{3-} and NO_3^- were also studied with solutions containing all components at three different initial concentrations: 0.5, 2.5 and 5 mmol/L, and NO_3^- for 1.8, 9.0 and 18 mmol/L (due to the nitrate content of metal solutions). These experiments confirm the effectiveness of CHA/MFC in Ni(II) and Cd(II) cases; no differences can be observed for the adsorption efficiency. Considering the removal efficiencies for PO_4^{3-} and NO_3^- , the adsorption efficiency was much higher for the one adsorbate solution. This indicates that there are fewer adsorption sites for anions on the surface of CHA/MFC, due to mutual competition between PO_4^{3-} and NO_3^-.

6.3 Adsorption mechanism

Papers II, IV and V present the suggested adsorption mechanisms of metal ions for APS/MFC, CHA/MFC and Fe_3O_4/MFC.

In the case of APS/MFC (Paper II) the amino groups are mainly responsible for the uptake of Cd(II), Cu(II) and Ni(II) ions as follows:

$$M^{2+} + RNH_2^+ \rightarrow M(RNH_2)^{2+} \qquad (15)$$

However, aminosilane-modified MFC was able to adsorb metals because of the amino ($-NH_2$) on aminosilane and/or hydroxyl (-OH) groups on cellulose fiber. Nitrogen and oxygen atoms have free electron doublets that can react with metal cations.

Another possible mechanism is the ion-exchange reaction of M^{2+} with the surface hydroxyl groups via the Si–O–M–O–Si bridging species (shown in Paper II, Figure 9). It is also possible that metal ions might react with one amine group and ion-exchange with an adjacent hydroxyl group (shown in Paper II, Figure 9).

In the case of CHA/MFC, the ion-exchange between the calcium and the bivalent ion is a possibility. The heavy metal replaces the calcium in the CHA lattice, according to the reaction:

$$Ca_{10}(PO_4)_6(OH)_2 + xMe^{2+} \leftrightarrow (Ca_{10-x})Me_x(PO_4)_6(OH)_2 + xCa^{2+} \quad (16)$$

Dissolution - precipitation is another suggested mechanism, which takes place in two steps: firstly, CHA is dissolved in solution; subsequently, the phosphate ion reacts with the metal to form a new insoluble phase. This mechanism is shown in the reactions below:

$$Ca_{10}(PO_4)_6(OH)_2 + 14H^+ \leftrightarrow 10Ca^{2+} + 6H_2PO_4^- + 2H_2O \quad (17)$$

$$10Me^{2+} + 6H_2PO_4^- + 2H_2O \leftrightarrow Me_{10}(PO_4)_6(OH)_2 + 14H^+ \quad (18)$$

Furthermore, FTIR-measurements confirmed the reaction between metal ions and phosphate groups (bi-modal phosphate peak in FTIR-spectra).

The adsorption of PO_4^{3-} and NO_3^- were also confirmed by FTIR-measurements (Paper IV). The adsorption of PO_4^{3-} does not induce any major changes in the FTIR spectra of CHA/MFC, however, the peaks of PO_4^{3-} are more intensive after adsorption due to an increase in the amount of phosphate. The adsorption of NO_3^- caused the new bands at around 1450-1370 cm^{-1} , which can be assigned to the nitro-complex stretching.

Paper V presents that the adsorption properties of Fe^0 are mainly due to the presence of OH_2^+, OH^-, and O^- functional groups on the adsorbent's surface. Fe^0 surface develops surface charges due to the different pH of water and, by adsorbing metal ions, completes coordination shells with OH groups, which either bind to or release H^+. At neutral and acidic conditions (less than 8), OH_2^+ and OH forms on surfaces are dominant and responsible for the selective binding of molecular and ionic forms of arsenic species.

As(V) adsorption onto hydrated Fe oxide/hydroxide from an aqueous solution can be expressed by the following formulae:

$$MFC - FeOH(s) + H_3AsO_{4(aq)} \leftrightarrow MFC - FeAsO_4^- + H^+_{(aq)} + H_2O \quad (19)$$

$$MFC - FeOH(s) + H_3AsO_{4(aq)} \leftrightarrow MFC - FeAsO_4^{2-} + 2H^+_{(aq)} + H_2O \quad (20)$$

The results of pH studies confirmed the observations above. EDX results provided evidence of the interaction between arsenic and nano-magneitc particles moieties resulting in the formation of the $FeAsO_4^{2-}$-complex.

6.4 Regeneration study

In Paper I, Zn(II), Ni(II), Co(II) and Cd(II) were desorbed from succinic-anhydride-modified nanocellulose using 1M nitric acid. Zn(II) ions desorption from the adsorbent was also conducted using 1M formic acid, 1M ascorbic acid and 1M acetic acid. After the first cycle of regeneration, the adsorption capacities of the adsorbents for Zn(II), Ni(II),Co(II) and Cd(II) decreased 11-25% and after second cycle they decreased 72-86%. The result also suggests that 15 s ultrasonic treatments after HNO_3 could effectively regenerate the adsorbent with regeneration efficiencies ranging from 96% to 100%.

In the study of Cd(II), Cu(II) and Ni(II) desorption from APS-modified MFC, 0.1 M HNO_3, 0.1 M NaOH and 0.1 M EDTA were used (Paper II). The results showed that the adsorption capacity remained the same or even improved after treatment with NaOH. After the first cycle of regeneration, the adsorption capacities of the adsorbents for Ni(II), Cu(II) and Cd(II) still remained the same. These results indicate the suitability of an alkaline regenerant for APS-modified MFC.

Ni(II) and Cd(II) were desorbed from CHA/ MFC using 0.01 M, 0.1M and 1.0 M HNO_3, and PO_4^{3-} and NO_3^- were desorbed using 0.01 M, 0.1M and 1 M NaOH. The adsorption efficiency

for metals was radically affected by regeneration with 0.1 M and 1 M HNO_3; the adsorbent lost its adsorption capacity completely. The results showed that 0.01 M HNO_3 is a potential regenerant for Cd(II): the adsorption capacity remained the same for Cd(II) after the fourth cycle. For Ni(II) the adsorption capacity decreased after every treatment; for the first cycle it was 99.7%, but after four cycles, the regeneration efficiency was 24.48% using 0.01 M HNO_3 as regenerant. Also for $PO_4^{3-,}$ adsorption capacity decreased after every treatment; from 64.2 % to 15.2 % during four treatments with 0.01 M NaOH. In general, it can be concluded that the weaker acid (0.01 M HNO_3) is a more effective regenerant for metals and the weaker base (0.01 M NaOH) is a more effective regenerant for PO_4^{3-}. The results showed that NO_3^- is not regeneration viable at all.

The results of the regeneration study in Paper V indicate that FeNP/MFC could not be used repeatedly using an adsorption–desorption cycle when NaOH was used as regenerant. After four cycles, the regeneration efficiency decreased by as much as 98 %. However, nanomaterials as adsorbents do not produce large volumes of waste sludge when disposal is a competitive option compared to the recycling of the used adsorbent. The results of regeneration studies for all of the studied adsorbents are summarized in Table 18.

Table 18. Ther results of regeneration studies.

Succinic Anhydride/MFC				
Type of adsorbate	Type of regenerant	No. Of cycle	Regeneration efficiency (%)	
Zn(II)	HNO_3 (0.1M)	2	95.28	
Ni(II)	HNO_3 (0.1M)	2	95.76	
Cu(II)	HNO_3 (0.1M)	2	106.25	Paper I
Co(II)	HNO_3 (0.1M)	2	106.25	
Cd(II)	HNO_3 (0.1M)	2	95.52	
APS/MFC				
Type of adsorbate	Type of regenerant	No. Of cycle	Regeneration efficiency (%)	
Ni(II)	NaOH (0.1M)	2	155.34	
Cu(II)	NaOH (0.1M)	2	110.82	Paper II
Cd(II)	NaOH (0.1M)	2	101.20	
CHA/MFC				
Type of adsorbate	Type of regenerant	No. Of cycle	Regeneration efficiency (%)	
Ni(II)	HNO_3 0.01M	4	24.48	
Cu(II)	HNO_3 0.01M	4	99.98	Paper IV
PO_4^{3-}	NaOH 0.01M	4	12.52	
NO_3^-	NaOH 0.01M	3	7.92	
FeNP/MFC				
Type of adsorbate	Type of regenerant	No. Of cycle	Regeneration efficiency (%)	
As(V)	NaOH(0.1M)	4	69.16	Paper V

7. CONCLUSIONS

The adsorptive removal of Zn(II), Ni(II), Cu(II), Co(II), Cd(II), As(V), H_2S, PO_4^{3-} and NO_3^- from aqueous solutions by five different nanostructured microfibrillated cellulose-based adsorbents was investigated in this thesis. The model adsorbents that were employed to study the adsorptive behavior of nanocellulose-based adsorbents were succinic-anhydride-modified mercerized nanocellulose for metal removal, aminosilane-modified nanostructured microfibrillated cellulose for hydrogen sulfide and metals removal, epoxy-modified nanostructured microfibrillated for hydrogen sulfide removal, hydroxyapatite-modified nanostructured microfibrillated cellulose for hydrogen sulfide, metals, phosphate and nitrate removal, and Fe^0 nanomagnetic-particle-activated microfibrillated cellulose for arsenate removal.

The adsorbents were characterized by FTIR, Elementary analyzer and SEM for verifying the functional groups of the surfaces and the surface morphology. The fibrous nanostructure of MFC remained largely unchanged after modifications. Hence, there were enough sites for the studied ion adsorption on the surface. Overall, the SEM analysis showed rather different surface morphologies due to different modifications.

Batch adsorption studies were conducted in order to optimize the experimental conditions to achieve maximum removal efficiencies. Overall, the studied adsorbents showed potential utility for the adsorption of the studied compounds. Modeling adsorption isotherms and adsorption kinetics gave information about the adsorbents' surface properties and the adsorption mechanism. In this study, various isotherm models were used to find the best fitting equations. The major results and findings of this thesis are presented below:

1. The use of succinic-anhydride-modified mercerized nanocellulose and aminosilane-modified nanostructured microfibrillated cellulose for removal of heavy metals from aqueous solutions exhibited promising results. The adsorption of metal ions was shown to be dependent on the solution pH. The kinetic studies demonstrated that during short contact times, adsorption by adsorbents was very fast for all the metals.

2. The results obtained for H_2S removal studies exhibited that aminosilane, epoxy and hydroxyapatite-modified nanostructured microfibrillated cellulose can be used as promising alternatives for H_2S removal from aqueous solutions. The bonding of H2S through the surfaces of the adsorbents are shown by the ATR-FTIR analysis.

3. Carbonated-hydroxyapatit$_e$-modified nanocellulose exhibited the ability to remove cations and anions using the same adsorbent. The results of adsorption study showed that the adsorbent was ve$_r$y effective for Ni(II), Cd(II) and PO_4^{3-} removal from an aqueous solution; the adsorption efficiency was > 90%. The adsorption efficiency for NO_3^- was > 50%. The results of the adsorption kinetic study indicate that adsorption was very fast for all the studied compounds. The competing anions, especially chloride and phophate, adversely affected the nitrate removal by competing with nitrate for similar binding sites.

4. The maghemite nanoparticles (Fe^0)-modified MFC was found to be a highly promising adsorbent for removal of As(V) from an aqueous solutions due to its magnetic properties, high surface area and a high adsorption capacity. The adsorption of As(V) was found to be effective at the lower pH range; maximum adsorption capacity was found to be the highest at pH 2. A comparison of the adsorption capacities of Fe^0 nanoparticles and FeNP/MFC for the removal of As(V) inidicated that the capacities of FeNP/MFC were relatively higher.

The research results of this thesis can be used as a foundation for future research in which modified MFC adsorbents can be employed in pilot/full-scale applications. In addition to batch studies, column studies are needed. Future investigations will focus upon the adsorption studies of various solution matrices, such as real wastewater samples for example. Multi-pollutant removal from municipal wastewater is a major challenge and an interesting matrix for adsorption studies. If nanocellulose-based adsorbents are used in full-scale applications, significantly higher amounts of adsorbents are needed for preparation, which brings more challenges to the process.

REFERENCES

1. Fu, F., Wang, Q., Removal of heavy metal ions from wastewaters: A review Journal of Environmental Management 92 (2011) 407-418.

2. Keng, P. -S., Lee, S - L., Ha, S. -T., Hung, Y. -T., Ong, S. -T., Cheap Materials to Clean Heavy Metal Polluted Waters, in: E. Lichtfouse et al. (eds.), Green Materials for Energy, Products and Depollution, Environmental Chemistry for a Sustainable World 3, Springer Science+Business Media Dordrecht, 2013, pp. 339-351.

3. Gupta, V. K., Ali, I., Water Treatment for Inorganic Pollutants by Adsorption Technology, Environmental Water (2013) 29-91.

4. Kurniawan, T.A., Chan, G.Y.S., Lo, W.H., Babel, S., Physico–chemical treatment techniques for wastewater laden with heavy metals, Chemical Engineering Journal 118 (2006) 3–98.

5. Krishnamurthy, N., Vallinayagam, P., Madhavan, D., Engineering Chemistry, Prentice-Hall Of India Pvt. Ltd., New Delhi (2007) pp. 58-59..

6. Mohammadi, T., Mohebb, A., Sadrzadeh, M., Razmi, A., Modeling of metal ion removal from wastewater by electrodialysis. Separation and Purifcation Technology 41 (2005) 73–82.

7. Babel, S., Kurniawan, T. A., Cost adsorbents for heavy metals uptake from contaminated water: a review, Journal of Hazardous Materials 97 (2003) 219-243.

8. Henriksson M, Berglund L.A., Structure and properties of cellulose nanocomposite films containing melamine formaldehyde, Journal of Applied Polymer Science 106 (2007) 2817–2824.

9. O'Connell, D.W., Birkinshaw, C., O'Dwyer, T.F., Heavy metal adsorbents prepared from the modification of cellulose: a review. Biores.Technol. 99 (2008) 6709–6724.

10. Faruk, O., Bledzki,A. K., Fink, H-P., Sain, M., Biocomposites reinforced with natural fibers: 2000–2010, Progress in Polymer Science 37 (2012) 1552– 1596.

11. Siro, I., Plackett, D., Microfibrillated cellulose and new nanocomposite materials: a review, Cellulose 17 (2010) 459–494.

12. Hon, D. N. S., (1996) Cellulose and its derivatives. In: Dumitriu S (ed) Polysaccharides in medicinal applications. Marcel Dekker, New York.

13. Wan Ngah, W. S., Hanafiah, M. A. K. M., Removal of heavy metal ions from wastewater by chemically modified plant wastes as adsorbents: A review, Bioresource Technology 99 (2008) 3935–3948.

14. Wojnarovits, L., Foldvary, Cs. M. Takacs, E., Radiation induced grafting of cellulose for adsorption of hazardous water pollutants: A review, Radiation Physics and Chemistry 79 (2010) 848–862.

15. Kubota, H., Shigehisa, Y., Introduction of amidoxime groups into cellulose and its ability to adsorb metal ions, Journal of Applied Polymer Science 56 (1995) 147–151.

16. Peng, T., Cheng, Y.L., PNIPAAm and PMAA cografted porous PE membranes: living radical co-grafting mechanism and multi-stimuli responsive permeability, Polymer 42 (2001) 2091–100.

17. Bellobono, I. R., Calgari, S., Leonari, M. C, Selli, E., Paglia, E. D., Photochemical grafting of acrylated azo dyes onto polymeric surfaces. IV. Grafting of 4-(N-ethyl N-2-acryloxyethyl) amino-40 nitroazobenzene onto cellulose, Die Angewandte Makromolekurare Chemie 100 (1981) 135–46.

18. Kubota, H., Suka, I. G., Kuroda, S., Kondo, T., Introduction of stimuli-responsive polymers into regenerated cellulose film by means of photografting, European Polymer Journal 37 (2001) 1367–1372.

19. Bhattacharya, A., Misra, B.N., Grafting: a versatile means to modify polymers: techniques, factors and applications, Progress in Polymer Science 29 (2004) 767–814.

20. Kubota, H., Suzuki, S., Comparative examinations of reactivity of grafted celluloses prepared by ultra violet and ceric salt-initiated graftings, European Polymer Journal 31 (1995) 701–704.

21. Hemvichian, K., Chanthawong, A., Suwanmala, P., Synthesis and characterization of superabsorbent polymer prepared by radiation-induced graft copolymerization of acrylamide onto carboxymethyl cellulose for controlled release of agrochemicals, *Radiation Physics and Chemistry*, *103 (2014)167-171.*

22. Desmet, G., Takács, E., Wojnárovits, L., Borsa, J., Cellulose functionalization via high-energy irradiation-initiated grafting of glycidyl methacrylate and cyclodextrin immobilization, Radiation Physics and Chemistry 80(2011)1358-1362.

21. Yamada, K., Nagano, R., Hirata, M., Adsorption and desorption properties of the chelating membranes prepared from the PE films, Journal of Applied Polymer Science 99 (2006) 1895–1902.

22. Yamada, K., Saitoh, Y., Haga, Y., Matsuda. K., Hirata, M., Adsorption and desorption properties of grafted polyethylene films modified with polyethylenimine chains, Journal of Applied Polymer Science 102 (2006) 5965–5976.

23. Waly, A., Abdel-Mohdy, F.A., Aly, A. S., Hebeish, A., Synthesis and characterization of cellulose ion exchanger. II. Pilot scale and utilization in dye–heavy metal removal, Journal of Applied Polymer Science 68 (1998) 2151–2157.

24. Nasef, M.M., El-Sayed, A.H., Preparation and applications of ion exchange membranes by radiation-induced graft copolymerisation of polar monomers onto non-polar films, Progress in Polymer Science 29 (2004) 499–561.

25. Chen, J., Iwata, H., Maekawa, Y., Yoshida, M., Tsubokawa, N., Grafting of polyethylene by g-radiation grafting onto conductive carbon black and application as novel gas and solute sensors, Radiation Physics and Chemistry, 67 (2003) 397–401.

26. Kumar, V., Bhardway, Y.K., Rawat, K.P., Sabharwal, S., Radiation-induced grafting of vinylbenzyltrimethylammonium chloride (VBT) onto cotton fabric and study of its anti-bacterial activities, Radiation Physics and Chemistry 73 (2005) 175–182.

27. Goel, N.K., Rao, M.S., Kumar, V., Bhardwaj, Y.K., Chaudhari, C.V., Dubey, K.A., Sabharwal, S., Synthesis of antibacterial cotton fabric by radiation- induced grafting of [2-(methacryloyloxy)ethyl]trimethylammonium chloride (MAETC) onto cotton, Radiation Physics and Chemistry 78 (2009) 399–406.

28. Roy, D., Semsarilar, M., Guthrie, J.T., Perrier, S., Cellulose modification by polymer grafting: a review, Chemical Society Reviews 38 (2009) 2046–2064.

29. Chauhan, G.S., Guleria, L., Sharma, R., Synthesis, characterization and metal sorption studies of graft copolymers of cellulose and glycidyl methacrylate and some comonomers, Cellulose 12 (2005) 97–110.

30. Tamada, M., Seko, N., Yoshii, F., Application of radiation-graft material for metal adsorbent and crosslinked natural polymer for healthcare product, Radiation Physics and Chemistry 71 (2004) 223–227.

31. Zhang, A.Y., Asakura, T., Uchiyama, G., The adsorption mechanism of uranium(VI) from seawater on a macroporous fibrous polymeric adsorbent containing amidoxime chelating functional groups, React. Funct. Polym. 57 (2003) 67–76.

32. Othman, S.H., Sohsah, M.A., Ghoneim, M.M., The effects of hazardous ions adsorption on the morphological and chemical properties of reactive cloth filter, Radiation Physics and Chemistry 78 (2009) 976–985.

33. Othman, S.H., Sohsah, M.A., Ghoneim, M.M., Sokker, H.H., Badawy, S.M., El-Anadouli, B.E., Adsorption of hazardous ions from radioactive waste on chelating cloth filter, Radiation Physics and Chemistry 75 (2006) 278–286.

34. Badawy, S.M., Sokker, H.H., Othman, S.H., Hashem, A., Cloth filters for recovery of uranium from radioactive waste, Radiation Physics and Chemistry 73 (2005) 125–130.

35. Bao-Xiu, Z., Peng, W., Tong, Z., Chun-yun, C., Jing, S., Preparation and adsorption performance of a cellulosic adsorbent resin for copper(II), Journal of Applied Polymer Science 99 (2006) 2951–2956.

36. Orlando, U.S., Baes, A., Nishijima, W., Okada, M., Preparation of chelating agents from sugarcane bagasse by microwave radiation as an alternative ecologically benign procedure, Green Chemistry 4 (2002) 555–557.

37. Abdel-Aal, S.E., Gad, Y.H., Dessouki, A.M., The use of wood pulp and radiation-modified starch in wastewater treatment, Journal of Applied Polymer Science Sci. 99 (2006) 2460–2469.

38. Bhattacharya, A., Das, A., De, A., Structural Influence on grafting of acrylamide based monomers on cellulose acetate, Indan Journal of Chemical Technology 5 (1998) 135–138.

39. Bhattacharya, A., Misra, B.N., Grafting: a versatile means to modify polymers: Techniques, factors and applications, Progress in Polymer Science 29 (2004) 767–814.

40. Shibi, I. G., Anirudhan, T. S., Polymer-grafted banana (Musa paradisiaca) stalk as an adsorbent for the removal of lead(II) and cadmium(II) ions from aqueous solutions: kinetic and equilibrium studies, Journal of Chemical Technology and Biotechnology 81 (2006) 433–444.

41. Okieimen, F. E., Sogbaike, C. E., Ebhoaye, J. E., Removal of cadmium and copper ions from aqueous solution with cellulose graft copolymers, Separation and Purification Technology 44 (2005) 85–89.

42. Eromosele, I. C., Bayero, S. S, Adsorption of chromium and zinc ions from aqueous solutions by cellulosic graft copolymers, Bioresource Technology 71 (2000) 279-281.

43. Guclu, G. Gurdag, G., Ozgumus, S., Competitive removal of heavy metal ions by cellulose graft copolymers, Journal of Applied Polymer Science 90 (2003) 2034–2039.

44. Aoki, Y., Tanaka, K., Sakamoto, M., Furuhata, K., Sorption of metal ions by bead cellulose grafted with amidoximated polyacrylonitrile, Sen'i Gakkaishi 55 (12) (1999) 569–575.

45. O'Connell, D.W., Birkinshaw, C., O'Dwyer, T.F., A chelating cellulose adsorbent for the removal of Cu(II) from aqueous solution. Journal of Applied Polymer Science Sci. 99 (2006) 2888–2897.

46. O'Connell, D.W., Birkinshaw, C., O'Dwyer, T.F., Removal of lead(II) from aqueous solution using a modified cellulose adsorbent, Adsorption Science and Technology, 24 (2006) 337–347.

47. O'Connell, D.W., Birkinshaw, C., O'Dwyer, T.F., A modified cellulose adsorbent for the removal of nickel(II) from aqueous solutions, Journal of Chemical Technology and Biotechnology 81 (2006) 1820–1828.

48. Navarro, R. R., Sumi, K., Matsumura, M., Improved metal affinity of chelating adsorbents through graft polymerization, Water Research 33 (1999) 2037–2044.

49. Anirudhan, T. S., Rauf, T.A., Adsorption performance of amine functionalized cellulose grafted epichlorohydrin for the removal of nitrate from aqueous solutions, Journal of Industrial and Engineering Chemistry 19 (2013) 1659-1667.

50. Anirudhan, T. S., Nima, J., Divya, P. L, Adsorption of chromium(VI) from aqueous solutions by glycidylmethacrylate-grafted-densified cellulose with quaternary ammonium groups, Applied Surface Science 279 (2013) 441– 449.

51. Çavuş, S., Gürdağ, G., Yaşar, M., Güçlü, K., Gürkaynak, M. L., The competitive heavy metal removal by hydroxyethyl cellulose-g-poly(acrylic acid) copolymer and its sodium salt: The effect of copper content on the adsorption capacity, Polymer Bulletin 57 (2006) 445–456.

52. Hajeeth, T., Vijayalakshmi, K., Gomathi, T., Sudha, P.N., Removal of Cu(II) and Ni(II) using cellulose extracted from sisal fiberand cellulose-g-acrylic acid copolymer, International Journal of Biological Macromolecules 62 (2013) 59–65.

53. Alila, S., Boufi, S., Removal of organic pollutants from water by modified cellulose fibres, Industrial Crops and Products 30 (2009) 93–104.

54. Misra. B. N., Dogra, R., Kaur, I., Jassal, J.K., Grafting onto cellulose. IV. Effect of complexing agents on Fenton's reagent ($Fe2^{+}$-H_2O_2)-initiated grafting of poly(vinyl acetate), Journal of Polymer Science Polymer Chemistry Edition 17 (1979) 1861–1863.

55. Zheng, L., Zhu, C., Dang, Z., Zhang, H., Yi, X., Liu, C., Preparation of cellulose derived from corn stalk and its application for cadmium ion adsorption from aqueous solution, Carbohydrate Polymers 90 (2012) 1008-1015.

56. Shibi, I. G., Anirudhan,T. S., Synthesis, characterisation, and application as a mercury(II) sorbent of banana stalk-polyacrylamide grafted copolymer bearing carboxyl groups, Industrial Engineering and Chemical Research 41 (2002) 5341–5352.

57. Bicak, N., Sherrington, D. C., Senkal, B. F., Graft copolymer of acrylamide onto cellulose as mercury selective sorbent, Reactive and Functional Polymers 41 (1999) 69–76.

58. Hashem, A., Amidoximated sunflower stalks (ASFS) as a new adsorbent for removal of Cu(II) from aqueous solution, Polymer–Plastics Technology and Engineering 45 (2006) 35–42.

59. Liu, M., Deng, Y., Zhan, H., Zhang, X., Adsorption and desorption of copper(II) from solutions on new spherical cellulose adsorbent, Journal of Applied Polymer Science 84 (2002) 478–485.

60. Liu, M., Deng, Y., Zhan, H., Zhang, X., Liu, W., Zhan, H., Removal and recovery of chromium(III) from aqueous solutions by a spheroidal cellulose adsorbent, Water Environmental Research 73 (3) (2001) 322–328.

61. Gaey, M., Marchetti, V., Clement, A., Loubinoux, B., Gerardin, P., Decontamination of synthetic solutions containing heavy metals using

chemically modified sawdusts bearing polyacrylic acid chains, Journal of Wood Science 46 (2000) 331–333.

62. Kondo, T., Ishizu, A., Nakano, J., Preparation of glycidyl celluloses from completely allylated methylcellulose and Tri-O-allylcellulose, Journal of Applied Polymer Science 37 (1989) 3003–3009.

63. Gurgel, L. V. A., de Melo, J. c. P., de Lena, J. C., Gil, L. F., Adsorption of chromium(VI) ion from aqueous solution by succinylated mercerized cellulose functionalized with quaternary ammonium groups, Bioresource Technology 100 (2009) 3214-3220.

64. Gurgel, L. V. A., Gil, L. F., Adsorption of Cu(II), Cd(II), and Pb(II) from aqueous single metal solutions by succinylated mercerized cellulose modified with triethylenetetramine, Carbohydrate Polymers 77 (2009) 142-149.

65. Gurgel, L.V.A., Júnior, O.K., Gil, R.P.d.F., Gil, L.F., Adsorption of Cu(II), Cd(II), and Pb(II) from aqueous single metal solutions by cellulose and mercerized cellulose chemically modified with succinic anhydride, Bioresource Technology 99 (2008) 3077-3083.

66. Melo, J. C. P., Filho, E. C. S., Santana, S. A. A., Airoldi, C.,Synthesized cellulose/succinic anhydride as an ion exchanger. Calorimetry of divalent cations in aqueous suspension, Thermochimica Acta 524 (2011) 29-34.

67. Hu, X., Zhao, M., Song, G., Huang, H., Modification of pineapple peel fibers with succinic anhydride for Cu(II), Cd(II), Pb(II) removal from aqueous solutions, Environmental Technology 32 (2011) 739-746.

68. Belhalfaoui, B., Aziz, A., Elandaloussi, E-H., Ouali, M. S., De Ménorval L. C, Succinate-bonded cellulose: A regenerable and powerful sorbent for cadmium-

removal from spiked high-hardness groundwater, Journal of Hazardous Materials 169 (2009) 831-837.

69. Nada, A. A. M. A., Hassan, M. L., Ion Exchange Properties of Carboxylated Bagasse, Journal of Applied Polymer Science 102 (2006) 1399–1404.

70. Chand, P., Shil, A. K., Sharma, M., Pakade, Y. B., Improved adsorption of cadmium ions from aqueous solution using chemically modified apple pomace: Mechanism, kinetics, and thermodynamics, International Biodeterioration & Biodegradation 90 (2014) 8-16.

71. Zhou, Y., Jin, Q., Hu, X., Zhang, Q., Ma, T., Heavy metal ions and organic dyes removal from water by cellulose modified with maleic anhydride, Journal of Material Science 47 (2012) 5019–5029.

72. Low, K.S., Lee, C.K., Mak, S.M., Sorption of copper and lead by citric acid modified wood, Wood Science and Technology 38 (2004) 629–640.

73. Gusmão, K. A. G., L Gurgel, L. V. A., Melo, T. M. S, de Freitas Carvalho, C., Gil, L. F., Adsorption studies of etherdiamine onto modified sugarcane bagasses in aqueous solution, Journal of Environmental Management 133(2014) 332-34.

74. Karnitz Jr., O., Gurgel, L. V., de Melo, J. C. P, Botaro, V. R., Melo, T. M. S., de Freitas Gil, R. M., Frédéric Gil L. F., Adsorption of heavy metal ion from aqueous single metal solution by chemically modified sugarcane bagasse, Bioresource Technology 98 (2007) 1291-1297.

75. Sciban, M., Klasnja, M., Skrbic, B., Modified hardwood sawdust as adsorbent of heavy metal ions from water, Wood Sci Technol 40 (2006) 217–227.

76. Huang, L., Xiao, C., Chen, B., A novel starch-based adsorbent for removing toxic Hg(II) and Pb(II) ions from aqueous solution, Journal of Hazardous Materials 192 (2011) 832-836.

77. Leyva-Ramos, R., Bernal-Jacome, L.A., Acosta-Rodriguez, I., Adsorption of cadmium(II) from aqueous solution on natural and oxidized corncob, Separation and Purification Technology 45 (2005) 41–49.

78. Nasernejad, B., Zadeh, T.E., Pour, B.B., Bygi, M.E., Zamani, A., Comparison for biosorption modeling of heavy metals (Cr(III), Cu(II), Zn(II)) adsorption from wastewater by carrot residues, Process Biochemistry 40 (2005) 1319–1322.

79. Pehlivan, E., Cetin, S., Yanık, B.H., Equilibrium studies for the sorption of zinc and copper from aqueous solutions using sugar beet pulp and fly ash. Journal of Hazardoud Materials 135 (2006) 193–199.

80. Wong, K.K., Lee, C.K., Low, K.S., Haron, M.J., Removal of Cu and Pb from electroplating wastewater using tartaric acid modified rice husk, Process Biochemistry 39 (2003) 437–445.

81. Acar, F.N., Eren, Z., Removal of Cu(II) ions by activated poplar sawdust (Samsun Clone) from aqueous solutions. Journal of Hazardous Materials 137 (2006) 909–914.

82. Khan, M.N., Wahab, M.F., Characterization of chemically modified corncobs and its application in the removal of metal ions from aqueous solution. Journal of Hazardous Materials 141 (2006) 237–244.

83. Özer, A., Özer, D., Özer, A., 2004. The adsorption of copper(II) ions onto dehydrated wheat bran (DWB): determination of equilibrium and thermodynamic parameters. Process Biochem. 39 (2004) 2183–2191.

84. Özer, A., Pirincci, H.B., 2006. The adsorption of Cd(II) ions on sulfuric acid-treated wheat bran. Journal of Hazardous Materials 137 (2006) 849–855.

85. Wong, K.K., Lee, C.K., Low, K.S., Haron, M.J., Removal of Cu and Pb by tartaric acid modified rice husk from aqueous solutions, Chemosphere 50 (2003) 23–28.

86. Velazquez-Jimenez, L.H., Pavlick, A., Rangel-Mendez, J. R., Chemical characterization of raw and treated agave bagasse and its potential as adsorbent of metal cations from water, Industrial Crops and Products 43 (2013) 200– 206.

87. Wartelle, L.H., Marshall, W.E., Citric acid modified agricultural byproducts as copper ion adsorbents. Advances in Environmental Research 4 (2000) 1–7.

88. Shin, E. W., Rowell, R.M.,Cadmium ion sorption onto lignocellulosic biosorbent modified by sulfonation: the origin of sorption capacity improvement, Chemosphere 60 (2005) 1054–1061.

89. Pangeni, B., Paudyal, H., Inoue, K.,Kawakita, H., Ohto, K., Alam, S.,Selective recovery of gold(III) using cotton cellulose treated with concentrated sulfuric acid, Cellulose 19 (2012) 381–391.

90. Filho, E. C. S, Santos Jr., L. S., Silva, M. M. F, Fonseca, M. G., Santana, S. A. A., Airoldi, C., Surface cellulose modification with 2-aminomethylpyridine for copper, cobalt, nickel and zinc removal from aqueous solution, Journal of Materials Research16 (2013) 79-87.

91. Musyoka, S. M., Mittal, H., Mishra, S. B., Ngila, J. C. Effect of functionalization on the adsorption capacity of cellulose forthe removal of methyl violet, International Journal of Biological Macromolecules 65 (2014) 389–397.

92. Zhou, Y., Jin, Q., Zhu,. T., Zhang, Q., Separation of chromium (vi) from aqueous solutions by cellulose modified with D-blucose and quaternary ammonium groups, Cellulose Chemistry and Technology, 46 (2012) 319-329.

93. Aoki, N., Fukushima, K., Kurakata, H., Sakamoto, M., Furuhata, K., 6-Deoxy-6-mercaptocellulose and its S-substituted derivatives as sorbents for metal ions, Reactive and Functional Polymers 42 (1999) 223–233.

94. Tashiro, T., Shimura, Y., Removal of mercuric ions by systems based on cellulose derivatives, Journal of Applied Polymer Science 27 (1982) 747–756.

95. Saito, T., Isogai, A., Ion-exchange behavior of carboxylate groups in fibrous cellulose oxidized by the TEMPO-mediated system, Carbohydrate Polymers 61 (2005) 183-190.

96. Maekawa, E., Koshijima, T., Properties of 2,3-dicarboxy cellulose combined with various metallic ions, Journal of Applied Polymer Science 29 (1984) 2289–2297.

97. Maekawa, E., Koshijima, T., Preparation and characterisation of hydroxamic acid derivatives and its metal complexes derived from cellulose, Journal of Applied Polymer Science 40 (1990) 1601–1613.

98. Foglarova, J. Prokop, M. Milichovsky, Oxidized Cellulose: An Application in the Form of Sorption Filter Materials Journal of Applied Polymer Science Sci., 112 (2009) 669-678.

99. Fox, S.C., Li, B., Xu, D., Edgar, K. J., Regioselective esterification and etherification of cellulose: a review, Biomacromolecules 12 (2011) 1956-1972.

100. Navarro, R.R., Sumi, K., Fujii, N., Matsumura, M., Mercury removal from wastewater using porous cellulose carrier modified with polyethyleneimine, Water Research 30 (1996) 2488–2494.

101. Anirudhan, T. S., Unnithan, M. S., Arsenic(V) removal from aqueous solutions using an anion exchanger derived from coconut coir pith and its recovery, Chemosphere 66 (2007) 60–66.

103. Zheng, L., Dang, Z., Yi, X., Zhang, H., Equilibrium and kinetic studies of adsorption of Cd(II) from aqueous solution using modified corn stalk, Journal of Hazardous Materials, 176 (2010) 650-656.

104. Saliba, R., Gauthier, H., Gauthier, R., Petit-Ramel, M., Adsorption of Copper(II) and Chromium(III) Ions onto Amidoximated Cellulose, Journal of Applied Polymer Science 75 (2000) 1624–1631.

105. Kalia, S., et al. (eds.), Cellulose Fibers: Bio- and Nano-Polymer Composites, Springer-Verlag Berlin Heidelberg 2011, pp. 43-48.

106. Carvalho, W. S., Martins, D. F., Gomes, F. R., Leite, I. R., da Silva, L. G., Ruggiero, R., Richter, E. M., Phosphate adsorption on chemically modified sugarcane bagasse fibres, Biomass and bioenergy 35 (2011) 3913-3919.

107. Min, S.H., Han, J.S., Shin, E.W., Park, J.K., Improvement of cadmium ion removal by base treatment of juniper fiber, Water Reseach 38 (2004) 1289–1295.

108. Sciban, M., Klasnja, M., Skrbic, B., Modified softwood sawdust as adsorbent of heavy metal ions from water, Journal of Hazardous Materials 136 (2006) 266–271.

109. Memon, S.Q., Memon, N., Shah, S.W., Khuhawar, M.Y., Bhanger, M.I., 2007. Sawdust – a green and economical sorbent for the removal of cadmium(II) ions, Journal of Hazardous Materials 139 (2007) 116–121.

110. Habib-ur-Rehman Shakirullah, M. Ahmad, I. Shah, S. Hameedullah, Sorption studies of nickel ions onto sawdust of Dalbergia sissoo, Journal of the Chinese Chemical Society 53 (2006) 1045–1052.

111. Hanafiah, M.A.K., Ngah, W.S.W., Zakaria, H., Ibrahim, S.C., Batch study of liquid-phase adsorption of lead ions using Lalang (Imperata cylindrica) leaf powder, Journal of Biological Sciences 7 (2007) 222–230.

112. Xie, Y., Hill, C. A. S., Xiao, Z., Militz, H., Mai, C., Silane coupling agents used for natural fiber/polymer composites: A review, Composites: Part A 41 (2010) 806–819.

113. Jorgetto, A. O. I., Silva, R. I. V. Longo, M.M., Saeki, M. J., Padilha, P. M., Martines, M. A. U., Rocha, B. P., Castro, G. R., Incorporation of dithiooxamide as a complexing agent into cellulose for the removal and pre-concentration of Cu(II) and Cd(II) ions from natural water samples, Surface Science 264 (2013) 368– 374 .

114. Abdul Khalil, H. P. S., Bhat,A. H., Yusra I.,A. F., Green composites from sustainable cellulose nanofibrils: A review, Carbohydrate Polymers 87 (2012) 963– 979.

115 Saber-Samandari, S., Saber-Samandari, S., Gazi, M., Cellulose-graft polyacrylamide/hydroxyapatite composite hydrogel with possible application in removal of Cu (II) ions, Reactive & Functional Polymers 73 (2013) 1523–1530.

116. Liu, Y., Wang, W., Wang, A., Adsorption of lead ions from aqueous solution by using carboxymethyl cellulose-g-poly (acrylic acid)/attapulgite hydrogel composites, Desalination 259 (2010) 258–264.

117. Jayalakshmi, A., Rajesh, R., Senthilkumar, S., D. Mohan, D., Epoxy functionalized poly(ether-sulfone) incorporated cellulose acetate ultrafiltration membrane for

the removal of chromium ions, Separation and Purification Technology 90 (2012) 120–132.

118. Qu, R. J., Sun, C. M.,Wang, M. H., Ji, C. N., Xu, Q., Zhang, Y., et al. (2009). Adsorption of Au(III) from aqueous solution using cotton fiber/chitosan composite adsorbents, Hydrometallurgy 100 (009) 65–71.

119. Sun, X. Q., Peng, B., Jing, Y., Chen, J., & Li, D. Q., Chitosan(chitin)/cellulose composite biosorbents prepared using ionic liquid for heavy metal ions adsorption, Separations 55 (2009) 2062–2069.

120. Zhang, L., Zhao, Y-H., Bai, R., Development of a multifunctional membrane for chromatic warning and enhanced adsorptive removal of heavy metal ions: Application to cadmium, Journal of Membrane Science 379 (2011) 69– 79.

121. Qu, R. J., Sun, C. M., Fang, M., Zhang, Y., Ji, C. N., Xu, Q., Removal of recovery of Hg(II) from aqueous solution using chitosan-coated cotton fibers, Journal of Hazardous Materials, 167 (2009) 17–727.

122. Tang, H., Chang, C., Zhang, L., Efficient adsorption of Hg2+ ions on chitin/cellulose composite membranes prepared via environmentally friendly pathway, Chemical Engineering Journal 173 (2011) 689– 697.

123. Zhou, D., Zhang, L., Guo, S., Mechanisms of lead biosorption on cellulose/chitin beads, Water Research 39 (2005) 3755–3762.

124. Trana, C. D., Duria, S., Delneri, A., Franko, M., Chitosan-cellulose composite materials: Preparation, Characterization and application for removal of microcystin, Journal of Hazardous Materials 252– 253 (2013) 355– 366.

125. Chen, J. H., Ni, J. C., Liu, Q. L., Li, S. X., Adsorption behavior of Cd(II) ions on humic acid-immobilized sodium alginate and hydroxyl ethyl cellulose blending porous composite membrane adsorbent, Desalination 285 (2012) 54–61.

126. Choi, S., Jeong, Y., The Removal of Heavy Metals in Aqueous Solution by Hydroxyapatite/Cellulose Composite, Fibers and Polymers 9 (2008) 267-270.

127. Yu, X., Tong, S., Ge, M., Zuo, J., Removal of fluoride from drinking water by cellulose@hydroxyapatite nanocomposites, Carbohydrate Polymers 92 (2013) 269–275.

128. Zhang, Y., Liub, Y., Wangb, X., Suna, Z., Mab, J., Wub, T., Xingb, F., Gao, J., Carbohydrate Porous graphene oxide/carboxymethyl cellulose monoliths, with highmetal ion adsorption, Polymers 101 (2014) 392– 400.

129. Zhou, C-H., Zhang, D., Tong D-S., Wua, L-M., Yu, W-H., Ismadji, S., Paper-like composites of cellulose acetate–organo-montmorillonite for removal of hazardous anionic dye in water, Chemical Engineering Journal 209 (2012) 223–234.

130. Ji, F., Li, C., Tang, B., Xu, J., Lu, G., Liu, P., Preparation of cellulose acetate/zeolite composite fiber and its adsorption behavior for heavy metal ions in aqueous solution, Chemical Engineering Journal 209 (2012) 325–333.

131. Inamuddin, A. M., Amin, A., Naushad, M., El-Desoky, G. E., Therm Anal Nicotinic acid adsorption thermodynamics study on carboxymethyl cellulose Ce(IV) molybdophosphate composite cation-exchanger, Journal of Thermal Analysis and Calorimetry 111 (2013) 831–838.

132. Inamuddin, A. L., Amin, A., Naushad, M., Eldesoky, G. E., Forward ion-exchange kinetics of heavy metal ions on the surface of carboxymethyl cellulose Sn(IV) phosphate composite nano-rod-like cation exchanger, Journal of Thermal Analysis and Calorimetry 110 (2012) 715–723.

133. Castillo-Ortega, M. M., Santos-Sauceda, I., Encinas, J. C., Rodriguez-Felix, D. E., del Castillo-Castro, T., Rodriguez-Felix, F., Valenzuela-García, J. L., Quiroz-Castillo, L. S., Herrera-Franco, P. J., Adsorption and desorption of a gold–iodide

complex onto cellulose acetate membrane coated with polyaniline or polypyrrole: a comparative study, Journal of Material Science 46 (2011) 7466–7474.

134 Çifci, C., Kaya, A., Preparation of poly(vinyl alcohol)/cellulose composite membranes for metal removal from aqueous solutions, Desalination 253 (2010) 175–179.

135. Villalobos-Rodríguez, R., Montero-Cabrera, M. E., Esparza-Ponce, H. E., Herrera-Peraza, E. F., Ballinas-Casarrubias, M. L., Uranium removal from water using cellulose triacetate membranes added with activated carbon, Applied Radiation and Isotopes 70 (2012) 872–881.

136. Barathi, M., Kumar, A. S. K. Rajesh, N., A novel ultrasonication method in the preparation of zirconium impregnated cellulose for effective fluoride adsorption, Ultrasonics Sonochemistry 21 (2014) 1090–1099.

137. Zhu, H.-Y., Fu, Y.-Q. , Jiang, R., Jiang, J.-H. Xiao, L., Zengc, G.-M. , Zhao, S.-L., Wang, Y., Adsorption removal of congo red onto magnetic cellulose/Fe3O4/activated carbon composite: Equilibrium, kinetic and thermodynamic studies, Chemical Engineering Journal 173 (2011) 494– 502.

138. Tasdelen, C., Aktas, S., Acma, E., Guvenilir, Y., Gold recovery from dilute gold solutions using DEAE-cellulose, Hydrometallurgy 96 (2009) 253–257.

139. Taha, A. A., Wu, Y., Wang, H., Li, F., Preparation and application of functionalized cellulose acetate/silica composite nanofibrous membrane via electrospinning for Cr(VI) ion removal from aqueous solution Journal of Environmental Management, 112 (2012)10-16.

140. Xu, Y. P., Wang, Z. J., Ke, R. H., Khan, S. U., Accumulation of organochlorine pesticides from water using triolein embedded cellulose acetate membranes., Journal of Environmental Science and Technology 39 (2005) 1152–1157.

141. Ke, R. H., Xu, Y. P., Wang, Z. J., Khan, S. U., Estimation of the uptake rate constants for polycyclic aromatic hydrocarbons accumulated by semipermeable membrane devices and triolein-embedded cellulose acetate membranes. Journal of Environmental Science and Technology 40 (2006) 3906–3911.

142. Faruk, O., Bledzki, A. K., Fink, H-P., Sain, M., Biocomposites reinforced with natural fibers: 2000–2010, Progress in Polymer Science 37 (2012) 1552– 1596.

143. Moon, R. J., Martini, A., Nairn, J., Simonsen, J., Youngblood, J., Cellulose nanomaterials review: Structure, properties and nanocomposites. Chemical Society Review 40 (2011) 3941–3994.

144. Habibi, Y., Lucia, L. A., & Rojas, O. J., Cellulose nanocrystals: Chemistry, self assembling, and applications, Chemical Reviews 110 (2010) 3479–3500.

145. Charreau, H., Foresti, M.L., Vazquez, A., Nanocellulose patents trends: a comprehensive review on patents on cellulose nanocrystals, microfibrillated cellulose and bacterial cellulose, Recent Patents on Nanotechnology 7 (2013) 56.

146. Siro, I., Plackett, D., Microfibrillated cellulose and new nanocomposite materials: A review. Cellulose 17 (2010) 459–494.

147. Aspler, J., Bouchard, J., Hamad, W., Berry, R., Beck, S., Drolet, F. and Zou, X., Review of nanocellulosic products and their applications. In: Dufresne, A.,

Thomas, S. and Pothan, L.A. (Eds.), Biopolymer nanocomposites. Wiley, Hoboken, NJ, USA, (2013), pp. 461-508.

148. Plackett, D. V., Letchford, K., Jackson, J. K., Burt, H. M., A review of nanocellulose as a novel vehicle for drug delivery, Nordic Pulp & Paper Research Journal 29 (2014) 105-112.

149. Dufresne, A., Nanocellulose: a new ageless bionanomaterial, Materials today (2013) 220–227.

150. Abdul Khalil, H.P.S., Davoudpour, Y., Islam, Md. N., Mustapha, A., Sudesh, K., Dungani, R., Jawaid, M., Production and modification of nanofibrillated cellulose using various mechanical processes: A review, Carbohydrate Polymers 99 (2014) 649– 665.

151. Klemm, D., Kramer, F., Moritz, S., Lindström, T., Ankerfors, M., Gray, D., Dorris, A., Nanocelluloses: A New Family of Nature-Based Materials, Angew. Chem. Int. Edition 50 (2011) 5438 – 5466.

152. Iguchi, M., Yamanaki, S., Budhiono, A., Review – Bacterial cellulose – a masterpiece of nature's arts, Journal of Material Science, 35 (200) 261-270.

153. Kardam, A., Raj, K. R., Srivastava, S., Srivastava, M. M., Nanocellulose fibers for biosorption of cadmium, nickel, and lead ions from aqueous solution, Clean Technologies and Environmental Policy 16 (2014) 385–393.

154. Donia, A. M., Atia, A. A., Abouzayed, F. I., Preparation and characterization of nano-magnetic cellulose with fast kinetic properties towards the adsorption of some metal ions, Chemical Engineering Journal 191 (2012) 22– 30.

155. Yu, X., Tong S, Ge, M., Wu, L., Zuo, J., Cao, C., Song, W., Adsorption of heavy metal ions from aqueous solution by carboxylated cellulose nanocrystals, Journal of Environmental Sciences 25 (2013) 933–943.

156. Sun, X., Yang, L., Li, Q., Zhao, J., Li, X., Wang, X., Liu, H., Amino-functionalized magnetic cellulose nanocomposite as adsorbent for removal of Cr(VI): Synthesis and adsorption studies, Chemical Engineering Journal 241 (2014) 175–183.

157. Singh, K., Arora J. K., Sinha, J. M. T., Srivastava, S., Functionalization of nanocrystalline cellulose for decontamination of Cr(III) and Cr(VI) from aqueous system: computational modeling, Approach in press, Clean Technologies and Environmental Policy 16 (2014) 1179-1191.

158. Lu, M. , Xu, Y., Guan, X., Wei, D., Preliminary research on Cr(VI) removal by bacterial cellulose, Journal Wuhan University of Technology, Materials Science Edition 25 (2012) 572-575.

159. Saumya S. Pillai, B. Deepa, Eldho Abraham, N. Girija, P. Geetha, Laly Jacob, Mathew Koshy, Biosorption of Cd(II) from aqueous solution using xanthated nano banana cellulose: Equilibrium and kinetic studies, Ecotoxicology and Environmental Safety 98 (2013) 352-360.

160. Musyoka, S., Ngila, C., Moodley, B., Kindness, A., Petrik, L., Greyling, C., Oxolane-2,5-dione modified electrospun cellulose nanofibers for heavy metals adsorption, Journal of Hazardous Materials 192 (2011) 922-927.

161. Karnitz Jr., O., Gurgel, L. V. A., de Freitas, R. P., Frédéric Gil, L. F., Adsorption of Cu(II), Cd(II), and Pb(II) from aqueous single metal solutions by mercerized cellulose and mercerized sugarcane bagasse chemically modified with EDTA dianhydride (EDTAD), Carbohydrate Polymers 77 (2009) 643–650.

162. Akama, Y., Ueda, T., Solid-phase extraction of PB from common salt and water samples by cellulose modified with anhydrous EDTA, Cellulose Chemistry and Technology 47 (2013) 479-486.

163. Shen, W., Chen, W., Shi, S., Li, X., Zhang, X., Hu, W., Wang, H., Adsorption of Cu(II) and Pb(II) onto diethylenetriamine-bacterial cellulose, Carbohydrate Polymers 75 (2009) 110-114.

164 Lu, M. , Xu, Y., Guan, X., Wei, D., Preliminary research on Cr(VI) removal by bacterial cellulose, Journal Wuhan University of Technology, Materials Science Edition 25 (2012) 572-575.

165. Chen, S., Zou, Y., Yan, Z., Shen, W., Shi, S., Zhang, X., Wang, H., Carboxymethylated-bacterial cellulose for copper and lead ion removal, Journal of Hazardous Materials 161 (2009) 1355-1359.

166. Sain, M., Oksman, K., Introduction to cellulose nanocomposites, Cellulose Nanocomposites: Processing, Characterization and Properties 938 (2006) 2-8.

167. Sanchez, C., Rozes, L., Ribot, F., Laberty-Robert, C., Grosso, D., Sassoye, C., Boissiere, C., Nicole, L., Chimie douce: A land of opportunities for the designed construction of functional inorganic and hybrid organic-inorganic nanomaterials, Comptes Rendus Chimie 1 (2010) 3-39.

168. Siro. I., Plackett, D., Microfibrillated cellulose and new nanocomposite materials: a review, Cellulose 17 (2010) 459–494.

169. Sun, X., Yang, L., Li, Q., Zhao, J., Li, X., Wang, X., Liu, H., Amino-functionalized magnetic cellulose nanocomposite as adsorbent for removal of Cr(VI):

Synthesis and adsorption studies, Chemical Engineering Journal 241(2014) 175-183.

170. Yang, J. Li, L. Yan, C. Zhong, Biosynthesis of spherical Fe_3O_4/bacterial cellulose nanocomposites as adsorbents for heavy metal ions, Carbohydrate Polymers 86 (2011) 1558–1564.

171. Wang, J., Wei, L., Ma, Y., Li, K., Li, M., Yu, Y., Wang, L., Qiu, H.,Collagen/cellulose hydrogel beads reconstituted from ionic liquid solution for Cu(II) adsorption, Carbohydrate Polymers 98 (2013)736-743.

172. Zhou, C., Lee, S., Dooley, K., Wu, Q., A facile approach to fabricate porous nanocomposite gels based on partially hydrolyzed polyacrylamide and cellulose nanocrystals for adsorbing methylene blue at low concentrations, Journal of Hazardous Materials 263 (2013) 334-341.

173. Mutututvari, M.T., Tran, C. D., Synergistic adsorption of heavy metal ions and organic pollutants by supramolecular polysaccharide composite materials from cellulose, chitosan and crown ether, Journal of Hazardous Materials 264 (2014) 449-459.

174. Angadi, S. C., Manjeshwar, L. M., Aminabhavi, T. M., Interpenetrating polymer network blend microspheres of chitosan and hydroxyethyl cellulose for controlled release of isoniazid, International Journal of Biological Macromolecules 47 (2010) 171-179.

175. Tang, H., Chang, C., Zhang, L., Efficient adsorption of Hg^{2+} ions on chitin/cellulose composite membranes prepared via environmentally friendly pathway, Chemical Engineering Journal 173 (2011) 689-697.

176. Ji, F., Li, C., Tang, B., Xu, J., Lu, G., Liu P., Preparation of cellulose acetate/zeolite composite fiber and its adsorption behavior for heavy metal ions in aqueous solution, Chemical Engineering Journal 209 (2012) 325-333.

177. Xie, K., Zhao, W., He, X., Adsorption properties of nano-cellulose hybrid containing polyhedral oligomeric silsesquioxane and removal of reactive dyes from aqueous solution, Carbohydrate Polymers 83 (2011) 1516–1520.

178. Tuutijarvi, T., Lu, J., Sillanpaa, M., and Chen, G., As(V) adsorption on maghemite nanoparticles ,Journal of Hazardous Materials 166 (2009) 1415-1420.

Paper I

Removal of heavy metals from aqueous solutions by succinic anhydride modified mercerized nanocellulose

Hokkanen, S., Repo, E., Suopajärvi, T., Liimatainen, H., Niinimäki, J., Sillanpää, M.

Chemical Engineering Journal 223 (2013) 40–47

Chemical Engineering Journal 223 (2013) 40–47

Contents lists available at SciVerse ScienceDirect

Chemical Engineering Journal

journal homepage: www.elsevier.com/locate/cej

Removal of heavy metals from aqueous solutions by succinic anhydride modified mercerized nanocellulose

Sanna Hokkanen *, Eveliina Repo [1], Mika Sillanpää [1]

Laboratory of Green Chemistry, Department of Energy and Environmental Technology, Faculty of Technology, Lappeenranta University of Technology, Sammonkatu 12, FI-50130 Mikkeli, Finland

HIGHLIGHTS

- Novel adsorbents combined beneficial properties of modified nanocellulose.
- Succinic anhydride modified merzerated nanocellulose were effective adsorbents for heavy metals.
- Modified nanocellulose could be regenerated after ultrasonic treatment.
- Porosity of the hybrid adsorbents affected the kinetics of the metal adsorption.
- Adsorption isotherms depended on the type of metal.

ARTICLE INFO

Article history:
Received 5 December 2012
Received in revised form 13 February 2013
Accepted 16 February 2013
Available online 27 February 2013

Keywords:
Modified nanocelluloses
Adsorption
Heavy metal removal
Water treatment

ABSTRACT

In this study, the removal of Zn(II), Ni(II), Cu(II), Co(II), and Cd(II) ions from aqueous solutions was investigated using succinic anhydride modified mercerized nanocellulose. The modified adsorbents were characterized using FTIR and SEM analyses. FTIR results showed the bands related to carboxyl groups and SEM-images clear increase in crystallinity after modification of nanocellulose. The effects of pH, contact time, regeneration, and the concentration of metals were studied in batch mode. The maximum metal uptakes ranged from 0.72 to 1.95 mmol/g following the order of: Cd > Cu > Zn > Co > Ni. Adsorption isotherms were demonstrated using Langmuir and Sips models with wet and dry weight of adsorbent. Both models were representative to simulate adsorption isotherms. Regeneration of the modified nanocellulose was accomplished using nitric acid and ultrasonic treatment.

1. Introduction

Investigation of heavy metals contaminated water has become essential focus of environmental scientists in recent years. The heavy metals in water could be derived from natural sources like volcanoes, weathering and erosion of bed rocks and ore deposits but also numerous anthropogenic activities, such as mining, industries, wastewater irrigation, and agriculture activities [1–3].

Heavy metals are essential to living organisms at low concentrations, but many of them are toxic at elevated concentrations [4]. Exposure to heavy metals has been linked with developmental retardation, various cancers, kidney damage, autoimmunity, and even death in extreme cases [5]. Therefore, their removal from contaminated, water is required prior to discharge. Metal removal from the waste streams is of relevance not only due to their toxicity but also due to the possibility to reuse metals in various industrial applications.

Conventional methods employed for the removal of heavy metal ions from industrial effluents include chemical precipitation, flocculation, membrane separation, ion exchange, evaporation, and electrolysis. Most of these methods are often costly or ineffective, especially in removing heavy metal ions from dilute solutions [6–8].

Adsorption has been shown to be one of the most efficient and technically feasible methods for the metal removal from aqueous solutions. Activated carbon is the most widely used adsorbent throughout the world for this purpose. However, it possesses disadvantages related to high operating costs, low selectivity, and its complex thermal regeneration requirements. Therefore, development of alternative adsorption materials is constantly under an intensive study. For example, natural bentonite [9,10], combination of natural zeolite–kaolin–bentonite [11], fruit peel [12,13], chitosan [14–16], and anaerobic granular sludge [17,18] have been tested for heavy metal removal. Heavy metal adsorption by inherently formed iron-based water treatment residuals (WTRs) and a boron processing waste (BW) has also seldom studied [19,20]. Promising materials for metal recovery are adsorbents functionalized with different

* Corresponding author. Tel.: +358 40 747 7843; fax: +358 15 336 013.
E-mail address: sanna.hokkanen@lut.fi (S. Hokkanen).
[1] Tel.: +358 40 747 7843; fax: +358 15 336 013.

1385-8947/$ - see front matter © 2013 Elsevier B.V. All rights reserved.
http://dx.doi.org/10.1016/j.cej.2013.02.054

chelating agents. This is due to the strong affinity of chelate forming groups towards metal ions, selectivity, and the possibility to regenerate the metal loaded adsorbent by a simple acid treatment [21,22].

Cellulose is regarded as the most abundant and renewable biopolymer in nature. The ongoing global trend to promote the production and usage of sustainable and biodegradable materials from natural resources have increased interest towards novel, high-value cellulose-based products and it is one of the most affordable raw materials available for the preparation of various functional materials. Moreover, nano- and microcelluloses are considered to be amongst the most potential bio-based materials for future high-end applications [23,24]. There are very few functional groups in cellulose fiber that are able to capture metals. Hence, many methods have been used to utilize cellulose as a metal scavenger through some derivatizations. Some of these methods are based on using carboxylate and amine groups as chelating agents [25–27] or catalytic and selective oxidation of primary hydroxyl groups of cellulose [28,29]. Succinylation reaction has also shown to be an alternative in cellulose modification [24,30–32].

Gurgel proposed the mercerization treatment as a way of increasing the fibers specific surface area and to make the hydroxyl groups of cellulose macromolecules more easily accessible for the modification with succinic anhydride (succinylation) and as continuation of that study they have described the preparation of two new chelating materials containing amine groups from succinylated mercerized cellulose [8,33].

As noted above, there are a few studies of modified cellulose as adsorbent for heavy metals, but, to the best of our knowledge, there are no studies on modification of nano- and microcellulose for this purpose. Modification of nano- and microcellulose can provide effective, stable, and regenerable adsorbents for metal recovery from various kinds of wastewaters. This study describes the preparation and evaluation of mercerized and succinic anhydride modified micro/nano cellulose to adsorb Zn(II), Ni(II), Cu(II), Co(II) and Cd(II) ions in aqueous solutions. Studies on pH dependence, adsorption kinetics and isotherms were investigated. Regeneration studies, using different acids at different concentrations, were also examined.

2. Materials and methods

2.1. Materials

Microfibrillated cellulose (MFC) was purchased from University of Oulu, Finland. All chemicals used in this study were of analytical grade and supplied by Sigma–Aldrich. Stock solutions of 1000 mg/L were prepared by dissolving appropriate amounts of Zn(II), Ni(II), Cu(II), Co(II) and Cd(II) nitrate salts in deionized water. Adjustment of pH was accomplished using 0.1 M NaOH or 0.1 M HNO_3.

2.2. Cellulose mercerization

Microfibrillated cellulose (MFC) (30 g) was treated with 0.20 L of NaOH solution (20 wt.%) at room temperature at least 16 h with magnetic stirring. The alkali-cellulose was separated from the solution using centrifuge and washed with distilled water down to pH 7.

2.3. Synthesis of celluloses

Mercerized cellulose (20 g) was reacted with succinic anhydride (35 g) under pyridine reflux (0.17 L) for 24 h. The modified cellulose was centrifugated and filtered, washed in sequence with dimethylformamide (DMF), ethanol 95%, distilled water, HNO_3 (0.01 mol/L), distilled water and finally with acetone. In order to liberate carboxylate functions for a better chelating function than the carboxylic group, succinylated cellulose was treated with a saturated sodium bicarbonate solution for 30 min under constant stirring and afterwards filtered and finally washed with distilled water and then acetone.

2.4. Characterization of celluloses

Fourier transform infrared spectroscopy (FTIR) type Vertex 70 by B Bruker Optics (Germany) was used to identify the surface groups of the synthesized nanocellulose. Attenuated Total Reflectance (ATR) technique was used. The FTIR spectra were recorded at 4 cm^{-1} resolution from 400 to 4000 cm^{-1} and 100 scans per sample. The surface morphology of the different treatment phases was examined using a Hitachi S-4100 scanning electron microscope (SEM).

2.5. Batch adsorption studies

Applicability of modified cellulose for Zn(II), Ni(II), Cu(II), Co(II) and Cd(II) removal was studied using batch experiments in a reaction mixture of 0.02 g of adsorbent and 0.004 L of metal solution containing each metals at concentrations ranging from 0.1 to 10.0 mmol/L. using own decanter glass for each metal reaction mixture. The kinetic study was carried out using five different containers for each metal solution (0.05 L) and 5 g of adsorbent was weighted in each container. 0.002 L samples were pipetted from the reaction mixtures according to schedule. The contact time was varied from 5 to 1140 min resulting overall 90 samples. Implementation under the same conditions as in the other adsorption tests (0.02 g adsorbent and 0.004 L metal solution, reacting in own sample container) would been very difficult because of large number of samples. Agitation was conducted under magnetic stirring and measurements conducted at the room temperature and temperature of 10 °C.

After centrifugation metal concentrations were analyzed by an inductively coupled plasma optical atomic emission spectrometry (ICP-OES) model iCAP 6300 (Thermo Electron Corporation, USA). Zn(II) was analyzed at a wavelength of 202.548 nm, Ni(II) at 231.605 nm, Cu(II) at 324.754 nm, Co(II) at 228.616 nm, and Cd(II) at 226.502 nm.

The amount of metal ions adsorbed per unit mass of modified nanocellulose (mmol/g) was calculated as follows:

$$q_e = \frac{(C_i - C_e)}{M} V \quad (1)$$

where C_i and C_e are the initial and the equilibrium concentrations (mmol/L), while M and V are the weight of the adsorbent (g) and the volume of the solution (L), respectively.

2.6. Regeneration studies

The regeneration of the modified nanocellulose was studied in Zn(II), Ni(II), Cu(II), Co(II) and Cd(II) solutions. At first adsorbents were loaded by metal ions by mixing 5 g of the adsorbent with 0.015 L of 1.8–3.4 mmol/L metal solution. Bigger dose was used in order to make separation of the adsorbent easier. After attaining equilibrium, the spent adsorbent was separated from the solution by centrifuge. Metal ions were eluted using 1 M HNO_3. The effect of different acids for the regeneration was tested with Zn(II) ions using 0.1 M formic acid, ascorbic acid, and acetic acid. The regeneration efficiency (%RE) of the adsorbent was calculated as follows:

$$(\%RE) = \frac{q_r}{q_0} \times 100 \quad (2)$$

where q_0 and q_r are the adsorption capacities of the adsorbents (mmol/g) before and after regeneration, respectively.

3. Results and discussions

3.1. FTIR analyses and SEM pictures

Characterization of succinic anhydride treated nanocellulose was accomplished by FTIR spectroscopy. Fig. 1 illustrates the FTIR spectra of pure cellulose (a) and modified cellulose (b). In spectrum a, the absorbances at 3378, 2875, 1628, 1381, 1325–1210, 1158, and 1052 cm^{-1} are associated with pure cellulose. The strong adsorption at 3378 cm^{-1} is due to the stretching of hydroxyl groups and at 2875 cm^{-1} to the C–H stretching. The band at 1628 cm^{-1} relates to the bending mode of the absorbed water. The peak at 1381 cm^{-1} and attributed to the O–H bending and the peaks 1325–1210 O–H-stretch. The absorption band at 1158 cm^{-1} corresponds to C–O antisymmetric bridge stretching [8,22].

A new peak at 1724 cm^{-1} assigned to asymmetric and symmetric stretching of ester C–O was observed in the spectrum of modified cellulose indicating occurrence of esterification reaction between cellulose and succinic anhydride during synthesis. Furthermore, after modification appearance of the bands at 1581 and 1425 cm^{-1} corresponding to asymmetric and symmetric stretching vibrations of the ionic carboxylic groups verified the introduction of carboxylic groups on the surface [8,34]. Noticeably, the –OH stretching adsorption band at 3378 cm^{-1} did not significantly change upon cellulose succinylation. This is because only the surface hydroxyls that are accessible to succinic anhydride can be succinylated during the chemical reaction [35].

SEM image of the raw cellulosic material used in this study is shown in Fig 2a. Cellulose microfibrils are typically composed of 1000–2000 glucan chains of the same polarity and they are spatially separated from each other [36]. Through the homogenization process, the cellulose bundles are split and degraded leaving microfibrillated cellulose strands with dimensions of 10–100 nm [37]. Because of the homogenization process the ratio of surface area to volume for the fibers is significantly increased.

It has been observed that the treatment of cellulose by alkalic solutions makes cellulose molecules to move segmentally, which leads to random chain folding and formation of folded-chain crystallites [38]. Fig 2b shows that treatment with 20% NaOH, caused the microfibrils become wavy and assemble into large bundles. These bundles were not present in the original disintegrated MFC (Fig. 2a). The formation of the cellulose bundles seems to be induced by partial swelling of the microfibril fragments, whose surfaces tend to adhere to one another.

The effect of the succinic anhydride treatment is shown in Fig. 2c. The fact that after succinylation procedure the nanocellulose fibers had very coarse surfaces strongly suggests that the considerable increase in roughness observed by these micrographs is associated with polymer growth induced by the chemical coupling of succinic anhydride with the surface OH groups. Specific surface area of the adsorbent increased with the increasing roughness of the surface, hence there are lot of sites for metal ions adsorption on the surface. Overall, the SEM analysis showed rather different kind of surface morphologies after different treatments of nanocellulose.

3.2. Adsorption studies

3.2.1. Effect of pH

The removal of metal ions from aqueous solutions by adsorption depends on the solution pH since acidity of the solution affects the ionization of the metal ions and concentration of the counter H^+ ions of the surface groups. To maximize the removal of heavy metals by the adsorbents, knowledge of an optimum pH is important. To study the effect of H^+ concentration on metal removal, the solution pH was varied from two to seven. The effect of pH on the adsorption of Zn(II), Ni(II), Cu(II), Co(II) and Cd(II) by the modified nanocellulose is presented in Fig. 4.

It is apparent from the figure that the extent of the metal removal was dependent on pH. The adsorption capacities of metals on modified nanocellulose increased with increasing pH. When the pH values were lower (pH < 3), the concentration of protons competing with metal ions for the active sites was higher [33]. The adsorbent surface was positively charged and metal ions with

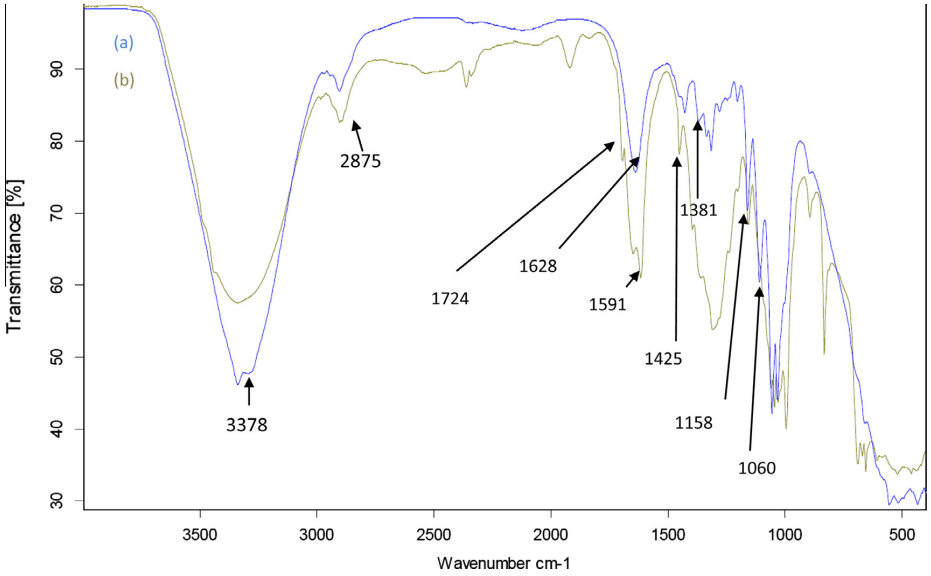

Fig. 1. FTIR spectrum of MFC (a) and succinic anhydride modified nanocellulose (b).

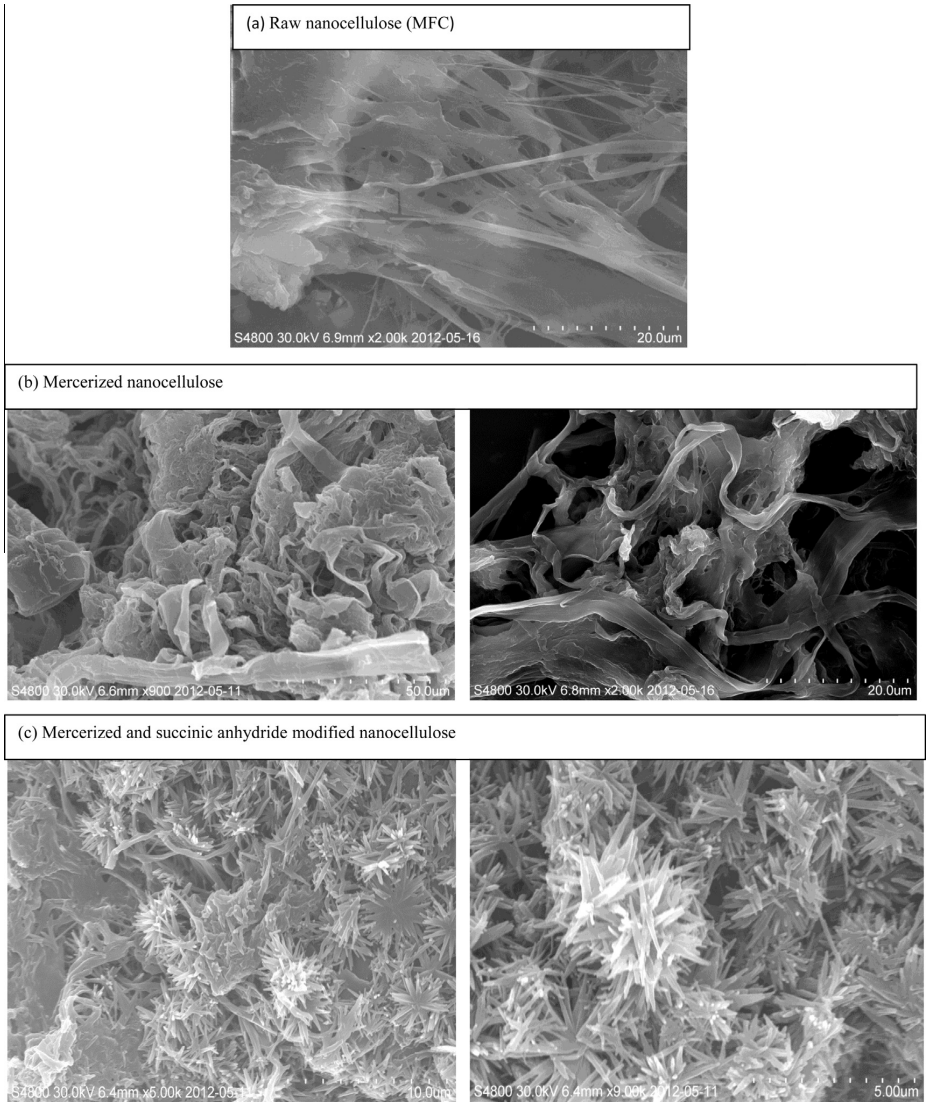

Fig. 2. SEM images of MFC (a), mercerized (b) and succinic anhydride modified (c) nanocellulose.

positive charge had difficulties to approach the functional groups due to electrostatic repulsion. Thus adsorption capacities were found to be lower at lower pH values. With increasing pH (pH > 3), the concentration of protons decreased and the adsorbent surface charge became negative when electrostatic attraction increased between the metal ions and the adsorbent. The maximum adsorption of metals occurred at pH range from 3 to 7. Any precipitation of metals was not observed at pH 7, but in order to be sure pH 5 was selected for the other experiments.

3.2.2. Effect of contact time

The effect of contact time on the adsorption of metals by modified nanocelluloses is shown in Fig. 3. Experiments were performed besides of room temperature at temperature of 10 °C in order to see how modified nanocellulose is performing at colder temperatures. During short contact times, adsorption was very fast for all the metals (within 5 min more than 50% was adsorbed) due to the presence of numerous active sites on the adsorbent surface. For Ni(II), Cu(II) and Co(II) adsorption efficiency remained rather similar until 90 min at room temperature and 120 min at 10 °C after which it started to increase again. This indicates that part of the metals was instantly adsorbed and after further mixing new adsorption sites became available possible due to the diffusion of metals inside the pores of cellulosic material. At colder temperatures, diffusion was slowed down and therefore the increase of adsorption efficiency occurred later than at room temperature. For Zn(II) and Cd(II) over 99% adsorption efficiency was instantly attained at both temperatures indicating that these metals were absorbed by readily available adsorption sites.

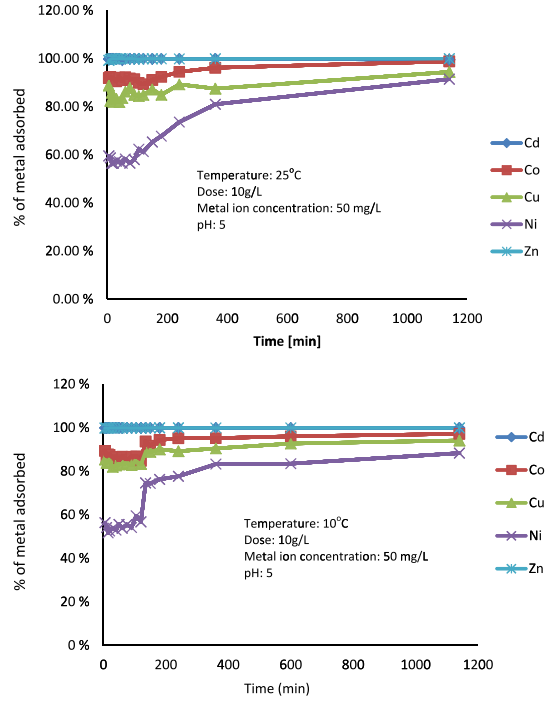

Fig. 3. Effects of contact time on adsorption of metal ions by modified nanocellulose at the room temperature and temperature of 10 °C.

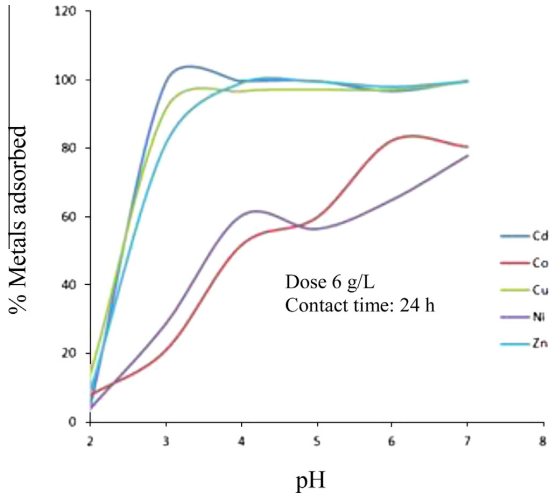

Fig. 4. Effect of pH on adsorption of metal ions by modified nanocellulose.

3.2.3. Adsorption isotherms

Adsorption isotherms describe the relationship between the amount of adsorbate that is adsorbed and the concentration of dissolved adsorbate in the liquid at equilibrium. Because of the high water concentration of the modified nanocellulose the isotherms were determined for the both wet and dry weight of the adsorbent. Dry weight was defined by drying 1 g of wet cellulose in an oven at 90 °C for 4 h and then storing it in a desiccator until its weight was unchanged. Water content of the modified nanocellulose was found to be 81%. In this study, the adsorption mechanisms were analyzed by one two-parameter (Langmuir) and one tree-parameter (Sips) isotherm models, which are commonly used to describe experimental results in a wide range of concentrations.

Langmuir isotherm model, which is probably most often applied adsorption isotherm, was originally developed to describe the gas–solid phase adsorption (in 1916). This model has produced a good concordance with a wide variety of experimental data and is expressed as follows:

$$q_e = \frac{q_m K_L C_e}{1 + K_L C_e} \tag{3}$$

where q_e (mmol/g) is the equilibrium adsorption capacity, q_m (mmol/g) is the maximum amount of the metal ion per unit weight of the adsorbent to form a complete monolayer coverage on the surface bound at high equilibrium metal ion concentration C_e (mmol/L) and K_L (L/mmol) is the Langmuir equilibrium constant related to the affinity of binding site. q_m represents the practical limiting adsorption capacity when the surface is fully covered with metal ions, assisting in the comparison of adsorption performance, and K_L indicates the bond energy of the adsorption reaction between metal and material. The Langmuir isotherm defines the equilibrium parameters of monolayer adsorption on homogenous surfaces by uniformly distributed adsorption sites [15].

Modeling calculations were conducted using Microsoft Office Excel 2007 software. Isotherm parameters were determined by minimizing the Sum of the Squares of the Errors (ERRSQ) function across the concentration range studied:

$$\sum_{i=1}^{p} \left(q_{e,exp} - q_{e,calc}\right)^2 \tag{4}$$

Fig. 4 shows that Langmuir isotherm model appeared to fit to the experimental data well and the correlation coefficients of the equations indicate that this model can explain metal ion adsorption by the modified celluloses satisfactorily (Table 1).

The estimated q_m values were very close to the experimentally obtained maximum metal uptakes for all the metal ions. The values

Table 1
The Langmuir and Sips parameters for Zn(II), Ni(II), Cu(II), Co(II) and Cd(II) ions adsorption.

Type of metal	q_m (mmol/g)	$q_{m,exp}$ (mmol/g)	K_L	R^2
Langmuir				
Zn(II) wet	0.306	0.285	59.213	0.902
Zn(II) dry	1.610	1.500	59.213	0.902
Ni(II) wet	0.141	0.135	12.318	0.964
Ni(II) dry	0.744	0.716	12.318	0.964
Cu(II) wet	0.361	0.342	58.889	0.849
Cu(II) dry	1.900	1.879	58.889	0.849
Co(II) wet	0.254	0.248	3.548	0.984
Co(II) dry	1.338	1.304	3.548	0.984
Cd(II) wet	0.392	0.371	695.101	0.923
Cd(II) dry	2.062	1.954	691.004	0.923

	q_m (mmol/g)	$q_{m,exp}$ (mmol/g)	n_S	K_S	R^2
Sips					
Zn(II) wet	0.306	0.301	0.426	53.677	0.993
Zn(II) dry	1.610	1.600	0.426	53.677	0.864
Ni(II) wet	0.141	0.140	0.540	4.694	0.949
Ni(II) dry	0.744	0.722	0.737	10.335	0.977
Cu(II) wet	0.361	0.347	0.808	56.190	0.857
Cu(II) dry	1.900	1.828	0.808	56.190	0.857
Co(II) wet	0.254	0.253	0.606	2.490	0.989
Co(II) dry	1.338	1.321	0.737	3.256	0.991
Cd(II) wet	0.392	0.389	0.579	555.179	0.962
Cd(II) dry	2.062	1.954	0.579	555.179	0.962

were in the range from 0.141 to 0.392 mmol/g and from 0.744 to 2.062 mmol/g using the wet and dry weight of the modified nanocellulose, respectively.

The major variations in K_L values of metal ions indicate that the adsorption energies between the adsorbent and metal ions were different. High K_L value of Cd(II) (695.2 and 691.0 mmol/L) correlated with very fast adsorption and also K_L values of the other metal ions are consistent with the results of kinetic study.

The Langmuir model is often too simple to describe the complex adsorption phenomena due to the surface heterogeneity or interactions between adsorbing species. Therefore, the Sips isotherm, which takes the surface heterogeneity into account, was tested as well. The Sips isotherm is a combination of the Langmuir and Freundlich isotherms and can be derived using either equilibrium or thermodynamic approach [39,40]. It has a form of

$$q_e = \frac{q_m (K_S C_e)^{n_S}}{1 + (K_S C_e)^{n_S}} \quad (5)$$

where K_S (L/mmol) is the affinity constant and n_S describes the surface heterogeneity. When n_S equals unity, the Sips isotherm returns to the Langmuir isotherm and predicts homogeneous adsorption. At high adsorbate concentrations, it predicts a monolayer sorption capacity of the Langmuir isotherm [41,42].

The plots of the Sips isotherm are illustrated in Fig. 5 and the examination of the results is presented in Table 1. Fig. 5 shows that the equilibrium data fitted as well with Sips as Langmuir isotherm. However, q_m values estimated by Sips model corresponded to the experimentally obtained values of $q_{m,exp}$ a little better than those estimated by Langmuir model. Moreover, correlation coefficients for Sips model were higher in most of the cases. The K_S indicated the highest affinity of Cd(II) and the other results are consistent with the Langmuir model. The heterogeneity factor (n_S) values were smaller than unity for all the metal ions with wet and dry adsorbent indicating heterogeneous adsorption [41].

Adsorption capacities obtained for different metals should be further compared. Based on the species distribution calculated by MINEQL software [43]. Cu(II) should be the most efficiently removed by succinyl modified cellulose. Stability constants of metal succine complexes in aqueous phase follow the order: Cu > Cd > Zn > Co > Ni. However, in the present study the observed order is Cd > Cu > Zn > Co > Ni suggesting that the immobilization of the functional group seems to play an important role. The primary hydration number (N) of the studied metals follows the order: Ni > Cu > Co > Zn > Cd and the hydrated radius (R_H) the opposite order: Cd > Zn > Co > Cu > Ni. Cd(II) has the lowest and Ni(II) the highest ratio of these parameters (N/R_H). The metals with lower N/R_H value have higher Columbic forces towards amorphous oxide surfaces [44] and therefore could have higher affinity towards cellulose surface, which also shows amorphous features [45]. This could explain the highest adsorption efficiency obtained for Cd(II) in this study as well as the fastest adsorption of Cd(II) and Zn(II) observed in the kinetic experiments (Fig. 3). Comparison of the adsorption efficiencies obtained in the present study to some earlier work is presented in Table 2. The similar mercerization treatment and the modification with succinic anhydride as Gurgel et al. [8] was used in this study. It seems that modification by succinyl groups produced the most effective adsorption material for most of the metals.

Even though the promising results obtained in this study it should be noted that preparation of nanocellulose is an expensive process at the moment. Therefore, practical applications of the studied adsorbent are still far away in the future. It seems that microcellulose modified in the similar manner gives better adsorption efficiency possible due to the fact that nanocellulose is more easily aggregated. Possible, further optimization of the synthetic route would improve the quality of the product. However, nanocellulose with its unique properties remains highly interesting

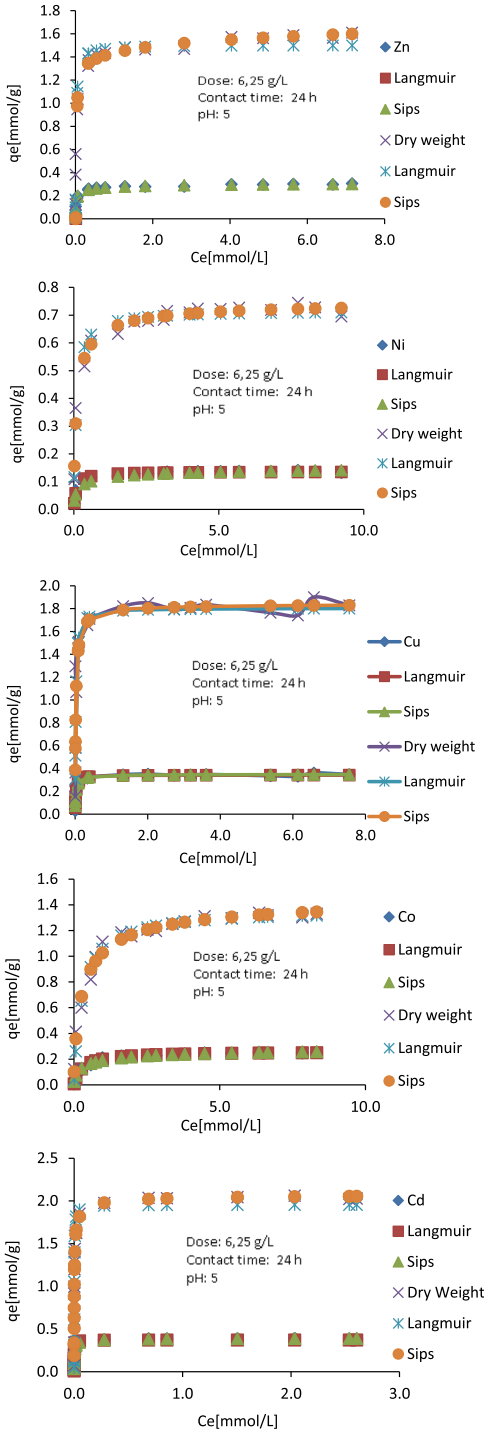

Fig. 5. Adsorption isotherms for Zn(II), Ni(II), Cu(II), Co(II) and Cd(II) adsorption by modified nanocellulose.

Table 2
Comparison of the Langmuir parameters obtained for the adsorption of different metals by modified cellulose based adsorbents.

Adsorbent	Activating agent	Modifying agent	Metal ion	q_m (mmol/g)	K_L (L/mmol)	Ref.
Cellulose (CelNN)	Phosphorous oxychloride	Ethylenediamine	Cu(II)	1.639		[35]
			Ni(II)	0.525		
			Zn(II)	1.059		
Cellulose (Celen)	Thionyl chloride	Ethylenediamine	Cu(II)	1.491	1.588	[36]
			Ni(II)	1.516	1.155	
			Zn(II)	1.118	0.196	
			Co(II)	2.011	1.532	
Mercerized cellulose	Pyridine	Succinic anhydride	Cu(II)	2.421	196.687	[8]
			Cd(II)	2.222	204.361	
			Pb(II)	2.413	1036.5	
Mercerized nanocellulose	Pyridine	Succinic anhydride	Co(II)	1.338	3.548	This study
			Ni(II)	0.744	12.318	
			Cu(II)	1.900	58.889	
			Zn(II)	1.610	59.213	
			Cd(II)	2.062	691.004	

material to work with and most likely its preparation will be less expensive in the future increasing its practical applicability.

3.3. Adsorption mechanism

The surface of the succinic anhydride and sodium bicarbonate solution treated nanocellulose contains ester functions including sodium ions or hydroxyl ions as functional groups. Based on the chemical interactions that might have occurred during metal removal by the adsorbent the mechanisms could be expressed as follows:

$$M^{n+} + n(-COONa) \leftrightarrow (-COONa)_nM \uparrow + nNa^+$$

$$M^{n+} + n(-COOH) \leftrightarrow (-COOH)_nM \uparrow + nH^+$$

where (–COONa) or (–COOH) represents the surface functional groups of modified nanocellulose and n is the coefficient of the reaction component depending on the oxidation state of the metal ion. M^{n+} represents metals: Zn^{2+}, Ni^{2+}, Cu^{2+}, Co^{2+}, or Cd^{2+}.

3.4. Regeneration study

Stability of the adsorbent was investigated by regeneration experiments. This procedure is necessary to restore the original adsorption capacity of the adsorbent and it also enables recovering valuable metals from wastewater streams. In this study, Zn(II), Ni(II), Co(II) and Cd(II) were desorbed from succinic anhydride modified nanocellulose using 1 M nitric acid. Zn(II) ions desorption from the adsorbent was also conducted using 1 M formic acid, 1 M ascorbic acid and 1 M acetic acid. Results with using HNO_3 as regenerant presented in Table 3 were obtained for different metals at the same conditions (metals concentration: 200 mg/L; dose of adsorbent: 3 g; volume of regenerant: 0.015 L).

The regeneration results after adsorption suggest that adsorption efficiency was affected by regeneration. After the first cycle of regeneration, the adsorption capacities of the adsorbents for Zn(II), Ni(II),Co(II) and Cd(II) decreased 11–25% and after second cycle decreased 72–86%. The result also suggests that 15 s ultrasonic treatments after HNO_3 could effectively regenerate the adsorbent with regeneration efficiencies ranging from 96% to 100%.

It seems that during the regeneration process the fibers of the succinic anhydride modified nanocellulose were intertwined or accumulated causing decrease in adsorption efficiency, but were again in the free spaces for the metal ions on the surface of adsorbent after ultrasonic treatment. This indicates the suitability of HNO_3 as the regenerant for succinic anhydride modified nanocellulose, but the ultrasonic treatment is necessary. The results of regeneration using the other acids without ultrasonic treatment after Zn(II) adsorption are presented in Table 4.

Table 3
Regeneration of modified nanocellulose for Zn(II), Ni(II), Co(II) and Cd(II) by 1 M HNO_3.

No.	Adsorption capacity		Regeneration efficiency (%)
	Before regeneration (mg/g)	After regeneration (mg/g)	
Zn			
1.	0.0106	0.0080	75.47
2.	0.0106	0.0015	14.15
After ultrasonic	0.0106	0.0101	95.28
Ni			
1.	0.0118	0.0088	74.57
2.	0.0118	0.0022	18.64
After ultrasonic	0.0118	0.0113	95.76
Co			
1.	0.0122	0.0100	89.28
2.	0.0122	0.0031	27.68
After ultrasonic	0.0122	0.0119	106.25
Cd			
1.	0.0067	0.0053	79.10
2.	0.0067	0.0019	28.36
After ultrasonic	0.0067	0.0064	95.52

Table 4 suggests that the regeneration efficiency using the other acids than HNO_3 was very low for Zn(II) ions. It should be noted that the regeneration efficiency between the first and the second regeneration cycle remained almost the same. It may indicate that the weak acids like ascorbic, formic and acetic acids are not suitable for regeneration process or the concentration of the acid solutions were not high enough.

A poor desorption of metal ions from adsorbent surface using acidic treatment may indicate that new amorphous contacts joint together by hydrogen bonds and additional Van der Waals bonds

Table 4
Regeneration of modified nanocellulose for Zn(II) by 0.1 M formic acid, ascorbic acid and acetic acid.

No.	Type of acid (0.1 M)	Adsorption capacity		Regeneration efficiency (%)
		Before regeneration (mg/g)	After regeneration (mg/g)	
1.	Formic acid	0.0033	0.0014	42.43
2.	Formic acid	0.0033	0.0013	39.39
1.	Ascorbic acid	0.0051	0.0014	27.45
2.	Ascorbic acid	0.0051	0.0013	25.49
1.	Acetic acid	0.0050	0.0012	24.00
2.	Acetic acid	0.0050	0.0011	22.00

between nanofibrils were formed. Therefore, free-adsorption surface area decreased and the high-power ultrasound treatment was needed for regeneration.

4. Conclusion

Succinic anhydride modified mercerized nanocellulose was found to effectively adsorb Zn(II), Ni(II), Cu(II), Co(II) and Cd(II) from aqueous solutions. The maximum adsorption capacities of adsorbent (Langmuir/Sips) ranged from 0.14/0.16 to 0.37/0.40 mmol/g. Because of the high water concentration of the modified nanocellulose the isotherms were also determined using the dry weight of the adsorbent. The same results using dry weight of adsorbent were from 0.71/0.74 to 1.96/2.08 mmol/g. Both models were representative to simulate adsorption isotherms. Moreover, modified nanocellulose could be regenerated after ultrasonic treatment with regeneration efficiencies ranging from 96% to 100%. On the whole, the succinic anhydride-modified nanocellulose showed the potential to be applied in different water treatment applications for the removal of heavy metals.

Acknowledgments

The authors are grateful to the fibre and particle engineering laboratory, University of Oulu for providing materials and consultation. Finnish Funding Agency for Technology and Innovation (Tekes) is thanked for the financial support. Łukasz Potoczny is acknowledged for his contribution in performing experiments in the laboratory.

References

[1] X. Huang, M. Sillanpää, B. Duo, E.T. Gjessing, Water quality in the Tibetan Plateau: metal contents of four selected rivers, Environ. Pollut. 156 (2008) 270–277.
[2] X. Huang, M. Sillanpää, E.T. Gjessing, R.D. Vog, Water quality in the Tibetan Plateau: major ions and trace elements in the headwaters of four major Asian rivers, Sci. Total Environ. 407 (2009) 6242–6254.
[3] S. Muhammad, M.T. Shah, S. Khan, Health risk assessment of heavy metals and their source apportionment in drinking water of Kohistan region, northern Pakistan, Microchem. J. 98 (2011) 334–343.
[4] F. Kieffer, In Metals and Their Compounds in the Environment, Occurrence, Analysis and Biological Relevance, Verlag Chemie, New York, 1991. pp. 1481–490.
[5] J. Glover-Kerkvilet, Environmental assault on immunity, Environ. Health Persp. 103 (1995) 236–237.
[6] J.C.Y. Ng, W.H. Cheung, G. Mckay, Equilibrium studies of the sorption of Cu(II) ions onto chitosan, J. Colloid Interface Sci. 255 (2002) 64–74.
[7] G. Bayramoglu, A. Denizli, S. Sektas, M.Y. Arica, Entrapment of *Lentinus sajor-caju* into Ca-alginate gel beads for removal of Cd(II) ions from aqueous solution: preparation and biosorption kinetics analysis, Microchem. J. 72 (2002) 63–76.
[8] L.V. Gurgel, O.K. Júnior, P.P. Gil, L.F. Gil, Adsorption of Cu(II), Cd(II), and Pb(II) from aqueous single metal solutions by cellulose and mercerized cellulose chemically modified with succinic anhydride, Bioresour. Technol. 99 (2008) 3077–3083.
[9] D. Zhao, S. Chen, S. Yang, X. Yang, S. Yang, Investigation of the sorption behavior of Cd(II) on GMZ bentonite as affected by solution chemistry, Chem. Eng. J. 166 (2011) 1010–1016.
[10] Y. Chen, B. Zhu, D. Wu, Q. Wang, Y. Yang, W. Ye, J. Guo, Eu(III) adsorption using di(2-thylhexly) phosphoric acid-immobilized magnetic GMZ bentonite, Chem. Eng. J. 181–182 (2012) 387–396.
[11] A. Salem, R. Akbari Sene, Removal of lead from solution by combination of natural zeolite–kaolin–bentonite as a new low-cost adsorbent, Chem. Eng. J. 174 (2011) 619–628.
[12] S. Schiewer, A. Balaria, Biosorption of Pb^{2+} by original and protonated citrus peels: equilibrium, kinetics, and mechanism, Chem. Eng. J. 146 (2009) 211–219.
[13] V.K. Gupta, A. Nayak, Cadmium removal and recovery from aqueous solutions by novel adsorbents prepared from orange peel and Fe_2O_3 nanoparticles, Chem. Eng. J. 180 (2012) 81–90.
[14] D. Kołodyńska, Chitosan as an effective low-cost sorbent of heavy metal complexes with the polyaspartic acid, Chem. Eng. J. 173 (2011) 520–529.
[15] E. Repo, J. Warchol, T.A. Kurniawan, M. Sillanpää, Adsorption of Co(II) and Ni(II) by EDTA- and/or DTPA-modified chitosan: kinetic and equilibrium modeling, Chem. Eng. J. 161 (2010) 73–82.
[16] X. Li, Y. Li, Z. Ye, Preparation of macroporous bead adsorbents based on poly(vinyl alcohol)/chitosan and their adsorption properties for heavy metals from aqueous solution, Chem. Eng. J. 178 (2011) 60–68.
[17] J. Virkutyte, E. Hullebusch, M. Sillanpää, P. Lens, Copper and trace element fractionation in electrokinetically treated anaerobic granular sludge, Environ. Pollut. 138 (2005) 518–529.
[18] A. Bhatnagar, M. Sillanpää, Utilization of agro-industrial and municipal waste materials as potential adsorbents for water treatment, a review, Chem. Eng. J. 157 (2010) 277–296.
[19] Y.W. Chiang, K. Ghyselbrecht, R.M. Santos, J.A. Martens, R. Swennen, V. Cappuyns, B. Meesschaert, Adsorption of multi-heavy metals onto water treatment residuals: sorption capacities and applications, Chem. Eng. J. 200–202 (2012) 405–415.
[20] N. Atar, A. Olgun, S. Wang, Adsorption of cadmium (II) and zinc (II) on boron enrichment process waste in aqueous solutions: batch and fixed-bed system studies, Chem. Eng. J. 192 (2012) 1–7.
[21] E. Repo, T.A. Kurniawan, J.K. Warchol, M.T.E. Sillanpää, Removal of Co(II) and Ni(II) ions from contaminated water using silica gel functionalized with EDTA and/or DTPA as chelating agents, J. Hazard. Mater. 171 (2009) 1071–1080.
[22] J. Rämö, M. Sillanpää, V. Vickackaite, M. Orama, L. Niinistö, Chelating ability and solubility of DTPA, EDTA and β-ADA in alkaline hydrogen peroxide environment, J. Pulp Pap. Sci. 26 (2000) 125–131.
[23] H. Liimatainen, J. Sirviö, A. Haapala, O. Hormi, J. Niinimäki, Characterization of highly accessible cellulose microfibers generated by wet stirred media milling, Carbohydr. Polym. 83 (2011) 2005–2010.
[24] T. Saito, A. Isogai, Ion-exchange behavior of carboxylate groups in fibrous cellulose oxidized by the TEMPO-mediated system, Carbohydr. Polym. 61 (2005) 183–190.
[25] R.R. Navarro, K. Sumi, N. Fujii, M. Matsumura, Mercury removal from wastewater using porous cellulose carrier modified with polyethyleneimine, Water Res. 30 (1996) 2488–2494.
[26] R.R. Navarro, K. Sumi, M. Matsumura, Improved metal affinity of chelating adsorbents through graft polymerization, Water Res. 33 (1999) 2037–2044.
[27] R.R. Navarro, K. Tatsumi, K. Sumi, M. Matsumura, Role of anions on heavy metal sorption of a cellulose modified with poly(glycidylmethacrylate) and polyethyleneimine, Water Res. 35 (2001) 2724–2730.
[28] A. Isogai, Y. Kato, Preparation of polyuronic acid from cellulose by TEMPO-mediated oxidation, Cellulose 5 (1998) 153–164.
[29] Y. Zhang, B. Sjögren, P. Engstrand, M. Htun, Determination of charged groups in mechanical pulp fibers and their influence on pulp properties, J. Wood Chem. Technol. 14 (1994) 83–102.
[30] F. Gellerstedt, P. Gatenholm, Surface properties of lignocellulosic fibers bearing carboxylic groups, Cellulose 6 (1999) 103–121.
[31] F. Gellerstedt, L. Wagberg, P. Gatenholm, Swelling behavior of succinylated fibers, Cellulose 7 (2002) 67–86.
[32] S. Mallon, C.A.S. Hill, Covalent bonding of wood through chemical activation, Int. J. Adhes. Adhes. 22 (2002) 465–469.
[33] M. Iqbal, A. Saeed, I. Kalim, Characterization of adsorptive capacity and investigation of mechanism of Cu^{2+}, Ni^{2+} and Zn^{2+} adsorption on mango peel waste from constituted metal solution and genuine electroplating effluent, Sep. Sci. Technol. 44 (2009) 3770–3791.
[34] W. Zhang, C. Li, M. Liang, Y. Geng, C. Lu, Preparation of carboxylate-functionalized cellulose via solvent-free mechanochemistry and its characterization as a biosorbent for removal of Pb^{2+} from aqueous solution, J. Hazard. Mater. 181 (2010) 468–473.
[35] H. Zhao, J.H. Kwak, Z.C. Zhang, H.M. Brown, B.W. Arey, J.E. Holladay, Studying cellulose fiber structure by SEM, XRD, NMR and acid hydrolysis, Carbohyd. Polym. 68 (2007) 235–241.
[36] A.N. Nakagatio, S. Iwamaoto, H. Yano, Bacterial cellulose: the ultimate non-scalar cellulose morphology for the production of high-strength composite, Appl. Phys. A: Mater. Sci. Proc. 80 (2005) 93–97.
[37] H. Shibazaki, S. Kuga, T. Okano, Mercerization and acid hydrolysis of bacterial cellulose, Cellulose 4 (1997) 75–87.
[38] S.J. Allen, G. Mckay, J.F. Porter, Adsorption isotherm models for basic dye adsorption by peat in single and binary component systems, J. Colloid Interface Sci. 280 (2004) 322–333.
[39] D.G. Kinniburgh, General purpose adsorption isotherms, Environ. Sci. Technol. 20 (1986) 895–904.
[40] Y.S. Ho, J.F. Porter, G. McKay, Equilibrium isotherm studies for the sorption of divalent metal ions onto peat: copper, nickel and lead single component systems, Water, Air Soil Pollut. 141 (2002) 1–33.
[41] T.V.N. Padmesh, K. Vijayaraghavan, G. Sekaran, M. Velan, Application of two and three parameters isotherm models: biosorption of acid red 88 onto *Azolla microphylla*, Biorem. J. 10 (2006) 37–44.
[42] M. Chutkowski, R. Petrus, J. Warchoł, P. Koszelnik, Sorption equilibrium in processes of metal ion removal from aqueous environment. Statistical verification of mathematical models, Przem, Chem. 87 (2008) 436–438.
[43] J.P. Gustafsson, Visual MINTEQ ver 2.53, 2007.
[44] P. Trivedi, L. Axe, Predicting divalent metal sorption to hydrous Al, Fe, and Mn oxides, Environ. Sci. Technol. 35 (2001) 1779–1784.
[45] Y. Liu, Y.-J. Liu, Biosorption isotherms, kinetics and thermodynamics, Sep. Purif. Technol. 61 (2008) 229–242.

Paper II

Adsorption of Ni(II), Cu(II) and Cd(II) from aqueous solutions by amino modified nanostructured microfibrillated cellulose

Hokkanen, S., Repo, E., Suopajärvi, T., Liimatainen, H., Niinimäki, J., Sillanpää, M.

Cellulose 21(2014) 1471-1487

Cellulose
DOI 10.1007/s10570-014-0240-4

ORIGINAL PAPER

Adsorption of Ni(II), Cu(II) and Cd(II) from aqueous solutions by amino modified nanostructured microfibrillated cellulose

Sanna Hokkanen · Eveliina Repo · Terhi Suopajärvi · Henrikki Liimatainen · Jouko Niinimaa · Mika Sillanpää

Received: 29 August 2013 / Accepted: 13 March 2014

Abstract The aim of the present study was to investigate the adsorption properties of aminopropyltriethoxysilane (APS) modified microfibrillated cellulose (MFC) in aqueous solutions containing Ni(II), Cu(II) and Cd(II) ions. The modified adsorbents were characterized using elemental analysis, Fourier transform infrared spectroscopy, SEM and zeta potential analysis. The adsorption and regeneration studies were conducted in batch mode using various different pH values and contact times. The maximum removal capacities of the APS/MFC adsorbent for Ni(II), Cu(II), and Cd(II) ions were 2.734, 3.150 and 4.195 mmol/g, respectively. The Langmuir, Sips and Dubinin-Radushkevich models were representative to simulate adsorption isotherms. The adsorption kinetics of Ni(II) Cu(II), and Cd(II) adsorption by APS/MFC data were modeled using the pseudo-first-order, pseudo-second-order and intra-particle diffusion kinetics equations. The results indicate that the pseudo-second-order kinetic equation and intra-particle diffusion model were adequate to describe the adsorption kinetics.

S. Hokkanen (✉) · E. Repo · M. Sillanpää
Laboratory of Green Chemistry, Department of Energy and Environmental Technology, Faculty of Technology, Lappeenranta University of Technology, Sammonkatu 12, 50130 Mikkeli, Finland
e-mail: sanna.hokkanen@lut.fi

T. Suopajärvi · H. Liimatainen · J. Niinimaa
Fiber and Particle Engineering Laboratory, University of Oulu, P.O. Box 4300, Oulu 90014, Finland

Published online: 26 March 2014

Keywords Nanocellulose · Adsorption · Surface modification · Wastewater treatment · Heavy metal removal

Introduction

The removal of heavy metal pollutants from wastewaters has become a critical issue because of their adverse effects on human health and the environment (Lin et al. 2011; Huang et al. 2011). Heavy metals such as Cd(II), Cu(II) and Ni(II) are toxic, non-biodegradable, and often accumulate in the food chain (Muhammad et al. 2011). Several industrial fields such as mining, metal plating, the metallurgical industry, and the manufacturing of plastics, fertilizers, and pigments produce waste waters containing heavy metals (Muhammad et al. 2011; Huang et al. 2008; Huang et al. 2009). The removal of metals from waste streams is important not only due to their toxicity but also to the possibility to recover and reuse metals in many industrial applications.

Conventional methods including chemical precipitation, flocculation, membrane separation, ion exchange, evaporation, and electrolysis have been used to remove heavy metal ions from various industrial effluents. These methods are often costly or ineffective, especially in removing heavy metal ions from dilute solutions (Ng et al. 2002; Bayramoglu et al. 2002). Adsorption has shown to be one of the most efficient and technically feasible methods for metal removal from aqueous

solutions. So far, activated carbon has been the most popular material in wastewater treatment for heavy metal removal. However, the high cost and difficult, energy consuming regeneration of this material makes its application less economically attractive on an industrial scale (Babel and Kurniawan 2003). Consequently, to reduce the operational costs, the search for alternative adsorbents has intensified in recent years. For example, natural bentonite (Babel and Kurniawan 2003), orange peel (Ajmal et al. 2000), chitosan (Repo et al. 2010; Bhatnagar and Sillanpää 2009; Guibal 2004), anaerobic granular sludge (van Hullebusch et al. 2005; Virkutyte et al. 2005) and activated carbon (Bhatnagar and Sillanpää 2010) have been tested for heavy metal removal. However, these materials usually have low adsorption capacities in as-received forms and further modifications are required to improve their applicability.

Cellulose is the most abundant renewable biopolymer in nature. Moreover, it is one of the most promising raw materials available in terms of cost for the preparation of various materials with designed properties and functionalities by means of self-assembly of different guest substrates, such as metal oxide thin films, small molecules, polymers, biomacromolecules, nanoparticles, carbon nanotubes and colloidal spheres (Huang and Gu 2011).

Nano- and micro-celluloses, consisting of a wide variety of minuscule particles from nano-sized whiskers to micron-sized microfibril aggregates, are considered to be amongst the most potential bio-based materials for future high-end applications. Being environmentally friendly, nanocellulose could be one of the most promising nanomaterials in environmental applications such as water purification, and biological and environmental monitoring, such as sensors and bioimaging (Razaq et al. 2012; Lan et al. 2012; Li et al. 2012.; Moritz and Geszke-Moritz 2013). The feasibility of nano- and micro-celluloses is further promoted by their large surface area, chemical accessibility and functional flexibility.

However, cellulose by itself cannot be satisfactorily applied for chelating or adsorbing heavy metal ions, and that is why many attempts have been made to utilize cellulose as a metal ion adsorbent through chemical and physical modification (Abdelmouleh et al. 2004; Vismara et al. 2009; Dahou et al. 2010; Ma et al. 2011; Zhao et al. 2009). Chemical modification using coupling agents enabled an interface to create a chemical bridge between the reinforcement and matrix. For that purpose, silanes are recognized as efficient coupling agents and they are already extensively used in composites and adhesive formulations (Rider and Arnott 2000). C-aminopropyltriethoxysilane (APS) is a kind of silane coupling agent bearing one amino group in one molecule. This silane coupling agent is easily hydrolyzed to the silanol group, and can be further dehydrated with surface hydroxyl groups of cellulose. Moreover, the amino groups could bind heavy metal anions and thus improve the adsorption capacity. Aminosilanes, especially APS, are most extensively studied literature as coupling agents between natural fibers and thermoplastics or thermosets (Bisanda and Ansell 1991; Maldas et al. 1989 Abdelmouleh et al. 2005; Serier et al. 1991; Matuana et al. 1998).

It is expected that amino functionalized cellulose poses a rather similar adsorbing environment than chitosan whom primary amino groups play an important role in complexing metal cations as well as anions. It has been observed that metals are coordinated by amino groups and hydroxyl groups (Wang et al. 2005), which are also present in amino functionalized cellulose. The affinity for different metals has followed an order of $Cu(II) > Hg(II) > Zn(II) > Cd(II) > Ni(II) > Co(II) \sim Ca(II)$ independently on the size and hardness of the ion (Rhazi et al. 2002). Similar behavior is also expected for the amino functionalized cellulose.

In this study, aminosilane (APS) modified nanostructured microfibrillated cellulose (MFC) was used to adsorb Cd(II), Cu(II) and Ni(II) from aqueous solutions. The effects of metal concentration, contact time, and pH on the adsorption were considered. The results related to the adsorption capacity and regeneration of the adsorbent used are very promising.

Materials and methods

Chemicals and solutions

All solutions were prepared in Millipore milliQ high-purity water. The reactant 3-aminopropyl-triethoxysilane (APTES) $\geq$98 % and all other chemicals used in this study were of analytical grade and supplied by Sigma-Aldrich (Germany). Metal stock solutions of 1000 mg/L were prepared by dissolving appropriate amounts of Ni(II), Cu(II) and Cd(II) nitrate salts in

deionized water. The pH was adjusted using 0.1 M NaOH or 0.1 M HNO_3.

Microfibrillated cellulose

Microfibrillated cellulose (MFC I) was purchased from the University of Oulu, Finland. Bleached birch (*Betula pendula*) chemical wood pulp obtained in dry sheets was used as a cellulose raw material after disintegration in deionized water. The polysaccharide content in the pulp was determined with high performance anion exchange chromatography (HPAEC–PAD) (Zuluaga et al. 2009), the lignin content by using (TAPPI-T 222 om-02) and the extractive content with (SCAN-CM 49:03). The cellulose content of the pulp was 74.8 % and the content of hemicelluloses (xylan and glukomannan) was 24.7 %. The amount of lignin was 0.4 % and that of acetone soluble extractives 0.08 %. Prior to homogenizing, the bleached birch pulp was grounded in a Valley beater at a consistency of 2.0 % for 50 h, utilizing 5,503 g of weight. The pulp was then diluted at a consistency of 0.7 % and homogenized with a homogenizer (Invensys APV 2000, Denmark) at a pressure of 350–1,200 bar to create MFC I.

Modification of microfibrillated cellulose

Microfibrillated cellulose (MFC I) (1.0 g) was reacted with a coupling agent, APTES (20 g) in a 80/20 v/v ethanol/water mixture under magnetic stirring for 2 h. The modified cellulose was centrifugted and washed once with an 80/20 v/v ethanol/water mixture and two times with distilled water (Abdelmouleh et al. 2005).

Optimization of the synthesis

The optimization of the synthesis is important due to a large infected area of the nano-size material. The concentration of the coupling agents and the synthesis time were optimized. The optimal amount of coupling agents was determined by adding different amounts (0, 10, 20, 25 and 30) of APTES to 1.0 g of cellulose suspension in an 80/20 v/v ethanol/water mixture and by stirring for 2 h. The optimal synthesis time was also tested using stirring times of 1, 2, 4, 6 and 24 h.

Because of the high water concentration of the modified nanocellulose, the isotherms were determined for the dry weight of the adsorbent. The dry weight was defined by drying 1 g of wet cellulose in an oven at 105 °C for 4 h and then storing it in a desiccator until its weight remained unchanged. The water content of the modified nanocellulose was 98 %.

Characterization of APS modified MFCs

Fourier transform infrared spectroscopy (FTIR) type Vertex 70 by B Bruker Optics (Germany) was used to identify the surface groups of the synthesized nanocellulose. An attenuated total reflection (ATR) -FTIR spectra were recorded at 4 cm^{-1} resolution from 400 to 4,000 cm^{-1} and 100 scans per sample. FESEM (Zeiss Ultra Plus, Germany) was used for imaging the samples. As pretreatment, the samples were filtered to a polycarbonate membrane with a pore size of 0.2 μm, followed by rapid freezing with liquid nitrogen and freeze-drying in a vacuum overnight. The dried samples were then sputter-coated with platinum. A voltage of 10 kV and a working distance of 5 mm were used when imaging the samples. The instrument used for C, H and N determination was Organic Elemental Analyzer Flash 2000 (Thermo Scientific, Germany). Approximately 2.5 mg of the sample in a capsule made of tin (assay of C, H and N) was burned at 920–1,000 °C. The quantity of each element is expressed in a percentage of dry mass. The surface charge and point of zero charge of the modified and unmodified cellulose were determined by isoelectric point titration as a function of pH by using Zetasizer Nano ZS (ZEN3500, Malvern).

Acid/based titration was used to determine the carboxyl group content of unmodified MFC. A few milligrams of model compounds or 0.40 g of unmodified MFC were dissolved in 10 mL of distilled water at room temperature. The coloured indicator was added (0.50 mL of 5 % (w/v) phenolphthalein) into the solution. The solution was titrated with 0.10 M HCl under magnetic stirring. The titration was stopped at the visual endpoint when the color change was stable. The titration procedure was repeated three times. The carboxyl group content of the sample is obtained according to

$$COOH = \frac{C_{HCl} * m_{HCl}}{m_{MFC}} \quad (1)$$

where C_{HCl} is the concentration of HCl (mmol/g), m_{HCl}, is the acid consumption during the titration (mg) and m_{MFC} is the mass of MFC solution sample (mg).

All presented values are the mean value of three parallel measurements.

Batch adsorption experiments

Batch adsorption tests were performed at room temperature to obtain equilibrium isotherms. For isotherm studies, adsorption experiments were carried out by stirring 0.05 g of APS modified MFC with a 0.015 L metal solution containing each metal at concentrations ranging from 0.1 to 10.0 mmol/L. The adsorption efficiency study of unmodified MFC was performed in the same conditions using a solution containing each metal at concentrations of 0.5 and 2.0 mmol/L.

The effect of contact time was studied in a reaction mixture of 0.30 g of adsorbent and 0.350 L of solution containing each metal at concentrations of 0.34 mmol/L. The mixtures were agitated under magnetic stirring using an individual decanter glass for each metal reaction mixture. Samples of 2 mL were pipetted from the reaction mixtures according to schedule. The contact time was varied from 1 to 2,880 min.

After centrifugation, metal concentrations were analyzed by an inductively coupled plasma optical atomic emission spectrometry (ICP–OES) model iCAP 6300 (Thermo Electron Corporation, USA). Ni(II) was analyzed at a wavelength of 231.605 nm, Cu(II) at 324.754 nm and Cd(II) at 226.502 nm.

In order to obtain the adsorption capacity (q), the amount of ions adsorbed per mass unit of APS modified MFC (mg/g) was calculated with the following formula:

$$q_e = \frac{(C_i - C_e)}{M} V \tag{2}$$

where C_i and C_e are the initial and the equilibrium concentrations (mmol/L), while M and V are the weight of the adsorbent (g) and the volume of the solution (L).

The removal efficiency (R %) of the adsorbent was calculated with the following formula:

$$\mathrm{R}(\%) = \left[\frac{C_i - C_e}{C_i}\right] \times 100 \tag{3}$$

Regeneration studies

The regeneration of the modified MFC was studied in Ni(II), Cu(II) and Cd(II) solutions. At first, adsorbents were loaded by metal ions by mixing 1 g of the adsorbent with 0.015 L of 1.8 to 3.4 mmol/L metal solution. After attaining equilibrium, the spent adsorbent was separated from the solution by centrifuge. Metal ions were eluted using 0.1 M HNO_3, 0.1 M NaOH and 0.1 M EDTA. The regeneration efficiency (%RE) of the adsorbent was calculated as follows:

$$(\%RE) = \frac{q_r}{q_0} \times 100 \tag{4}$$

where q_0 and q_r are the adsorption capacities of the adsorbents (mmol/g) before and after regeneration, respectively.

Results and discussions

Characterization of APS modified MFC

The characterization of APS treated MFC was accomplished by FTIR spectroscopy, SEM images, an elementary analyzer and zeta potential measurements. Figure 1 shows the FTIR spectrum of APS modified (I) and pure MFC (II). The spectrum of both materials showed a broad –OH absorption band in the region of 3,250–3,500 cm^{-1}. For APS treated MFC, the absence of the characteristics of free NH_2 modes (3,470 cm^{-1}) is attributed to the hydrogen bonding between almost all of the NH_2 groups and the nearby attached hydrogen atoms (Abdelmouleh et al. 2004; Metwalli et al. 2006). Two absorbing peaks emerged at 2,920 and 2,850 cm^{-1}, corresponding to the tension and vibration of $–CH_2$. A new peak appeared at 1,625 cm^{-1}, implying the vibration and bending of N–H. The bands at 1,575 and 1,480 cm^{-1} are typical for the deformation modes of the NH_2 groups hydrogen bonded to the OH functions of both silanol moieties and cellulosic substrate. The peaks from 1,350 to 1,250 cm^{-1} may imply the extension bending of C–N. The large intense bands around 1,100 and 980 cm^{-1} are related to the –Si–O–Si– linkage and –Si–O–Cellulose bond (Wu et al. 2000; Barbot et al. 2007; Wu et al. 1999).

The morphological characteristic of the unmodified and modified MFC was investigated with FESEM. Figure 2a shows a typical surface morphology for both APS modified and unmodified cellulose fiber. The fibrous nanostructure of MFC remained largely unchanged after modification. Hence there were enough sites for metal ion adsorption on the surface.

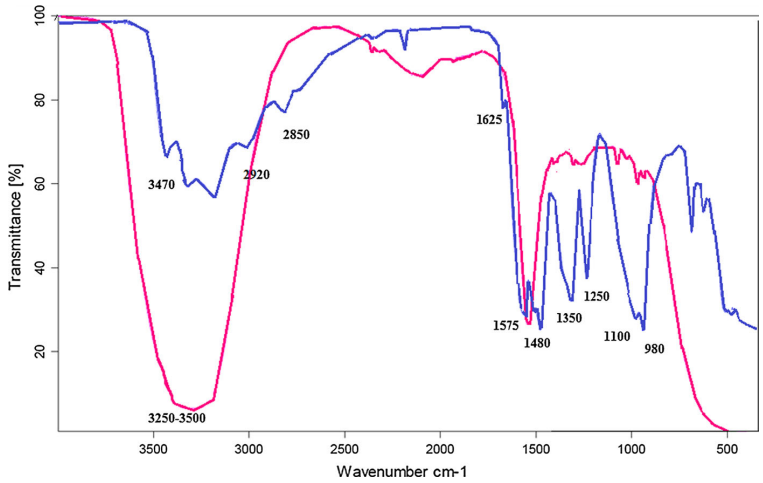

Fig. 1 FTIR spectra of unmodified and APS modified MFC

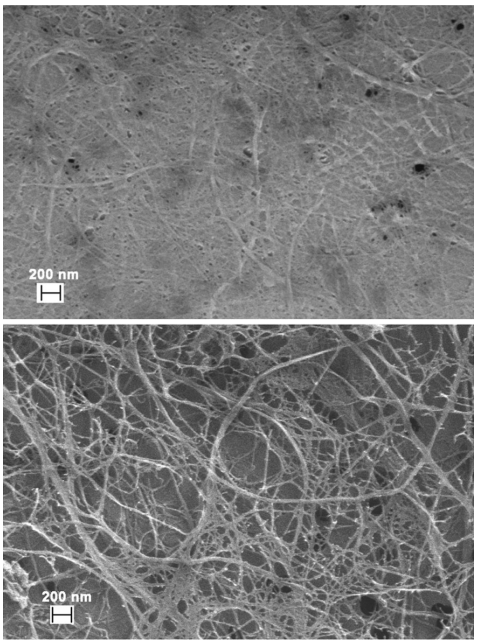

Fig. 2 SEM picture of unmodified and APS modified MFC

Overall, the FESEM analysis showed rather different surface morphologies due to modification by APS. FESEM images also verified that the structure of the adsorbent material was nano-sized (50 nm).

Table 1 The content of N in APS modified MFC obtained from elemental analysis

Material	M (mg)	Content of amine groups (mmol/g)	Molar percentages			
			C	H	N	O
Unmodified MFC	2.61		33.05	0.44		66.51
APS/MFC	2.53	2.3	35.46	0.48	3.43	60.70

The elemental analysis of unmodified and APS modified MFC (Table 1) shows a high level of carbon (33.05 and 35.46 mol%) and oxygen (66.51 and 60.70 mol%), and a low level of hydrogen (0.44 and 0.46 mol%) and nitrogen (3.43 mol% only for APS modified MFC). After modification with aminosilane, an obvious increase in nitrogen content can be observed, which corresponds to the introduction of amine groups on the cellulose surface. Thus, the elemental analysis results also confirm the success of grafting.

The isoelectric point was determined by zeta potential measurements for both unmodified MFC and APS/MFC. For APS/MFC, the isoelectric point was found to be at pH 5.65, while it was roughly pH 3.9 for unmodified MFC (Fig. 3). The latter is consistent with earlier results obtained for nanocellulosic materials (Lee et al. 2011). A change in the isoelectric point after modification is caused by the

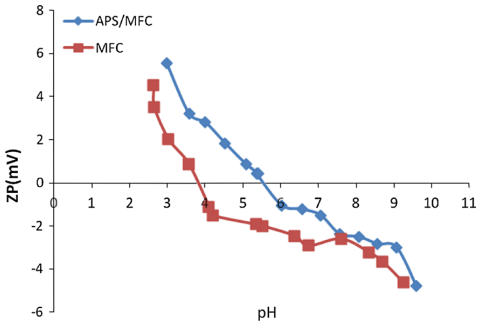

Fig. 3 Zeta potentials as a function of pH

amino groups on the surface of the modified cellulose. The isoelectric point was shifted towards alkaline pH close to the value determined for example for chitosan (pH ∼ 6.5), which is also an amino-functionalized natural biopolymer (Ahire et al. 2007).

The surface charge dependency on the solution pH of the both unmodified and modified MFC followed a similar trend. A positive surface charge at acidic pH indicated a protonation of the surface groups and negative surface charge at alkaline conditions the release of protons into the solution. However, nanocellulose with quaternized amine groups have shown overall positive surface charge even at pH 8.3 (Olszewska et al. 2013) indicating its higher cationic nature compared to the cellulose with primary amino groups used in this study.

Synthesis optimization

Synthesis was optimized with respect to the contact time and concentration of APTES by following metal adsorption on the modified MFC. Figure 4a, b shows that 40 % (0.20 g) of the APTES concentration of the nanocellulose weight and a 2 h contact time were the optimal conditions for interaction between all available hydroxyls of MFC fibers and silanes.

The interaction of silane coupling agents with natural fibers may mainly proceed through hydrolysis, self-condensation or oligomer condensation, adsorption (and grafting) (Salon et al. 2007; Arkles et al. 1992) (Fig. 5). In hydrolysis reaction, the silane monomers are hydrolyzed in the presence of water liberating alcohol and yielding reactive silanol groups. During the hydrolysis process, the condensation of silanols (aging) also takes place. The reaction is shown

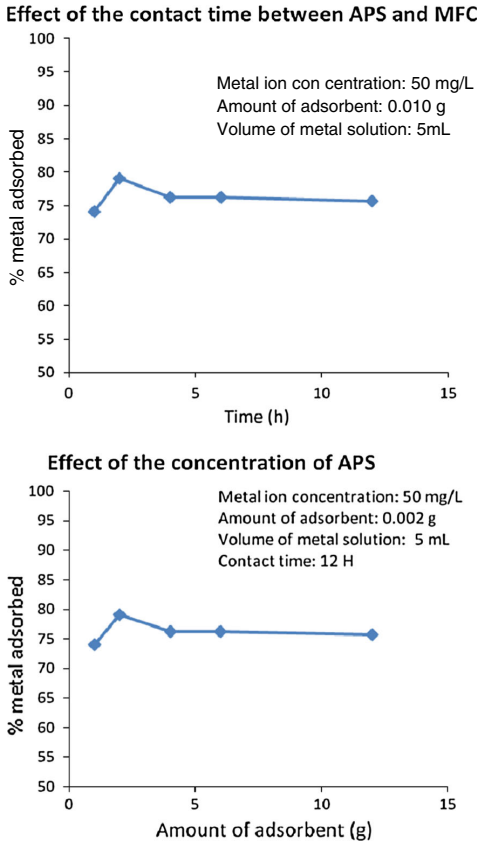

Fig. 4 Optimizing synthesis conditions. **a** Effect of the contact time between APS and MFC. **b** Effect of the concentration of APS

in Fig. 5. Figure 4a shows that the adsorption capacity of APS/MFC decreased after 2 h of synthesis. This may indicate that the condensation reaction dominated after 2 h; hence, the amount of free silanols decreased. The condensed silanol groups cannot be adsorbed by the hydroxyl groups of MFC. In general, the amount of binding sites for metal ions decreases if the synthesis time is excessive.

The reactive silanol monomers or oligomers are physically adsorbed to hydroxyl groups of MFC via hydrogen bonds of the cellulose surfaces (surface coating), which depends on the molecular size of silanol monomers/oligomers formed (Fig. 5) (Salon et al. 2007; Arkles et al. 1992). Free silanols also adsorb and react

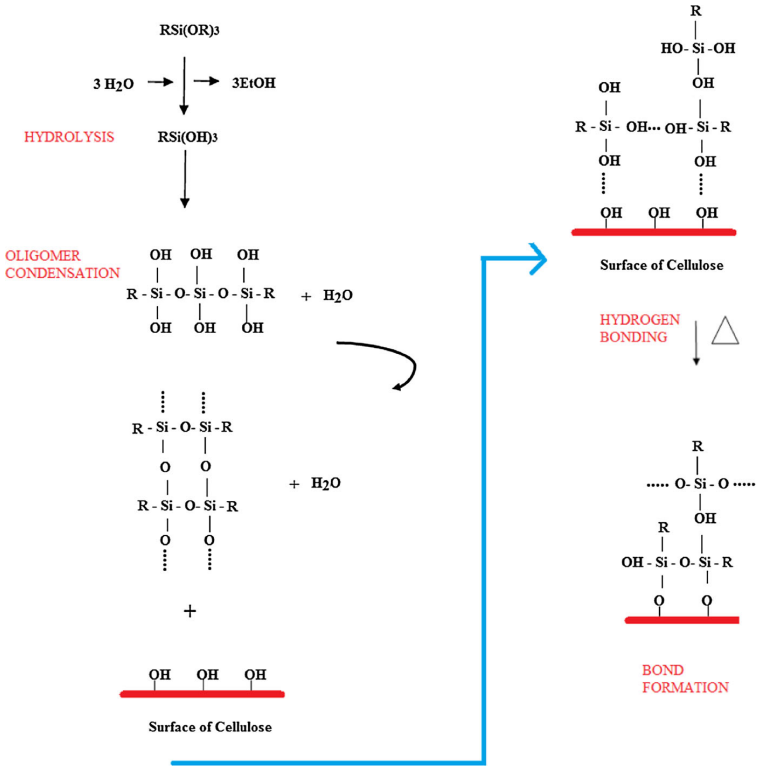

Fig. 5 Silane monomers are hydrolyzed in the presence of liberating alcohol and yielding reactive silanol groups. The hydrogen bonds between silanols and hydroxyl groups of fibers can be converted into the covalent bonds liberating water

with each other, thereby forming rigid polysiloxane structures linked with a stable –Si–O–Si– bond.

Grafting occurs as a general rule under heating conditions, when the hydrogen bonds between the silanols and the hydroxyl groups of fibers can be converted into covalent –Si–O–C– bonds liberating water. The residual silanol groups in the fibers will further condense with each other. The bonds of –Si–O–C– may not be stable towards hydrolysis; however, this bond is irreversible when the water is removed at a raised temperature. This step is not possible with MFC because drying makes nanocellulose material stone-like, rendering its use as an adsorbent impossible.

Adsorption studies

Effect of pH

The removal of metal ions from aqueous solutions by adsorption is dependent on the solution pH because it affects the adsorbent surface charge, the degree of ionization, and the speciation of adsorbates. Figure 6 shows that at solution pH = 2, the adsorption efficiency of Cd(II), Cu(II) and Ni(II) by APS/MFC was nearly zero. In an acidic environment (pH < 3), a relatively high concentration of protons strongly competed with cationic metal ions for free amine sites, and thus, the adsorption of metal ions significantly decreased. On the other hand, the protonation of the amine groups led to a strong electrostatic repulsion towards the metal ions to be adsorbed. With an increasing pH, the competition of protons with metal ions for the amine groups became less significant, and more amine groups existed in their neutral form. This reduced the electrostatic repulsion between the surface and metal ions enhancing adsorption.

At alkaline conditions (pH > 7), metal ions precipitate as $M(OH)_2(s)$, and the amount of aqueous forms of M^{2+}, $M(OH)^+$, $M(OH)M(OH)_2^0$,$M(OH)_3^-$ and $M(OH)_4^{2-}$ vary with the solution pH. Hydroxyl

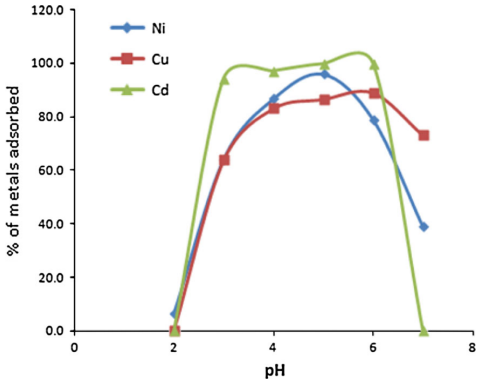

Fig. 6 Effect of pH on the adsorption of Cd(II), Cu(II), and Ni(II) ions by APS/MFC (dose 0.86 g/L; metal ion concentration 50 mg/L; contact time 20 h)

forms of metal species are not adsorbed effectively on the anionic surfaces. For Cu(II), hydroxyl forms are dominating already at pH 7, where the amount of Cu^{2+} is 22.7 %, $Cu_2OH_2^{2+}$ 14.1 %, $Cu_3OH_4^{2+}$ 14.1 %, and $CuOH^+$ 6.5 % (Visual MINTEQ). This explains decreasing adsorption capacity of Cu(II) at these conditions

Figure 6 also indicates that Cd(II) adsorption decreased when the solution pH exceeded 6 and its adsorption was completely inhibited at pH 7. Ni(II) adsorption decreased when the solution pH exceeded 5. Cd(II) and Ni(II) do not form hydroxides in this pH range (Visual MINTEQ), but it is likely that at more alkaline conditions amino groups bound on the cellulose surface contribute to a fast hydrolysis reaction of the Si–O–C bond leading the leaching of APTES into the solution. This observation was confirmed by studying the leaching of the APTES from the surface of APS modified MFC by reaction with alkaline solutions at pH ranging from 6 to 9. The experiments were carried out by stirring 0.05 g of APS modified MFC with a 0.015 L alkaline solution over a period of 8 h. After centrifugation, the nitrogen concentrations were analyzed by using a photometric analyzer (Thermo Scientific Aquakem 250, Finland). Table 2 shows that when pH was varied from 6 to 9 the leaching of the functional groups from the surface of the adsorbent increased. This has also been observed earlier for APTES modified silica gel (Etienne and Walcarius 2003). As a result, the optimum pH for

Table 2 The effect of the pH for the leaching of APTES (=nitrogen) into the solution

pH of the solutions	Nitrogen concentration of solution (μg/L)
6	240
7	310
8	1,200
9	1,700

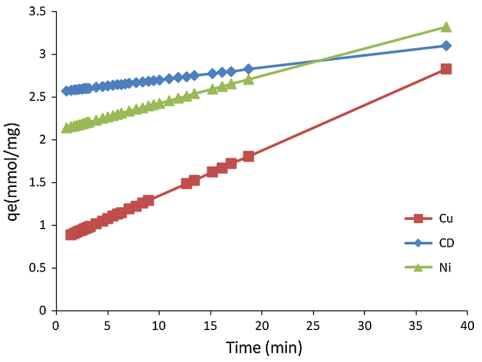

Fig. 7 Effect of contact time on the uptake of Cd(II), Cu(II), and Ni(II) ions by APS/MFC (initial concentration 50 mg/L; dose 0.86 g/L; pH 5.0)

Cd(II), Cu(II) and Ni(II) adsorption by APS/MFC was found to be in the pH range of 4–6, and all further experiments were carried out at pH = 5.

Effect of contact time

In order to establish the equilibration time for the maximum adsorption capacity and to define the rate of the adsorption process, the adsorption capacities of Cd(II, Cu(II) and Ni(II) on APS/MFC were measured as a function of time and the results are shown in Fig. 7.

As shown in Fig. 7, all metals were rapidly removed by adsorbent. During the first 5 min, 97 % of Cd(II), 75 % of Cu(II) and 83 % of Ni(II) were removed by APS/MFC, indicating that these metals were absorbed by readily available adsorption sites.

It is seen that the adsorption rate was initially fast with 50 % of the Cd(II) adsorbed within 1 min, and adsorption equilibrium was attained in <8 min. For Cu(II) and Ni(II), 50 % adsorption was completed

Table 3 Kinetic parameters for Ni(II), Cu(II) and Cd(II) adsorption on APS/MFC

Metal	C_0 (mmmol/L)	$q_{e,exp}$ (mmol/g)	q_e (mmol/g)	k_1 (min^{-1})	R^2
Pseudo-firs-order					
Cd(II)	0.34	2.91	2.83	0.5038	0.642
Cu(II)	0.34	2.93	2.32	0.0235	0.798
Ni(II)	0.34	2.96	2.98	0.1190	0.970
Metal	C_0 (mmol/L)	$q_{e,exp}$ (mmol/g)	q_e (mmol/g)	k_2 (min^{-1})	R^2
Pseudo-second-order					
Cd(II)	0.34	2.91	2.92	0.3380	0.927
Cu(II)	0.34	2.93	2.56	0.0123	0.895
Ni(II)	0.34	2.96	3.1484	0.0566	0.942

within 80 and 8 min, respectively, and adsorption equilibrium was attained within 160 and 35 min, respectively. An inspection of the uptake–time curves shows that the maximum uptake follows the order Cd(II) > Ni(II) > Cu(II) at all time intervals. The kinetic curves for Cd(II) and Ni(II) ions show that the adsorption was initially rapid. The fast rate observed in this study may, to some extent, be attributed to the higher concentration of functional groups on the APS/MFC surface enabled by its nanostructure.

It is known that the adsorption process could be controlled by various mechanisms such as mass transfer, diffusion, chemical reactions and particle diffusion (Unlua and Ersoz 2006). In order to clarify the adsorption process, several adsorption models such as pseudo-first-order and pseudo-second-order models were used to identify the rate and kinetics of adsorption of Cd(II), Cu(II), and Ni(II) on the APS/MFC adsorbent.

The linear pseudo-first-order equation is represented by

$$\ln(q_e - q_t) = \ln q_e - \frac{k_1}{2.303} t \tag{5}$$

where k_1 (min^{-1}) is the pseudo-first-order adsorption rate constant, q_t is the amount of metal adsorbed at time t (min), and q_e denotes the amount of metal adsorbed at equilibrium, both in mmol/g.

The linear pseudo-second-order equation can be expressed as

$$\frac{t}{q_t} = \frac{1}{k_2 q_e^2} + \frac{t}{q_e} \tag{6}$$

where k_2 [g/(mmol min)] is the adsorption rate constant of the pseudo-second-order.

The kinetic parameters for adsorption of Cd(II), Cu(II), and Ni(II) are given in Table 3. The experimental q_e values are in agreement with the calculated values of both pseudo-first-order and pseudo-second-order kinetics.

Based on the obtained correlation coefficients, the pseudo-second-order equation was the model that yielded the best fit for the experimental kinetic data with Ni(II), Cd(II) and Cu(II). This suggests that chemical sorption is the rate-limiting step of the adsorption mechanism and that mass transfer is not involved in the solution (Monier et al. 2010; Atia et al. 2008; Guibal et al. 1998; Repo et al. 2010). Meanwhile, the data was found not to fit the pseudo-first order model, as indicated by the low R^2 values (Table 3). Generally, all the R^2 values were rather low for both of the pseudo kinetic models, which can be attributed to very fast adsorption occurring at the beginning of the experiments. However, the results can be used to notify the fastest removal rate of Cd(II) indicated by its highest rate constant value.

To investigate if the film or pore diffusion was the controlling step in the adsorption, a model of intraparticle diffusion was tested as follows:

$$q_t = X + K_i t^{0.5} \tag{7}$$

where q_t is the amount of metal ion adsorbed at time t, K_i is the intraparticle diffusion rate constant (mmol/g $min^{-0.5}$), and X represents the boundary layer diffusion effects. As the value of X decreases, the effect of boundary layer diffusion decreases. The plot of adsorption capacity versus the square root of time (Fig. 7) gives a straight line that does not pass through the origin. This indicates that the adsorption of metals

by modified MFC is controlled by intraparticle diffusion along with the boundary layer diffusion, and adsorption may take place through a multi-step mechanism comprising (I) external surface adsorption or instantaneous adsorption, (II) intraparticle diffusion and (III) interaction between the adsorbate and active site. At the final stage, the intraparticle diffusion starts to slow down due to the low metal concentration in the solution (Guibal et al. 1998; Cheung et al. 2007).

Adsorption studies and isotherms

The equilibrium adsorption isotherm is fundamental in describing the interactive behavior between the adsorbate and adsorbent, and the relationship between the concentration of adsorbed and dissolved adsorbate at equilibrium. For the adsorption isotherm studies, the initial metal ion concentrations were in the range of 10–300 mg/L.

In this study, the adsorption mechanisms were analyzed by one two-parameter (Langmuir) and one tree-parameter (Sips) isotherm models, which are commonly used to describe experimental results in a wide range of concentrations.

The Langmuir isotherm model was originally developed to describe the gas–solid phase adsorption. It models the monolayer coverage of the adsorptive surface. The model assumes that adsorption occurs at specific homogeneous adsorption sites within the adsorbent, and intermolecular forces decrease rapidly with the distance from the adsorptive surface. The Langmuir adsorption model further assumes that all the adsorption sites are energetically identical and adsorption occurs on a structurally homogeneous adsorbent. The Langmuir equation is expressed as follows:

$$q_e = \frac{q_m K_L C_e}{1 + K_L C_e} \tag{8}$$

where q_e (mmol/g) is the equilibrium adsorption capacity and q_m (mmol/g) is the maximum amount of the metal ions adsorbed per unit weight of the adsorbent. The latter also describes the formation of complete monolayer coverage on the surface at high equilibrium metal ion concentration C_e (mmol/L). Furthermore, q_m represents the practical limiting adsorption capacity when the surface is fully covered with metal ions, assisting in the comparison of adsorption performances of different adsorbents. K_L (L/mmol) is the Langmuir equilibrium constant related to the affinity of the binding sites and indicates the bond energy of the adsorption reaction between metal and material (Ho et al. 2002; Repo et al. 2010).

Modeling calculations were conducted using Microsoft Office Excel 2007 software. Isotherm parameters were determined by minimizing the Sum of the Squares of the Errors (ERRSQ) function across the concentration range studied:

$$\sum_{i=1}^{p} \left(q_{e,\exp} - q_{e,\mathrm{calc}}\right)^2 \tag{9}$$

Figure 8 shows that the Langmuir isotherm fit rather well with the experimental data, and especially for Ni(II), the adsorption was supported also by the estimated q_m value and high R^2 value (Table 4). For Cu(II), however, the Langmuir model could not predict the experimental behavior indicating more complex adsorption phenomena than simple monolayer formation. Significant variations in K_L values of metal ions indicate that the adsorption energies between the adsorbent and metal ions were different. The high K_L values of Cd(II) and Ni(II) ions correlated well with theast adsorption and low K_L value of Cu(II) with the slower adsorption seen in kinetic experiments.

The Langmuir model is often too simple to describe the complex adsorption phenomena due to the surface heterogeneity or interactions between adsorbing species. The Sips isotherm is a three-parameter isotherm appearing as a combination of the Langmuir and Freundlich isotherms and is therefore also called the Langmuir–Freundlich (Sips) isotherm (Guibal et al. 1998; Ho et al. 2002). Generally, the Sips isotherm is an appropriate equation to fit the experimental equilibrium data of a wide variety of adsorbents. It takes the following form:

$$q_e = \frac{q_m (K_S C_e)^{n_s}}{1 + (K_S C_e)^{n_s}}$$

where q_m is the total number of binding sites (mg/g), K_s is the median association constant (mL/mg) and n_s is the heterogeneity factor. If the value for n_s is <1, the Sips isotherm will become a Freundlich isotherm, which indicates that it is a heterogeneous adsorbent. While the value for n_s is getting closer to one the Sips isotherm equation reduces to the Langmuir equation and adsorption takes place on the homogeneous

surface (Allen et al. 2004; Repo et al. 2010). Table 4 shows that all n_s values obtained were higher than 1, indicating more homogeneous binding sites.

The plots of the Sips isotherm are illustrated in Fig. 8 and the examination of the results is presented in Table 4. Results show that for Cd(II), the q_m value estimated by the Sips model corresponded to the experimentally obtained $q_{m,exp}$ significantly better than that estimated by the Langmuir model. For Ni(II), the Langmuir model seemed to provide a better approximation for q_m, but the R^2 values were higher for all the metals with the Sips model. The results for the maximum adsorption capacity of the experimental data for Ni(II) (2.734 mmol/g), Cu(II) (3.150 mmol/g) and Cd(II) (4.195 mmol/g) correlated quite well with the results given by the elementary analysis for the amount of active sites (2.3 mmol/g). However, higher capacities indicate that part of the metals were adsorbed by other surface groups than amines. It is also possible that the amount of amino groups varied from sample to sample due to the high water content and heterogeneous structure of the modified MFC.

The different behavior of the studied metals may be attributed to the formation of hydroxides, which is observed for Cu(II) (Visual MINTEQ). This may cause the highly heterogeneous adsorption of Cu(II), while Cd(II) and Ni(II) are adsorbed more homogeneously (no hydroxide formation within the pH range used). Relatively poor correlation coefficients (R^2 values < 0.990) observed for all of the metal ions with both Langmuir and Sips models may be attributed to the unequal distribution of the adsorption surface area and active sites in samples due to the high water concentration of APS modified nano cellulose.

It can be seen that APS/MFC has a relatively high adsorption capacity for Cd(II), Cu(II) and Ni(II) ions, indicating that it has significant potential for the removal of these metal ions from aqueous solutions. A comparison of the adsorption efficiency of APS/MFC to some commercial as well as cellulose-based adsorbents/ion-exchangers is presented in Table 5. It can be seen that APS/MFC provides clearly better adsorption properties compared to the commercial adsorption resins as well as some other cellulose based materials.

The Dubinin-Radushkevich (D-R) isotherm model was applied to the data in order to deduce the heterogeneity of the surface energies of adsorption and the characteristic porosity of the adsorbent. The linear form of the D-R isotherm is given as follows:

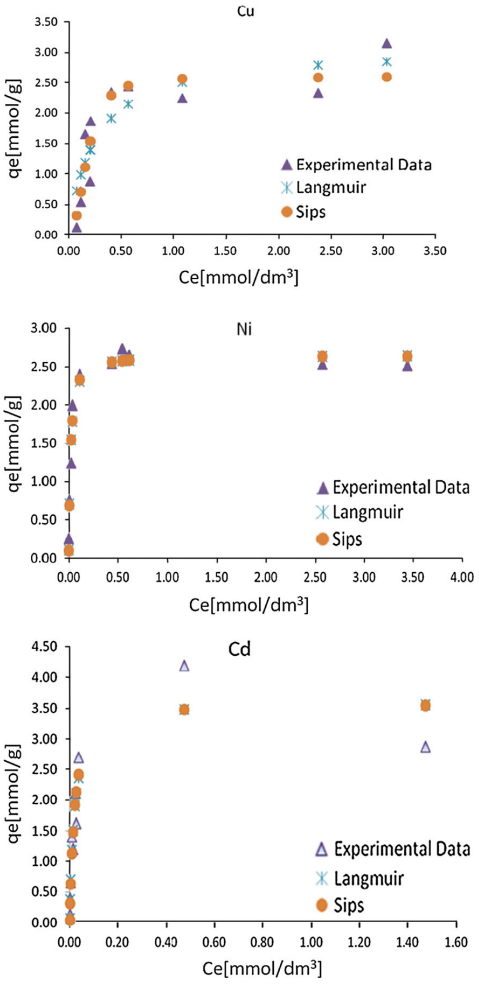

Fig. 8 Adsorption isotherms of Ni(II), Cu(II) and Cd(II) on APS/MFC (dose 0.67 mg/L, contact time 12 h; pH 5)

$$\ln q_e = \ln q_D - B_D\left(RT\ln\left(1+\frac{1}{C_e}\right)^2\right) \tag{11}$$

The apparent energy of adsorption, E was calculated by

$$E = \frac{1}{(2B_D)^{1/2}} \tag{12}$$

The constants q_D(mol/g) is the D-R constant representing the theoretical saturation capacity and

Table 4 Isotherm constants of APS/MFC for Ni(II), Cu(II) and Cd(II)

Type of metal	q_m (mmol/g)	$q_{m,exp}$ (mmol/g)	n_s	K_S	R^2
Sips					
Cd(II)	3.472	4.195	1.100	53.667	0.894
Cu(II)	2.593	3.150	2.387	5.761	0.965
Ni(II)	3.092	2.724	1.038	62.973	0.970
Type of metal	q_m (mmol/g)	$q_{m,exp}$ (mmol/g)		K_L	R^2
Langmuir					
Cd(II)	3.611	4.195		61.298	0.892
Cu(II)	3.078	3.150		4.072	0.770
Ni(II)	2.663	2.734		52.194	0.969
Type of metal	q_D (mmol/g)	$q_{m,exp}$ (mmol/g)	B_d	E	R^2
Dubinin-Radushkevich					
Cd(II)	1.445	4.195	0.007	8.111	0.964
Cu(II)	1.446	3.150	0.007	8.379	0.805
Ni(II)	1.048	2.734	0.007	8.392	0.981

Table 5 Comparison of APS/MFC to other adsorption materials

Adsorbent	Metal	pH	Contact time (min)	q_m (mmol/g)	Reference
Amberlite IRC-748	Cu(II)	5	1,440	1.69	Ling et al. 2010
	Cd(II)			0.61	
Lewatit CNP 80	Ni(II)	8	120	0.32	Pehlivan and Altun 2007
	Cu(II)			0.16	
	Cd(II)			0.04	
MCGT	Cu(II)	5	7	1.50	Donia et al. 2012
Cellulose acetate/zeolite composite fiber	Cu(II)	5	–	0.18	Ji et al. 2012
	Ni(II)			0.19	
EABC	Cu(II)	4.5	10–80	0.98	Shen et al. 2009
CelNN/ethylenediamine	Cu(II)	5	–	1.63	Torres et al. 2006
	Ni(II)			0.53	
Succinic anhydried modified cellulose	Cu(II)		–	2.42	Gurgel et al. 2008
	Cd(Ii)		–	2.22	
EMMB	Cu(II)	5.3	10	1.43	Karnitz et al. 2009
	Cd(II)	5.3		1.33	
APS/MFC	Cu(II)	5	300	2.74	This study
	Cd(II)		300	3.45	
	Ni(II)		300	2.63	

$B_D(mol^2/J^2)$ is a constant related to the mean free energy of adsorption per mol of the adsorbate, R is the ideal gas constant, (8.314 J/mol K), T(K) is the temperature of adsorption and E(kJ/mol) is the mean free energy of adsorption per molecule of the adsorbate when transferred to the surface of the solid from infinity in solution. The constants q_D and B_D were calculated from the intercept and the slope, which were determined by the plot of lnq_e against $[RTln(1 + 1/Ce)]^2$.

The D-R isotherm parameters are given in Table 4. If the value of E lies between 8 and 16 kJ/mol the nature of the sorption process is chemical, while values below 8 kJ/mol indicate a physical adsorption process. The values of the apparent energy of adsorption (8.392, 8.379 and 8.111 kJ/mol) obtained indicated chemisorptions between Ni(II), Cu(II) and Cd(II) ions, respectively (Chen et al., 2008).

The removal efficiency of unmodified MFC was also studied. Table 6 shows that the interaction between unmodified MFC and metal ions is observed due to the carboxylic groups on MFC surface. The value of the carboxyl group content obtained by the acid/based titration for unmodified MFC sample is 1.062 mmol/g. The interactions between metals and carboxylic groups can be expressed as follows:

$$M^{n+}n(-COOH) \rightarrow (-COOH)_nM \uparrow +nH^+ \qquad (13)$$

where (–COOH) represents the carboxylic groups of unmodified MFC and n is the coefficient of the reaction component depending on the oxidation state of the metal ion. The comparison between APS/MFC and unmodified MFC indicate the radically better removal efficiency of APS/MFC.

Adsorption mechanism

Amino groups are mainly responsible for the uptake of Cd(II), Cu(II) and Ni(II) ions as follows (Repo et al. 2010):

Table 6 The adsorption efficiency of unmodified MFC and APS/MFC using tree different concentration of Cu(II), Ni(II) and Cd(II) solutions

Concentration of metal solution (mg/L)	MFC q_e (mmol/g)	APS/MFC q_e (mmol/g)
Ni(II)		
50	0.0400	1.2449
100	0.0138	2.3938
200	0.2556	2.7344
Cu(II)		
50	0.0708	0.8757
100	0.0944	1.8681
200	0.2596	2.3367
Cd(II)		
50	0.0708	0.8756
100	0.0084	1.2449
200	0.0400	2.6992

$$M^{2+} + RNH_2^+ \rightarrow M(RNH_2)^{2+} \qquad (14)$$

However, aminosilane modified MFC is able to adsorb metals because the amino (–NH_2) on aminosilane and/or hydroxyl (–OH) groups on cellulose fiber. Nitrogen and oxygen atoms have free electron doublets that can react with metal cations. At higher solution pH values of 5–6 (lower proton concentrations), fewer protons are available to protonate –NH_2 to –NH_3^+. The removal efficiency (R %) of the adsorbent decreases by increasing the initial metal ion (M^{2+}) concentration due to the saturation of binding sites (Kudryavtsev et al. 1990). The adsorption yield was calculated using Eq. (2). At the beginning of the M^{2+} adsorption process on aminosilane modified MFC, the ions tie with two ligands to form $[M(RNH_2)_2]^{2+}$complexes as shown in Fig. 9(1). Based on the adsorption energy values obtained from D-R isotherm, chemical adsorption takes place and bonds between nitrogen and metals are coordinative. Other coordination sites of metal ion are occupied by water molecules or hydroxyl groups of cellulose as in the case of chitosan (Wang et al. 2005). At higher M^{2+} concentrations, some of the $[M(RNH_2)_2]^{2+}$ complexes convert into $[M(RNH_2)]^{2+}$ (Fig. 9(2)), leading to a higher adsorption capacity. At low concentrations, all M^{2+} ions present in the solution could interact with two binding sites, leading to a higher adsorption yield. As seen in Fig. 10, when the dilute solutions, i.e. 30 mg/L, were used, over 85 % of metals were removed. This confirms the high sensitivity of the adsorbent to such cations, which is a crucial parameter to design the Cd(II), Cu(II) and Ni(II) separation process based on adsorption. As mentioned earlier, some of the amine groups might be hydrogen-bonded to the cellulose surface hydroxyl groups, as shown in Fig. 9(3), diminishing their availability for adsorption.

Another possible mechanism is the ion-exchange reaction of M^{2+} with the surface hydroxyl groups via the Si–O–M–O–Si bridging species, as shown in Fig. 9(4). It is also possible that metal ions might react with one amine group and ion-exchange with an adjacent hydroxyl group, as shown in Fig. 9(4).

For cationic metal ions, there is a direct relationship between the charge to radius ratio (Z/r) and adsorption capacity (Demirbas et al. 2005; Breviglieri et al. 2000). Thus, according to the Z/r ratio of the cations Cd(II) (2.11), Cu(II) (2.74) and Ni(II) (2.90), the selectivity sequence is expected to be Ni(II) > Cu(II) > Cd(II) for

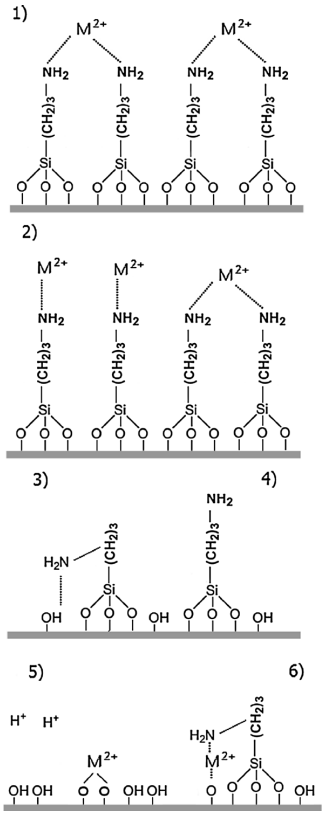

Fig. 9 Proposed mechanisms for Ni(II), Cu(II) or Cd(II) (=M^{2+}) adsorption on APS/MFC

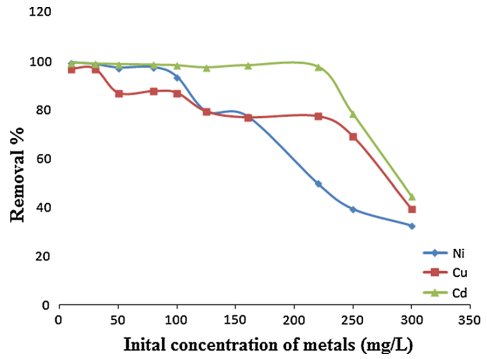

Fig. 10 The removal capacity of Ni(II), Cu(II) and Cd(II) MFC (dose 0.67 mg/L, contact time 12 h; pH 5)

Table 7 Regeneration of APS/MFC

Type of regenerant	No. of cycle	Adsorption capacity of **Ni(II)**		Regeneration efficiency (%)	Adsorption capacity of **Cu(II)**		Regeneration efficiency (%)	Adsorption capacity of **Cd(II)**		Regeneration efficiency (%)
		Before regeneration (mmol/g)	After regeneration (mmol/g)		Before regeneration (mmol/g)	After regeneration (mmol/g)		Before regeneration (mmol/g)	After regeneration (mmol/g)	
HNO_3 (0.1 M)	1	0.927	0.215	23.19	0.813	0.297	36.53	0.803	0.196	24.41
	2	0.927	0.190	20.49	0.813	0.070	0.09	0.803	0.206	25.65
NaOH (0.1 M)	1	0.927	0.963	103.88	0.813	0.980	120.54	0.803	0.796	99.13
	2	0.927	1.440	155.34	0.813	0.901	110.82	0.803	0.804	101.12
EDTA (0.1 M)	1	0.927	0.264	28.48	0.813	0.181	22.26	0.803	0.330	41.10
	2	0.927	0.332	25.81	0.813	0.223	27.43	0.803	0.197	24.53

divalent ions. The results in Table 3 confirm this. It should be noted that this selectivity sequence is different compared to chitosan (see introduction).

The maximum removal capacities of the APS/MFC adsorbent for Ni(II), Cu(II), and Cd(II) ions were 2.734, 3.150 and 4.195 mmol/g, respectively.

Regeneration study

The stability of the adsorbent was investigated by regeneration experiments. This procedure is necessary to restore the original adsorption capacity of the adsorbent, and it also enables recovering valuable metals from wastewater streams. In this study, Cd(II), Cu(II) and Ni(II) were desorbed from APS modified MFC using 0.1 M HNO_3, 0.1 M NaOH and 0.1 M EDTA. Results presented in Table 7 were obtained for different metals at the same conditions (metal concentration of 100 mg/L; adsorbent dose of 0.020 g; regenerant volume of 0.010 L).

Table 7 shows that the adsorption efficiency was radically affected by regeneration with HNO_3 and EDTA treatment; the adsorbent lost its adsorption capacity completely. The adsorption capacity remained the same or even improved after treatment with NaOH. After the first cycle of regeneration, the adsorption capacities of the adsorbents for Ni(II), Cu(II) and Cd(II) still remained the same. These results indicate the suitability of an alkaline regenerant for APS modified MFC.

Conclusions

The nanostructured APS modified MFC adsorbent for heavy metals was successfully prepared using a very quick and easy method. Moreover, preparation of the adsorbent was carried out without environmentally harmful chemicals. The modified MFC was very effective for Ni(II), Cu(II) and Cd(II) removal from contaminated water. The adsorption of Ni(II), Cu(II), and Cd(II) ions was shown to be dependent on the solution pH, and the optimum pH value for the adsorption was 5. The kinetic study demonstrated that the kinetic mechanism for the adsorption of metal ions followed a pseudo-second-order model, which provided the best correlation with the experimental data. Also the intraparticle diffusion model was well fitted. In the isotherm studies, the experimental maximum adsorption capacities ranged from 2.72 to 4.20 mmol/g. The Sips isotherm model provided the best fit to the experimental adsorption data for these ions, revealing maximum adsorption capacities of 3.09, 2.59, and 3.47 mmol/L for Ni(II), Cu(II) and Cd(II), respectively. The regeneration of APS/MFC was best accomplished by an alkaline regenerant.

Acknowledgments The authors thank the Finnish Funding Agency for Technology and Innovation (Tekes) for its financial support.

References

Abdelmouleh M, Boufi S, Belgacem MN, Duarte AP, Salah BA, Gandini A (2004) Modification of cellulosic fibres with functionalised silanes: development of surface properties. Int J Adhes Adhes 24:43–54

Abdelmouleh M, Boufi S, Belgacem MN, Dufresne A, Gandini A (2005) Modification of cellulose fibers with functionalized silanes: effect of the fiber treatment on the mechanical performances of cellulose–thermoset composites. J Appl Polym Sci 98:974–984

Ahire VJ, Sawant KK, Doshi JB, Ravetkar SD (2007) Chitosan microparticles as oral delivery system for tetanus toxoid. Drug Dev Ind Pharm 33:1112–1124

Ajmal M, Rao RAK, Ahmad R, Ahmad J (2000) Adsorption studies on Citrus reticulate (fruit peel of orange): removal and recovery of Ni(II), from electroplating wastewater. J Hazard Mater 79:117–131

Allen SJ, Mckay G, Porter JF (2004) Adsorption isotherm models for basic dye adsorption by peat in single and binary component systems. J Colloid Interface Sci 280:322–333

Arkles B, Steinmetz JR, Zazyczny J, Mehta P (1992) Factors contributing to the stability of alkoxysilanes in aqueous solution. J Adhes Sci Technol 6:193–206

Atia AA, Donia AM, Awed HW (2008) Synthesis of magnetic chelating resins functionalized with tetraethylenepentamine for adsorption of molybdate anions from aqueous solutions. J Hazard Mater 155:100–108

Babel S, Kurniawan TA (2003) Low-cost adsorbents for heavy metals uptake from contaminated water: a review. J Hazard Mater 97:219–243

Barbot C, Bouloussa O, Szymczak W, Plaschke M, Buckau G, Durand J-P, Pieri J, Kim JI, Goudard F (2007) Self-assembled monolayers of aminosilanes chemically bonded onto silicon wafers for immobilization of purified humic acids. Colloids Surf A: Physicochem Eng Asp 297:221–239

Bayramoglu G, Denizli A, Sektas S, Arica MY (2002) Entrapment of *Lentinus sajor-caju* into Ca-alginate gel beads for removal of Cd(II), ions from aqueous solution: preparation and biosorption kinetics analysis. Microchem J 72:63–76

Bhatnagar A, Sillanpää M (2009) Applications of chitin- and chitosan-derivatives for the detoxification of water and wastewater: a short review. Adv Colloid Interface Sci 152:26–38

Bhatnagar A, Sillanpää M (2010) Utilization of agro-industrial and municipal waste materials as potential adsorbents for water treatment: a review. Chem Eng J 157:277–296

Bisanda ETN, Ansell MP (1991) The effect of silane treatment on the mechanical and physical properties of sisal-epoxy composites. Compos Sci Technol 41:165–178

Breviglieri ST, Cavalheiro RTG, Chierice GO (2000) Correlation between ionic radius and thermal decomposition of Fe(II), Co(II), Ni(II), Cu(II) and Zn(II) diethanoldithiocarbamates. Thermochim Acta 356:79–84

Chen A-H, Liu S-C, Chen C-Y, Chen C-Y (2008) Comparative adsorption of Cu(II), Zn(II), and Pb(II) ions in aqueous solution on the crosslinked chitosan with epichlorohydrin. J Hazard Mater 154:184–191

Cheung WH, Szeto YS, McKay G (2007) Intraparticle diffusion processes during acid dye adsorption onto chitosan. Bioresour Technol 98:2897–2904

Dahou W, Ghemati D, Oudia A, Aliouche D (2010) Preparation and biological characterization of cellulose graft copolymers. Biochem Eng J 48:187–194

Demirbas A, Pehlivan E, Gode F, Altun T, Arslan G (2005) Adsorption of Cu(II), Zn(II), Ni(II), Pb(II), and Cd(II) from aqueous solution on Amberlite IR-120 synthetic resin. J Colloid Interface Sci 282:20–25

Donia AM, Atia AA, Abouzayed FA (2012) Preparation and characterization of nano-magnetic cellulose with fast kinetic properties towards the adsorption of some metal ions. Chem Eng J 191:22–30

Etienne M, Walcarius A (2003) Analytical investigation of the chemical reactivity and stability of aminopropyl-grafted silica in aqueous medium. Talanta 59:1173–1188

Guibal E (2004) Interactions of metal ions with chitosan-based sorbents: a review. Sep Purif Technol 38:43–74

Guibal E, Milot C, Tobin JM (1998) Metal-anion sorption by chitosan beads: equilibrium and kinetic studied. Ind Eng Chem Res 37:1454–1463

Gurgel LV, Karnitz O Jr, de Freitas RP, Gil LF (2008) Adsorption of Cu(II), Cd(II) and Pb(II), from aqueous single metal solutions by cellulose and mercerized cellulose chemically modified with succinic anhydride. Bioresour Technol 99:3077–3083

Ho YS, Porter JF, Mckay G (2002) Equilibrium isotherm studies for the sorption of divalent metal ions onto peat: copper, nickel and lead Single component systems. Water Air Soil Pollut 141:1–33

Huang J, Gu Y (2011) Self-assembly of various guest substrates in natural cellulose substances to functional nanostructured materials. Curr Opin Colloid Interface Sci 16:470–481

Huang X, Sillanpää M, Duo B, Gjessing ET (2008) Water quality in the tibetan plateau: metal contents of four selected rivers. Environ Pollut 156:270–277

Huang X, Sillanpää M, Duo B, Gjessing ET (2009) Water quality in the tibetan plateau: major ions and trace elements in the headwaters of four major Asian rivers. Environ Pollut 156:270–277

Huang CH, Chang KP, Ou HD, Chiang YC, Wang CF (2011) Adsorption of cationic dyes onto mesoporous silica. Microporous Mesoporous Mater 141:102–109

Ji F, Li C, Tang B, Xu J, Lu G, Liu P (2012) Preparation of cellulose acetate/zeolite composite fiber and its adsorption behavior for heavy metal ions in aqueous solution. Chem Eng J 209:325–333

Karnitz O Jr, Gurgel LVA, de Freitas RP, Gil LF (2009) Adsorption of Cu(II), Cd(II), and Pb(II), from aqueous single metal solutions by mercerized cellulose and mercerized sugarcane bagasse chemically modified with EDTA dianhydride (EDTAD). Carbohydr Polym 77:643–650

Kudryavtsev GV, Miltchenko DV, Yagov VV, Lopatkin AA (1990) Ion sorption on modified silica surface. J Colloid Interface Sci 140:114–122

Lan E, Male KB, Chong JH, Leung ACW, Luong JHT (2012) Applications of functionalized and nanoparticle-modified nanocrystalline cellulose: a review. Trends Biotechnol 30:283–290

Lee K-Y, Quero F, Blaker JJ, Hill CAS, Eichhorn SJ, Bismarck A (2011) Surface only modification of bacterial cellulose nanofibres with organic acids. Cellulose 18:595–605

Li X, Wang Y, Yang X, Chen J, Fu H, Cheng T, Wang Y (2012) Conducting polymers in environmental analysis: a review. Trends Anal Chem 39:163–179

Lin YF, Chen HW, Chien PS, Chiou CS, Liu CC (2011) Application of bifunctional magnetic adsorbent to adsorb metal cations and anionic dyes in aqueous solution. J Hazard Mater 185:1124–1130

Ling P, Liu F, Li L, Jing X, Yin B, Chen K, Li A (2010) (Adsorption of divalent heavy metal ions onto IDA-chelating resins: simulation of physicochemical structures and elucidation of interaction mechanisms. Talanta 81:424–432

Ma H, Hsiao B, Chu B (2011) Ultrafine cellulose nanofibers as efficient adsorbents for removal of UO22+ in water. ACS Macro Lett 1:213–216

Maldas D, Kokta BV, Daneault C (1989) Influence of coupling agents and treatments on the mechanical properties of cellulose fiber–polystyrene composites. J Appl Polym Sci 37:751–775

Marinich JA, Ferrero C, Jiménez-Castellanos MR (2009) Graft copolymers of ethyl methacrylate on waxy maize starch derivatives as novel excipients for matrix tablets: physicochemical and technological characterization. Eur J Pharm Biopharm 80:674–681

Matuana LM, Woodhams RT, Balatinecz JJ, Park CB (1998) Influence of interfacial interactions on the properties of PVC/cellulosic fiber composites. Polym Compos 19:446–455

Metwalli E, Haines D, Becker O, Conzone S, Pantano CGC (2006) Surface characterizations of mono-, di-, and triaminosilane treated glass substrates. J Colloid Interface Sci 298:825–831

Monier M, Ayad DM, Wei BY, Sarhan AA (2010) Preparation and characterization of magnetic chelating resin based on chitosan for adsorption of Cu(II), Co(II), and Ni(II) ions. React Funct Polym 70:257–266

Moritz M, Geszke-Moritz M (2013) The newest achievements in synthesis, immobilization and practical applications of antibacterial nanoparticles. Chem Eng J 228:596–613

Muhammad S, Shah MT, Khan S (2011) Health risk assessment of heavy metals and their source apportionment in drinking water of Kohistan region, northern Pakistan. Microchem J 98:334–343

Ng JCY, Cheung WH, Mckay G (2002) Equilibrium studies of the sorption of Cu(II), ions onto chitosan. J Colloid Interface Sci 255:64–74

Olszewska AM, Kontturi E, Laine J, Österberg M (2013) All-cellulose multilayers: long nanofibrils assembled with short nanocrystals. Cellulose 20:1777–1789

Pehlivan E, Altun T (2007) Ion-exchange of Pb2+ , Cu2+ , Zn2+ , Cd2+, and Ni2+ ions from aqueous solution by Lewatit CNP 80. J Hazard Mater 140:299–307

Razaq A, Nyholm L, Sjodin M, Stromme M, Mihranyan A (2012) Paper-based energy-storage devices comprising carbon fiber-reinforced polypyrrole-cladophora nanocellulose composite electrodes. Adv Energy Mater 2:445–454

Repo E, Warchol JK, Kurniawan TA, Sillanpää MET (2010) Adsorption of Co(II), and Ni(II), by EDTA- and/or DTPA-modified chitosan: kinetic and equilibrium modeling. Chem Eng J 161:73–82

Rhazi M, Desbrieres J, Tolaimate A, Rinaudo M, Vottero P, Alaguic A, Meray ME (2002) Influence of the nature of the metal ions on the complexation with chitosan. Eur Polym J 38:1523–1530

Rider AN, Arnott DR (2000) Boiling water and silane pretreatment of aluminium alloys for durable adhesive bonding. Int J Adhes Adhes 20:209–220

Salon MCB, Gerbaud G, Abdelmouleh M, Bruzzese C, Boufi S, Belgacem MN (2007) Studies of interactions between silane coupling agents and cellulose fibers with liquid and solid-state NMR. Magnet Reson Chem 45:473–483

Serier A, Pascault JP, Lam TM (1991) Reaction in aminosilane-epoxy prepolymer systems II Reactions of alkoxysilane groups with or without the presence of water. J Polym Sci, Part A: Polym Chem 29:1125–1131

Shen W, Chen S, Shi S, Li X, Zhang X, Hu W, Wang H (2009) Adsorption of Cu(II), and Pb(II), onto diethylenetriamine-bacterial cellulose. Carbohydr Polym 75:110–114

Torres JD, Faria EA, Prado A (2006) Thermodynamic studies of the interaction at the solid/liquid interface between metal ions and cellulose modified with ethylenediamine. J Hazard Mater 129:239–243

Unlua N, Ersoz M (2006) Adsorption characteristics of heavy metal ions onto a low cost biopolymeric sorbent from aqueous solutions. J Hazard Mater 136:272–280

van Hullebusch ED, Peerbolte A, Zandvoort MH, Lens PNL (2005) Sorption of cobalt and nickel on anaerobic granular sludges: isotherms and sequential extraction. Chemosphere 58:493–505

Virkutyte J, Hullebusch E, Sillanpaa M, Lens P (2005) Copper and trace element fractionation in electrokinetically treated anaerobic granular sludge. Environ Pollut 138:517–528

Vismara E, Melonea L, Gastaldi G, Cosentinob C, Torri G (2009) Surface functionalization of cotton cellulose with glycidyl methacrylate and its application for the adsorption of aromatic pollutants from wastewaters. J Hazard Mater 170:798–808

Wang XH, Du YM, Fan LH, Liu H, Hu Y (2005) Chitosan-metals complexes as antimicrobial agent: synthesis, characterization and structure-activity study. Polym Bull 55:105–113

Wu FC, Tseng RL, Juang RS (1999) Role of pH in metal adsorption from aqueous solutions containing chelating agents on chitosan. Ind Eng Chem Res 38:270–275

Wu B, Guangzhao M, Ng KYS (2000) Stepwise adsorption of a long trichlorosilane and a short aminosilane. Physicochem Eng 162:203–213

Zhao Y, Huang M, Wu W, Jin W (2009) Synthesis of the cotton cellulose based Fe(III) -loaded adsorbent for arsenic(V), removal from drinking water. Desalination 249:1006–1011

Zuluaga R, Putaux JL, Cruz J, Velez J, Mondragon I, Ganan P (2009) Cellulose microfibrils from banana rachis: effect of alkaline treatments on structural and morphological features. Carbohydr Polym 76:51–59

Paper III

Adsorption of hydrogen sulphide from aqueous solutions using modified nano/micro fibrillated cellulose

Hokkanen, S., Repo, E., Bhatnagar, A., Tang W. Z., Sillanpää, M.

Environmental Technology 35(2014)2334-2346

Environmental Technology
Publication details, including instructions for authors and subscription information:
http://www.tandfonline.com/loi/tent20

Adsorption of hydrogen sulphide from aqueous solutions using modified nano/micro fibrillated cellulose

Sanna Hokkanen[a], Eveliina Repo[a], Amit Bhatnagar[b], Walter Zhonghong Tang[c] & Mika Sillanpää[a]

[a] Laboratory of Green Chemistry, LUT Savo Sustainable Technologies, Lappeenranta University of Technology, Sammonkatu 12, Mikkeli FI-50130, Finland

[b] Department of Biology and Environmental Science, Faculty of Health and Life Sciences, Linnaeus University, Kalmar SE-391 82, Sweden

[c] Department of Civil and Environmental Engineering, Florida International University, Miami, FL 33174, USA

Published online: 08 Apr 2014.

To cite this article: Sanna Hokkanen, Eveliina Repo, Amit Bhatnagar, Walter Zhonghong Tang & Mika Sillanpää (2014): Adsorption of hydrogen sulphide from aqueous solutions using modified nano/micro fibrillated cellulose, Environmental Technology, DOI: 10.1080/09593330.2014.903300

To link to this article: http://dx.doi.org/10.1080/09593330.2014.903300

Environmental Technology, 2014
http://dx.doi.org/10.1080/09593330.2014.903300

Taylor & Francis
Taylor & Francis Group

Adsorption of hydrogen sulphide from aqueous solutions using modified nano/micro fibrillated cellulose

Sanna Hokkanen[a]*, Eveliina Repo[a], Amit Bhatnagar[b], Walter Zhonghong Tang[c] and Mika Sillanpää[a]

[a]*Laboratory of Green Chemistry, LUT Savo Sustainable Technologies, Lappeenranta University of Technology, Sammonkatu 12, Mikkeli FI-50130, Finland;* [b]*Department of Biology and Environmental Science, Faculty of Health and Life Sciences, Linnaeus University, Kalmar SE-391 82, Sweden;* [c]*Department of Civil and Environmental Engineering, Florida International University, Miami, FL 33174, USA*

(*Received 11 July 2013; accepted 8 February 2014*)

In the present study, microfibrillated cellulose (MFC) was modified by aminopropyltriethoxysilane (APS), hydroxycarbonated apatite (HAP), or epoxy in order to produce novel nanostructured adsorbents for the removal of hydrogen sulphide (H_2S) from the aqueous solutions. Structural properties of the modified MFC materials were examined using a scanning electron microscope, Fourier transform infrared spectroscopy and acid/base titration. These methods were used to verify the presence of nanostructures on the adsorbents surfaces as well as functionalities suitable for H_2S adsorption. Adsorption of H_2S by prepared adsorbents was investigated in batch mode under different experimental conditions, i.e. varying pH and H_2S concentrations. H_2S uptake was found to be 103.95, 13.38 and 12.73 mg/g by APS/MFC, HAP/MFC and epoxy/MFC, respectively from 80 mg/L H_2S solution. The equilibrium data were best described by the Langmuir isotherm for HAP/MFC and APS/MFC and the Sips isotherm for epoxy/MFC.

Keywords: adsorption; hydrogen sulphide; nanocellulose; water treatment; isotherms

1. Introduction

Hydrogen sulphide (H_2S) is one of the important toxic industrial compounds which can occur at objectionable levels in natural water and wastewaters being a very important pollution index for water quality. H_2S dissolves in ground water causing irritating rotten egg smell and unpleasant taste making water undrinkable. H_2S concentrations can be detected by human beings as low as 0.003–0.2 mg/L.[1] At a low concentration, H_2S can produce personal distress while at a higher concentration it can result in loss of consciousness, permanent brain damage or even death through asphyxiation. Exposure for 30 min at concentrations of 300 mg/L can cause unconsciousness and more than 30 min at concentrations of greater than 600 mg/L have been fatal.[2–4]

Hydrogen sulphide is introduced into water environments through two main routes: (1) sulphate can be reduced to hydrogen sulphide under anaerobic conditions; (2) water generated from industrial processes, such as the petrochemical industries, always contains some amounts of hydrogen sulphide.[5,6] In solution, hydrogen sulphide can exist in three forms, H_2S, HS^- and S^{2-}, depending on the pH, and all these forms have been reported to harmful to organisms.[7] It can also influence the biogeochemistry of sediments, because hydrogen sulphide inhibits the ability of phosphorus to bind in sediments thereby increasing the internal loading of phosphorus in aqueous environment.[8]

Various methods have been used to remove H_2S from water and wastewater with varying degrees of success. In general, adsorption is the one of the most promising methods for the removal of a wide variety of aquatic pollutants. The focus has now shifted for development of the selective adsorbents for the removal of inorganic pollutants from water. Different adsorbents such as metal oxides,[9,10] activated carbon,[11–14] activated carbon fibre cloth-supported metal oxides [15] and sludges [16,17] have been well studied for the removal of H_2S; however, they may not be suitable in practice due to their high cost. Furthermore, most of the adsorption studies related to H_2S removal have been conducted in gaseous phase. However, hydrogen sulphide is a very problematic inorganic compound in high-salinity groundwater.[18,19] Therefore, it is important to find cost-efficient adsorbents for efficient hydrogen sulphide removal from aqueous solutions. In recent years, nano-technology has emerged as one of the promising technologies in water treatment and various nano-adsorbents have been developed and examined for their efficacy in water purification. The recent process

*Corresponding author. Email: sanna.hokkanen@lut.fi

developments of nanocellulose have enabled energy consumption to be reduced by a total of 98%, representing a saving of 29,000 kWh per tonne. In future, nanocellulose can be produced in large scale, which is a promising route to reduce the cost of nanocellulose, and thereby increase the use of nanocellulose in environmental protection applications.[14–20]

Nano- and microcelluloses, which cover a wide variety of tiny particles from nano-sized whiskers to micron-sized microfibril aggregates, are considered to be amongst the potential bio-based materials for versatile applications such as electronic components, textiles, high adsorbency products, thermoplastic products, nourishing, cosmetics and pharmaceuticals.[21] Due to its biocompatibility, nanocellulose could also provide attractive alternatives for environmental applications such as water purification. The feasibility of nano- and microcelluloses is further promoted by their high surface area, chemical accessibility and flexibility of functionalization making them potential to possess novel and improved performance compared with present synthetic water treatment chemicals. Cellulose is inexpensive and abundant in hydroxyl groups, which can anchor other functionalities through a variety of chemical modifications.

There are only a few reports available dealing with adsorptive removal of contaminants by nanocellulose and adsorption of H_2S from aqueous matrix. Therefore, a potential novel solution to a serious environmental problem is investigated in this study. Three different modified nanocelluloses are employed as adsorbents to remove hydrogen sulphide from aqueous solutions. The equilibrium isotherms of hydrogen sulphide of these adsorbents under different pH are studied. The developed adsorbents were also characterized by Fourier transform infrared spectroscopy (FTIR) to identify the role of different functional groups present on adsorbents surface during H_2S adsorption. Scanning electron microscopy (SEM), zeta-potential analyse and elemental analysis provided an insight on the characteristics of adsorbents.

2. Materials and methods

2.1. Materials

Microfibrillated cellulose (MFC), bleached birch pulp (Betula Verrucosa and Betula Pendula) was obtained as dry sheets and used as cellulose source after disintegration in deionized water. Prior to homogenizing, pulp was ground to MFC in a Valley beater at the consistency of 2.0% for 50 h, utilizing 5503 g of weight. The sample was then diluted at the consistency of 0.7% and homogenized with a homogenizer (Invensys APV 2000) at a pressure of 350–1200 bar to create nanofibrillated cellulose. MFC was purchased from the University of Oulu, Finland. All the chemicals used in this study were of analytical grade and supplied by Sigma-Aldrich.

2.2. Adsorbents

2.2.1. APS-modified MFC

MFC (2 g) was reacted with a coupling agent, aminopropyltriethoxysilane, APS (20 g) in a 80/20v/v ethanol/water mixture under magnetic stirring for 2 h at room temperature. The modified cellulose was centrifuged and washed with 80/20v/v ethanol/water mixture and distilled water three times.[21]

2.2.2. HAP-modified MFC

MFC (3.0 g) and NaOH-urea solution containing NaOH (7.0 g), urea (12.0 g) and distilled water (1 mL), were reacted together under magnetic stirring during 1 h at room temperature. The solution was then cooled at 5°C for 12–18 h.[13,22]

After cooling, 50 mL of MFC-NaOH-urea solution was mixed with 25 mL of $CaCl_2 \cdot 2H_2O$ solution (0.402 mol/L) and 25 mL of $NaH_2PO_4 \cdot H_2O$ (0.802 mol/L) under vigorous stirring (for how long) at room temperature. The mixture was then transferred into an oven where the temperature was set to 160°C for 6 h. After heating, cellulose/HAP mixture was centrifuged at 4000 rpm for 5 min. Cellulose/HAP mixture was washed four times by water and ethanol and centrifuged.[22]

2.2.3. Epoxy-modified MFC

MFC (5.7 g) was mercerized using 200 mL of 8 M NaOH solution at room temperature for 20 min. Then, the solution was centrifuged and washed several times with ultra-pure water. After mercerization MFC was prepared by crosslinking in a mixture composed of 20 mL of 6.25 M NaOH, 50 mL of epichlorohydrin and 75 mL of dimethyl sulfoxide (DMSO). MFC-NaOH-epichlorohydrin-DMSO solution was stirred for 2 h at 50°C. Then, the solution was centrifuged and washed with ultra-pure water until filtrate became neutral.[23]

Treated MFC was added into reacting solution containing 32.5 mL of DMSO, 17.5 mL of 1,4-butanediol diglycidyl ether and 17.5 mL of 1 M NaOH. This mixture was stirred for 2 h at room temperature. After reaction MFC/epoxide was centrifuged, washed until neutrality and filtered.[23]

2.3. Solutions

A pH buffer was prepared by dissolving appropriate amounts of sodium hydroxide and l(+)-ascorbic acid in ultra-pure water to achieve concentrations of 2 and 0.2 mol/L, respectively.[24,25]

Hydrogen sulphide solution was prepared using sodium sulphide-y-hydride ($Na_2S \cdot 3H_2O$) at the concentration of 116.25 mg/L. This corresponds the 30 mg/L of hydrogen sulphide.[25]

2.4. Instrumentation

H_2S concentration was analysed by an inductively coupled plasma optical atomic emission spectrometry (ICP-OES) model iCAP 6300 (Thermo Electron Corporation, USA). The operating parameters are shown in Table 1.

A vapour-generating device was used to produce H_2S through the reaction of sodium sulphide-y-hydride with hydrochloric acid (10 M HCl) in the reaction coil. The acid was added using an own pump system to the sample flow via a *T*-piece placed in junction of the sample coil and the reaction coil.[24] The instrumentation is shown in Figure 1.

2.5. Characterization of modified MFC

FTIR type Vertex 70 by Bruker Optics (Germany) was used to identify the surface functional groups of the synthesized nanocellulose. The FTIR spectra were recorded at 4 cm^{-1} resolution from 400 to 4000 cm^{-1} and 100 scans per sample. The surface morphology of the different adsorbents was examined using a Hitachi S–4100 SEM. Surface charge and a point of zero charge of the modified and unmodified MFC were determined by isoelectric point titration as a function of pH by using Zetasizer Nano ZS (ZEN3500, Malvern). The determination of C, H, N and O was obtained using Organic Elemental Analyzer Flash 2000 (Thermo Scientific, Germany). About 2.5 mg of the sample in a capsule made of tin (assay of C, H and N) or silver (assay of O) was burned at 920–1000°C. The quantity of each element is expressed in percentage of dry mass. After reaction between H_2S and hydroxy-carbonated apatite (HAP)/MFC, solubility product equilibrium constant (Ksp) of calcium sulphide (CaS) was determine by acid/based titration. 22 mg HAP/MFC was dissolved in 10 ml of distilled water and 0.5 mL of 0.5% phenolphthalein indicator was added to the solution under the magnetic stirring. The solution was titrated with 0.10 M HCl. The titration procedure was repeated three times.

Table 1. ICP operating parameters.

RF power	1350 W
Nebulizer gas flow	0.5 mL/min
Auxiliary gas flow	0.2 mL/min
Plasma gas flow	15 L/min
Sample flow rate	3.529 mL/min
Acid flow rate	0.643 mL/min
S wavelength	180.731; 180.034 nm

2.6. Batch adsorption experiments

Batch adsorption tests were performed with different adsorbents at room temperature and 10 min stirring time to obtain equilibrium isotherms. For isotherm studies, adsorption experiments were carried out by stirring 0.020–0.038 g of modified MFC with 0.010 L of H_2S solution (pH 6) with concentrations ranging from 5.0 to 80.0 mg/L under nitrogen gas flow. Nitrogen gas was used to inhibit the evaporation of sulphide from the solution. Reference samples were used as duplicates to determine the amount of evaporated sulphide during 10 min reaction time. The optimal time for adsorption was studied using the hydrogen sulphide solution without adsorbent as reference samples under the same conditions were the batch adsorption tests were performed. It was observed that after 10 min the evaporation of the higher H_2S concentrations increased significantly. After 10 min, 3 mL of sample was injected into test tube containing 3 mL of buffer.

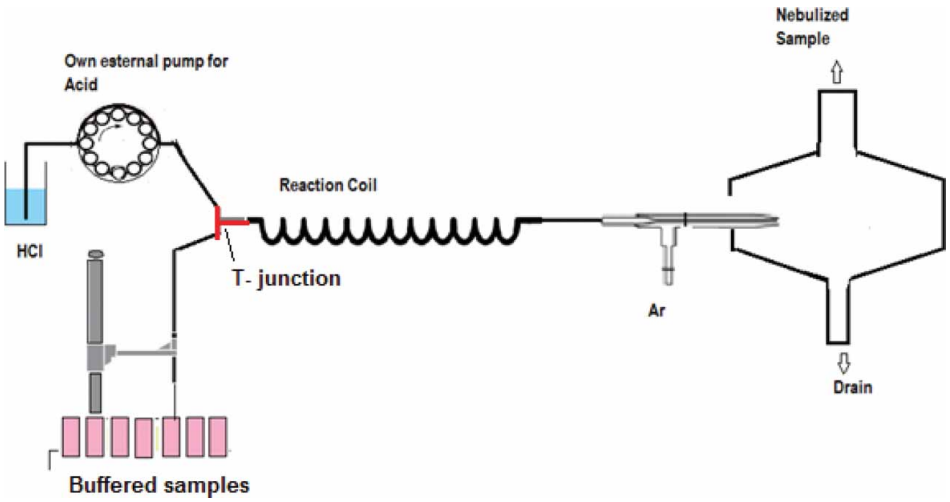

Figure 1. Schematic representation of ICP instrumentation.

In order to obtain the adsorption capacity (q_e), the amount of ions adsorbed per mass unit of modified cellulose (mg/g) was calculated with the following formula:

$$q_e = \frac{(C_i - C_e)}{M} V, \quad (1)$$

where C_i and C_e are the initial and the equilibrium adsorbate concentrations (mmol/L), while M and V are the weight of the adsorbent (g) and the volume of the solution (L).

3. Results and discussions

3.1. FTIR, SEM analyses, zeta-potential analyse and elemental analysis

3.1.1. FTIR of unmodified MFC and APS/MFC

The spectrum of unmodified MFC is shown in Figure 2. The band found at around 2900 cm^{-1} belongs to O−H stretching, while the O−H bending mode of adsorbed water is registered at around 1640 cm^{-1}. The weak band at 1590 cm^{-1} confirms the presence of the COO− group. The other weak bands at 1428 cm^{-1} are assigned to HCH and OCH vibrations and the band at 1366 cm^{-1} to the CH bending mode. The band at 895 cm^{-1} is corresponding to the COC, CCO and CCH deformation modes.[26,27]

Figure 3 shows the FTIR spectrum of (a) APS/MFC and (b) APS/MFC after H_2S adsorption. In both spectra two absorbing peaks were observed at 2920 cm^{-1} and 2850 cm^{-1} corresponding to the tension and vibration of $-CH_2$. A new peak appeared at 1625 cm^{-1} implying the vibration and bending of N−H. The bands at 1575 and 1480 cm^{-1} are typical for the deformation modes of the NH_2 groups hydrogen bonded to the OH function group of both silanol moieties and cellulosic substrate. The peaks from 1350 to 1250 cm^{-1} may imply the extension bending of C−N. The large intense bands around 1100 and 980 cm^{-1} are related to the −Si−O−Si− linkage and −Si−O−cellulose bond.[27–31] A new peak at 2574 cm^{-1} corresponding SH-stretching vibration modes appeared after H_2S adsorption.[32]

3.1.2. FTIR of HAP/MFC

The FTIR spectra of the HAP modified MFC (a) before and (b) after H_2S adsorption are shown in Figure 4. A weak band corresponding to hydroxyl stretching is observed at around 3330 cm^{-1}. The bands at around 1640 cm^{-1} are assigned to the bending mode of OH- groups and band at 601 cm^{-1} ascribed to the liberation mode of the O–H vibration. The asymmetric and symmetric stretching vibrations of PO_4^{3-} are found at 962–1023 cm^{-1} and 562–643 cm^{-1}, respectively. The bands at 1420 cm^{-1} corresponding to CO_3^{2-} CO_3^{2-} are present due to the presence of carbonate (CO_3^{2-}), which is also indicated by the band around 878 cm^{-1}.[33,34] The peaks in the region between 2182 and 1996 cm^{-1} may assignable to the combination and overtone bands of PO_4^{3-} ions in the adsorbent.[19] After H_2S adsorption, new bands due to SH-stretching vibration modes appeared at 2574 cm^{-1}.[35]

3.1.3. FTIR of epoxy/MFC

FTIR spectrum of MFC/epoxy composite (a) before and (b) after adsorption is shown in Figure 5. It shows a

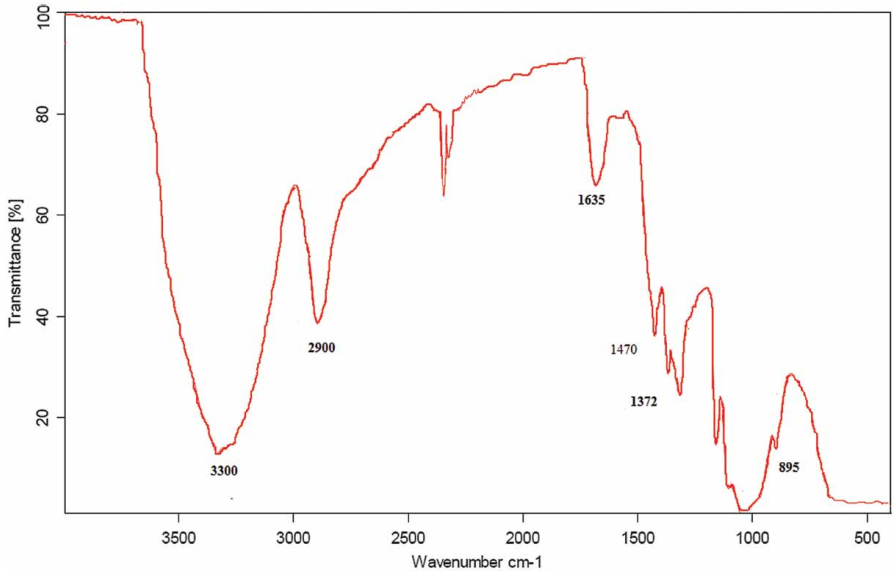

Figure 2. FTIR spectra of unmodified MFC.

broad peak in the region between 3125 and 3425 cm^{-1} corresponding to the hydroxyl (OH)-stretching vibration of free and hydrogen bonded −OH groups.[27–40] The absorbance peak observed at 1650 cm^{-1} indicates the (OH) bending vibration of absorbed water.[33,36,37] The peaks at 1422 and 1358 cm^{-1} may be attributed to CH_2 and CH_3 bending vibration of cellulose fibres, respectively.[34] The absorption peaks around 1000–1100 cm^{-1} may correspond to C−O stretching of cellulose fibre. The peaks at 2930 and 2890 cm^{-1} may belong to the asymmetric and symmetric stretching of CH_2 and CH_3 of the epoxy resin.[36,40] The peaks at 1608, 1580 and 1497 cm^{-1} can be assigned to the benzene ring of epoxy or C−C stretching of aromatic ring. The peaks appearing at 1244 and 920 cm^{-1} may be attributed to the C−O stretching of epoxide ring vibration.[36,37,41–43] New peaks after H_2S adsorption

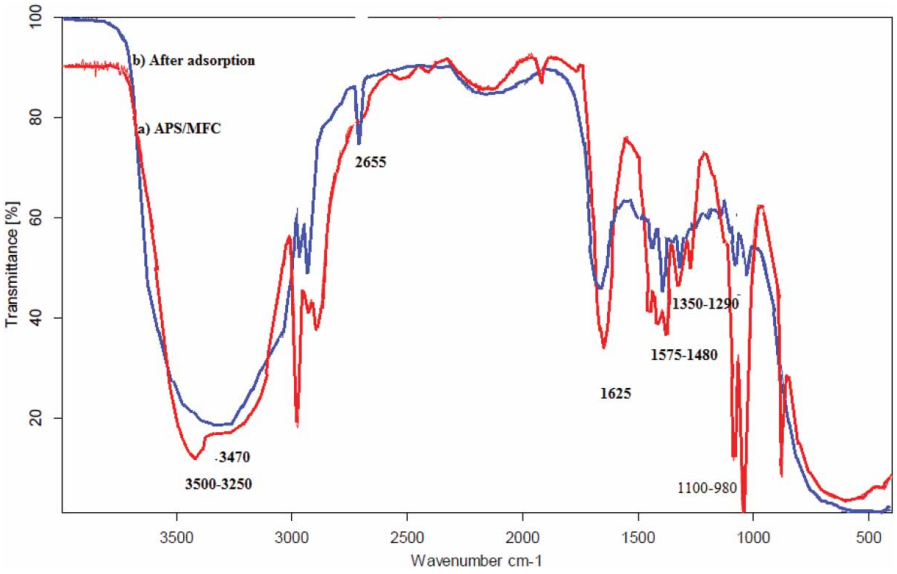

Figure 3. FTIR spectra of APS/MFC (a) before and (b) after H_2S adsorption.

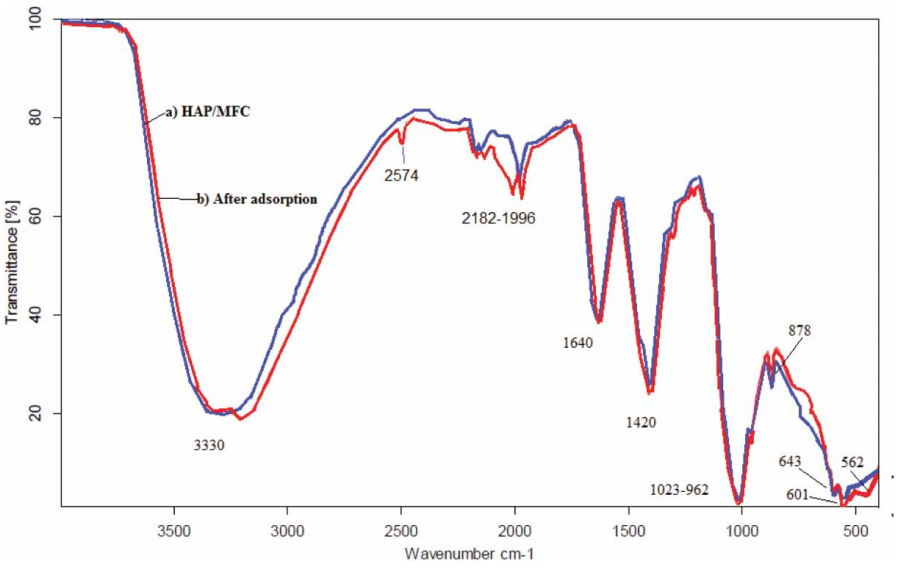

Figure 4. FTIR spectra of HAP/MFC (a) before and (b) after H_2S adsorption.

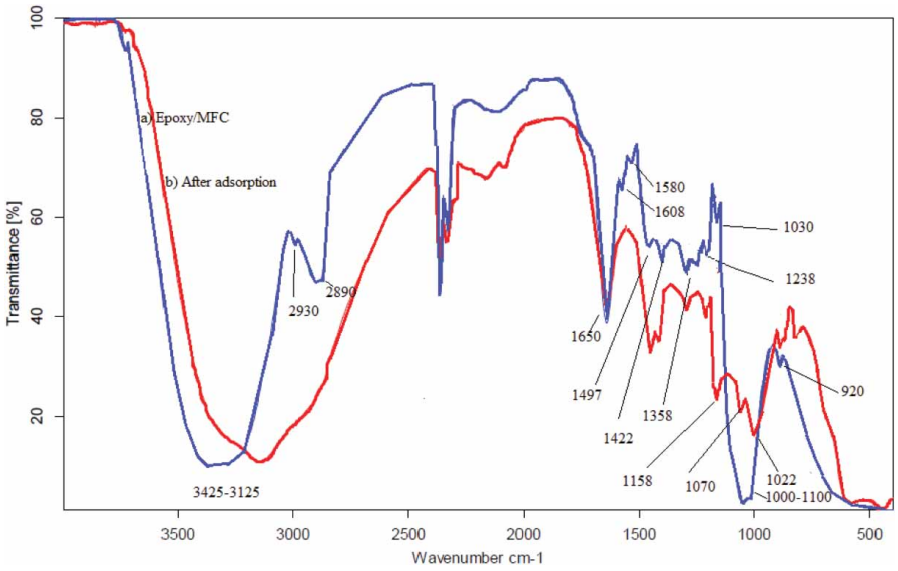

Figure 5. FTIR spectra of epoxy/MFC (a) before and (b) after H_2S adsorption.

at 1158, 1070 and 1022 cm^{-1} are characteristic for the molecular vibrations of C−S bonds.[44]

3.1.4. *SEM pictures, zeta-potential analyse and elemental analysis*

Morphological characteristics of APS/MFC, HAP/MFC and epoxy/MFC were investigated by SEM analysis. Figure 6(a) and 6(b) shows a typical non-homogenous surface morphology for both APS modified and unmodified cellulose fibre. Comparison of unmodified area (Figure 5(a)) and APS modified (Figure 6(b)) adsorbent shows an observed increase in surface area after modification. Observed crystalline sizes of 100 nm or lower confirm the presence of nanostructured surface.

It has been observed (Figure 6(c)) that the treatment of cellulose by alkaline solutions before the activation of the cellulose membrane by epoxy reagents makes cellulose molecules to move segmentally, which leads to random chain folding and formation of folded-chain crystallites.[45–47]

The SEM images of HAP/MFC (Figure 6(c) and 6(d)) show that the surface of the cellulose is completely covered by the HAP layers. This indicates the success of the synthesis and increase in the surface area due to the HAP treatment. For HAP/MFC crystalline sizes were around 50–100 nm. Overall, the SEM analysis showed rather different kinds of surface morphologies after different treatments of nanocellulose.

Figure 6(e) shows that treatment with NaOH, made the microfibrils wavy and assemble into large bundles. The effect of the epoxy reagents treatment is shown in Figure 6(f). After epoxydation procedure the nanocellulose fibres had very coarse surfaces. This strongly suggests that a considerable increase in roughness observed in these micrographs is associated with polymer growth induced by the chemical coupling of epoxy with the surface OH groups. Specific surface area of the adsorbent increased with the increasing roughness of the surface (crystalline sizes as low as 10 nm can be observed), which increases the number of the sites for H_2S adsorption.

The isoelectric point was determined by zeta-potential measurements for unmodified MFC, APS/MFC and epoxy/MFC. The measurements for HAP/MFC were not possible due to the very alkaline surface of the adsorbent. For APS/MFC isoelectric point was found to be at pH 5.65. The isoelectric point for unmodified MFC was around pH 3.9 (Figure 7). A change in isoelectric point after modification is caused by the amino groups on the surface of the modified cellulose. As can be seen from Figure 7, the epoxy/MFC surface acquired a negative charge at pH above 6.5, which was its isoelectric point.

The elemental analysis results of unmodified and modified MFC are shown in Table 2. A high content of carbon (31.91% and 37.38%) and oxygen (55.110% and 50.60%), and low content of hydrogen (4.98% and 6.39%) and nitrogen (3.18% only for APS modified MFC) were observed. After modification with aminosilane (APS/MFC), an obvious increase in nitrogen content corresponds to the introduction of amine groups on the cellulose surface. The most notable difference in contents of elements was observed between the unmodified MFC and HAP/MFC. The level of

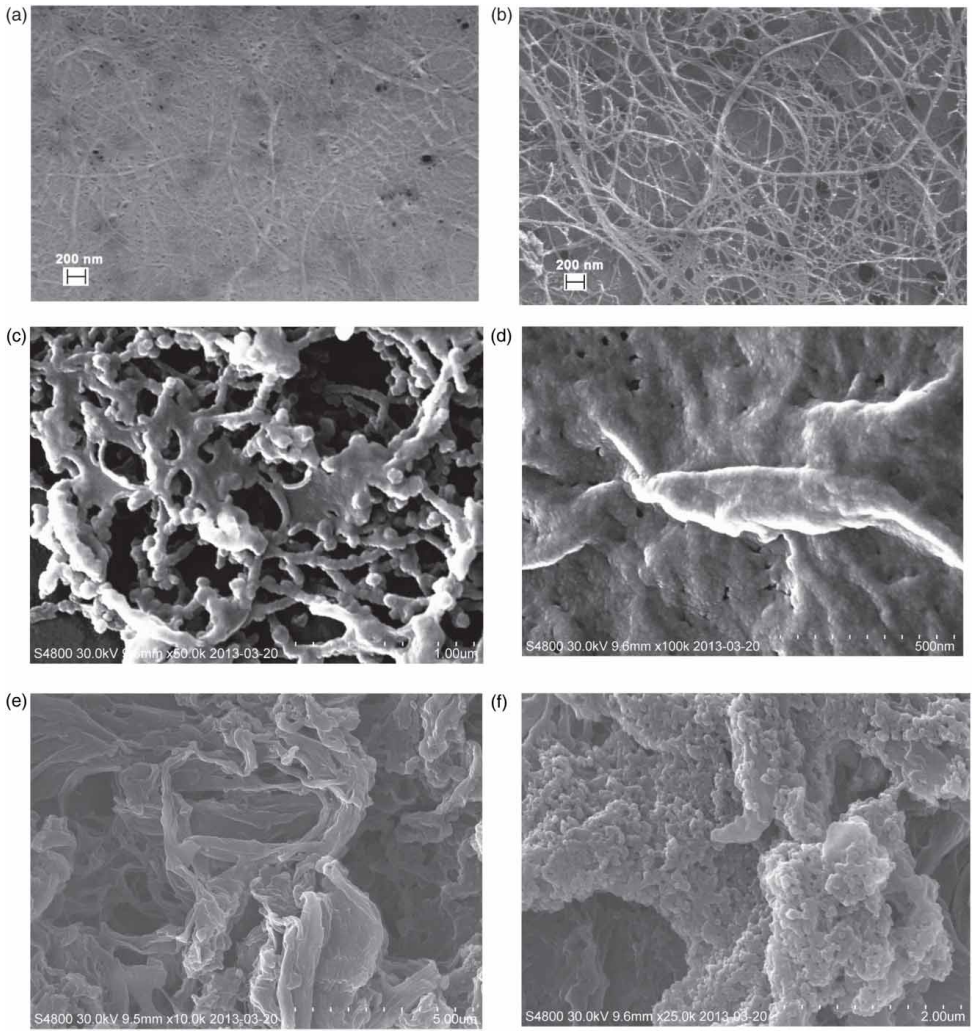

Figure 6. The SEM images of (a) unmodified MFC (b) APS/MFC, (c-d) HAP/MFC, (e) MFC after treatment of cellulose by alkaline solutions and (f) epoxy/MFC.

carbon was much lower with HAP/MFC and the levels of hydrogen and oxygen higher due to the high amount of the calcium caused by the modification.

3.2. *Adsorption studies*

3.2.1. *Effect of pH*

The removal of hydrogen sulphide from aqueous solutions by adsorption depends on the solution pH because it affects adsorbent surface charge, the degree of ionization and the speciation of adsorbate. The adsorption of H_2S on prepared adsorbents was examined at different pH ranging from 6 to 9 and results are presented in Figure 8. In the case of HAP/MFC, the Ca^{2+} would be precipitated after pH increases to 7 and CaS is also a precipitate.[43] Therefore, hydrogen sulphide cannot be adsorbed on the surface of HAP/MFC at such high pH. Ksp of CaS was 6.02×10^{-8} $(mol/L)^2$ at the temperature of 25°C. The value was determined from the resulting information of HCl titration.

It was observed that at solution pH 9, the adsorption of H_2S by all the adsorbents was lowest. At this pH, negatively charged HS^- was dominating in the solution phase (Visual MINTEQ) and based on the zeta-potential measurements, the surface charge of the adsorbents was also found to be negative indicating electrostatic repulsion between

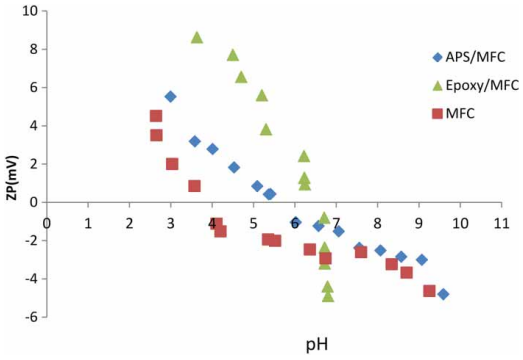

Figure 7. Zeta potential as a function of pH of different adsorbents.

Table 2. The content of C, H, N and O in unmodified and unmodified MFC obtained from elemental analysis.

Adsorbent	%			
	Percentage of dry weight			
Unmodified MFC 2.61 mg	C	H	N	O
	31.91	4.98		55.11
APS/MFC 2.53 mg				
	C	H	N	O
	39.38	6.39	3.18	50.60
HAP/MFC 2.48 mg				
	C	H	P (calculated)	O
	7.05	0.35	70.24	21.65
Epoxy/MFC 2.23 mg				
	C	H	N	O
	41.23	5.98		52.73

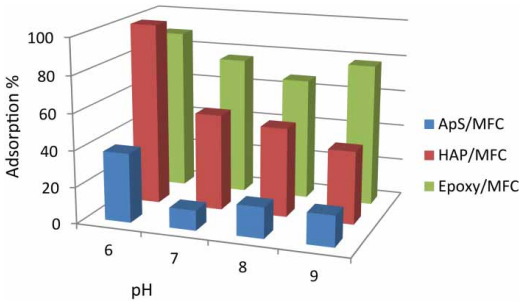

Figure 8. Effect of H_2S solution initial pH on adsorption using APS, HAP and epoxy-modified MFC.

the surface and dissolved species. Adsorption efficiency increased when approaching the neutral pH and at pH < 7, the adsorption efficiency was highest for all the adsorbents studied. This can be attributed to the increasing positive surface charge of the adsorbents with decreasing pH (surface protonation) making surface more attractive for sulphide species (H_2S and HS^-).

3.2.2. *Adsorption capacities of APS/MPS, HAP/MPS and epoxy/MPS*

The experimental maximum adsorption capacities were 103.95, 13.38 and 12.73 mg/g for APS/MPS, HAP/MPS and epoxy/MPS, respectively. In this paper, the maximum adsorption capacity was compared also with the couple of reported results of adsorption for gaseous H_2S because there are only few reports, including the maximum adsorption capacities of hydrogen sulphide in water. The maximum adsorption capacities were 12.00, 45.00–68.00, and 58.87 mg/g (the Thomas model) for crushed oyster shell, cupric oxide, and ferric and alum water treatment residuals, respectively.[21,48–50] The maximum adsorption capacities for gaseous H_2S were 2.3–71, 0.53–12.00, 14.00–1530.00, 117.17–206.97 and 24.20–228.10 mg/g for activated carbons, montmorillonites, an activated carbon catalyst, silica–aluminas and mixed zinc/cobalt hydroxides.[50–54]

3.2.3. *Adsorption isotherms*

Adsorption isotherms indicate how the adsorbate (H_2S) interacts with adsorbents and how adsorption uptakes vary with adsorbate concentrations at given pH values and temperatures. In this study, initial H_2S concentrations were in the range of 5.0–80.0 mg/L for the adsorption isotherm studies.

The isotherms were determined for dry weight of the adsorbent due to the high water concentration of the modified nanocellulose. Dry weight was defined by drying 1 g of wet cellulose in an oven at 105°C for 4 h and then storing it in a desiccator until its weight remained unchanged. Water contents of APS/MFC, HAP/MFC and epoxy/MFC were 98%, 71% and 64%, respectively.

In this study, the adsorption mechanisms were analysed by the Langmuir, Freundlich and Sips isotherm models, which are commonly used to describe experimental results in a wide range of concentrations.

3.2.4. *Langmuir isotherm*

The Langmuir model is a very simple theoretical model for monolayer adsorption onto a surface with finite number of identical adsorption sites.[55] The Langmuir model was originally developed as a theoretical equilibrium isotherm for a gas phase adsorption. The equation is applicable for homogeneous systems where adsorption process has equal activation energy, based on the following basic assumptions: (a) molecules are adsorbed at a fixed number of well-defined localized sites, (b) each site can hold one adsorbate molecule, (c) all sites are energetically equivalent and (d) there are no interactions between molecules adsorbed on neighbour sites.[56]

The general Langmuir equation is written as follows:

$$q_e = \frac{q_m K_L C_e}{1 + K_L C_e}, \tag{2}$$

where q_e (mmol/g) is the equilibrium adsorption capacity and q_m (mmol/g) is the maximum amount of the ions adsorbed per unit weight of the adsorbent. Latter also describes a formation of the complete monolayer coverage on the surface at high equilibrium H_2S concentration C_e (mmol/L) and practical limiting adsorption capacity. K_L (L/mmol) is the Langmuir equilibrium constant related to the affinity of the binding sites and also indicates the binding energy of the adsorption reaction between adsorbate and adsorbent.

3.2.5. *Freundlich isotherm*

Freundlich expression is an empirical equation applicable for non-ideal adsorption on heterogeneous surface as well as multilayer adsorption.[55,56] The model is given as

$$q_e = K_f C_e^{1/nf}. \tag{3}$$

If the concentration of the solute in the solution at equilibrium, C_e, is raised to the power of $1/nf$ with the amount of solute adsorbed being q_e, $C_e^{1/nf}/q_e$ is constant at a given temperature. K_f is a relative indicator of adsorption capacity, while the dimensionless $1/nf$ indicates the energy or intensity of the reaction and suggests the favourability and capacity of the adsorbent/adsorbate system. According to the theory, $nf > 1$ represents favourable adsorption conditions.

3.2.6. *Sips isotherm*

The Sips isotherm model is a combination of the Langmuir and Freundlich isotherm type models and is expected to describe heterogeneous surface much better than these two. At low adsorbate concentrations, the Sips isotherm approaches the Freundlich isotherm, whereas it approaches the Langmuir isotherm at high concentrations. The model can be written as

$$q_e = \frac{q_m (K_S C_e)^{n_S}}{1 + (K_S C_e)^{n_S}}, \tag{4}$$

where q_m (mg/g) is the maximum amount of H_2S adsorbed per unit mass of adsorbent, K_S (L/mg) is the Sips constant related to the energy of adsorption, and n_S could be regarded as a parameter characterizing the system heterogeneity.

Modelling calculations were conducted using Microsoft Office Excel 2007 software. Isotherm parameters were determined by minimizing the Sum of the Squares of the Errors (ERRSQ) function across the concentration range studied

$$\sum_{i=1}^{p} \left(q_{e,exp} - q_{e,calc}\right)^2. \tag{5}$$

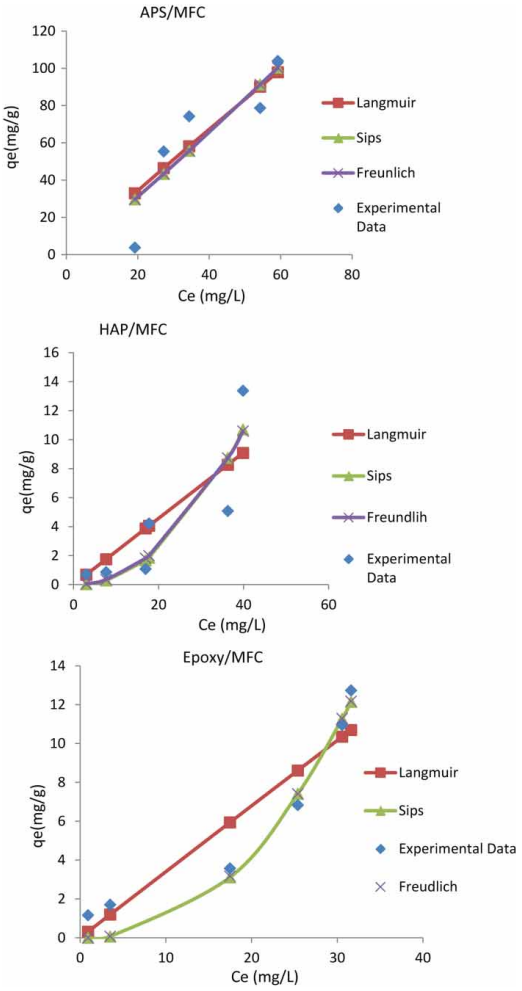

Figure 9. Adsorption isotherms of H_2S on APS/MFC, HAP/MFC and epoxy/MFC.

The experimental equilibrium data for H_2S adsorption on APS/MFC, HAP/MFC and epoxy/MFC, calculated from Equation (1), were fitted with Langmuir, Freundlich and Sips isotherms, Equations (2)–(4). The plots of H_2S adsorption are presented in Figure 9. The calculated constants of the three isotherm equations along with R^2 values are presented in Table 2.

For APS/MFC, all the isotherm models tested showed a poor fit to the experimental data with low R^2. The R^2 values of the three models descended in the order of: Langmuir > Sips > Freundlich.

For HAP/MFC, R^2 values descended in the order of: Freundlich = Sips > Langmuir. Poor fitting results were observed with all the models. In the case of H_2S adsorption on epoxy/MFC, the tested models fitted better with the experimental data than for APS/MFC and HAP/MFC. The Langmuir model was found to represent the equilibrium data best with R^2 value of 1000 suggesting the homogenous surface adsorption of H_2S on epoxy/MFC (Table 3).

In addition to low correlation coefficients ($R^2 < 0.95$), Figure 7 shows that generally the equilibrium data did not fit well with the tested isotherms.

Table 3. Isotherm constants of APS/MFC, HAP/MFC and epoxy/MFC for H_2S adsorption.

APS/MFC			
Langmuir			
q_m (mg/g)	K_L (L/mg)		R^2
1807.564	0.000967		0.759
Freundlich			
	K_f	n_f	R^2
	1.215150	1.081	0.644
Sips			
q_m (mg/g)	K_S (L/mg)	ns	R^2
0.513	0.816887	1.081	0.677
HAP/MFC			
Langmuir			
q_m (mg/g)	K_L (L/mg)		R^2
1549.752	0.000148		0.687
Freundlich			
	K_f	n_f	R^2
	0.005306	2.062	0.770
Sips			
q_m (mg/g)	K_S (L/mg)	n_s	R^2
709.476	0.003689	2.180	0.770
Epoxy/MFC			
Langmuir			
q_m (mg/g)	K_L (L/mg)		R^2
1267.150	0.000269		1.000
Freundlich			
	K_f	n_f	R^2
	0.004806	2.268	0.959
Sips			
q_m (mg/g)	K (L/mg)	n_s	R^2
173.170	0.010727	2.390	0.958

Table 4. Calculated R_L values for H_2S adsorption on APS/MFC, HAP/MFC and epoxy/MFC.

	R_L Adsorbents		
C_0 (mg/L)	APS/MFC	HAP/MFC	Epoxy/MFC
5		1.001	1.001
10		1.001	1.003
20	1.019	1.003	1.008
30	1.039	1.004	1.013
50	1.048	1.007	1.018
80	1.068	1.012	1.022

The essential feature of the Langmuir isotherm can be expressed by means of parameter R_L, a dimensionless constant referred to as separation factor or equilibrium parameter for predicting whether an adsorption system is favourable or unfavourable. R_L is calculated using the following equation:[55]

$$R_L = \frac{1}{1 + K_L C_0}, \quad (6)$$

where C_0 is the initial H_2S concentration (mg/L). As the R_L values lie between 0 and 1, the adsorption process is favourable. The values of R_L included in Table 4 are very close to unity for all the adsorbents and concentrations, suggesting that the APS/MFC, HAP/MFC and epoxy/MFC are favourable for the adsorption of H_2S under conditions used in this study. These results are consistent with the Freundlich model, which gave $nf > 1$ for all the adsorbents suggesting favourable adsorption.

Poor fitting results of the isotherm models tested may be attributed to the high water concentration of the used adsorbents. Wet adsorbents were used in this study because a dry modified MFC becomes very hard and loses its adsorption capacity. When wet adsorbent is used, it is difficult to know the exact water concentration in each sample. Therefore, the samples were not homogenous with regard to the adsorbent. Furthermore, the volatility of H2S could also affect the fitting results. Reference samples were used for detecting the volatility and the average volatility was +/− 0.44 mg/L per sample.

3.3. *Mechanisms of adsorption*

Huang and Yang [56] used XPS for analysing the surface groups of amino-functionalized silica-based adsorbents before and after reaction with H_2S. They observed the formation of a NH_3^+HS- group due to a weak chemical reaction between H_2S and surface amine groups ($-NH_2$) in the 3-aminopropyl functional silica xerogel and MCM-48. Tian et al. (2009) achieved comparable results using aminosilane-modified-activated carbon for the removal of H_2S from gas streams.[57] Based on the findings, H_2S is thought to react with the amine groups by proton transfer, which is similar to the reaction taking place during aqueous absorption processes with amines. The reaction between amine groups ($-NH_2$) fixed on MFC and H_2S can be presented as follows:

$$-\text{MFC} - \text{NH}_2 + \text{H}_2\text{S} \rightarrow -\text{MFC} - \text{NH}_3^+\text{SH}^- \quad (7)$$

The result of FTIR confirms the findings above. After the adsorption of H_2S the $-NH_2$ bands weakened slightly and new bands due to SH-stretching vibration modes appeared. These results suggest a presence of similar weak interactions between H_2S and $-NH_2$ on the surface of APS/MFC.

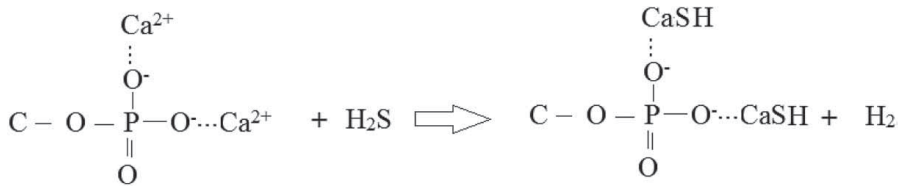

Figure 10. The adsorption of H_2S on the surface of HAP/MFC.

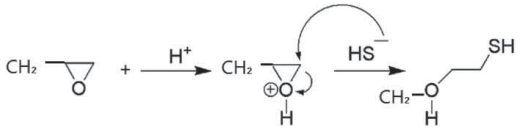

Figure 11. The adsorption of H_2S on the surface of epoxy-modified MFC.

The reaction between H_2S and HAP/MFC is illustrated in Figure 10. In this reaction pathway, positively charged calcium ions are forming complexes with sulfate ions.[58] A new peak on the FTIR spectrum at the region of thiols (2574 cm^{-1}) after adsorption indicates the bond formation between H_2S and the surface of HAP/MFC. Furthermore, the surface PO-bands did not weakened by the adsorption of H_2S. This proved that the adsorption sites of H_2S on the HAP/MFC surface were not P−OH groups.

Finally, the reaction mechanism between H_2S and epoxy groups is illustrated in Figure 11.[59] As can be seen, this reaction is favourable in acidic conditions, which is also supported by the poor adsorption performance of epoxy/MFC observed at alkaline pH. However, the FTIR spectrum after adsorption of H_2S confirms the reactions between epoxy groups and hydrogen sulphide.

4. Conclusions

The characteristics and mechanisms of H_2S adsorption by APS, HAP, and epoxy-modified MFC from aqueous solutions were studied. The obtained results clearly suggest that all the developed adsorbents could be successfully utilized for the removal of H_2S from the aqueous environments. The H_2S removal capacity of the studied adsorbents followed the order of: APS/MFC > HAP/MFC > Epoxy/MFC with APS/MFC having much higher capacity than the other two adsorbents. The adsorption performance was strongly dependent on the initial pH of the solution. The optimum pH was found to be 6 for all the adsorbents. The experimental data were fitted using the Langmuir, Freundlich and Sips isotherms showing favourable adsorption of H_2S for all the MFC-based adsorbents studied. In summary, the prepared adsorbents could provide a viable solution for the treatment of H_2S contaminated waters.

References

[1] Alharthi ESR, Ghaly AE. Removal of hydrogen sulphide from water. Am J Environ Sci. 2011;7:295–305.

[2] Feng W, Kwon S, Borguet E, Vidic R. Adsorption of hydrogen sulfide onto activated carbon fibers: effect of pore structure and surface chemistry. Environ Sci Technol. 2005;39:9744–9749.

[3] Cosoli P, Ferrone M, Pricl S, Fermeglia M. Hydrogen sulphide removal from biogas by zeolite adsorption. Part I. GCMC molecular simulations. Chem Eng J. 2008;145:86–92.

[4] Bassindale T, Hosking M. Deaths in Rotorua's geothermal hot pools: hydrogen sulphide poisoning. Foren Sci Int. 2011;207:28–29.

[5] Oriowo MA, Bevan RD, Bevan JA. Reactive adsorption of hydrogen sulfide on visible light photoactive zinc (hydr), pp.oxide/graphite oxide and zinc (hydr), pp.oxychloride/graphite oxide composites. Appl Catal B: Environ. 2013;132–133:321–331.

[6] Vaiopoulou E, Melidis P, Aivasidis A. Sulfide removal in wastewater from petrochemical industries by autotrophic denitrification. Water Res. 2005;39:4101–4109.

[7] Wang C, Pei Y. The removal of hydrogen sulfide in solution by ferric and alum water treatment residuals. Chemosphere. 2012;88:1178–1183.

[8] Beauchamp RO, Bus JS, Popp JA, Boreiko CJ, Andjelkovich DA. A critical review of the literature on hydrogen sulfide toxicity. Crit Rev Toxicol. 1984;13:25–48.

[9] Holmer M, Storkholm P. Sulphate reduction and sulphur cycling in lakes sediments: a review. Freshwater Biol. 2011;46:431–451.

[10] Seredych M, Bandosz TJ. Reactive adsorption of hydrogen sulfide on graphite oxide/$Zr(OH)_4$ composites. Chem Eng J. 2011;166:1032–1038.

[11] Hamon L, Serre C, Devic T, Loiseau T, Millange F, Férey G. Comparative study of hydrogen sulfide adsorption in the MIL-53(Al, Cr, Fe), MIL-47(V) MIL 100(Cr) and MIL-101(Cr) metal-organic frameworks at room temperature. J Am Chem Soc. 2009;131:8775–8777.

[12] Sitthikhankaew R, Predapitakkun S, Kiattikomol R, Pumhiran S, Assabumrungrat S, Laosiripojana N. Comparative study of hydrogen sulfide adsorption by using alkaline impregnated activated carbons for hot fuel gas purification. Energy Proc. 2011;9:15–24.

[13] Erdogan FO, Kopac T. Dynamic analysis of sorption of hydrogen in activated carbon. Int J Hydrogen Energy. 2007;32:3448–3456.

[14] Pääkkö M, Ankerfors M, Kosonen H, Nykänen A, Ahola A, Österberg M, Ruokolainen J, Laine J, Larsson PT, Ikkala O, Lindström T. Enzymatic hydrolysis combined with mechanical shearing and high-pressure homogenization for nanoscale cellulose fibrils and strong gels. Biomacromolecules. 2007;8:1934–1941.

[15] Le Leuch LM, Subrenat A, Le Cloirec P. Hydrogen sulfide and ammonia removal on activated carbon fiber cloth-supported metal oxides. Environ Technol. 2005;11:1243–1254.
[16] Moussavi G, Naddafi K, Mesdaghinia A, Deshusses MA. The removal of H_2S from process air by diffusion into activated sludge. Environ Technol. 2007;28:987–993.
[17] Ros A, Montes-Moran MA, Fuente E, Nevskaia DM, Marti MJ. Dried sludges and sludge-based chars for h2s removal at low temperature: influence of sewage sludge characteristics. Environ Technol. 2006;40:302–309.
[18] Wågberg L, Decher G, Norgren M, Lindström T, Ankerfors M, Axnäs K. The build-up of polyelectrolyte multilayers of microfibrillated cellulose and cationic polyelectrolytes. Langmuir. 2008;24:784–795.
[19] Siró I, Plackett D, Hedenqvist M, Ankerfors M, Lindström T. Highly transparent films from carboxymethylated microfibrillated cellulose: the effect of multiple homogenization steps on key properties. J Appl Polym Sci. 2011;119:2652–2660.
[20] Ankerfors M, Lindström T. Method for providing a nanocellulose involving modifying cellulose fibers. US patent 20,110,036,522 A1. 2011 Feb 17.
[21] Asaoka S, Yamamoto T, Kondo S, Haykawa S. Removal of hydrogen sulfide using crushed oyster shell from pore water to remediate organically enriched coastal marine sediments. Bioresour Technol. 2009;100:4127–4132.
[22] Tanaka H, Tsuda E, Nishikawa H, Fuji M. FTIR studies of adsorption and photocatalytic decomposition under UV irradiation of dimethyl sulfide on calcium hydroxyapatite. Adv Powder Technol. 2012;23:115–119.
[23] He M, Chang C, Peng N, Zhang L. Structure and properties of hydroxyapatite/cellulose nanocomposite films. Carbohyd Polym. 2012;87:2512–2518.
[24] Hokkanen S, Repo E, Sillanpää M. Removal of heavy metals from aqueous solutions by succinic anhydride modified mercerized nanocellulose. Chem Eng J. 2013;223:40–47.
[25] Metwalli E, Haines D, Becker O, Conzone S, Pantano CG. Surface characterizations of mono-, di-, and tri-aminosilane treated glass substrates. J Colloid Interface Sci. 2006;298:825–831.
[26] Abdelmouleh M, Boufi S, Belgacem MN, Duarte AP, Ben Salah A, Gandini A. Modification of cellulosic fibres with functionalised silanes: development of surface properties. Inter J Adhes Adhes. 2004;24:43–54.
[27] Wu B, Guangzhao M, Ng KYS. Stepwise adsorption of a long trichlorosilane and a short aminosilane. Colloid Surf A. 1997;162:203–213.
[28] Barbot C, Bouloussa O, Szymczak W, Plaschke M, Buckau G, Durand J-P, Pieri J, Kim JI, Goudard F. Self-assembled monolayers of aminosilanes chemically bonded onto silicon wafers for immobilization of purified humic acids. Colloids Surf A: Physicochem Eng Aspects. 2007;297:221–239.
[29] Dartois E, Duret Ph, Marboeuf U, Schmitt B. Hydrogen sulfide clathrate hydrate FTIR spectroscopy: A help gas for clathrate formation in the Solar System? Icarus. 2012;220:427–434.
[30] Wan YZ, Huang Y, Yuan CD, Raman S, Zhu Y, Jiang HJ, He F, Gao C. Biomimetic synthesis of hydroxyapatite/bacterial cellulose nanocomposites for biomedical applications. Mater Sci Eng C. 2007;27:855–864.
[31] Petrovic M, Colovic B, Jokanovic V, Markov D. Self assembly of biomimetic hydroxyapatite on the surface of different polymer thin films. J Ceramic Proc Res. 2012;13:398–404.
[32] Koranyi TI, Moreau F, Rozanov VV, Rozanova EA. Identification of SH groups in zeolite-supported HDS catalysts by FTIR spectroscopy. J Molec Struct. 1997;41:103–110.
[33] Jia N, Li S-M, Zhu J-F, Ma M-G, Xu F, Wang B, Sun R-C. Microwave-assisted synthesis and characterization of cellulose-carbonated hydroxyapatite nanocomposites in NaOH–urea aqueous solution. Mater Lett. 2010;64:2223–2225.
[34] Alamri H, Low IM. Mechanical properties and water absorption behaviour of recycled cellulose fibre reinforced epoxy composites. Polym Testing. 2012;31:620–628.
[35] Karbowiak T, Ferret E, Debeaufort F, Voilley A, Cayot P. Investigation of water transfer across thin layer biopolymer films by infrared spectroscopy. J Membr Sci. 2011;370:82–90.
[36] Lasagabaster A, Abad MJ, Barral L, Ares A, Bouza R. Application of FTIR spectroscopy to determine transport properties and water–polymer interactions in polypropylene (PP./poly(ethylene-co-vinyl alcohol) (EVOH) blend films: effect of poly(ethylene-co-vinyl alcohol)content and water activity. Polymer. 2009;50:2981–2989.
[37] Tserki V, Zafeiropoulos NE, Simon F, Panayiotou C. A study of the effect of acetylation and propionylation surface treatments on natural fibres. Composites: Part A. 2005;36:1110–1118.
[38] Deka BK, Maji TK. Study on the properties of nanocomposite based on high density polyethylene polypropylene polyvinyl chloride and wood. Composites: Part A. 2011;42:686–693.
[39] Shukla DK, Kasisomayajula SV, Parameswaran V. Epoxy composites using functionalized alumina platelets as reinforcements. Composit Sci Technol. 2008;68:3055–3063.
[40] Rajasekaran R, Karikalchozhan C, Alagar M. Synthesis characterization and properties of organoclaymodified polysulfone/epoxy interpenetrating polymer network nanocomposites. Chin J Polym Sci. 2008;26:669–678.
[41] Bellamy LJ. The infrared spectra of complex molecules. New York: Wiley; 1957; p. 18–20.
[42] Chozhan CK, Alagar M, Sharmila RJ, Gnanasundaram P. Thermo mechanical behaviour of unsaturated polyester toughened epoxy—clay hybrid nanocomposites. J Polym Res. 2007;14:319–328.
[43] Shibazaki H, Kuga S, Okano T. Mercerization and acid hydrolysis of bacterial cellulose. Cellulose. 1997;4:75–87.
[44] Recillasa S, Rodríguez-Lugo V, Montero ML, Viquez-Cano S, Hernandez L, Castaño VM. Studies on the precipitation behavior of calcium phosphate solutions. J Ceram Proc Res. 2012;13:5–10.
[45] Haimour NM, El-Bishtawi R, Ail-Wahbi A. Equilibrium adsorption of hydrogen sulfide onto CuO and ZnO. Desalin. 2005;181:145–152.
[46] Changhui W, Yuansheng P. The removal of hydrogen sulfide in solution by ferric and alum water treatment residuals. Chemosphere. 2012;88:1178–1183.
[47] Guo J, Luo Y, Lua AC, Chi R, Chen Y, Bao X, Xiang S. Adsorption of hydrogen sulphide (H_2S) by activated carbons derived from oil-palm shell. Carbon. 2007;45:330–336.
[48] Xiao Y, Wang S, Wu D, Yuan Q. Experimental and simulation study of hydrogen sulfide adsorption on impregnated activated carbon under anaerobic conditions. J Hazard Mater. 2008;153:1193–1200.
[49] Nguyen-Thanh D, Block K, Bandosz TJ. Adsorption of hydrogen sulfide on montmorillonites modified with iron. Chemosphere. 2005;59:343–353.
[50] Bashkova S, Baker FS, Wu X, Armstrong TR, Schwartz V. Activated carbon catalyst for selective oxidation of hydrogen sulphide: on the influence of pore structure surface characteristics and catalytically-active nitrogen. Carbon. 2007;45:1354–1363.

[51] Tagliabue M, Bellussi G, Broccia P, Carati A, Millini R, Pollesel P, Rizzo C. High pressure hydrogen sulphide adsorption on silica–aluminas. Chem Eng J. 2012;210:398–403.
[52] Ahmed MJ, Dhedan SK. Equilibrium isotherms and kinetics modeling of methylene blue adsorption on agricultural wastes-based activated carbons. Fluid Phase Equilibr. 2012;317:9–14.
[53] Abdullah MA, Chiang L, Nadeem M. Comparative evaluation of adsorption kinetics and isotherms of a natural product removal by Amberlite polymeric adsorbents. Chem Eng J. 2009;146:370–376.
[54] Mabayoje O, Seredych M, Bandosz TJ. Enhanced adsorption of hydrogen sulfide on mixed zinc/cobalt hydroxides: Effect of morphology and an increased number of surface hydroxyl groups. J Colloid Interface Sci. 2013;405: 218–225.
[55] Worden RH, Smalley PC. H2S-producing reactions in deep carbonate gas reservoirs: Khuff formation Abu Dhabi. Chem Geol. 1996;133:157–171.
[56] Huang HY, Yang RT. Amine-grafted MCM-48 and silica xerogel as superior sorbents for acidic gas removal from natural gas. Ind Eng Chem Res. 2003;42:2427–2433.
[57] Tian S, Mo H, Zhang R, Ning P, Zhou T. Enhanced removal of hydrogen sulfide from a gas stream by 3-minopropyltriethoxysilane-surface-functionalized activated carbon. Adsorption. 2009;15:477–488.
[58] Tomar M, Abdullah THA. Evaluation of chemicals to control the generation of malodorous hydrogen sulfide in waste water. Wat Res. 1994;28:2545–2552.
[59] Seredych M, Bandosz TJ. Reactive adsorption of hydrogen sulfide on graphite oxide/$Zr(OH)_4$ composites. Chem Eng J. 2011;166:1032–1038.

Paper IV

Adsorption of $Ni^{2+,}$ Cd^{2+}, PO_4^{3-} and NO_3^- from aqueous solutions by nanostructured microfibrillated cellulose modified with carbonated hydroxyapatite

Hokkanen, S., Repo, E., Johansson Westholm , L., Lou, S., Sainio, T., Sillanpää, M.

Chemical Engineering Journal 252 (2014) 64–74

Chemical Engineering Journal 252 (2014) 64–74

Contents lists available at ScienceDirect

Chemical Engineering Journal

journal homepage: www.elsevier.com/locate/cej

Adsorption of Ni^{2+}, Cd^{2+}, PO_4^{3-} and NO_3^- from aqueous solutions by nanostructured microfibrillated cellulose modified with carbonated hydroxyapatite

Sanna Hokkanen [a,*], Eveliina Repo [a,1], Lena Johansson Westholm [b], Song Lou [c], Tuomo Sainio [d], Mika Sillanpää [a,1]

[a] Laboratory of Green Chemistry, LUT GreenTech Faculty of Technology, Lappeenranta University of Technology , Sammonkatu 12, FI-50130 Mikkeli, Finland
[b] School of Business, Society and Engineering, Mälardalen University, P.O. Box 883, SE-721 23 Västerås, Sweden
[c] Medical School, University of Minnesota, 321 Church Street SE, Minneapolis, MN 55455, USA
[d] Lappeenranta University of Technology, Laboratory of Separation Technology, P.O. Box 20, FI-53851 Lappeenranta, Finland

HIGHLIGHTS

- CHA/MFC has a relatively high adsorption capacity for Ni^{2+}, Cd^{2+}, PO_4^{3-} and NO_3^- from aqueous solutions.
- The same adsorbent is applicable for cationic and anionic compounds.
- The adsorption rate is fast.
- The adsorption is not dependent on the solution pH.

GRAPHICAL ABSTRACT

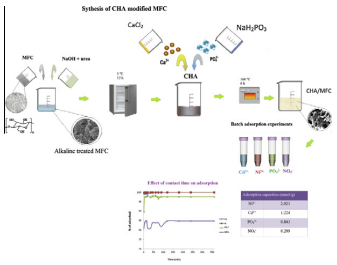

ARTICLE INFO

Article history:
Received 3 March 2014
Received in revised form 24 April 2014
Accepted 25 April 2014
Available online 9 May 2014

Keywords:
Adsorption
Carbonated hydroxyapatite (CHA)
Nanocellulose
Water treatment
Ni^{2+}, Cd^{2+}, PO_4^{3-} and NO_3 removal
Isotherms

ABSTRACT

The adsorption of Ni^{2+}, Cd^{2+}, PO_4^{3-} and NO_3^- by carbonated hydroxyapatite (CHA) modified microfibrillated cellulose (MFC) was studied in the aqueous solution. The modified adsorbent was characterized using elemental analysis, FTIR, SEM and EDAX analysis. The adsorption studies were conducted in batch mode. The effects of pH, contact time, the concentration of metals and the regeneration efficiency were studied. The removal of Ni^{2+}, Cd^{2+}, PO_4^{3-} and NO_3^- was not pH dependent. The maximum removal capacities of the CHA/MFC adsorbent for Ni^{2+}, Cd^{2+}, PO_4^{3-} and NO_3^- were 2.021, 1.224, 0.843 and 0.209 mmol/g, respectively. The Langmuir and Sips models were representative to simulate adsorption isotherms. The results of adsorption kinetic indicate that adsorption was very fast for all studied compounds.

1. Introduction

Phosphates (PO_4^{3-}) and nitrates (NO_3^-) are essential, often limiting, nutrients for growth of organisms in most ecosystems [1]. Primarily, PO_4^{3-} can enter into freshwater ecosystems through agricultural runoff, domestic sewages and industrial effluents [2,3]. PO_4^{3-} and NO_3^- are directly responsible for the extraordinary growth of algae in water bodies such as rivers and lakes [4,5]. Removal of these nutrients, especially PO_4^{3-} by advanced treatment is beneficial when the euthrophication impacts are expected in the receiving aquatic environment [6,7].

* Corresponding author. Tel.: +358 40 747 7843; fax: +358 15 336 013.
E-mail address: sanna.hokkanen@lut.fi (S. Hokkanen).
[1] Tel.: +358 40 747 7843; fax: +358 15 336 013.

http://dx.doi.org/10.1016/j.cej.2014.04.101
1385-8947/

There are a wide range of technologies used to remove phosphorus and nitrates from wastewaters, such as physical, chemical, biological and combination methods, which typically require considerable capital investment and maintenance costs for infrastructure and operational costs [8]. Among all the approaches proposed, the use of adsorbents with high phosphorus and nitrate sorption capacity to remove them in wastewaters have become popular worldwide. These adsorbents include minerals (limestone, opoka, wollastonite, bauxite and zeolites), soils (laterite and marl), industrial byproducts (fly ash, red mud, burnt oil shale and slag materials) and man-made products (lightweight aggregates) effluents [2,3].

Literature shows that excellent and efficient phosphorus and nitrate adsorbents are all characterized by their high aluminum, iron or carbonated contents and that they can effectively remove phosphorus from wastewaters by the adsorption and/or precipitation of chemically stable phosphorus phases [9–14]. Thus, substrates with high contents of aluminum, iron or calcium may have the potential to be phosphorus-removing adsorbents.

The removal of heavy metals from wastewater has become a critical issue because of their adverse effects on human health and the environment [15,16]. Adsorption has been proved to be a useful method also for the treatment of wastewater contaminated by metal ions. Nowadays, almost all the adsorbents developed for the removal of heavy metal ions and rely on the interaction of the target compounds with the functional groups that are present on the surfaces of the adsorbents.

As indicated above, the wastewaters vary in terms of the pollutant composition depending on the origin of the industry. There are also water waters that contain as well as nutrients and heavy metals, for example storm wastewater and municipal wastewater. In the cases where a complex water composition and several of the pollutants need to be removed, it would be interesting to find a single adsorbent that has the potential to be utilized for treatment of that kind of wastewater due to the ability of removal of nutrients and heavy metals.

For these aims, we attempted in this work to study the adsorption and regeneration of nickel (Ni), cadmium (Cd), PO_4^{3-} and NO_3^- using the same adsorbent, carbonated hydroxyapatite (CHA) modified nanocellulose (CHA/MFC). CHA has a composition and structure analogous to the bone apatite and shows higher bioactivity than pure hydroxyapatite (HA) [17–19]. Due to small size and high specific surface area, CHA nanostructures can effectively interact with the cellulose structures, resulting in the enhancement of properties of their nanocomposite [20]. To make the adsorption process more economical and to also enable recovering valuable metals from wastewater streams it is necessary to regenerate the spent adsorbent.

2. Materials and methods

2.1. Raw material and chemicals

Microfibrillated cellulose (MFC) was purchased from University of Oulu, Finland. Bleached birch (*Betula Verrucosa and Pendula*) chemical wood pulp was used as the raw material of MFC. The cellulose, xylan and glucomannan contents of the pulp were 74.8%, 23.6% and 1.1%, respectively. The amount of lignin was 0.4% and acetone soluble extractives 0.08%. Prior to homogenising, the bleached birch was ground in a Valley beater to a dry weight of 2.0% over 50 h, yielding 5503 g of weight. The samples where then diluted to a dry weight of 0.7% and homogenised with a homogeniser at a pressure of 350–1200 bar to create MFC (Suopajärvi et al. 2013).

All solutions were prepared in Millipore milliQ high-purity water. All chemicals used in this study were of analytical grade and supplied by Sigma–Aldrich (Germany). Metal stock solutions of 1000 mg/L were prepared by dissolving appropriate amounts of Ni^{2+} and Cd^{2+} nitrate salts in deionized water. PO_4^{3-} and NO_3^- stock solution were prepared dissolving dose of $NaHPO_4{\cdot}7H_2O$ and $NaNO_3$ salts in deionized water. Adjustment of pH was accomplished using 0.1 M NaOH or 0.1 M HNO_3.

2.2. Synthesis of CHA modified MFC

MFC (3.0 g) and NaOH–urea solution containing NaOH (7.0 g), urea (12.0 g) and distilled water (100 mL), were mixed under magnetic stirring for 5 min at room temperature. The solution was then cooled to 5 °C for 12–18 h (Jia et al., 2010).

After cooling, 50 mL of MFC–NaOH–urea solution was mixed with 25 mL of $CaCl_2{\cdot}2H_2O$ solution (0.402 mol/L) and 25 mL of $NaH_2PO_4{\cdot}H_2O$ (0.802 mol/L) under vigorous stirring for 2 h at room temperature. The mixture was then transferred into an oven where the temperature was set to 160 °C for 6 h. After heating, HCA/MFC mixture was centrifuged at 4000 rpm for 5 min. HCA/MFC mixture was washed four times by water and ethanol and centrifuged [21].

2.3. Characterization of modified MFC

Fourier transform infrared spectroscopy (FTIR) type Vertex 70 by B Bruker Optics (Germany) was used to identify the surface groups of the synthesized nanocellulose. An attenuated total reflection (ATR) -FTIR spectra were recorded at 4 cm^{-1} resolution from 400 to 4000 cm^{-1} and 100 scans per sample. FESEM (Zeiss Ultra Plus, Germany) was used for imaging the samples. As pretreatment, the samples were filtered to a polycarbonate membrane with a pore size of 0.2 μm, followed by rapid freezing with liquid nitrogen and freeze-drying in a vacuum overnight. The dried samples were then sputter-coated with platinum. A voltage of 10 kV and a working distance of 5 mm were used when imaging the samples. HPLC (High Performance Liquid Chromatograph, Shimadzu) was used for the analysis of PO_4^{3-} and NO_3^-. The used anion columns were IC SI-50 4E and SI-90G (Shodex®) and 3.2 mM Na_2CO_3 + 1.0 mM $NaHCO_3$ was used as the eluent.

Surface charge and a point of zero charge of the modified and unmodified MFC were determined by isoelectric point titration as a function of pH by using Zetasizer Nano ZS (ZEN3500, Malvern). The determination of C, H, N and O was obtained using Organic Elemental Analyzer Flash 2000 (Thermo Scientific, Germany). About 2.5 mg of the sample in a capsule made of tin (assay of C, H and N) or silver (assay of O) was burned at 920–1000 °C. The quantity of each element is expressed in percent of dry mass.

2.4. Batch adsorption experiments

Batch experiments were performed at ambient temperature using the optimum conditions of all pertinent factors such as dose, pH and contact time. For isotherm and adsorption capacity studies the experiments were carried out by stirring 0.250 g of adsorbent with 0.025 L $NaHPO_4$ solution containing adsorbate at concentrations ranging from 0.1 to 20.0 mmol/L and 0.025 L $NaNO_3$ solution containing adsorbate at concentrations ranging from 0.1 to 10.0 mmol/L. The same experiments for Ni and Cd were carried out by stirring 0.099 g of adsorbent with 0.020 L metal solutions containing metals concentration ranging from 0.1 to 15 mmol/L.

The effect of contact time was studied in a reaction mixture of 1.2 g of adsorbent and 0.350 L of solution containing each adsorbates at concentrations of 1.7 mmol/L. Agitation was conducted under magnetic stirring using own decanter glass for each metal

reaction mixture. 2 mL samples were pipetted from the reaction mixtures according to schedule. The contact time was varied from 1 to 2400 min.

After centrifugation metal concentrations were analyzed by an inductively coupled plasma optical atomic emission spectrometry (ICP–OES) model iCAP 6300 (Thermo Electron Corporation, USA).

In order to obtain the adsorption capacity (q), the amount of ions adsorbed per mass unit of CAH/MFC (mg/g) was calculated with the following formula:

$$q_e = \frac{C_i - C_e}{M} V. \quad (1)$$

where C_i and C_e are the initial and the equilibrium concentrations (mmol/L), while M and V are the weight of the adsorbent (g) and the volume of the solution (L).

2.5. Regeneration studies

The regeneration of the modified MFC was studied in Ni^{2+}, and Cd^{2+} solutions. At first adsorbents were loaded by metal ions by mixing 1 g of the adsorbent with 0.015 L of 1.8–3.4 mmol/L metal solution, 1 mmol/L phosphate solution and 0.5 mmol/L nitrate solution. After attaining equilibrium, the spent adsorbent was separated from the solution by centrifuge. Metal ions were eluted using 0.1 M HNO_3 and 0.01 M HNO_3, phosphate and nitrate were eluted using 0.1 M NaOH and 0.01 M NaOH. The regeneration efficiency (%RE) of the adsorbent was calculated as follows:

$$(\%RE) = \frac{q_r}{q_0} \times 100 \quad (2)$$

where q_0 and q_r are the adsorption capacities of the adsorbents (mmol/g) before and after regeneration, respectively.

3. Results and discussions

3.1. Characterization of CHA/MFC

Characterization of CHA treated MFC was accomplished by FTIR spectroscopy, FESEM images, elementary analyzer and zeta potential measurements. The FTIR analysis was carried out to understand the chemical structure of modified and unmodified nanocellulose. Fig. 1 shows the FTIR spectra of both pristine unmodified MFC and CHA/MFC. In both spectra two absorbing peaks were observed at 2900 corresponding to the tension and vibration of —CH_2 [22]. A weak band at around 3330 cm^{-1} corresponding to hydroxyl stretching is observed. The other characteristic peaks for pure MFC are the CH and OCH in-plane bending vibrations at 1428 cm^{-1}, the CH deformation vibration at 1366 cm^{-1}, the COC, CCO, and CCH deformation modes and stretching vibrations in which the motions of the C-5 and C-6 atoms are at 895 cm^{-1} [16].

In spectra of CHA/MFC the bands at around 1640 cm^{-1} are indicated to the bending mode of OH— groups and band at 601 cm^{-1} ascribed to the liberation mode of the O—H vibration. The asymmetric and symmetric stretching vibrations of PO_4^{3-} are found at 962–1023 cm^{-1} and 562–643 cm^{-1}, respectively. The bands at 1420 cm^{-1} corresponding to CO_3^{2-} are present due to the presence of carbonate (CO_3^{2-}), which is also indicated by the band around 878 cm^{-1} [23,24].

The spectrum of MFC shows that the band found at around 2900 cm^{-1} belongs to O—H stretching, while the O—H bending mode of adsorbed water is registered at around 1640 cm^{-1}. The weak band at 1590 cm^{-1} confirms the presence of the COO— group. The other weak bands at 1428 cm^{-1} are assigned to HCH and OCH vibrations and the band at 1366 cm^{-1} to the CH bending mode. The band at 895 cm^{-1} is corresponding to the COC, CCO and CCH deformation modes [25].

The elemental analysis of unmodified and CHA modified MFC (Table 1) shows a high level of carbon (C) (31.91% and 11.04%) and oxygen (O) (55.11% and 21.65%) and low level of hydrogen (H) (4.98% and 1.70%), respectively. After modification with CHA, an obvious increase in nitrogen (N) and the other elements can be observed, which corresponds to the introduction of CHA onto the cellulose surface.

The X-ray diffraction results are supported by EDX analysis of the composite surfaces. The contents of elements (Fig. 2) on the surface in a weight and atomic percent are collected in Table 1. Besides, the elemental concentration distribution of solid sample can be analyzed using the mapping analysis of SEM/EDAX. The elemental distribution mapping of EDAX for the sample of CHA treated MCA is illustrated in Fig. 2. The bright points represent the signal of phosphorus or calcium element from the solid sample. Both elements were spread over the surfaces of MFC. Results indicated that CHA produces chemical bond with MFC.

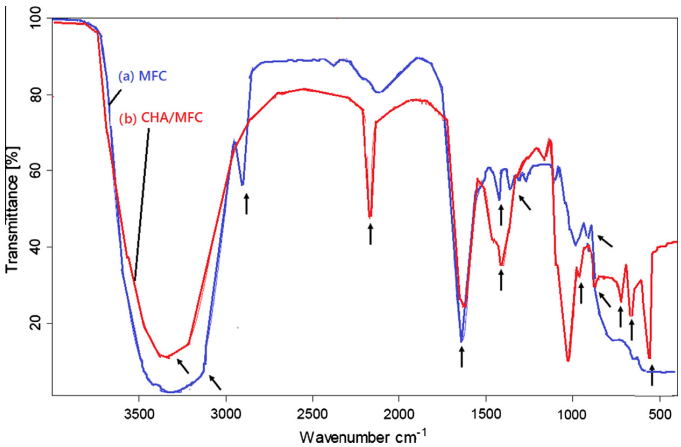

Fig. 1. FTIR spectra of unmodified MFC (a) and CHA/MFC (b).

Table 1
The elemental analysis results of unmodified and modified MFC.

Percentage of dry weight (%)					
Unmodified MFC 2.61 mg		C	H	O	
		31.91	4.98	55.11	
Percentage of dry weight (%)					
HAP/MFC 2.48 mg	N	C	H	O	Ca, Na, P and Cl (calculated)
	1.7	11.04	1.65	21.65	63.93

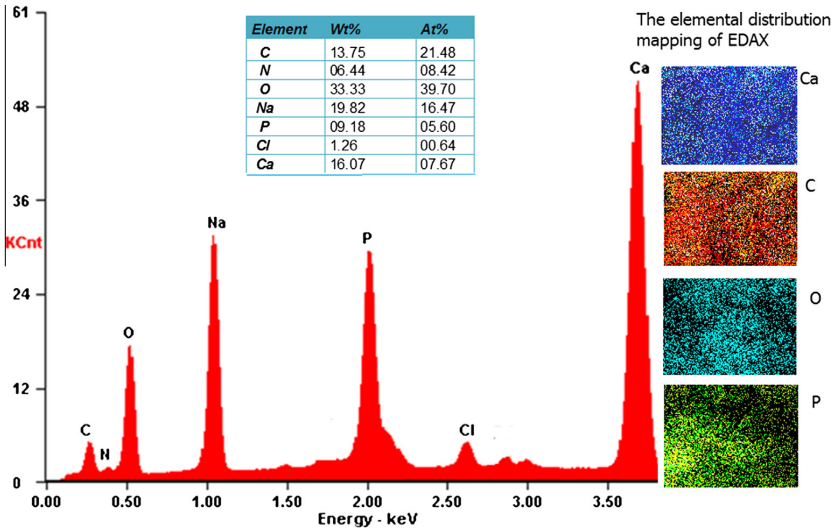

Fig. 2. EDAX spectra, contents of elements and the elemental distribution mapping for the sample of CHA treated MCA.

The SEM images of unmodiriede MFC (Fig. 3a) and CHA/MFG (Fig. 3b) show that the surface of the cellulose is completely covered by the CHA layers. This indicates the success of the synthesis and increase of the surface area due to the CHA treatment.

Clear relationship was found between EDAX analysis and the elementary analysis (Fig. 2) in CHA/MFC. Low concentrations of C and high concentrations of Ca and P indicate that MFC can bind to a much larger amount of CHA than its own mass. Cl, Na and N originate from the starting materials of synthesis; urea, NaOH, $CaCl_2$ and NaH_2PO_4.

3.2. Adsorption studies

3.2.1. Effect of pH

The removal of metal ions from aqueous solutions by adsorption depends on the solution pH, because it affects the adsorbent's surface charge, the degree of ionization, and the speciation of adsorbates.

Adsorption of Ni^{2+}, Cd^{2+}, PO_4^{3-} and NO_3^- by CHA/MFC was studied using the initial pH range from 2 to 8. At higher pH values, most metal ions precipitate as hydroxides. Nickel can be removed by precipitation as hydroxide at pH ranging from 10 to 11 and cadmium by precipitation as hydroxide at pH ranging from 8 to 11. Therefore, the effect of pH was not investigated at pH values above 8. After 20 h of contact time, equilibrium pH values were measured, as well as the residual metal concentrations. The effect of initial pH for adsorption is presented in Fig. 4a. The results illustrate that the results the pH does not affect the percentage of Ni^{2+}, Cd^{2+}, PO_4^{3-} and NO_3^- removed for pH 5 and above. However in the pH below 5 it has a significant effect.

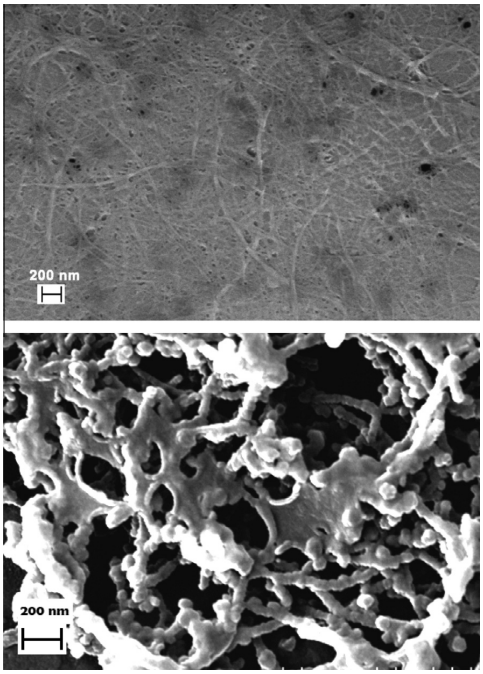

Fig. 3. The SEM images of (a) MFC and (b) CHA/MFC.

Table 2
Kinetic parameters for of Ni^{2+}, Cd^{2+}, PO_4^{3-} and NO_3^-.

Type of metals	q_e (mmol/g)	Pseudo-first-order			Pseudo-second-order		
		q_t, (mmol/g)	k_1 (1/min)	R^2	q_t, (mmol/g)	k_2 (g/mg min)	R^2
Cd	0.495	0.494	4.58	1.000	0.495	158.7	1.000
Ni	0.497	0.489	4.25	1.000	0.490	93.4	0.998
PO_4	0.207	0.204	3.02	1.000	0.204	71.8	0.993
NO_3	0.415	0.415	1.00	1.000	0.451	1.56	0.998

Fig. 4b. shows that the buffering properties of CHA/MFC depended on the adsorbates. For all adsorbates the final pH was alkaline regardless of the initial pH range 2–10. The change was smaller for metals: for the initial pH range 3–6 for Ni^{2+} and 2–6 for Cd^{2+} the final pH values were almost constant (8.5–9). The plateau parts of final pH versus initial pH plots, correspond to the pH range where the buffering effect of HAP surface takes place. In that area acidic, as well as basic solutions are buffered after the reaction with CHA/MFC to value 8.5–9. In the initial pH range 6–10, the final pH changed to value of 11.5 for Ni^{2+} and 12 for Cd^{2+}. These values are close to the pH of CHA/MFC (11.6). Generally, Ni^{2+} and Cd^{2+} aqueous concentrations diminished rapidly at initial pH 6 with the increase of final pH, due to both adsorption of hydrolytic species and precipitation of insoluble hydroxides.

At the initial pH range 2–6 for PO_4^{3-}, the final pH values were around 10.5. At the higher initial pH range the final pH increased gradually until to pH value of 11.4. For NO_3^-, at the initial pH range 2–6, the final pH increased gradually until to pH value of 11.4 and thereafter remained unchanged.

The buffering characteristics of CHA are causing the acid–base reactions of the reactive surface sites. According to Wu et al. and Smiciklas et al. the reactions responsible for the surface properties of CHA in aqueous solutions are [26,27]:

$$\equiv PO^- + H^+ \leftrightarrow \equiv PHO^0 \quad (3)$$

$$\equiv CaOH_2^+ \leftrightarrow \equiv CaOH^0 + H^+ \quad (4)$$

For the alkaline initial pH values consumption of protons from the solution by the protonation of surface ≡PO— and ≡$CaOH^0$ groups caused the increase of final pH. In the acidic solutions the positively charged ≡$CaOH^{2+}$ and neutral ≡POH^0 sites predominate on CHA/MFC surface, making it positive. Secondly, decrease of final pH occurs in the alkaline pH conditions due to OH— consumption via deprotonation of surface ≡$CaOH^{2+}$ and ≡POH^0 sites. Thereby, in alkaline solutions CHA/MFC surface becomes negative due to neutral ≡$CaOH^0$ and negatively charged ≡PO— species predominate in those conditions [26,27].

3.2.2. Effect of contact time

The effect of contact time on the adsorption of Ni^{2+}, Cd^{2+}, PO_4^{3-} and NO_3^- by modified CHA/MFC is shown in Fig. 5a–d using single component solution and multi component solution (Ni^{2+}, Cd^{2+}, PO_4^{3-}, NO_3^- in same solution). The adsorption was very fast for all the studied components in the both cases. For metals more than 95%, for PO_4^{3-} more than 85% and for NO_3^- more than 80% was adsorbed within 5 min in the case of single component solution. This indicates the presence of numerous active sites on the adsorbent surface. On the basis of these results, it can be observed that CHA/MFC can be used to remove these ions, however, the removal capacity for the different ions on the CHA/MFC is in order of $Ni^{2+} \sim Cd^{2+} > PO_4^{3-} > NO_3^-$.

As shown in Fig. 5a–d, in the case of multi component solution, the other components are hardly effecting on the adsorption of Ni^{2+} and for Cd^{2+} ions. This indicates that the adsorbent had enough adsorption sites for both metals. Instead, in the presence of other ions the adsorption capacity of NO_3^- decreased drastically and the adsorption kinetics became irregular (Fig. 5d). This is due to the metal solutions were prepared by dissolving appropriate amounts of Co(II) and Ni(II) nitrate salts in deionized water for which reason the total nitrate concentration was much more higher than the other compound in multi component solution. In a recent publication [28,29] were observed that chloride and carbonate ions, for example, influenced the nitrate adsorption. Furthermore, the CHA/MFC residue contains some chlorides (Fig. 2) which may have decreased the nitrate removal efficiency. For PO_4^{3-} maximum adsorption capacity decreased and the equilibrium

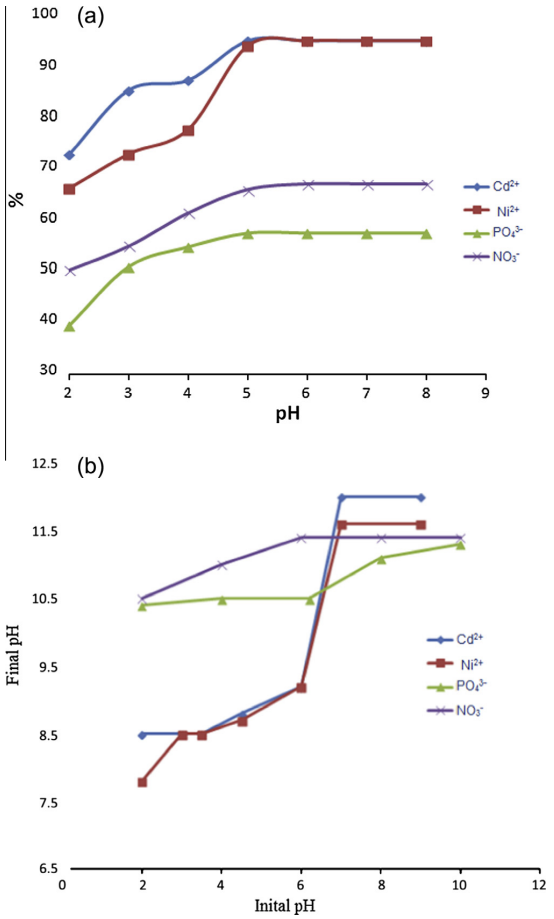

Fig. 4. (a) Effect of initial pH on adsorption and (b) relationships between initial and final pH values obtained after equilibration of CHA/MFC with Ni^{2+} and Cd^{2+} solution.

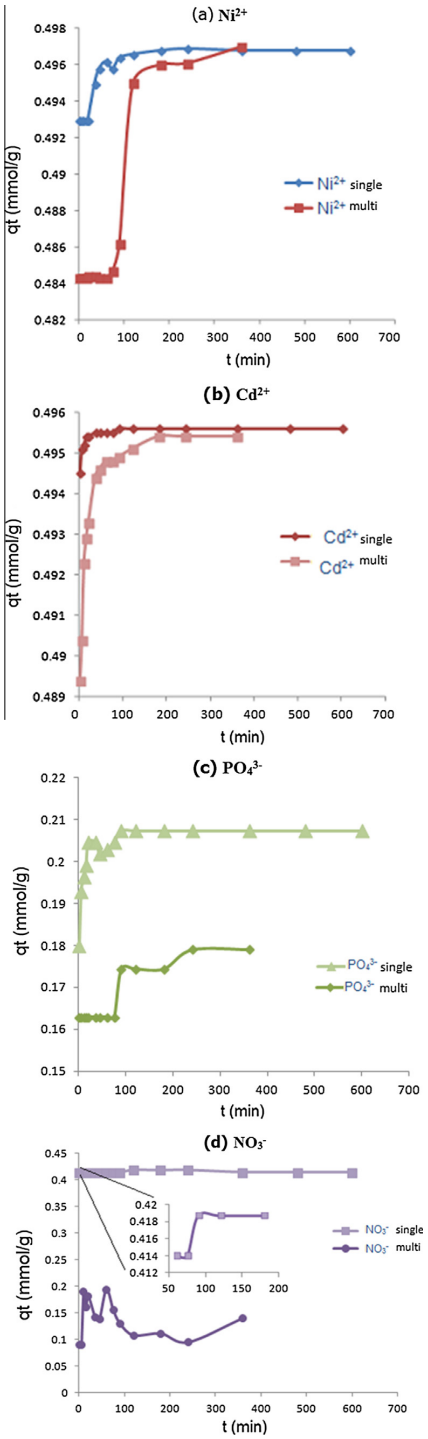

Fig. 5. (a–d) Effect of contact time on adsorption of Ni^{2+}, Cd^{2+}, PO_4^{3-} and NO_3^- by the adsorbent in single and multi component solution (at initial concentration for Ni^{2+}, Cd^{2+}, PO_4^{3-} 1.7 mmol/L and for NO_3^- 5.7 mmol/L respectively; dose of each adsorbent: 3 g/L; volume of solution: 0.350 L).

time was 90 min, while in the case PO_4^{3-} one-component solution, it was 5 min. This indicates that there are less adsorption sites for anions on the surface of CHA/MFC. Hence, PO_4^{3-} and NO_3^- have to compete with each other for the free adsorption sites.

The kinetics of Ni^{2+}, Cd^{2+}, PO_4^{3-} and NO_3^- adsorption on CHA/MFC was also analyzed using pseudo-first-order and pseudo-second-order kinetic models. The pseudo-first-order kinetic model is commonly used to predict adsorption kinetics and is expressed as [30]:

$$\log(q_e - q_t) = \log(q_e) - \frac{k_1}{2.303}t \quad (5)$$

The pseudo-second-order rate equation is:

$$\frac{t}{q_t} = \frac{1}{q_e^2 k_2} + \frac{1}{q_e} + t \quad (6)$$

The adsorption kinetics can be considered as a pseudo-second order reaction non linear, which can be described by the following equation:

$$q_t = \frac{q_e^2 k_2 t}{1 + q_e k_2 t} \quad (7)$$

where q_t and q_e (mg/g) are the adsorption capacity at time t and at equilibrium, respectively, k_1 (1/min) and k_2 (g/mg min) are the adsorption rate constant.

Fig. 6 and Table 2 indicate that both models were found to be in good agreement with experimental data and can be used to favorably explain the sorption of Ni^{2+}, Cd^{2+}, PO_4^{3-} and NO_3^- on CHA/MFC, but the pseudo-first-order model gave the best fit to the experimental data since $q_{e,exp}$ and $q_{e,model}$ were very close to each other.

3.2.3. Adsorption isotherms

Adsorption isotherm studies are important to determine the efficacy of adsorption. The equilibrium adsorption isotherm is fundamental in describing the interactive behavior between the adsorbate and adsorbent, and the relationship between the concentration of adsorbed and dissolved adsorbate at equilibrium. For the adsorption isotherm studies, the initial metal ion concentrations were in the range of 10–700 mg/L, initial phosphorus and nitrate concentration of 10–620 mg/L.

In this study, the adsorption mechanisms were analyzed by one two-parameter (Langmuir) and one tree-parameter (Sips) isotherm models, which are commonly used to describe experimental results in a wide range of concentrations.

The Langmuir adsorption model further assumes that all the adsorption sites are energetically identical and adsorption occurs on a structurally homogeneous adsorbent. The Langmuir equation is expressed as follows:

$$q_e = \frac{q_m K_L C_e}{1 + K_L C_e} \quad (8)$$

where q_e (mmol/g) is the equilibrium adsorption capacity and q_m (mmol/g) is the maximum amount of the metal ions adsorbed per unit weight of the adsorbent. Latter also describes the formation of a complete monolayer coverage on the surface at high equilibrium metal ion concentration C_e (mmol/L). Furthermore, q_m represents the practical limiting adsorption capacity when the surface is fully covered with metal ions, assisting in the comparison of adsorption performances of different adsorbents. K_L (L/mmol) is the Langmuir equilibrium constant related to the affinity of the binding sites and indicates the bond energy of the adsorption reaction between metal and material [30,31].

Modeling calculations were conducted using Microsoft Office Excel 2007 software. Isotherm parameters were determined by

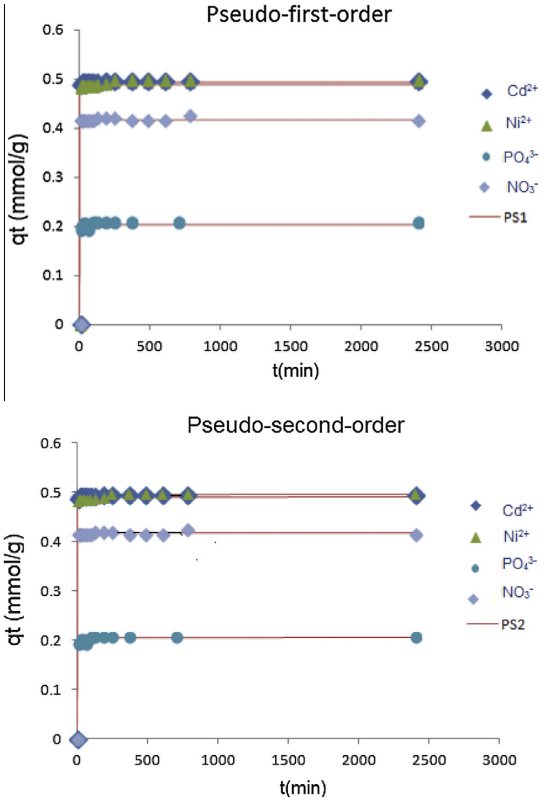

Fig. 6. Kinetic modeling of Ni^{2+}, Cd^{2+}, PO_4^{3-} and NO_3^- adsorption by CHA/MFC.

minimizing the Sum of the Squares of the Errors (ERRSQ) function across the concentration range studied:

$$\sum_{i=1}^{p}(q_{e,exp} - q_{e,calc})^2 \quad (9)$$

Fig. 7 and Table 4 show that the Langmuir isotherm fitted rather well to the experimental data and especially for *P* adsorption supported also by the estimated q_m value and high R^2 value. For NO_3^-, however, the Langmuir model could not predict the experimental behavior indicating more complex adsorption phenomena than simple monolayer formation. Significant variations in K_L values of metal ions indicate that the adsorption energies between the adsorbent and metal ions were different. Very high K_L values of Ni^{2+} and Cd Cd^{2+} ions correlated well with their fast adsorption and low K_L value of PO_4^{3-} and NO_3^- its slower adsorption observed in kinetic experiments.

The Langmuir model is often too simple to describe the complex adsorption phenomena due to the surface heterogeneity or interactions between adsorbing species.

The Sips isotherm model is obtained by introducing a power law expression of the Freundlich isotherm into the Langmuir isotherm and is therefore also called as Langmuir–Freundlich (Sips) isotherm. The non-linearized form of Sips isotherm model can be given as follows:

$$q_e = \frac{q_m(K_sC_e)^{n_s}}{1 + (K_sC_e)^{n_s}} \quad (10)$$

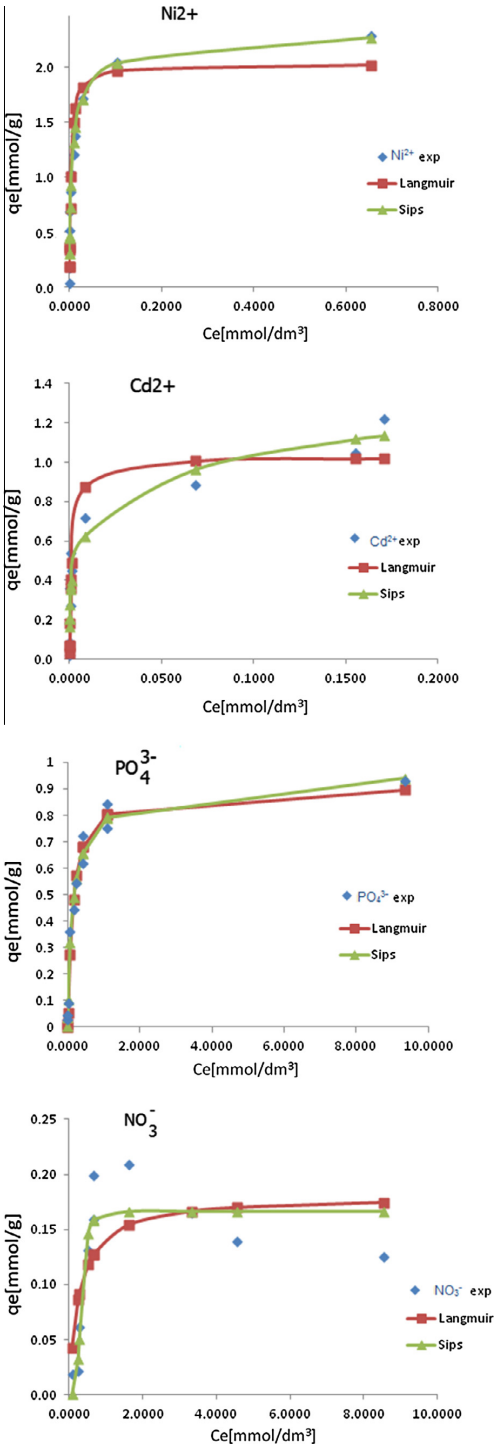

Fig. 7. Adsorption isotherms of Ni^{2+}, Cd^{2+} (initial concentration 10–100 mg/L; dose of CHA/MFC: 3.96 g/L; volume of solution 0.025 L), PO_4^{3-} and NO_3^- (initial concentration rage 10–620 mg/L; dose of CHA/MFC: 11.2 g/L; volume of solution 0.025 L), pH 5.0, room temperature.

Table 3
Langmuir and Sips parameters and average adsorption capacity.

Type of adsorbate	$q_{m,exp}$ (mmol/g)	q_m (mmol/g)	K_L	R^2	Average adsorption capacity (%)
Langmuir					
Ni^{2+}	2.021	2.277	293.040	0.931	99.334
Cd^{2+}	1.224	1.028	676.279	0.878	99.300
PO_4^{3-}	0.843	0.911	6.995	0.977	91.703
NO_3^-	0.209	0.180	3.665	0.561	55.000
Type of adsorbate	$q_{m,exp}$ (mmol/g)	q_m (mmol/g)	n_s	K_S	R^2
Sips					
Ni^{2+}	2.021	0.616	0.735	5.984	0.965
Cd^{2+}	1.224	1.688	0.293	1.950	0.917
PO_4^{3-}	0.843	0.974	0.673	4.559	0.979
NO_3^-	0.209	7.591	4.538	2.945	1.000

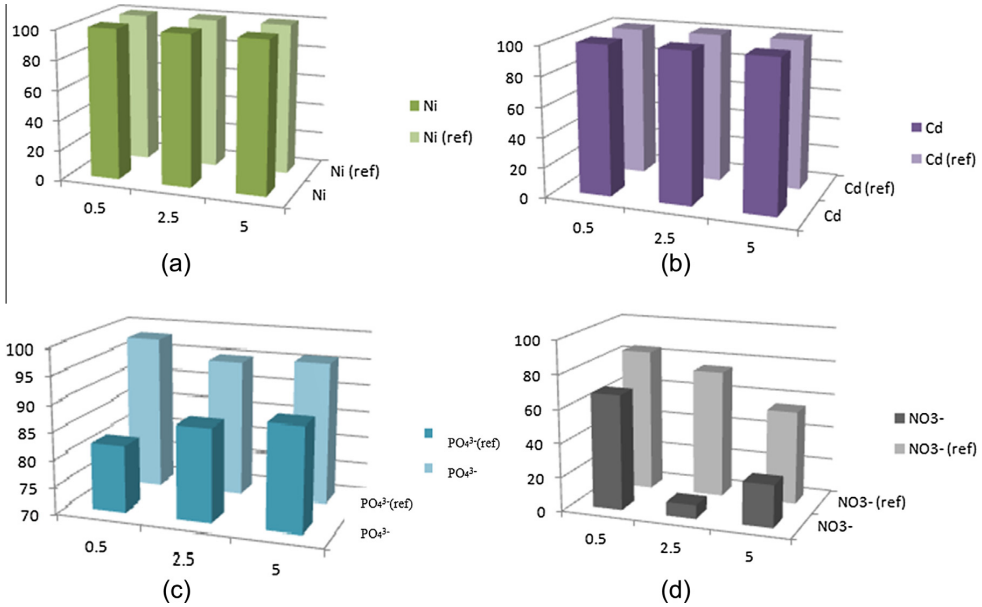

Fig. 8. The adsorption efficiency of multi adsorbate solution in compared with results of adsorption efficiency with one adsorbate solution: (a) Ni^{2+}, (b) Cd^{2+}, (c) PO_4^{3-} and (d) NO_3^-.

Table 4
The adsorption efficiency of multi adsorbate solution in compared with results of adsorption efficiency with one adsorbate solution.

Initial concentration of the adsorbate (mol/g)	Ni^{2+}	Cd^{2+}	PO_4^{3-}	NO_3^-
Adsorption efficiency with one adsorbate solution (%)				
0.5	100	100	98	84
2.5	100	100	95	75
5	100	100	96	55
Adsorption efficiency of multi adsorbate solution (%)				
0.5	100	100	82	68
2.5	100	100	87	8.1
5	100	100	89	25

Generally, the Sips isotherm is an appropriate equation to fit experimental equilibrium data of the wide variety of adsorbents. At low adsorbate concentrations, Sips isotherm effectively reduces to the Freundlich isotherm, while at high adsorbate concentrations it predicts a monolayer adsorption capacity characteristic of the Langmuir isotherm [30]. It has a form of where, q_{max} (mg/g) is the maximum monolayer surfactant adsorption capacity on sandstone. K_S [$(L/mg)_s^n$] is the Sips isotherm constant representing the energy of adsorption. n_s is the empirical constant. If the value of K_S approaches 0, the Sips isotherm will become a Freundlich isotherm. While the value of $m_s = 1$ or closer to 1, the Sips isotherm equation reduces to the Langmuir equation; that is, adsorption takes place on homogeneous surface [30–32].

The plots of the Sips isotherm are illustrated in Fig. 7 and the results are presented in Table 3. The results show that for adsorbates q_m value estimated by the Sips model corresponded to the experimentally obtained $q_{m,exp}$ better than that estimated by the Langmuir model, especially for NO_3^-. For Ni^{2+} the Langmuir model seemed to provide a better approximation for q_m, but the R^2 values were higher for all the metals with Sips model. Relatively poor correlation coefficients (R^2 values <0.990) observed for all the metal ions with both Langmuir and Sips models may be attributed to the unequal distribution of the adsorption surface area and active sites in samples due to the high water concentration of CHA/MFC.

The results for average adsorption efficiency (%) within concentration range 10–700 mg/L for Ni^{2+} and Cd^{2+}, within concentration range 10–620 mg/L for P and NO_3^- are illustrated in Table 3. The results indicate that CHA/MFC have very high, > 90% adsorption efficiency for Ni^{2+}, Cd^{2+} and PO_4^{3-}, and >50% for NO_3^-.

Table 5
Regeneration of CHA/MFC for Ni^{2+}, Cd^{2+}, PO_4^{3-} and NO_3^- by different regenerats.

Type of regenerant	No. of cycle	Adsorption capacity of Ni^{2+}		Regeneration efficiency (%)	Adsorption capacity of Cd^{2+}		Regeneration efficiency (%)
		Before regeneration (mmol/g)	After regeneration (mmol/g)		Before regeneration (mmol/g)	After regeneration (mmol/g)	
HNO_3 1.0 M	1	0.0437	0.0081	18.30	0.0288	0.0000	0.00
	2	0.0437	0.0021	4.57	0.0288	0.0000	0.00
	3	0.0437	0.0010	2.28	0.0288	0.0000	0.00
	4	0.0437	0.0027	6.16	0.0288	0.0000	0.00
HNO_3 0.1 M	1	0.0437	0.0210	48.05	0.0288	0.0071	24.62
	2	0.0437	0.0024	5.49	0.0288	0.0000	0.00
	3	0.0437	0.0015	3.43	0.0288	0.0000	0.00
	4	0.0437	0.0043	9.83	0.0288	0.0013	5.51
HNO_3 0.01 M	1	0.0437	0.0436	99.77	0.0288	0.0288	100.00
	2	0.0437	0.0190	43.70	0.0288	0.0288	100.00
	3	0.0437	0.0155	35.46	0.0288	0.0288	100.00
	4	0.0437	0.0107	24.48	0.0288	0.0220	99.98
Type of regenerant	No. of cycle	Adsorption capacity of PO_4^{3-}		Regeneration efficiency (%)	Adsorption capacity of NO_3^-		Regeneration efficiency (%)
		Before regeneration (mmol/g)	After regeneration (mmol/g)		Before regeneration (mmol/g)	After regeneration (mmol/g)	
NaOH 1.0 M	1	0.1709	0.0263	15.39	0.0619	0.0000	0.00
	2	0.1709	0.0215	12.58	0.0619	0.0000	0.00
	3	0.1709	0.0186	9.60	0.0619	0.0000	0.00
	4	0.1709	0.0164	8.26	0.0619	0.0000	0.00
NaOH 0.1 M	1	0.1709	0.0822	48.10	0.0619	0.0000	0.00
	2	0.1709	0.0384	22.47	0.0619	0.0000	0.00
	3	0.1709	0.0280	16.38	0.0619	0.0000	0.00
	4	0.1709	0.0202	11.82	0.0619	0.0000	0.00
NaOH 0.01 M	1	0.1709	0.1097	64.19	0.0619	0.0049	7.92
	2	0.1709	0.0367	21.48	0.0619	0.0049	7.92
	3	0.1709	0.0244	14.28	0.0619	0.0000	7.92
	4	0.1709	0.0214	12.52	0.0619	0.0000	0.00

Experiments were also performed with solutions containing both metals and PO_4^{3-} for three different initial concentrations: 0.5, 2.5 and 5 mmol/L, and NO_3^- for 1.8, 9.0 and 18 mmol/L (due to the nitrate content of metal solutions) Fig. 8a–c shows the adsorption efficiency in comparison with results of adsorption efficiency with one adsorbate solution. As it can be seen from Table 4, these experiments confirm the effectiveness of CHA/MFC in Ni^{2+} and Cd^{2+} cases; any differences cannot observed for the adsorption efficiency. Considering the removal efficiencies for PO_4^{3-} and NO_3^- (Table 5), the adsorption efficiency was much higher for the one adsorbate solution. This indicates that there are fewer adsorption sites for anions on the surface of CHA/MFC, due to mutual competition between PO_4^{3-} and NO_3^- .

3.3. Removal mechanism

The adsorption of metal ions, PO_4^{3-} and NO_3^- by CHA/MFC can take place via various possible mechanisms. Factors that affect the preference for the adsorption may be related to the characteristics of the binding sites (e.g. functional groups, structure, surface properties, etc.), the properties of the sorbet (e.g. concentration, ionic size, ionic charge, molecular structure, etc.) and the solution chemistry (e.g. pH, ionic strength, etc.). In the context of sorption on apatite, a number of properties have been suggested for use in the ordering of affinity rank, including ionic radius and Pauling electronegativity [33,34].

In the case of metals, ion-exchange between the calcium and the bivalent ion is one possibility. The heavy metal replaces the calcium in the CHA lattice, according to the reaction:

$$Ca_{10}(PO_4)_6(OH)_2 + xMe^{2+} \leftrightarrow (Ca10 - x)Me_x(PO_4)_6(OH)_2 + xCa^{2+} \quad (11)$$

Dissolution–precipitation is another suggested mechanism, which takes place in two steps: firstly, CHA is dissolved in solution; subsequently, the phosphate ion reacts with the metal to form a new insoluble phase. This mechanism is shown in the reactions below:

$$Ca_{10}(PO_4)_6(OH)_2 + 14H^+ \leftrightarrow 10Ca^{2+} + 6H_2PO_4^- + 2H_2O \quad (12)$$

$$10Me^{2+} + 6H_2PO_4^- + 2H_2O \leftrightarrow Me_{10}(PO_4)_6(OH)_2 + 14H^+ \quad (13)$$

The adsorption of PO_4^{3-}- or NO_3^- ions can be best explained as exchange of ions. Probably OH^- ions are exchanged by PO_4^{3-}- or NO_3^- ions.

FTIR spectra of the CHA/MFC before and after metal ion sorption are shown in Fig. 9. The reaction of Ni^{2+} and Cd^{2+} with the apatitic structure of CHA was very similar and led to some changes of IR vibrations of functional groups. The spectrum of CHA/MFC after metal adsorption shows a decrease in the intensity of carbonate vibrations, which might be due to the partial decarbonation when CHA sorbents were in contact with acidic Cd^{2+} and Ni^{2+} nitrate (initial pH of 5.2). The bi-modal peak at 1010 and 980 cm^{-1} and peaks at around 600–560 cm^{-1} were characterized as phosphate vibrations in Cd^{2+} and Ni^{2+} substituted CHA. [35,36]. The phosphate peaks are also weaker after metal adsorption which may caused the reaction between metal ions and phosphate groups of the CHA.

The adsorption of PO_4^{3-} on the CHA/MFC does not induce any major changes in the FTIR spectra of CHA/MFC (Fig. 9).The peaks of PO_4^{3-} are more intensive after adsorption due to the amount of the phosphate was increased. The results demonstrated that there were significant differences between the FTIR spectra of CHA/MFC before and after adsorption of NO_3^-. After adsorption, the new bands at around 1450–1370 cm^{-1} can be assigned to the nitro complex stretching [37].

In the ion exchange mechanism, equilibrium is attained when forward and reverse exchange reactions occur at equal rates. In the latter case, the dissolution and precipitation reaction rates are equal at equilibrium and the reaction is the same as in Eq. (13). If the initial concentration of Ca atoms in the hydroxyapatite structure is denoted by q^0_{Ca}, and the concentration of metal atoms exchanged to the structure is denoted by q_{Me}, the forward and reverse exchange reaction rates can be written as:

$$r_{fwd} = k_{fwd} C_{Me^{2+}} (q^0_{Ca} - q_{Me})^m \quad (14)$$

where $C_{Me^{2+}}$ is the concentration of metal cations in the liquid phase, k_{fwd} is a rate constant, and m is an empirical correction factor that takes into account non-idealities in the solid phase structure. In case of ideal ion exchange, the correction factor $m = 1$. Analogously, the reverse exchange reaction rate can be written as:

$$r_{rev} = k_{rev} (q_{Me})^m \quad (15)$$

Eqs. (12) and (13) yield the following expression at equilibrium:

$$q_{Me} = \frac{q^0_{Ca} \left(\frac{k_{fwd}}{k_{rev}} C_{Me^{2+}}\right)^{\frac{1}{m}}}{1 + \left(\frac{k_{fwd}}{k_{rev}} C_{Me^{2+}}\right)^{\frac{1}{m}}} \quad (16)$$

which can be written in a simplified form by setting $K = k_{fwd}/k_{rev}$, $n = 1/m$, and $q_m = q^0_{Ca}$

$$q_{Me} = \frac{q_m K (C_{Me^{2+}})^n}{1 + K (C_{Me^{2+}})^n} \quad (17)$$

Eq. (13) is formally analogous to the Sips isotherm and reduces to the Langmuir isotherm in the case $n = 1$.

3.4. Regeneration study

In this study, Ni^{2+} and Cd^{2+} were desorbed from CHA/MFC using 0.01 M, 0.1 M and 1.0 M HNO_3, PO_4^{3-} and NO_3^- were desorbed using 0.01 M, 0.1 M and 1 M NaOH. The regeneration data are summarized in Table 5. The results show that the adsorption efficiency for Ni^{2+} and Cd^{2+} was radically affected by regeneration with 0.1 M and 1 M HNO_3; the adsorbent lost its adsorption capacity completely. The adsorption capacity remained the same for Cd^{2+} after the fourth cycle using 0.01 M HNO_3 as regenerant. For Ni^{2+}, the adsorption capacity decreased after every treatment. For Ni^{2+} adsorption capacity decreased after every treatment, the first cycle it was 99.7, but after four cycles, the regeneration efficiency was 24.48% using 0.01 M HNO_3 as regenerant. Also for PO_4^{3-} adsorption capacity decreased after every treatment; from 64.18% to 15.22% during four treatments with 0.01 M NaOH. In general, it can be concluded that the weaker acid (0.01 M HNO_3) is a more effective regenerant for metals and the weaker base (0.01 M NaOH) is a more effective regenerant for PO_4^{3-}. The results in Table 5 show that NO_3^- is not regeneration viable at all.

4. Conclusions

The present study focused on the adsorption of Ni^{2+}, Cd^{2+}, PO_4^{3-} and NO_3^- from aqueous solution using the CHA/MFC as adsorbent. Adsorption of Ni^{2+}, Cd()II, PO_4^{3-} and NO_3^- was found to be independent of the initial pH due to the amphoteric and buffering properties of CHA/MFC. The results of adsorption study showed that CHA modified MFC was very effective for Ni^{2+}, Cd^{2+} and PO_4^{3-} removal from aqueous solution; adsorption efficiency was >90%. The adsorption efficiency for NO_3^- was >50%. Equilibrium isotherm data was fitted using Langmuir and Sips models. Among these models, Sips model was in good agreement with the experimental data with high R^2. Kinetic studies showed very fast adsorption for all adsorbates. The mechanism of adsorption includes mainly ionic interactions (ion-exchange) between adsorbates and CHA/MFC. The adsorption–desorption cycle results demonstrated that the regeneration and subsequent use the CHA/MFC would enhance the economics of practical applications for the removal of Ni^{2+} and Cd^{2+} from water and wastewater. This study shows that CHA/MFC is an easily handled, natural and environmentally friendly absorbent with excellent removal efficiency for metals and phosphorus, moderate removal efficiency for nitrates.

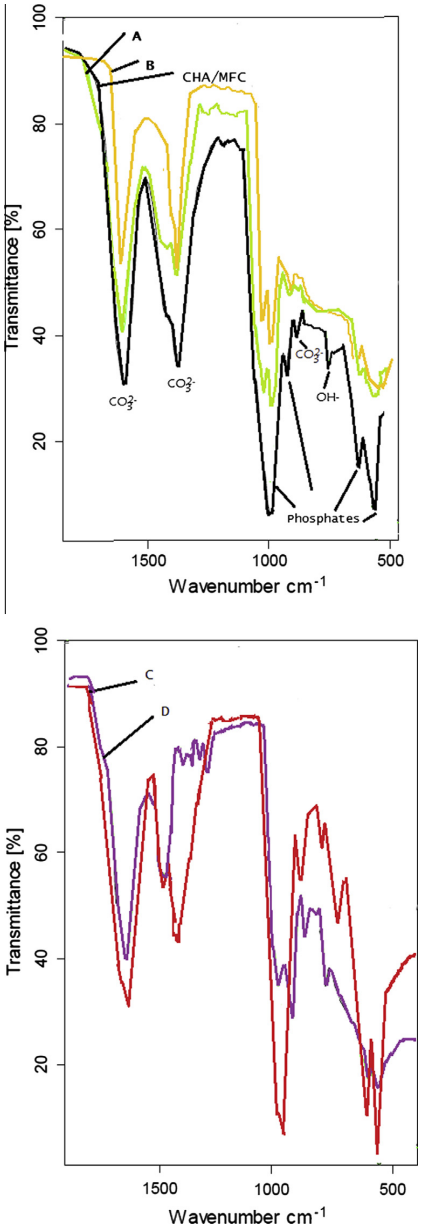

Fig. 9. The FTIR- spectra of CHA/MFC; (A) after adsorption of Ni^{2+}; (B) Cd^{2+}; (C) PO_4^{3-}; (D) and NO_3^-.

Acknowledgments

The authors are grateful to the Fibre and particle engineering laboratory, University of Oulu for providing materials and consultation. Finnish Funding Agency for Technology and Innovation (Tekes) is thanked for the financial support.

References

[1] D.L. Correll, The role of phosphorus in the eutrophication of receiving waters: a review, J. Environ. Qual. 27 (1998) 261–266.
[2] J.A. Rentz, I.P. Turner, J.L. Ullman, Removal of phosphorus from solution using biogenic iron oxides, Water Res. 43 (2009) 2029–2035.
[3] A. Drizo, C.A. Forst, K.A. Grace, Physico-chemical screening of phosphate removing substrates for use in constructed wetland systems, Water Res. 33 (2009) 3595–3602.
[4] P.S. Lau, N.F.Y. Tam, Y.S. Wong, Wastewater nutrients (N and P) removal by carrageenan and alginate immobilized *Chlorella vulgaris*, Environ. Technol. 18 (1997) 945–951.
[5] C. Trépanier, S. Parent, Y. Comeau, J. Bouvrette, Phosphorus budget as a water quality management tool for closed aquatic mesocosms, Water Res. 36 (2002) 1007–1017.
[6] O. Oenemaa, L. Van, O. Liereb, Schoumansa, effects of lowering nitrogen and phosphorus surpluses in agriculture on the quality of groundwater and surface water in the Netherlands, J. Hydrol. 4 (2005) 289–301.
[7] A. Kontas, F. Kucuksezgin, O. Altay, E. Uluturhan, Monitoring of eutrophication and nutrient limitation in the Izmir Bay (Turkey) before and after wastewater treatment plant, Environ. Int. 29 (2004) 1057–1062.
[8] L. Johansson Westholm, Substrates for phosphorus removal—potential benefits for on-site wastewater treatment?, Water Res 40 (2006) 23–26.
[9] M.Koiv Vohla, H. John Bavor, F. Chazarenc, U. Mander, Filter materials for phosphorus removal from wastewater in treatment wetlands—a review, Ecol. Eng. 37 (2011) 70–89.
[10] V. Cucarella, G. Renman, Phosphorus sorption capacity of filter materials used for on site wastewater treatment determined in bath experiments—a comparative study, J. Environ. Qual. 38 (2009) 381–392.
[11] A. Kaasik, C. Vohla, R. Motlp, U. Mander, K. Kirsima, Hydrated calcareous oilshale ash as potential filter media for phosphorus removal in constructed wetlands, Water Res. 42 (2008) 1315–1323.
[12] M. Liira, M. Koiv, U. Mander, R. Motlep, C. Vohla, K. Kirsimae, Active filtration of phosphorus on Ca-rich hydrated oil shale ash: does longer retention time improve the process?, Environ Sci. Technol. 43 (2009) 3809–3814.
[13] P. Sibrell, G.A. Montgomery, K.L. Ritenour, T.W. Tucker, Removal of phosphorus from agricultural wastewaters using adsorption media prepared from acid mine drainage sludge, Water Res. 43 (2009) 2240–2250.
[14] Y. Hongbin, Y. Ye, Z. Yinlong, F. Fana, Phosphate removal from wastewaters by a naturally occurring, calcium-rich sepiolite, J. Hazard. Mater. 198 (2011) 362–369.
[15] Y.N. Mata, M.L. Blázquez, A. Ballester, F. González, J.A. Muñoz, Biosorption of cadmium, lead and copper with calcium alginate xerogels and immobilized fucus vesiculosus, J. Hazard. Mater. 163 (2–3) (2009) 555–562.
[16] S. Hokkanen, E. Repo, M. Sillanpää, Removal of heavy metals from aqueous solutions by succinic anhydride modified mercerized nanocellulose, Chem. Eng. J. 223 (2013) 40–47.
[17] W.L. Suchanek, P. Shuk, K. Byrappa, R.E. Riman, K.S. TenHuisen, V.F. Janas, Mechanochemical–hydrothermal synthesis of carbonated apatite powders at room temperature, Biomaterials 23 (2002) 699–710.
[18] E. Landi, A. Tampieri, G. Celotti, L. Vichi, M. Sandri, Influence of synthesis and sintering parameters on the characteristics of carbonate apatite, Biomaterials 25 (2004) 1763–1770.
[19] X.K. Cheng, Q.J. He, L.Z. Huang, R.A. Chi, Control of pore size of the bubble-template porous carbonated hydroxyapatite microsphere by madjustable pressure, Cryst. Growth Des. 9 (2009) 2770–2775.
[20] A. Bhatnagar, M. Sillanpää, A review of emerging adsorbents for nitrate removal from water, Chem. Eng. J. 168 (2011) 493–504.
[21] N. Jia, S.-M. Li, J. Zhu, M.-G. Ma, F. Xu, B. Wang, R.-C. Sun, Microwave-assisted synthesis and characterization of cellulose–carbonated hydroxyapatite nanocomposites in NaOH–urea aqueous solution, Mater. Lett. 64 (2010) 2223–2225.
[22] S.Y. Oh, D.I. Yoo, Y. Shin, G. Seo, FTIR analysis of cellulose treated with sodium hydroxide and carbon dioxide, Carbohydr. Res. 340 (2005) 417–428.
[23] Y.Z. Wan, Y. Huang, C.D. Yuan, S. Raman, Y. Zhu, H.J. Jiang, F. He, C. Gao, Biomimetic synthesis of hydroxyapatite/bacterial cellulose nanocomposites for biomedical applications, Mater. Sci. Eng. C 27 (2007) 855–864.
[24] M. Petrovic, B. Colovic, V. Jokanovic, D. Markov, Self assembly of biomimetic hydroxyapatite on the surface of different polymer thin films, J. Ceram. Process. Res. 13 (2012) 398–404.
[25] M. He, C. Chang, N. Peng, L. Zhang, Structure and properties of hydroxyapatite/cellulose nanocomposite films, Carbohydr. Polym. 87 (2012) 2512–2518.
[26] L. Wu, W. Forsling, P.W. Schindler, Surface complexation of calcium minerals in aqueous solutions. 1. Surface protonation of fluoroapatite water interfaces, J. Colloid Interface Sci. 147 (1991) 178–185.
[27] I. Smiciklas, S. Dimovic, I. Plecas, M. Mitric, Removal of Co^{2+} from aqueous solutions by hydroxyapatite, Water Res. 40 (2006) 2267–2274.
[28] A. Bhatnagar, E. Kumar, M. Sillanpää, Nitrate removal from water by nano-alumina: characterization and sorption studies, Chem. Eng. J. 163 (2010) 317–323.
[29] S. Kilpimaa, H. Runtti, T. Kangas, U. Lassila, T. Kuokkanen, Removal of phosphate and nitrate over a modified carbon residue from biomass gasification, Chem. Eng. Res. Des. (in press) (available online 04.04.14).
[30] E. Repo, J.K. Warchol, T.A. Kurniawan, M.E. Sillanpaa, Adsorption of Co(II) and Ni(II) by EDTA- and/or DTPA-modified chitosan: kinetic and equilibrium modeling, Chem. Eng. J. 161 (2010) 73.
[31] S.J. Allen, G. Mckay, J.F. Porter, Adsorption isotherm models for basic dye adsorption by peat in single and binary component systems, J. Colloids Interface Sci. 280 (2004) 322–333.
[32] D.G. Kinniburgh, General purpose adsorption isotherms, Environ. Sci. Technol. 20 (1986) 895–904.
[33] Z. Elouear, J. Bouzid, N. Boujelben, M. Feki, F. Jamoussi, A. Montiel, Heavy metal removal from aqueous solutions by activated phosphate rock, J. Hazard. Mater. 156 (2008) 412–420.
[34] J. Perrone, B. Fourest, E. Giffaut, Sorption of nickel on carbonate fluoroapatites, J. Colloid Interface Sci. 239 (2001) 303–313.
[35] J.C. Elliott, Studies in Inorganic Chemistry 18: Structure and Chemistry of the Apatites and Other Calcium Orthophosphates, Elsevier, Amsterdam, London, New York, Tokyo, 1994.
[36] D.P. Minh, N.D. Tran, A. Nzihou, P. Sharrock, Hydroxyapatite gel for the improved removal of Pb^{2+} ions from aqueous solution, Chem. Eng. J. 232 (2013) 128–138.
[37] M.C.P.M. da Cunha, M. Weber, F.C. Nart, On the adsorption and reduction of NO_3^- ions at Au and Pt electrodes studied by in situ FTIR spectroscopy, J. Electroanal. Chem. 414 (1996) 163–170.

Paper V

Removal of Arsenic(V) onto magnetic Fe_3O_4 activated Microfibrillated Cellulose (MFC)

Hokkanen, S., Repo, E., Lou, S., Sillanpää, M.

Chemical Engineering Journal 260 (2015) 886–894

Chemical Engineering Journal 260 (2015) 886–894

Contents lists available at ScienceDirect

Chemical Engineering Journal

journal homepage: www.elsevier.com/locate/cej

Removal of arsenic(V) by magnetic nanoparticle activated microfibrillated cellulose

Sanna Hokkanen [a,*], Eveliina Repo [a], Song Lou [b], Mika Sillanpää [a]

[a] Laboratory of Green Chemistry, LUT Savo Sustainable Technologies, Lappeenranta University of Technology, Sammonkatu 12, FI-50130 Mikkeli, Finland
[b] Medical School, University of Minnesota, 321 Church Street SE, Minneapolis, MN 55455, USA

HIGHLIGHTS

- MFC/Fe_2O_3 has a relatively high adsorption capacity for As(V) from aqueous solutions.
- That adsorption capacity of Fe_3O_4/MFC was relatively higher than bare Fe_3O_4 nanoparticles.
- The adsorption rate is fast.
- The adsorption is dependent on the solution pH.

GRAPHICAL ABSTRACT

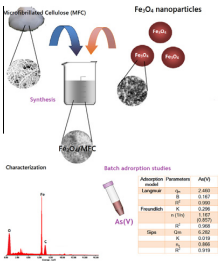

ARTICLE INFO

Article history:
Received 16 May 2014
Received in revised form 24 August 2014
Accepted 25 August 2014

Keywords:
Arsenic
Magnetic nanoparticles
Adsorption
Nanocellulose
Water treatment

ABSTRACT

In this study a novel adsorbent, magnetic iron nanoparticles modified microfibrillated cellulose (FeNP/MFC), was used for arsenate (As(V)) removal from aqueous solutions. The modified cellulose was characterized by FTIR, elemental analysis, zeta potential analyzer, SEM, and TEM. In order to demonstrate the adsorption performance of synthesized material, the effects of contact time, pH, initial As(V) concentration, and regeneration were investigated. The equilibrium adsorption data were fitted to Langmuir, Freundlich, and Sips adsorption models, and the model parameters were evaluated. The monolayer adsorption capacity of the adsorbent, as obtained from the Langmuir isotherm, is 2.460 mmol/g. The adsorption process could be described by pseudo-second-order kinetic model. Iron nanoparticle modified MFC was found to be an exceptional adsorbent material due to its magnetic properties, high surface area and a good adsorption capacity.

1. Introduction

Arsenic is one of the most toxic elements in the world [1]. It is a metalloid, possessing thus both metallic and non-metallic properties, and is ubiquitously present in air, soil, natural water, mineral deposits and rocks and biota [2–4] in varying concentrations. Arsenic is present in water as a result of both natural and anthropogenic activities. Natural processes are volcanic emissions, biological activities, burning of fossil fuels and weathering of arsenic bearing rocks and minerals such as realgar (AsS), orpiment (As_2S_3), arsenopyrite (FeAsS), and lollingite ($FeAs_2$) [5]. Anthropogenic sources include applications of arsenical pesticides and insecticides [6,7], wood preservatives, paints, drugs, dyes, semiconductors, incineration of arsenic containing substances, industrial wastewater discharge, mine tailing/landfill leaching, and manufacturing of arsenic compounds [8,9]. Inorganic arsenic can occur in the environment in several forms depending on the ambient environment (i.e. pH, Eh) and microbial activity [10]. The most common valence states of arsenic in water are oxidized (+V oxidation state, (As(V)) and reduced (+III oxidation state, (III)) forms. As(V) is less toxic than As(III) and is a main species in natural waters [11].

* Corresponding author. Tel.: +358 40 747 7843.

http://dx.doi.org/10.1016/j.cej.2014.08.093
1385-8947/

The arsenic contamination in groundwater is a major threat to human health in many regions of the world. Arsenic dissolved in water is acutely toxic, mutagenic and carcinogenic. Also Arsenicosis due to long-term arsenic exposure can lead to a number of health problems, such as pigmentation of the skin and the development of hard patches of skin on the palm of the hands and soles of the feet. Arsenic poisoning finally leads to skin, bladder, kidney, lung, liver and prostate cancers [12,13]. Due to its high toxicity to human health, USEPA and WHO established an international maximum contaminant level for arsenic in drinking water, which is 0.01 mg/L or 10 ppb [13–16].

Various technologies such as oxidation [15,17], precipitation/coprecipitation [18], coagulation [19,20], sorption [21,22], ion-exchange [23], reverse osmosis [24] and electrokinetic methods [25] have been studied for the removal of arsenic from water. These methods have been widely employed, but they have several drawbacks: high operating and waste treatment costs, high consumption of reagents and large volume of sludge formation [26]. Among all the treatment processes mentioned, adsorption is recognized as an effective approach due to the low cost, high concentration efficiency, and environmental friendliness.

Conventional adsorbents used in arsenic removal are activated carbons and alumina, soils, and resins, which can be coated with different materials like iron or alumina [27–31]. The major detriments of these techniques are difficult separation, waste formation and in many cases poor adsorption capacity [32]. However, because of the selectivity and affinity of Fe(III) toward inorganic arsenic species, Fe(III)-bearing materials are widely used in arsenic adsorption [33–36]. Though these materials are selective and efficient in removing arsenic, their applicability is often limited due to their cost [37].

Within recent decade iron-based nanoparticles have been widely applied for arsenic removal from soils and aqueous surroundings [27,38,39] The popularity of these nanosized particles arises from their unique characteristics such as high surface area, interfacial reactivity, and magnetic properties. However, applicability of the iron nanoparticles is shown to suffer from their poor chemical stability and mechanical strength and tendency to aggregate. Furthermore, these nanoparticles as such are not suitable for fixed-bed column or flow-through systems due to for instance mass transport problems and significant pressure drops. To overcome the above drawbacks different solid supports have been used in order to prepare composite materials without losing the beneficial properties of the nanoparticles. Especially, polymeric supports with proper functional groups despite offering the required stability may even enhance the adsorptive properties of the nanoparticles under study [40,41].

Due to intensified "green thinking" in process industry as well as environmental protection, adsorption of arsenic using natural products has emerged as a viable option. Cellulose is most widely available and renewable biopolymer in nature. It is a very promising raw material available at low cost for the preparation of various functional materials. Due to the presence of hydroxyl groups, cellulose is considered to be an excellent material for surface modification [42,43]. At the same time, a combination between bioadsorbents and iron oxide nanoparticles can pose an efficient biocomposite material, which could possibly show high adsorption capacity, intensified stability, and easy recovery from treated effluents by applying a magnet [27].

In the present study, a novel adsorbent, magnetic iron oxide modified microfibrillated cellulose, was synthesized for the selective removal of arsenic from aqueous solutions. The modified cellulose was characterized by FTIR, elemental analysis, zetasizer, SEM, and TEM. In adsorption studies, the effects of contact time, pH, initial arsenate concentration, and regeneration were investigated.

2. Materials and methods

2.1. Chemicals and materials

Microfibrillated cellulose (MFC) was obtained from the University of Oulu, Finland. Zero-valent iron nanoparticles in aqueous dispersion were supplied by the NANOIRON®. All solutions were prepared in Millipore milliQ high-purity water. All other chemicals used in this study were of analytical grade and supplied by Sigma–Aldrich (Germany). Stock solution of 1000 mg/L was prepared by dissolving appropriate amount of As(V) oxide at first in 25% NaOH following instant neutralization with 2 M HCl and dilution with deionized water. Adjustment of pH was accomplished using 0.1 M NaOH or 0.1 M HNO_3.

2.2. Preparation of FeNP modified MFC

Preparation of modified MFC was conducted according to Zhu et al. with some modifications [44]. 8.9 wt% NaOH/5.5 wt% sulfocarbamide/6.0 wt% urea mixed aqueous solution was pre-cooled to −4 °C in a refrigerator. MFC (2 g) was immediately dispersed into the mixed aqueous solution under vigorous stirring for 5 min at ambient temperature to obtain a transparent cellulose solution with 2% concentration. The resultant cellulose solution was centrifuged at 4000 rpm for 5 min at room temperature to eliminate insoluble components and air bubbles. 1 g of Fe^0 nanoparticles were added into cellulose solution under dynamoelectric stirring for 1 h. The resulting suspension was poured into a coagulation bath containing 10 wt% NaCl under vigorous stirring.

After aged for 12 h, 5 mL of epichlorohydrin was slowly added into the above mixture with stirring for 45 min and its temperature was raised to 75 °C with stirring for another 150 min to obtain wet FeNP/MFC. FeNP/MFC was washed with double distilled water and ethanol for three times.

2.3. Characterization of materials

Fourier transform infrared spectroscopy (FTIR) type Vertex 70 by B Bruker Optics (Germany) was used to identify the surface groups of the modified nanocellulose. The FTIR spectra were recorded at 4 cm^{-1} resolution from 400 to 4000 cm^{-1} and 100 scans per sample. The surface morphology and chemical composition of FeNP/MFC was examined using a Hitachi S-4100 scanning electron microscope (SEM) and energy dispersive analysis of X-rays (EDAX), respectively. Distribution of nanoparticles on the cellulose surface was further verified using transmission electron microscope (HT7700 120 kV High-Contrast/High-Resolution Digital TEM). TEM sample was prepared by dispersing a small amount of modified MFC in ethanol and placing a drop of this mixture on the carbon coated copper grid. The instrument used for C, H and N determination was Organic Elemental Analyzer Flash 2000 (Thermo Scientific, Germany). About 2.5 mg of the sample in a capsule made of tin (assay of C, H and N) or silver (assay of O) was burned at 920–1000 °C. The quantity of each element is expressed in percent of dry mass. Surface charge and point of zero charge of the modified and unmodified cellulose were determined by isoelectric point titration as a function of pH by using Zetasizer Nano ZS (ZEN3500, Malvern).

2.4. Batch adsorption studies

Applicability of FeNP/MFC for As(V) removal was studied using batch experiments in a reaction mixture of 0.100 g of adsorbent and 0.015 L of metal solution containing As(V) at concentrations ranging from 0.14 to 10.68 mmol/L. The effect of contact time

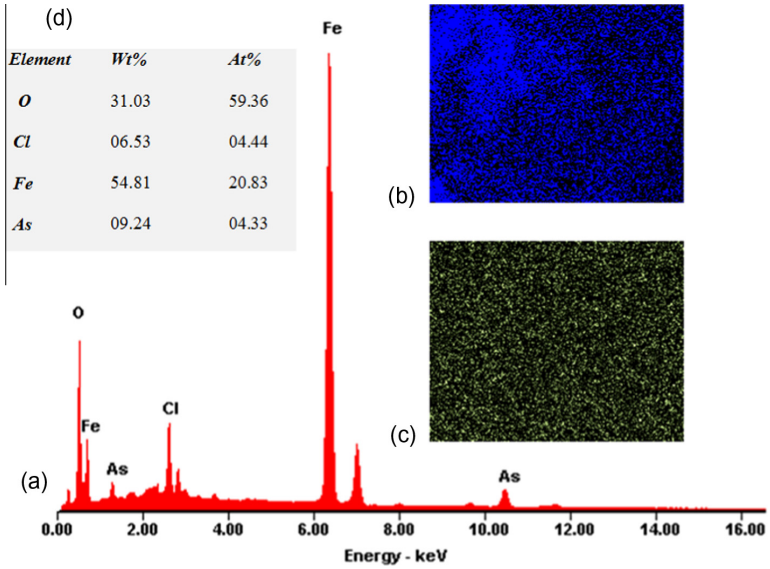

Fig. 1. (a) EDAX spectrum of FeNP/MFC after As(V) adsorption. Inset: elemental X-ray images of (b) O and (c) Fe. (d) The contents of elements on the surface in a weight and atomic percent.

Table 1
The elemental analysis results of unmodified and FeNP modified MFC.

	Percentage of dry weight (%)			
Unmodified MFC 2.61 mg	C 31.91	H 4.98	O 55.11	
FeNP/MFC 3.13 mg	C 11.83	H 7.58	O 21.44	Fe (calculated) 59.15

was studied in reaction mixture of 5 g of adsorbent and 0.350 L of solution containing 0.68 mmol/L of As(V). Agitation was conducted under mechanic stirring. 2 mL samples were pipetted from the reaction mixtures according to schedule. The contact time was varied from 5 to 600 min and measurements were conducted at the room temperature.

After centrifugation metal concentrations were analyzed by an inductively coupled plasma optical atomic emission spectrometry (ICP-OES) model iCAP 6300 (Thermo Electron Corporation, USA).

The concentration retained in adsorbent phase (q_t, mg/g) and removal efficiency (n, %) were calculated by Eqs. (1) and (2), respectively.

$$q_t = \frac{(C_0 - C_t)V}{W} \quad (1)$$

$$n\,(\%) = \frac{(C_0 - C_t)}{C_0} \times 100 \quad (2)$$

where C_0 (mg/L) is initial As(V) concentration and C_t (mg/L) is As(V) concentration at time t (min), V (L) is volume of solution and W (g) is weight of adsorbent.

2.5. Regeneration studies

The regeneration of the FeNP/MFC was also studied. At first adsorbent was loaded by As(V) ions by mixing 0.09 g of the adsorbent with 0.010 L of 0.53 mmol/L As(V) solution. After attaining equilibrium, the spent adsorbent was separated from the solution by centrifuge. Metal ions were eluted using 1.0 M NaOH. The regeneration efficiency (%RE) of the adsorbent was calculated as follows:

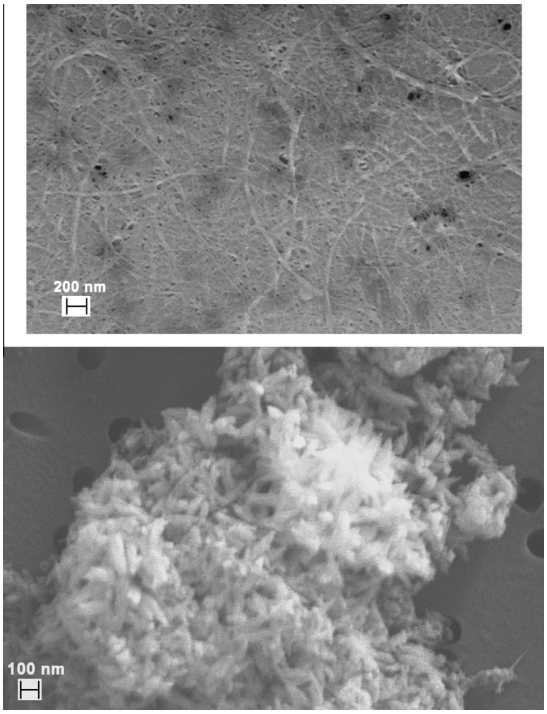

Fig. 2. The SEM picture of (a) unmodified MFC and (b) after FeNP treatment.

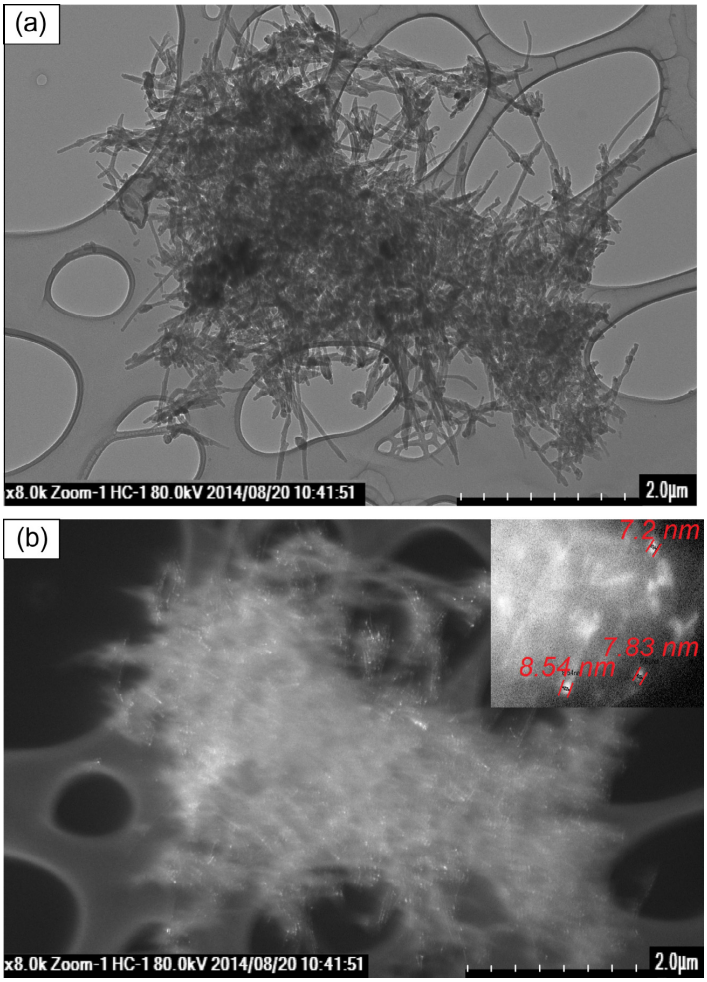

Fig. 3. FTIR–ATR spectra of FeNP nanoparticles, unmodified MFC and FeNP/MFC.

$$(\%\mathrm{RE}) = \frac{q_r}{q_0} \times 100 \quad (3)$$

where q_0 and q_r are the adsorption capacities of FeNP/MFC (mmol/g) before and after regeneration, respectively.

3. Results and discussions

3.1. Characterization

The elemental distribution for the sample of iron nanoparticle modified MFC is illustrated in Fig. 1. Bright spots in Fig. 1b and c represent the signal of the Fe and O elements from the solid sample. Fe was spread over the whole surface of MFC indicating the success of the synthesis. The EDAX spectrum for FeNP/MFC after As(V) adsorption is illustrated in Fig. 1a. Signals observed in spectrum indicate the fact that As(V) was adsorbed on the surface of FeNP/MFC. Low concentration of C and high concentration of Fe are in a good agreement with the results of the elementary analysis shown in Table 1. The SEM images of the adsorbent (Fig. 2) show that the surface roughness of the cellulose increased after modification. This could be attributed, based on the elemental distribution mapping, to the iron nanoparticles covering the cellulose fibers.

TEM analysis was used to confirm the distribution of iron nanoparticles on the MFC surface. High resolution TEM image (Fig. 3a) shows overall structure of the studied material and dark field image (Fig. 3b) locations of the nanoparticles seen as white dots. The size of the nanoparticles is just below 10 nm although some aggregation is also observed. Furthermore, both SEM and TEM analysis show that most of the material is composed of very short fibers indicating that hydrolysis of cellulose occurred during the modification step.

The FTIR–ATR spectra of bare Fe^0 nanoparticles, unmodified MFC and FeNP/MFC are shown in Fig. 3. In the case of Fe^0 nanoparticles, the band at 580 cm^{-1} corresponding to the vibration of the Fe–O bonds, indicates that Fe^0 was partly corroded into its oxide/hydroxide forms (magnetite, maghemite, and lepidocrocite) [38].

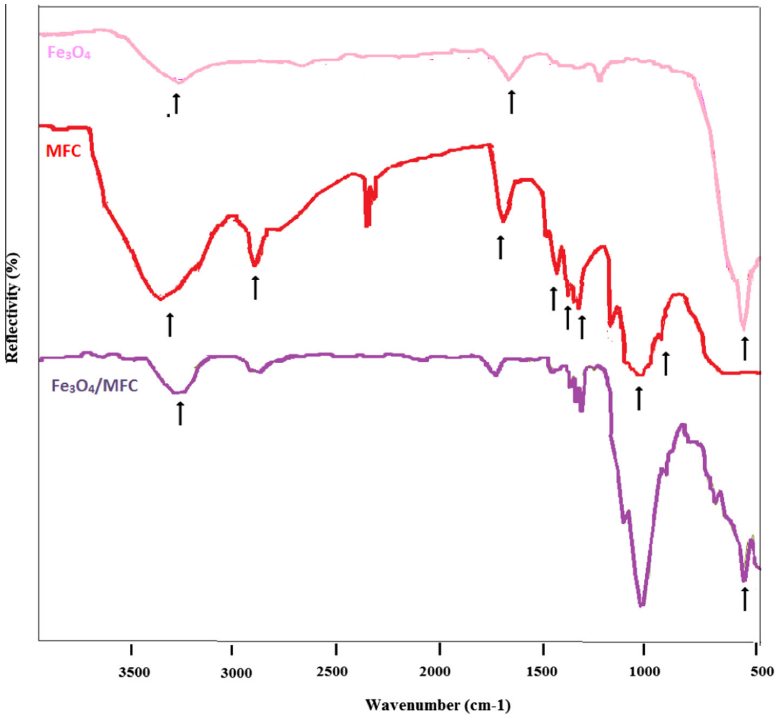

Fig. 4. Effect of initial pH for adsorption (T = 25 °C; adsorbent dosage = 0.067 g/L).

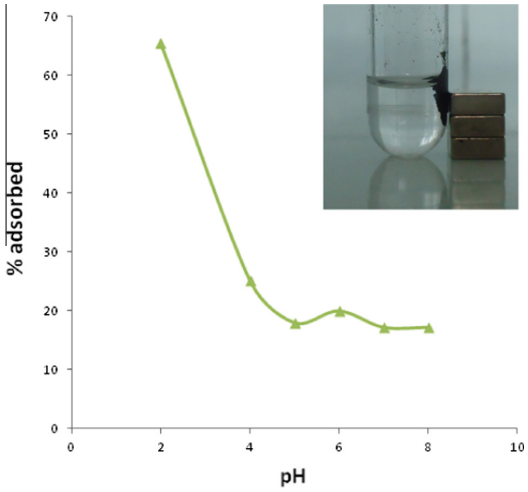

Fig. 5. Effect of initial pH for adsorption of As(V) by FeNP/MFC (T = 25 °C; adsorbent dosage = 0.067 g). Inset: Illustration of magnetic separation.

The high density O regions in elemental mapping could correspond to iron oxide/hydroxide particles (Fig. 1b). This is also supported by the characteristic bands of hydroxyl groups, 1630 and 3405 cm^{-1} present in the spectrum.

The spectrum of unmodified MFC shows the band at around 2900 cm^{-1} which belongs to O–H stretching, while the O–H bending mode of adsorbed water is registered at around 1640 cm^{-1}. The weak band at 1590 cm^{-1} confirms the presence of the COO− groups. The other weak bands at 1428 cm^{-1} are assigned to HCH and OCH vibrations and the band at 1366 cm^{-1} to the CH bending mode. The band at 895 cm^{-1} corresponds to the COC, CCO and CCH deformation modes. For FeNP/MFC, the characteristic peak at around 580 cm^{-1}, caused by the strong vibration of the Fe–O bond, indicates the presence of iron oxide or the bond formed between Fe nanoparticles and surface hydroxyl groups. Thus, the FTIR analysis confirms the interaction of the surface groups of cellulose backbone with the iron nanoparticles at the surface. On the whole, it can be suggested that both Fe^0 and iron oxide nanoparticles exist on the surface.

3.2. Batch adsorption experiments

3.2.1. Effect of pH on As(V) removal

Fig. 5 shows that As(V) was strongly adsorbed on the FeNP/MFC surface from acidic solutions (pH 2). It can be stated that at least two pH dependent factors affected the As(V) adsorption efficiency: point of zero charge (pHpzc) of the adsorbent and As(V) speciation. At acidic conditions surface charge of the adsorbent was positive and accordingly more attractive to As(V), which appears to be in form of $H_2AsO_4^-$ between pH 2 and 5 [45].When pH value exceeded pHpzc (5.2) the surface sites became negatively charged causing repulsive electrostatic effect towards As(V) species as verified by lower adsorption efficiency. Moreover, stronger form of arsenate oxyanion ($HAsO_4^{2-}$) is present at alkaline conditions [45] when electrostatic repulsion dominates even more evidently.

3.2.2. Kinetic studies

As(V) removal by modified MFC as a function of contact time is shown in Fig. 6. The kinetic curve for As(V) ions showed that the

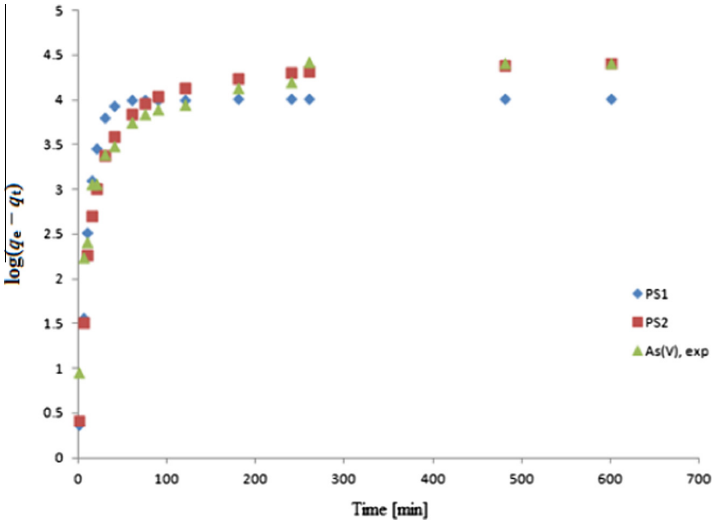

Fig. 6. Non-linear regressions of kinetic plots: pseudo-first-order model (PS1) and pseudo-second-order model (PS2) (T = 25 °C; adsorbent dosage = 0.132 g/L; n pH 2).

Table 2
Kinetic parameters for As(V) adsorption by FeNP/MFC.

	k_1 (min^{-1})	q_1 (mol/g)	R^2
First-order model			
	0.099	4.016	0.854
k_2 (g/(mol min))	q_2 (mmol/g)	h (mmol/(g min))	R^2
Second-order model			
0.037569404	4.270	0.685	0.957

Table 3
Parameters of Langmuir, Freundlich and Sips isotherms for adsorption of As(V) on FeNP/MFC.

Adsorption model	Parameters	As(V)
Langmuir	q_m	2.460
	B	0.167
	R^2	0.990
Freundlich	K	0.296
	n (1/n)	1.167 (0.857)
	R^2	0.968
Sips	q_m	6.282
	K	0.019
	n_s	0.866
	R^2	0.919

adsorption was initially rapid and reached equilibrium after approximately 75 min. Investigating the mechanism of adsorption and its potential rate-controlling steps including mass transport and chemical reaction processes, kinetic models were exploited to analyze the experimental data. Pseudo-first-order (PS1) and pseudo-second-order (PS2) models were applied to find out the adsorption mechanism. The PS1 model, which is widely used for sorption in liquid/solid systems, is expressed as [46,47]:

$$\ln(q_e - q_t) = \ln q_e - k_1 t \quad (4)$$

and the PS2 model, which assumes that the rate-determining step may be a chemical surface reaction, is presented as follows:

$$\frac{t}{q_t} = \frac{1}{k_2 q_e^2} + \frac{1}{q_e} t \quad (5)$$

where q_t and q_e (mmol/g) represent the amount of metals adsorbed at time t (min) and at equilibrium, respectively, while k_1 (1/min) and k_2 (g/mmol min) are the rate constants of PS1 and PS2 sorption. The initial adsorption rate (h) can be determined from k_2 and q_e values using [48]:

$$h = k_2 q_e^2 \quad (6)$$

Fig. 6 and Table 2 indicate that the PS1 kinetic model did not describe the sorption system as well as the PS2 model. The theoretical q_e value calculated from the PS1 kinetic model was evidently less than the experimental value, and the correlation coefficient was also very low (0.854), indicating that this model could not explain the adsorption process. This is due to the fact that the PS1 kinetic model cannot fit well to the whole time range, but is usually applicable only at the initial stage of adsorption [47]. According to Fig. 4 and Table 3, the PS2 model was better fitted to the experimental data since the calculated q_e was closer to the experimental one, and the correlation coefficient was 0.957. The PS2 model is based on the assumption that the rate-determining step may be a chemical sorption involving valence forces through sharing of electrons between adsorbent and adsorbate [48]. Therefore, the PS2 kinetic model was feasible to describe the adsorption process of As(V) on the FeNP/MFC.

3.2.3. Adsorption isotherms

The information of the equilibrium relationship between the concentration of adsorbate in the liquid phase and adsorbed phase, also known as the adsorption isotherm is of great importance in the adsorption studies. Three adsorption isotherm models namely Langmuir, Sips and Freundlich, were used to evaluate adsorption equilibrium data of single component system.

The adsorption theory of Langmuir model is based on the kinetic principle and it proposes the monolayer surface adsorption on the ideal solid with definite localized sites that are energetically identical [49]. This model further presumes that the adsorbate molecules can only accommodate one localized site without lateral interactions between the adsorbed molecules, even on the adjacent sites. Graphically, Langmuir isotherm is characterized by a plateau curve. It means that further adsorption cannot occur when equilibrium is established.

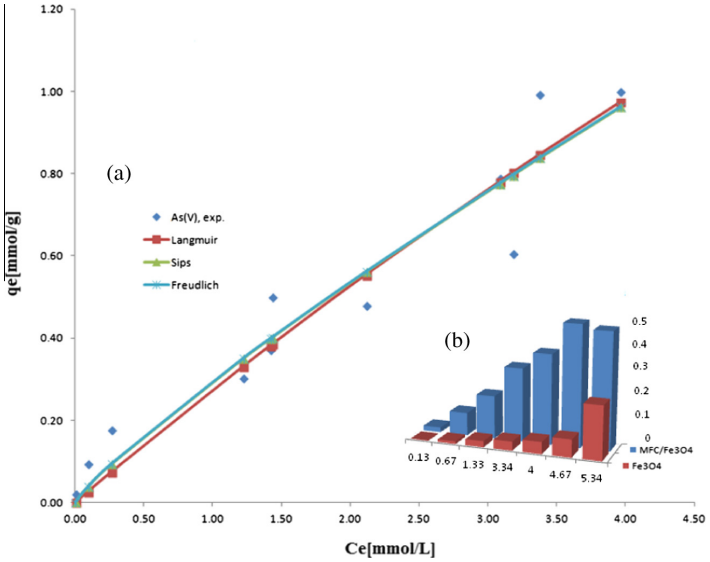

Fig. 7. (a) Langmuir, Freundlich and Sips isotherms for adsorption of As(V), (b) comparison of the adsorption capacities of Fe^0 nanoparticles and FeNP/MFC for the removal of As(V) from water (T = 25 °C; adsorbent dosage = 0.067 g/L; n pH 2).

Table 4
Values of separation factor (R_L) for adsorption of As(V) on FeNP/MFC.

Initial concentration (ppm)	R_L
10	0.995
50	0.975
100	0.951
200	0.885
250	0.865
300	0.846
350	0.828
400	0.793
500	0.762
600	0.733
700	0.706
800	0.995

Langmuir model was originally developed for describing adsorption phenomena in the gas phase, but it has been extensively used for the correlation of adsorption equilibrium data of various solute-sorbent interactions in the liquid phase. The mathematical form of Langmuir isotherm model is given as follows:

$$q_e = \frac{K_L b C_e}{(1 + bC_e)} \tag{7}$$

where q_e is the maximum adsorptive capacity of the solid (mmol/g), which corresponds to the monolayer surface coverage (i.e. the adsorbate layer is one molecule in thickness) and K_L is Langmuir constant of adsorption affinity (L/mmol). As the value of C_e becomes lower, the term of $K_L \cdot C_e$ is much less than unity and Langmuir isotherm will obey Henry's law behavior. In contrast, when the value of C_e is getting higher, the saturation point of adsorption will be reached and the concentration of solute on the solid surface will be equal to the maximum sorption capacity. The essential characteristic of Langmuir isotherm on the adsorption nature can be assessed by a dimensionless equilibrium parameter [49]:

$$R_L = \frac{1}{1 + C_0 K_L} \tag{8}$$

where R_L is a dimensionless equilibrium parameter or the separation factor and C_0 is the initial concentration of metal solution (mmol/L). The value of R_L denotes the adsorption nature to be unfavorable ($R_L > 1$), favorable ($0 < R_L < 1$), irreversible ($R_L = 0$), or linear ($R_L = 1$).

The Freundlich isotherm model (Freundlich, 1906), which assumes a heterogeneous surface and a multilayer adsorption with an energetic non-uniform distribution, can be expressed as [50]:

$$q_e = kC_e^{1/n} \tag{9}$$

where k and n are constants for a given adsorbent–adsorbate system.

The Sips (Sips, 1948) isotherm model is obtained by introducing a power law expression of the Freundlich equation into the Langmuir equation [51]. The non-linearized form of Sips isotherm model can be given as follows:

$$q_e = \frac{q_m S (K_S C_e)^{n_S}}{1 + (K_S C_e)^{n_S}} \tag{10}$$

where q_e is the adsorbed amount at equilibrium (mmol/g), C_e the equilibrium concentration of the adsorbate (mmol/L), q_{mS} the Sips maximum adsorption capacity (mmol/g), K_S the Sips equilibrium constant (L/mmol), and n_S the Sips model exponent describing heterogeneity.

At low adsorbate concentrations, the Sips isotherm effectively reduces to the Freundlich isotherm and thus does not obey the Henry's law. At high adsorbate concentrations, it predicts a monolayer adsorption capacity, characteristic of the Langmuir isotherm.

As shown in Fig. 7 and Table 3, according to the correlation coefficients (R^2), a suitability order of the three models tested was Langmuir, Freundlich and Sips. Thus, the Langmuir model was the most adequate to describe the adsorption process of arsenate onto FeNP/MFC surface suggesting a monolayer adsorption process. The maximum adsorption capacity (q_m) for As(V) from Langmuir model was 2.460 mmol/g. According to Eq. (8), the values of R_L were 0.706–0.964 for As(V), indicating that the adsorption process was favorable (Table 4). Furthermore, the value of 1/n

Table 5
The results of regeneration study.

Regenerant NaOH 1.0 M	No. of cycle	Adsorption capacity of As(V)		Regeneration efficiency (%)
		Before regeneration (mmol/g)	After regeneration (mmol/g)	
	1	0.0509	0.0532	104.52
	2	0.0509	0.0489	96.07
	3	0.0509	0.0501	98.42
	4	0.0509	0.0352	69.16

obtained from Freundlich model was less than 1, which also suggested the favorable adsorption of arsenate onto adsorbent. This is consistent with the result of Langmuir model.

Comparison of the adsorption capacities of bare Fe^0 nanoparticles and FeNP/MFC for the removal of As(V) shows that the capacity of Fe_3NP/MFC was significantly higher (Fig. 7). The Langmuir maximum adsorption capacity for FeNP/MFC was 2.460 mmol As(V)/g and for Fe^0 0.042 mmol As(V)/g.

3.3. Mechanisms of As(V) adsorption

The removal of arsenic species by Fe^0 has been explained by their adsorption on the corrosion product surface of original Fe particles. Thus, when contacted with a solution, Fe^0 gradually oxidizes enabling arsenate ions to form inner-sphere complexes with the oxidized sites [38]. Therefore, the adsorption properties are mainly due to the presence of OH_2^+, OH^-, and O^- functional groups on adsorbent surface. Due to exposed to water at different pH iron oxide surface develop surface charges and, by adsorbing metal ions complete coordination shells with OH groups, which either bound to or release H^+. At neutral and acidic conditions (less than 8), OH_2^+ and OH forms on surface are dominant and responsible for the selective binding of molecular and ionic forms of arsenate species [52].

As(V) adsorption onto hydrated Fe oxide/hydroxide from an aqueous solution can be expressed by the following formula [53]:

$$MFC-FeOH(s)+H_3AsO_{4(aq)} \leftrightarrow MFC-FeAsO_4^- + H^+_{(aq)} + H_2O \quad (11)$$

$$MFC-FeOH(s)+H_3AsO_{4(aq)} \leftrightarrow MFC-FeAsO_4^{2-} + 2H^+_{(aq)} + H_2O \quad (12)$$

Fig. 4 shows the removal efficiencies of As(V) by the FeNP/MFC adsorbent at different pH. As known, the pH of the solution has a major influence on its ionic strength. The removal efficiencies of As(V) showed obvious change with the increase of the pH from 2 to 8. As suggested by Goldberg and Johnston (2001), the adsorption of arsenic species will decrease with the increase of ionic strength, if arsenic species form outer-sphere surface complexes, while the adsorption of arsenic species will not change or increase with the increase of ionic strength, if arsenic species form inner-sphere surface complexes [54]. Therefore, As(V) adsorption in the present study presumably followed the inner-sphere complex mechanism.

3.4. Regeneration

For a practical use of an adsorbent, the regeneration of the material is very important to decrease operational costs. In this study the regeneration procedure was carried out for four times using 10 mL of 1.0 M NaOH as eluent and the results are shown in Table 5. After three cycles the regeneration efficiency was still over 98% indicating that FeNP/MFC could be used repeatedly using an adsorption–desorption cycle. On the other hand, nanomaterials as adsorbents do not produce large volumes of waste sludge when disposal is a competitive option compared to the recycling of the used adsorbent.

4. Conclusions

In the present study, magnetic iron nanoparticles modified microfibrillated cellulose was synthesized and characterized. Analysis indicated that nanoparticles were well dispersed on the surface of MFC providing a highly potential adsorption material for As(V) removal. Indeed, FeNP/MFC showed greatly improved As(V) uptake properties compared to original Fe nanoparticles. Adsorption of As(V) was found to be effective at the lower pH range; maximum adsorption capacity was found to be the highest at pH 2. Equilibrium isotherm data was fitted using three different adsorption models. Among these models, the Langmuir model was in a good agreement with the experimental data with high correlation coefficient. Kinetic study showed that the pseudo-second order model was appropriate to describe the adsorption process. Furthermore, regeneration of studied material was possible using NaOH solution. Feasible improvements in the uptake properties along with the magnetic properties encourage efforts for FeNP/MFC obtained to be used in water and wastewater treatment.

References

[1] D.K. Nordstrom, Worldwide occurrences of arsenic in ground water, Science 296 (2002) 2143–2145.
[2] J. Matschullat, Arsenic in the geosphere—a review, Sci. Total Environ. 249 (2000) 297–312.
[3] X. Huang, M. Sillanpää, B. Duo, E.T. Gjessing, Water quality in the Tibetan plateau: metal contents of four selected rivers, Environ. Pollut. 156 (2008) 270–277.
[4] X. Huang, M. Sillanpää, E.T. Gjessing, R.D. Vogt, Water quality in the Tibetan Plateau: major ions and trace elements in the headwaters of four major Asian rivers, Sci. Total Environ. 407 (2009) 6242–6254.
[5] X. Huang, M. Sillanpää, E.T. Gjessing, S. Peräniemi, R.D. Vogt, Water quality in the southern Tibetan plateau: chemical evaluation of the Yarlung Tsangpo (Brahmaputra), River Res. Appl. 27 (2011) 113–121.
[6] W.R. Cullen, K.J. Reimer, Arsenic speciation in the environment, Chem. Rev. 89 (1989) 713–764.
[7] N.E. Korte, Q. Fernando, A review of arsenic(III) in groundwater, Crit. Rev. Environ. Control 21 (1991) 1–39.
[8] F.J. Peryea, T.L. Creger, Vertical distribution of lead and arsenic in soils contaminated with lead arsenate pesticide residues, Water Air Soil Pollut. 78 (1994) 297–306.
[9] J.M. Azcue, J.O. Nriagu, Arsenic: historical perspectives, in: J.O. Nriagu (Ed.), Arsenic in the Environment, Part 1: Cycling and Characterization, John Wiley & Sons, New York, 1994, pp. 1–15.
[10] A.H. Welch, M.S. Lico, J.L. Hughes, Arsenic in groundwater of the western United States, Ground Water 26 (1988) 333–347.
[11] R.N. Yong, C.N. Mulligan, Natural Attenuation of Contaminants in Soils, CRC Press, Boca Raton, FL, 2004.
[12] F. El-Hadri, A. Morales-Rubio, M. de la Guardia, Atomic fluorescence spectrometric determination of trace amounts of arsenic and antimony in drinking water by continuous hydride generation.nta, Talanta 52 (2000) 653.
[13] R. Stone, Arsenic and paddy rice: a neglected cancer risk?, Science 321 (5886) (2008) 184–185
[14] World Health Organization (WHO), Guidelines for Drinking Water Quality, Geneva, (2008).
[15] European Commission, The Quality of Water Intended for Human Consumption, Council Directive 98/83/EC (1998).
[16] U.S. Environmental Protection Agency (USEPA), "Minor clarification of national primary drinking water regulation for arsenic", Federal register, 68 (57), 14502–14507 (2003).
[17] T.M. Gihring, G.K. Druschel, R.B. Mccleskey, R.J. Hamers, J.F. Banfield, Rapid arsenite oxidation by *Thermus aquaticus* and *Thermus thermophilus*: field and laboratory investigations, Environ. Sci. Technol. 35 (2001) 3857–3862.
[18] M. Zaw, M.T. Emett, Arsenic removal from water using advanced oxidation processes, Toxicol. Lett. 133 (2002) 113–118.

[19] M. Bissen, F.H. Frimmel, Arsenic—a review. Part II: oxidation of arsenic and its removal in water treatment, Acta Hydrochim. Hydrobiol. 31 (2003) 97–107.
[20] T. Yuan, F.-Q. Luo, J.-Y. Hu, S.-L. Ong, W.-N. Ng, A study on arsenic removal from household drinking water, J. Environ. Sci. Health 38A (2003) 1731–1744.
[21] P.R. Kumar, S. Chaudhari, K.C. Khilar, S.P. Mahajan, Removal of arsenic from water by electrocoagulation, Chemosphere 55 (2004) 1245–1252.
[22] B.A. Manning, S. Goldberg, Adsorption and stability of arsenic(III) at the clay mineral–water interface, Environ. Sci. Technol. 31 (1997) 2005–2011.
[23] J. Pattanayak, K. Mondal, S. Mathew, S.B. Lalvani, A parametric evaluation of the removal of As(V) and As(III) by carbon-based adsorbents, Carbon 38 (2000) 589–596.
[24] T.-F. Lin, J.-K. Wu, Adsorption of arsenite and arsenate within activated alumina grains: equilibrium and kinetics, Water Res. 35 (2001) 2049–2057.
[25] P. Isosaari, M. Sillanpää, Effects of oxalate and phosphate on electrokinetic removal of arsenic from mine tailings, Sep. Purif. Technol. 86 (2012) 26–34.
[26] J. Kim, M.M. Benjamin, Modeling a novel ion exchange process for arsenic and nitrate removal, Water Res. 38 (2004) 2053–2062.
[27] T. Tuutijärvi, J. Lu, M. Sillanpää, G. Chen, As(V) adsorption on maghemite nanoparticles, J. Hazard. Mater. 166 (2009) 1415–1420.
[28] L. Lorenzen, J.S.J. van Deventer, W.M. Landi, Factors affecting the mechanism of the adsorption of arsenic species on activated carbon, Miner. Eng. 8 (1995) 557–569.
[29] I. Rau, A. Gonzalo, M. Valiente, Arsenic(V) removal from aqueous solutions by iron(III) loaded chelating resin, J. Radioanal. Nucl. Chem. 246 (2000) 597–600.
[30] S. Chakravarty, V. Dureja, G. Bhattacharyya, S. Maity, S. Bhattacharjee, Removal of arsenic from groundwater using low cost ferruginous manganese ore, Water Res. 36 (2002) 625–632.
[31] Y. Kim, C. Kim, I. Choi, S. Rengaraj, J. Yi, Arsenic removal using mesoporous alumina prepared via a templating method, Environ. Sci. Technol. 38 (2004) 924–931.
[32] Z. Gu, J. Fang, B. Deng, Preparation and evaluation of GAC-based iron-containing adsorbents for arsenic removal, Environ. Sci. Technol. 39 (2005) 3833–3843.
[33] Q. Liu, H. Guo, Y. Li, H. Xiang, Acclimation of arsenic-resistant Fe(II)-oxidizing bacteria in aqueous environment, Int. Biodeterior. Biodegrad. 76 (2013) 86–91.
[34] K. Wu, R. Liu, T. Li, H. Liu, J. Peng, J. Qu, Removal of arsenic(III) from aqueous solution using a low-cost by-product in Fe-removal plants—Fe-based backwashing sludge, Chem. Eng. J. 226 (15) (June 2013) 393–401.
[35] Yaping Zhao, Minsheng Huang, Wu Wei, Wei Jin, Synthesis of the cotton cellulose based Fe(III)-loaded adsorbent for arsenic(V) removal from drinking water, Desalination 249 (2009) 1006–1011.
[36] Sanjoy Kumar Maji, Yu-Hsuan Kao, Chin-Jen Wang, Guang-Sin Lu, Jia-Jing Wu, Chen-Wuing Liu, Fixed bed adsorption of As(III) on iron-oxide-coated natural rock (IOCNR) and application to real arsenic-bearing groundwater, Chem. Eng. J. 203 (2012) 285–293.
[37] A. Gupta, V.S. Chauhan, N. Sankararamakrishnan, Preparation and evaluation of iron–chitosan composites for removal of As(III) and As(V) from arsenic contaminated real life groundwater, Water Res. 43 (2009) 3862–3870.
[38] S.R. Kanel, B. Manning, L. Charlet, H. Choi, Removal of arsenic (III) from groundwater by nanoscale zero-valent iron, Environ. Sci. Technol. 39 (5) (2005) 1291–1298.
[39] S.R. Kanel, J.M. Greneche, H. Choi, Arsenic (V) removal from groundwater using nano scale zero-valent iron as a colloidal reactive barrier material, Environ. Sci. Technol. 40 (6) (2006) 2045–2050.
[40] S. Sarkar, E. Guibal, F. Quignard, A.K. SenGupta, Polymer-supported metals and metal oxide nanoparticles: synthesis, characterization, and applications, J. Nanopart. Res. 14 (2) (2012) 1–24.
[41] X. Zhao, L. Lv, B. Pan, W. Zhang, S. Zhang, Q. Zhang, Polymer-supported nanocomposites for environmental application: a review, Chem. Eng. J. 170 (2) (2011) 381–394.
[42] Y. Habibi, L.A. Lucia, O.J. Rojas, Cellulose nanocrystals: chemistry, selfassembly, and applications, Chem. Rev. 110 (6) (2010) 3479–3500.
[43] S. Hokkanen, E. Repo, E. Sillanpää, Removal of heavy metals from aqueous solutions by succinic anhydride modified mercerized nanocellulose, Chem. Eng. J. 223 (2013) 40–47.
[44] H.-Y. Zhu, Y.-Q. Fu, R. Jiang, J.-H. Jiang, L. Xiao, G.-M. Zeng, S.-L. Zhao, Y. Wang, Adsorption removal of congo red onto magnetic cellulose/Fe_3O_4/activated carbon composite: equilibrium, kinetic and thermodynamic studies, Chem. Eng. J. 173 (2011) 494–502.
[45] M. Streat, K. Hellgardt, N.L.R. Newton, Hydrous ferric oxide as an adsorbent in water treatment, Part 2. Adsorption studies, Process Saf. Environ. Prot. 86 (2008) 11–20.
[46] L. Zhou, Y. Wang, Z. Liua, Q. Huang, Characteristics of equilibrium, kinetics studies for adsorption of Hg(II), Cu(II), and Ni(II) ions by thiourea-modified magnetic chitosan microspheres, J. Hazard. Mater. 161 (2009) 995–1002.
[47] Y.-S. Ho, Second-order kinetic model for the sorption of cadmium onto tree fern: a comparison of linear and non-linear methods, Water Res. 40 (2006) 119–125.
[48] I. Langmuir, The adsorption of gases on plane surfaces of glass, mica and platinum, J. Am. Chem. Soc. 40 (1918) 1361–1403.
[49] F.E. Soetaredjo, A. Kurniawan, A.L. Ki, S. Ismadji, Incorporation of selectivity factor in modeling binary component adsorption isotherms for heavy metals-biomass system, Chem. Eng. J. 2 (91) (2013) 137–148.
[50] H.M.F. Freundlich, Over the adsorption in solution, J. Phys. Chem. 57 (1906) 385–470.
[51] R. Sips, On the structure of a catalyst surface, J. Chem. Phys. 16 (1948) 490–495.
[52] N.B. Issa, V.N. Rajaković-Ognjanović, B.M. Jovanović, L.V. Rajaković, Determination of inorganic arsenic species in natural waters – benefits of separation and preconcentration on ion exchange and hybrid resins, Anal. Chim. Acta 673 (2010) 185–193.
[53] R. Chen, C. Zhi, H. Yang, Y. Bando, Z. Zhang, N. Sugiur, D. Golberg, Arsenic (V) adsorption on Fe_3O_4 nanoparticle-coated boron nitride nanotube, J. Colloid Interface Sci. 359 (2011) 261–268.
[54] S. Goldberg, C.T. Johnston, Mechanisms of arsenic adsorption on amorphous oxides evaluated using macroscopic measurements, vibrational spectroscopy, and surface complexation modeling, J. Colloid Interface Sci. 234 (1) (2001) 204–216.

ACTA UNIVERSITATIS LAPPEENRANTAENSIS

546. HYYPIÄ, MIRVA. Roles of leadership in complex environments
Enhancing knowledge flows in organisational constellations through practice-based innovation processes. 2013. Diss.

547. HAAKANA, JUHA. Impact of reliability of supply on long-term development approaches to electricity distribution networks. 2013. Diss.

548. TUOMINEN, TERHI. Accumulation of financial and social capital as means to achieve a sustained competitive advantage of consumer co-operatives. 2013. Diss.

549. VOLCHEK, DARIA. Internationalization of small and medium-sized enterprises and impact of institutions on international entrepreneurship in emerging economies: the case of Russia. 2013. Diss.

550. PEKKARINEN, OLLI. Industrial solution business – transition from product to solution offering. 2013. Diss.

551. KINNUNEN, JYRI. Risk-return trade-off and autocorrelation. 2013. Diss.

552. YLÄTALO, JAAKKO. Model based analysis of the post-combustion calcium looping process for carbon dioxide capture. 2013. Diss.

553. LEHTOVAARA, MATTI. Commercialization of modern renewable energy. 2013. Diss.

554. VIROLAINEN, SAMI. Hydrometallurgical recovery of valuable metals from secondary raw materials. 2013. Diss.

555. HEINONEN, JARI. Chromatographic recovery of chemicals from acidic biomass hydrolysates. 2013. Diss.

556. HELLSTÉN, SANNA. Recovery of biomass-derived valuable compounds using chromatographic and membrane separations. 2013. Diss.

557. PINOMAA, ANTTI. Power-line-communication-based data transmission concept for an LVDC electricity distribution network – analysis and implementation. 2013. Diss.

558. TAMMINEN, JUSSI. Variable speed drive in fan system monitoring. 2013. Diss.

559. GRÖNMAN, KAISA. Importance of considering food waste in the development of sustainable food packaging systems. 2013. Diss.

560. HOLOPAINEN, SANNA. Ion mobility spectrometry in liquid analysis. 2013. Diss.

561. NISULA, ANNA-MAIJA. Building organizational creativity – a multitheory and multilevel approach for understanding and stimulating organizational creativity. 2013. Diss.

562. HAMAGUCHI, MARCELO. Additional revenue opportunities in pulp mills and their impacts on the kraft process. 2013. Diss.

563. MARTIKKA, OSSI. Impact of mineral fillers on the properties of extruded wood-polypropylene composites. 2013. Diss.

564. AUVINEN, SAMI. Computational modeling of the properties of TiO2 nanoparticles. 2013. Diss.

565. RAHIALA, SIRPA. Particle model for simulating limestone reactions in novel fluidised bed energy applications. 2013. Diss.

566. VIHOLAINEN, JUHA. Energy-efficient control strategies for variable speed controlled parallel pumping systems based on pump operation point monitoring with frequency converters. 2014. Diss.

567. VÄISÄNEN, SANNI. Greenhouse gas emissions from peat and biomass-derived fuels, electricity and heat – Estimation of various production chains by using LCA methodology. 2014. Diss.

568. SEMYONOV, DENIS. Computational studies for the design of process equipment with complex geometries. 2014. Diss.

569. KARPPINEN, HENRI. Reframing the relationship between service design and operations: a service engineering approach. 2014. Diss.

570. KALLIO, SAMULI. Modeling and parameter estimation of double-star permanent magnet synchronous machines. 2014. Diss.

571. SALMELA, ERNO. Kysyntä-toimitusketjun synkronointi epävarman kysynnän ja tarjonnan toimintaympäristössä. 2014. Diss.

572. RIUNGU-KALLIOSAARI, LEAH. Empirical study on the adoption, use and effects of cloud-based testing. 2014. Diss.

573. KINNARINEN, TEEMU. Pressure filtration characteristics of enzymatically hydralyzed biomass suspensions. 2014. Diss.

574. LAMMASSAARI, TIMO. Muutos kuntaorganisaatiossa – tapaustutkimus erään kunnan teknisestä toimialasta. 2014. Diss.

575. KALWAR, SANTOSH KUMAR. Conceptualizing and measuring human anxiety on the Internet. 2014. Diss.

576. LANKINEN, JUKKA. Local features in image and video processing – object class matching and video shot detection. 2014. Diss.

577. AL-SAEDI, MAZIN. Flexible multibody dynamics and intelligent control of a hydraulically driven hybrid redundant robot machine. 2014. Diss.

578. TYSTER, JUHO. Power semiconductor nonlinearities in active d*u*/d*t* output filtering. 2014. Diss.

579. KERÄNEN, JOONA. Customer value assessment in business markets. 2014. Diss.

580. ALEXANDROVA, YULIA. Wind turbine direct-drive permanent-magnet generator with direct liquid cooling for mass reduction. 2014. Diss.

581. HUHTALA, MERJA. PDM system functions and utilizations analysis to improve the efficiency of sheet metal product design and manufacturing. 2014. Diss.

582. SAUNILA, MINNA. Performance management through innovation capability in SMEs. 2014. Diss.

583. LANA, ANDREY. LVDC power distribution system: computational modelling. 2014. Diss.

584. PEKKARINEN, JOONAS. Laser cladding with scanning optics. 2014. Diss.

585. PELTOMAA, JYRKI. The early activities of front end of innovation in OEM companies using a new FEI platform as a framework for renewal. 2014. Diss.

586. ROZHANSKY, IGOR. Resonant tunneling effects in semiconductor heterostructures. 2014. Diss.

587. PHAM, THUY DUONG. Ultrasonic and electrokinetic remediation of low permeability soil contaminated with persistent organic pollutants. 2014. Diss.